THE UNIVERSITY
of EDINBURGH

Novel capillary defects in Spinal Muscular Atrophy

Eilidh Somers

Declaration

I declare that this thesis was composed entirely by myself and the work on which it is based is my own, unless clearly stated in the text.

Eilidh Somers

Acknowledgements

During my time at the University of Edinburgh I have been fortunate enough to work with some excellent scientists who just also happen to be lovely people. I would like to take the opportunity now to thank them.

First, my supervisors Simon Parson and Tom Gillingwater. Your endless enthusiasm, encouragement, support and knowledge have been greatly appreciated. It has been a privilege to work with you and to learn so much from you both. Above all I would like to thank you for giving me such a fantastic opportunity.

I would also like to thank the members of the Parson and Gillingwater labs, past and present. Sarah and Sophie, I can't think of two better people to share this experience with. Thank you for your company, advice, knowledge, support and most importantly, your friendship. Thank you to Tom Wishart, Laura Comely and Chantal Mutsaers for teaching and training me when I started and for making the lab so welcoming. Thank you to Derek Thomson for knowing everything, being able to solve any problem and for his excellent hugs. Thank you to Gillian for her endless patience and excellent book club selections. Thank you to Arwin for sharing her cell culture expertise and for being so much fun to work with. Thank you to Rachel for humouring me and laughing no matter how bad the joke. Thank you to Inès for always having the one email I needed and being polite enough to share it. Thank you to Ross and Ewout, two stand up gents who've always listened and cheered me up. I would also like to thank my friends in Edinburgh beyond the lab, Anjali, Sarah, Katie and Anatomy Scott, whose friendships are so important and special to me.

I would also like to thank the Anatomy Department for funding my studentship and for providing me with the opportunity to teach alongside such an inspiring team.

Last but by no means least, I would like to thank my family whom I love dearly and would be lost without. The 100,000 word limit isn't enough to thank my parents for all that they have done for me in the past four years, never mind the 22 before that! So I'll be brief. Thank you for everything. Thank you to my brother Andrew, the coolest person I know, and to Jacqueline, the best friend I could ever ask for. And finally, to my fiancé Scott who gave me the courage to try and the strength to keep going. Your patience, support, love and good humour know no bounds. I look forward to spending the rest of my life making you as happy as you have made me.

Abstract

Spinal Muscular Atrophy (SMA) is an autosomal, recessive form of childhood motor neuron disease and the most common genetic cause of infant mortality in the western world. SMA displays the characteristic hallmarks of a motor neuron disease, including loss of motor neurons in the spinal cord and atrophy of skeletal muscles. However, mounting evidence suggests that multiple tissues and body systems, beyond the neuromuscular system, are affected in SMA. Previous studies have highlighted alterations in the vascular system in both SMA patients and in a variety of mouse models of the disease, reporting alterations in vessel structure and perfusion abnormalities in peripheral tissues. In this project a detailed morphological investigation of the capillary beds of skeletal muscle and the spinal cord, two of the key pathological tissues in SMA was undertaken. This work was conducted in the $Smn^{-/-}$;SMN2, $Smn^{-/-}$;$SMN2^{tg/+}$ and $Smn^{-/-}$;SMN2;Δ7 mouse models of SMA. Significant alterations in the form and extent of the skeletal muscle and spinal cord capillary bed in SMA mice were identified, the most striking of which being a reduction in capillary density in SMA tissue when compared to control littermate tissue. In skeletal muscle, this reduction in capillary density was found to be a postnatal phenomenon, which occurred independently of denervation, in a variety of phenotypically distinct muscles and in all three SMA mouse models investigated. In the spinal cord, the capillary defect was seen to develop in a similar postnatal pattern to that observed in skeletal muscle. Importantly, a reduction in capillary density was observed in the ventral horn of the spinal cord, which houses motor neuron cell bodies, a known pathological target in SMA. These motor neurons were seen to be surrounded by fewer capillaries than their control counterparts. Using an injectable

marker of hypoxia, it was determined that the cells of the ventral horn of SMA spinal cords are hypoxic. This suggests that the capillary defect identified has a functional impact on the tissues it is observed in. Having established the presence of capillary defect in SMA tissue, the effect of potential SMA therapeutics on the capillary defect was then investigated. The effect of HDAC inhibitors, which have been successfully shown to increase the levels of the disease causing Smn protein, was investigated. Treatment with the HDAC inhibitor SAHA was found to ameliorate the capillary defect, significantly improving capillary density in SMA skeletal muscle. This implies that the capillary defect is related to Smn levels in tissue and is amenable to therapeutics which increase Smn levels. Having characterised the capillary defect in SMA tissues in detail, a selection of tools were then used to investigate the underlying mechanisms resulting in the defect. First, using primary cell cultures, the growth and morphology of the key cellular component of capillaries, the endothelial cell, was examined. While displaying reduced levels of the Smn protein, endothelial cells isolated from SMA tissues showed no difference in growth rate, morphology or endothelial cell marker expression when compared to endothelial cells isolated from control tissue. This suggests that the defects seen in SMA capillary beds are not the result of defects in the structure and growth of endothelial cells. Second, retinas from SMA mice were found to exhibit similar capillary defects to those observed in SMA skeletal muscle and spinal cord. Given the entirely postnatal development of the retinal capillary network, the retina was identified as a useful experimental preparation for the further investigation of the mechanisms underlying the capillary defect in SMA. In summary, this work highlights the incidence and importance of capillary defects in mouse models of spinal muscular atrophy.

Table of contents

Abbreviations

ACh	Acetylcholine
AChR	Acetylcholine receptor
ALS	Amyotrophic lateral sclerosis
ASO	Antisense Oligonucleotide
BBB	Blood Brain Barrier
BSCB	Blood Spinal Cord Barrier
BCA	Bicinchoninic acid (assay)
BTX	Bungarotoxin
Cl-5	Claudin-5
CNS	Central nervous system
DeSyn	Delayed synapsing
DMSO	Dimethyl sulfoxide
E	Embryonic (i.e. E10 = embryonic day 10)
ECG	Electrocardiogram
EMND	Equine motor neuron disease
FaSyn	Fast synapsing
FITC	Fluorescein isothiocyanate

GSL-1	Griffonia Simplicifolia Isolectin 1
HDAC	Histone deacytelase
IGF-1	Insulin-like Growth Factor 1
ISS-N1	Intronic splicing silencer N1
JNJ	JNJ-2648158
LAL	Levator auris longus
MND	Motor neuron disease
NMJ	Neuromuscular junction
P	Postnatal (i.e. P5 = postnatal day 5)
PAGE	Polyacrylamide gel electrophoresis
PBS	Phosphate buffered saline
PCR	Polymerase chain reaction
PECAM 1	Platelet Endothelial Cell Adhesion Molecule 1
PFA	Paraformaldehyde
RIPA	Radio-immunoprecipitation assay
scAAV9	Self-complimentary adeno-associated virus serus number 9
SAHA	Suberoylanilide hydroxamic acid
SMA	Spinal muscular atrophy

Smn/SMN/Smn	Murine/human survival motor neuron gene/protein
snRNP	Small nuclear ribonucleoproteins
SOD 1	Superoxide dismutase 1
TRITC	Tetramethylrhodamineisothiocyanate
TVA	Transversus Abdominus
VEGF	Vascular Enodothelial Growth Factor
ZO-1	Zona occluden-1

Introduction

1.1 Autosomal Recessive Proximal Spinal Muscular Atrophy

The term motor neuron disease encompasses a variety of disorders which are caused by the degeneration and loss of motor neurons in the brain and spinal cord. This loss of motor neurons results in a progressive weakening and wasting of skeletal muscles which leads to paralysis and, in the most severe disorders, death (Rezania & Ross, 2013). Included in this collection of disorders is Autosomal Recessive Proximal Spinal Muscular Atrophy (SMA), a childhood form of motor neuron disease. Initially characterised by physicians Werdnig and Hoffman in 1891, SMA has since been identified as the most common genetic cause of infant death in the western world, with an incidence rate of 1 in 6000-10000 live births and a carrier frequency of 1 in 38 (Pearn, 1978; Feldkotter et al., 2002; Lunn &Wang, 2008).

1.1.2 Clinical Classifications

SMA can be classified into four distinct disease types based on the age of symptom onset and the motor milestones achieved by the patient. Of these four classifications, Type I SMA is the most common and most severe (Markowitz et al., 1990; Lunn & Wang, 2008).

Type I SMA, also referred to as Werdnig-Hoffman disease, is characterised by a profound infantile hypotonia. Type I infants display flaccid paralysis of muscles on both sides of the body within the first six months of life. This weakness affects the muscles of the limbs and trunk, preventing patients from sitting unaided and from

supporting their own heads. While the intercostal muscles, involved in breathing, are affected in SMA, the diaphragm is spared. This results in characteristic paradoxical breathing, where the normal movements of the chest wall during breathing are reversed. These breathing difficulties are the main cause of death in Type I patients within the first two years of life (Lunn & Wang, 2008), though this lifespan can be extended with respiratory support (Bach, 2007).

Type II SMA is of an intermediate severity, with symptoms becoming apparent within 7–18 months of age (Lunn & Wang, 2008). Type II patients are capable of sitting without support and some patients have been reported to stand with the support of leg braces. However, the motor milestone of independent walking is never achieved. Other motor symptoms, particularly finger tremors, are observed. Weakness of the tongue is also commonly reported, with patients experiencing difficulties chewing and swallowing, affecting the nutritional status and the ability of patients to gain weight as they grow (Messina et al., 2008). Scoliosis, the abnormal curvature of the spine, is also observed in Type II patients, in particular Kyphoscoliosis which affects both the coronal and sagittal planes of the spine and so compromises lung ventilation. This, combined with the weakness of the intercostal muscles, results in respiratory insufficiency, the most frequent cause of death in Type II patients (Lunn & Wang, 2008).

Type III SMA, also referred to as Kugelberg-Welander disease, is the most variable form of SMA. Symptom presentation and age of onset vary greatly, with most patients displaying muscle weakness after 18 months of age. The majority of patients reach all major motor milestones, including independent walking. Some patients will require wheelchair assistance in childhood, while others will continue to walk

unaided into adult life. Some patients display joint overuse, as a result of muscle weakness. Scoliosis is often observed in Type III patients. However, this does not develop as early or progress as rapidly as the scoliosis observed in Type II patients (Fujak et al., 2013).

Finally, in addition to these childhood forms of SMA, a fourth adult onset form of the disease has also been identified (Lunn & Wang, 2008). In Type IV SMA, muscle weakness develops in the second and third decades of life. This weakness is mild, resulting in slight motor impairments but without any additional respiratory or nutritional impairment. As a result, Type IV patients lead relatively normal lives (Zerres et al., 1995; Lunn & Wang, 2008).

1.1.3 Genetics

SMA is caused by mutations in the Survival Motor Neuron (SMN) gene (Lefebrve et al., 1995). Early linkage analysis of Type II and Type III SMA patients determined that, although distinct in phenotype, these different forms of SMA were genetically homogenous (Brzustowicz et al., 1990; Melki et al., 1990). These linkage analyses identified the 5q12-13 region on the long arm of chromosome five as the location of the SMA causing defect (Brzustowicz et al., 1990; Melki et al., 1990). Further physical and genetic mapping of the region highlighted inherited and *de novo* deletions in the region (Melki et al., 1994). Genomic DNA from this candidate region was used to probe a human foetal brain cDNA library, identifying SMN as the disease causing gene (Lefebvre et al., 1995). Restriction mapping revealed the structure and organisation of the SMN gene (Lefebvre et al., 1995; Bürglen et al., 1995).

In the human genome, a large inverted duplication was found within the 5q13 region (Lefebrve et al., 1995). This duplication resulted in numerous copies of the SMN gene: a single telomeric copy, known as the SMN1 gene, and varying numbers of centromeric copies, known as the SMN2 gene. The SMN gene itself is approximately 20kb in length and consists of 9 exons interrupted by 8 introns (Bürglen et al., 1995). Further amplification and sequence analysis revealed that the telomeric SMN1 and the centromeric SMN2 genes differed from one another by only 5 nucleotides in their 3" ends, allowing SMN1 to be distinguished from SMN2. Full length cDNA from SMN1 and SMN2 is almost completely identical save for a single nucleotide difference in both exon7 and exon 8 (Monani et al., 1999). These differences result in two gene transcripts: full length Smn protein from the SMN1 gene and truncated SMN2 product which lacks exon 7 (Lefebvre et al., 1995). This suggests that the critical nucleotide exchange occurs in exon 7. Complete sequencing of the genes identified this key difference to be a C to T base exchange, 6 base pairs inside exon 7 (Monani et al., 1999). This single alteration is sufficient to alter the splicing pattern of the genes, resulting in the loss of exon 7 from the SMN2 product. This shortened SMN2 product is non-functional and degrades rapidly in comparison to the full length, fully functioning SMN1 product (Lorson & Androphy, 2000). In healthy individuals this altered splicing is inconsequential. In SMA patients however this difference is crucial.

In SMA, the SMN1 gene is lost or disrupted. In more than 98% of SMA patients the SMN1 gene is homozygously deleted. In the remaining cases the instability of the 5q12-13 region results in gene conversions or mutations which disrupt the SMN1 gene (Melki et al., 1994; Prior, 2007). While SMN1 is lost, each patient retains at

least one copy of SMN2 and while the majority of the SMN2 transcripts are erroneously spliced, correct splicing occurs in approximately 10% of SMN2 transcripts. These transcripts are translated into functioning, full length Smn protein (Lefebvre et al., 1995), as shown in Figure 1 taken from the 2009 review by Burghes and Beattie.

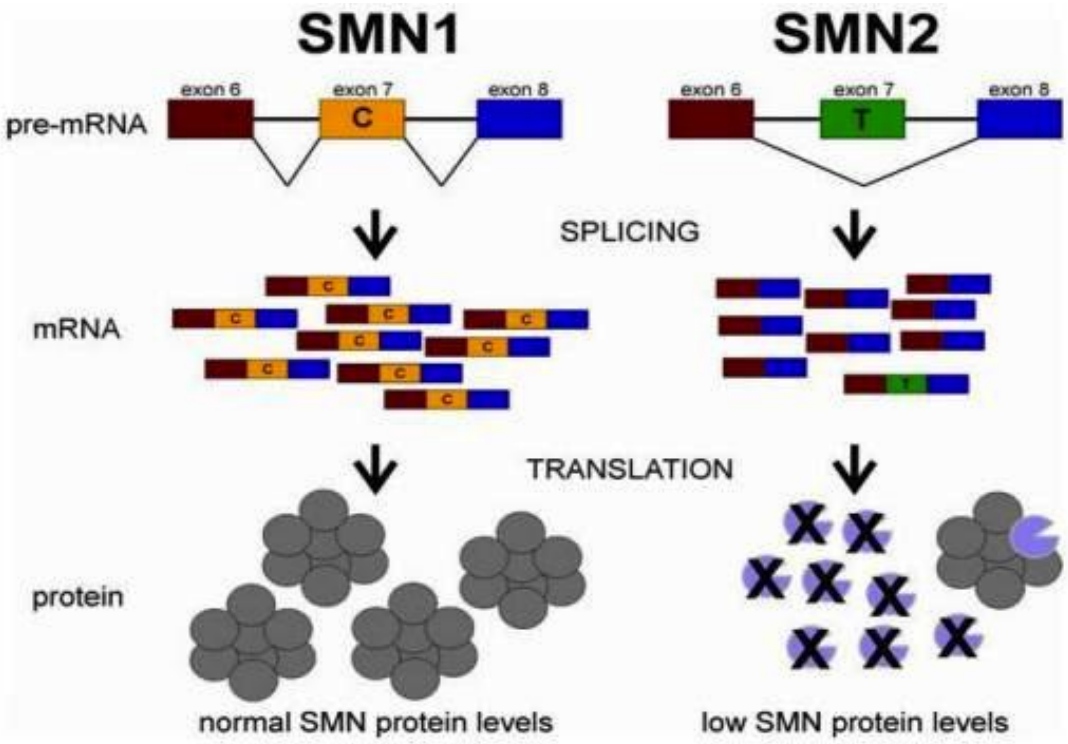

Figure 0.1 SMN1 and SMN2 genes, structure and splicing. The SMN1 and SMN2 have identical gene structure and are 99.9% identical at the sequence level. The essential difference between the two genes is a single nucleotide change in exon 7 (C or T as indicated). This single nucleotide change affects the splicing of the gene. Thus the majority of SMN transcripts from SMN2 lack exon 7 whereas those from SMN1 contain exon 7. However, because SMN2 does produce some full-length SMN it can be viewed as a gene with reduced function but not loss of function. The loss of amino acids that are encoded by exon 7 results in the production of SMN protein with severely decreased stability. (Burghes & Beattie, 2009)

The very low levels of Smn produced from the SMN2 gene cannot fully compensate for the loss of SMN1 in SMA and so Smn levels are drastically reduced in SMA patients. However, SMN2 copy number has been identified as a positive modifier of

disease severity, with patients possessing increased SMN2 copy number showing later symptom onset and an improved prognosis (Wirth et al., 2006). In SMA patients a clear correlation is observed between SMN2 copy number and disease severity (Wirth et al., 2006). Clinical reports have shown that 80-95% of Type I SMA patients possess one or two copies of SMN2. In Type II patients this number is increased to 3 copies in 96% of patients and 96% of Type III patients were found to carry 3 or 4 copies of SMN2 (Feldkotter et al., 2002; Mailman et al., 2009; Wirth et al 2006; Arkblad et al., 2009).

1.1.4 Role of Smn protein

Smn is an ubiquitously expressed 294 amino acid, 38 kDa protein encoded for by 9 exons interrupted by 8 introns (Bürglen et al., 1995; Lefebvre et al., 1995). Homozygous deletion of murine SMN is embryonic lethal, with massive cell death occurring early in development in $SMN^{-/-}$ embryos (Schrank et al., 1997). This emphasises the essential role of Smn in normal cell function.

Immunolocalisation studies indentified Smn presence in both the cytoplasm (Battaglia et al., 1997) and the nucleus (Lui & Dreyfuss, 1996). In the nucleus Smn is highly enriched within bodies called Gems, which show close association with Cajal bodies (Lui & Dreyfuss, 1996). Cajal bodies contain high concentrations of the elements involved in the transcription and processing of nuclear RNAs (Gubitz et al., 2004). Cajal bodies are thought to be the site where the machinery responsible for transcription and processing is assembled and modified (Gubitz et al., 2004). This suggested a potential role for the Smn protein in similar functions.

Within the nuclear Gems, Smn forms a stable complex with an array of Gemin proteins (Gubitz et al., 2004). This Smn-Gemin complex plays a key role in the assembly of splicesomal small nuclear ribonucleoproteins (snRNPs) which are responsible for splicing pre-mRNA. snRNPs recognise intron splice sites and catalyse splicing, resulting in mature, spliced mRNAs (Will & Lührmann, 2001; Nilson, 2003). snRNPs are composed of 7 common core Smn proteins and one uridine-rich small nuclear RNA (snRNA). The Smn-Gemin complex is responsible for assembling these two constituent components to form the snRNP. This is achieved by the binding of the Smn-Gemin complex to the Sm protein core and the snRNA. The Smn-Gemin complex then joins the snRNA onto the Sm protein core in an ATP-dependent manner to form the snRNP (Lui & Dreyfuss 1996; Pellizzoni et al., 2002; Workman et al., 2012). These investigations detail the essential cellular function of Smn. The characteristic degeneration and loss of motor neurons in SMA has prompted the investigation for motor neuron specific roles of Smn.

Smn protein has been identified in the growth cones and filopodia of cultured motor neurons (Fan et al., 2002), suggesting a role for Smn in neuronal outgrowth. In fact, investigations of SMA model zebrafish with reduced Smn levels have reported aberrant outgrowth of motor axons and defects in motor axon pathfinding (McWhorter et al., 2003; Beattie et al., 2007). The Smn protein has also been reported to be involved in the transport of axonal mRNAs along axons (Rossoll et al., 2003) particularly β-actin mRNA, which is important in the outgrowth and pathfinding of motor axons during development (Rossoll et al., 2003). These additional functions of Smn in axon outgrowth and pathfinding could explain why spinal motor neurons, particularly their distal axons, are vulnerable in SMA.

1.2 Animal Models of SMA

As the genetic basis of SMA is well characterised and understood, it has been possible to generate a variety of transgenic animals which recapitulate the human disease.

1.2.1 Mouse Models of SMA

Unlike humans, mice possess only one Smn gene. Homozygous deletion of this gene results in embryonic lethality (Schrank et al., 1997; Monani et al., 2000). To overcome this, transgenic mice expressing human SMN2 have been created (Monani et al., 2000; Hseih-li et al., 2000; Le et al., 2005).

1.2.1.1 Severe SMA Mouse Model

In 2000 Monani et al., reported the generation of a mouse model of severe SMA. The resulting $Smn^{-/-}$;SMN2 mice are hereafter referred to as Severe SMA mice. To generate these mice the human SMN2 gene was inserted into fertilised mouse oocytes. The adult mice were then bred with C57BL6J$Smn^{-/-}$ mice to produce $Smn^{+/-}$;SMN2 heterozygous carrier mice. These mice were then bred to produce $Smn^{-/-}$;SMN2 Severe SMA mice.

Severe SMA mice survive for 4 to 6 days. In the first 48 hours of life Severe SMA mice are indistinguishable from their unaffected littermates. This initial healthy period is followed by a rapid deterioration in which mice display decreased movement, a lack of suckling and laboured breathing. By 72-96 hours after birth Severe SMA mice display a marked phenotype with decreased weight, limb tremors, difficulty in righting and bell-shaped trunks similar to those observed in Type I

patients. At birth Severe SMA mice have a normal number of motor neuron cell bodies in the spinal cord but this number is drastically reduced by P5, when the mice die. This closely resembles the pattern of motor neuron loss seen in Type I SMA patients. Along with these motor and neuronal defects the most striking difference between Severe SMA mice and their unaffected littermates is their very small size. At the time of death Severe SMA mice are on average 68% smaller than their unaffected littermates, with affected mice being both smaller in overall size and less than half the weight of unaffected littermates (Monani et al., 2000).

This model closely mimics the symptoms and disease progression seen in Type I SMA patients. A high SMN2 copy number generated alongside the single copy Severe SMA line shows that SMN2 has the same positive modified effects in transgenic mouse models as it has in patients. $Smn^{-/-}$ mice with 8 copies of the human SMN2 transgene displayed no obvious SMA phenotype or impaired survival (Monani et al., 2000). The only apparent difference between high copy SMN2 Smn null mice and their Smn+/- littermates was a shortened, thickened tail. Increased SMN2 copy number in humans results in later symptom onset and an improved survival. A similar trend is observed in SMA model mice with an increased SMN2 transgene number.

1.2.1.2 Taiwanese SMA Mouse Model

In 2000 Hsieh-Li et al created $Smn^{-/-}$;SMN2 mice by introducing the human SMN2 transgene to $Smn^{+/-}$ mice on a variety of backgrounds. This generated 5 independent SMN2 transgenic founder lines that were crossed with Smn+/- mice to give a variety of $Smn^{-/-}$;SMN2 mice which developed progressive motor neuron disease, the

severity of which depended on the number of SMN2 copies. In 2010 Riessland et al., adapted the breeding strategy of Hsieh-Li and co-workers to produce consistent SMA phenotype mice on a pure FVB/N background with no other contributing mouse strains.

Riessland and co-workers initially bred mice carrying four copies of SMN2, two copies per allele, on a Smn null background onto a pure FVB/N rather than mixed background. These $Smn^{-/-}$:$SMN2^{tg/tg}$ mice survived and bred normally without an obvious SMA phenotype, although the mice did display shortened and necrotic tails and ears. These founder mice were then crossbred with heterozygous $Smn^{+/-}$ mice lacking the SMN2 transgene. This resulted in litters where 50% of mice were control $Smn^{+/-}$;$SMN2^{tg/0}$ carriers and 50% were SMA affected $Smn^{-/-}$;$SMN2^{tg/0}$ mice, hereafter referred to as Taiwanese SMA mice. Taiwanese SMA mice survive on average for 11 days and develop a severe SMA phenotype displaying a reduced body weight, muscle wasting and motor neuron degeneration by P6-7.

Survival is further extended in a third mouse model where in addition the SMN2 transgene, the SMNΔ7 transgene has also been inserted.

1.2.1.3 SMNΔ7 Mouse Model

Alternative splicing of the SMN2 transgene results in the truncated SMNΔ7 transcript which lacks exon 7. When the SMNΔ7 transgene was added to the $Smn^{-/-}$;SMN2 genotype, survival was extended to 14 days (Le et al., 2005).

To generate SMNΔ7 transgenic mice, SMN cDNA lacking exon 7, the SMNΔ7 transcript, was inserted into fertilised FVB/N oocytes. The resulting SMNΔ7 transgenic mice were then crossed with mice lacking endogenous murine Smn but

possessing the human SMN2 transgene. This created double transgenic SMNΔ7;SMN2;$Smn^{+/-}$ mice on a pure FVB/N background. These founder mice were interbred to obtain $Smn^{-/-}$;SMN2;SMNΔ7 mice, hereafter referred to as SMNΔ7 SMA mice.

SMNΔ7 SMA mice survive between 10 to 14 days. Differences in weight gain between SMNΔ7 SMA mice and control littermates are apparent by P5 and once established the reduced weight gain persists throughout the rest of life. At P5 motor defects are also apparent and SMNΔ7 SMA mice show difficulty righting. This weakness becomes progressively more pronounced over the following days and by P10 SMNΔ7 SMA mice have difficulty moving and display an abnormal gait and limb tremors when they do move. Alongside these motor deficits a reduction in motor neuron number in the lumbar spinal cord is also seen. While motor neuron loss is evident at earlier timepoints (P4) the loss is not significant. This suggests that the timeline of motor neuron loss is related to disease severity, with earlier motor neuron loss observed in mouse models which lack the SMNΔ7 transcript (Monani et al., 2000; Monani et al., 2003).

Mouse models are a useful tool in the study of SMA. The generation of transgenic mice allows for the close mirroring of the genetic basis of SMA and the resultant molecular phenotype where Smn protein is present in every cell albeit at markedly reduced levels. Manipulation of SMN2 copy number and additions of the SMNΔ7 transcript have established a variety of mouse models of varying disease severity similar to that seen in human SMA patients. These models also mimic the molecular pathologies, symptoms and disease progression seen in SMA patients. While the work in this thesis will focus on mouse models of SMA, it should be noted that other

SMA model organisms are also available. These include *Drosophila,* zebrafish and the roundworm *C.elegans*.

1.2.2 Other Animal Models of SMA

In 2003 Chan and co-workers isolated a *Drosophila* Smn mutant, with similar point mutations to those seen in SMA patients. These mutants displayed abnormal motor behaviour showing a progressive loss of mobility and coordination before death. Physiological experiments revealed reduced post-synaptic currents and disorganised motor neuron boutons, indicative of neuromuscular junction (NMJ) defects. *Drosophila* models have proven to be a particularly useful tool for the identification of modifiers of Smn with a single study highlighting 27 genetic modifiers of Smn (Chang et al., 2008). Along with *Drosophila* models, zebrafish SMA models are also useful for the testing and analysis.

Knockdown of Smn levels in zebrafish resulted in a drastic SMA-like motor axon degeneration (Winkler et al., 2005). Morpholino knockdown reduced Smn levels to 16% of that seen in control animals. In these Smn knockdown animals motor axons were truncated and erroneously branched, indicative of axon outgrowth and pathfinding defects (Winkler et al., 2005). Zebrafish models benefit from their relative ease of genetic and protein manipulation and their transparent nature which allows for the real time study of motor axon development and growth (Winkler et al 2005; McWhorter et al., 2005; Wishart et al., 2014).

Finally, the orthologue of the human SMN1 gene, smn-1, has been identified in *C.elegans*. When knocked down with RNA interference techniques, reduced smn-1 levels resulted in late larval arrest, reduced lifespan, sterility and impaired locomotor

and pharyngeal activity in *c.elegans* (Briese et al., 2009). The rapid lifecycle and ease of maintenance of *C.elegans* and *Drosophila* model SMA animals provide a useful starting tool for the identification of genetic modifiers and potential therapeutics.

1.3 Tissue Pathology in SMA

SMA displays the characteristic hallmarks of a motor neuron disease. SMA patients exhibit a loss of motor neurons in the spinal cord which is followed by an atrophy of skeletal muscles, leading to paralysis and eventually death. This has lead to the in depth investigation of the neuromuscular system in SMA.

1.3.1 Neuromuscular Pathology in SMA

The neuromuscular system is the connection between the nervous system and skeletal muscle which work in combination to permit movement. The neuromuscular system is composed of lower motor neurons and the muscles they innervate. The cell bodies of lower motor neurons are located in the ventral horn of the spinal cord. From here their projecting axons exit the spinal cord via the ventral spinal roots and travel, as peripheral nerves, to reach their target muscles. Within the muscle, axons branch multiple times to supply a number of muscle fibres. This collection of muscles and the motor axon innervating them is called a motor unit (Sanes & Lichtman, 1999). These axons make contact with the muscle at a specialised synapse: the neuromuscular junction (NMJ). This junction is composed of a skeletal muscle fibre, the motor nerve terminal, terminal Schwann cells and the capping kranocyte (Sanes & Lichtman, 1999; Court et al., 2008). In neuromuscular disorders,

such as SMA, the association between the nervous and muscular system is disrupted. In SMA, the NMJ is an early pathological target.

Morphological, molecular and functional defects are observed at the NMJ in SMA model mice (Murray et al., 2008, Kong et al., 2009, Ruiz et al., 2010, Wyatt & Keusted et al., 2010; Dachs et al., 2001). These abnormalities are seen in both the pre and post-synaptic compartments of the NMJ. A characteristic feature of the NMJ in SMA is the loss of presynaptic motor nerve terminals which results in the denervation of the underlying muscle fibre. Along with this loss, structural alterations of the motor nerve at the NMJ are also observed. These include accumulations of neurofilament and poor arborisation of the nerve terminal. Post-synaptically defects in acetylcholine receptors (AChRs) are also seen. AChRs in SMA retain an immature plaque-like structure rather than developing into the mature pretzel-like structure seen in age matched control mice (Kariya et al., 2008). AChRs are also found to contain the embryonic γ-subunit which during normal development should be replaced by the adult ε-subunit. This suggests that the reduced levels of Smn found in SMA cause a delay in the development of AChRs. This resulted in intermittent transmission failures along with alterarations to quantal content and end-plate potentials in SMA mice (Kariya et al., 2008). Along with these physiological and morphological defects, molecular defects are also seen at the NMJ in SMA.

Key proteins involved in the targeting of synaptic vesicles and the release of neurotransmitters are downregulated in the presynaptic terminal of NMJs in SMA (Dachs et al., 2011; Ruiz et al., 2010). Importantly these defects are observed prior to extensive denervation (Dachs et al., 2011; Ruiz et al., 2010). Similarly, many of the morphological defects at the NMJ are seen prior to the degeneration of axons and the

loss of motor neurons (Murray et al., 2008, Kong et al., 2009, Dachs et al., 2011). Loss of synaptic inputs and abnormal neurofilament accumulations are seen in early to mild symptomatic Severe SMA mice (Murray et al., 2008) and defects in terminal organisation are seen in Severe SMA mice without great spinal cord motor neuron loss (Dachs et al., 2011). In addition to these morphological and molecular defects, functional defects have also been reported at the NMJ in SMA, in particular the release of neurotransmitters (Kong et al., 2009, Ruiz et a., 2010). Overall synaptic vesicle density is reduced by almost 50% in Severe SMA mouse NMJs (Kong et al., 2009) and when analysed the release of neurotransmitter at the NMJ was significantly reduced (Ruiz et al., 2010).

These studies highlight the NMJ as an early pathological target in SMA mice. Recent investigations have confirmed similar defects in the NMJs of Type I SMA patients (Kariya et al., 2008; Martinez-Hernadez et al., 2013).

Abnormal accumulations of neurofilaments and poorly developed motor endplates are seen in the diaphragm of Type I SMA patients (Kariya et al., 2008). Further investigation revealed defects in the foetal development of the diaphragm and limb muscles in SMA foetuses (Martinez-Hernadez et al., 2013). Detailed microscopic analysis of these muscles revealed alterations in AChR clustering, abnormal prenatal vesicle accumulations and aberrant nerve terminal structure (Martinez-Hernadez et al., 2013).

These studies emphasise the nature of the NMJ as a pathological target in SMA. However, not all NMJs display pathology in SMA. NMJs from different muscles show a varied susceptibility to low Smn levels. Studies have been conducted to

identify the factors which contribute to synapse vulnerability in SMA (Murray et al., 2008; Ling et al., 2012; Thomson et al., 2012).

In general, axial muscles are more vulnerable to NMJ defects than limb muscles. However both proximal and distal limb regions contain a mix of vulnerable and resistant muscles (Ling et al., 2012). This suggests that muscle location cannot be used as a determinant of muscle vulnerability.

In Amyotrophic Lateral Sclerosis (ALS), fibre type predisposes muscle vulnerability with fast-twitch muscle fibres innervated by fast fatiguing motor neurons being more vulnerable than slow twitch muscles (Hegedus et al., 2007). In SMA however no such correlation is observed between fibre type and NMJ vulnerability (Murray et al., 2008; Ling et al., 2012). Similarly, no correlation is observed between NMJ vulnerability and motor unit size, total axonal arbour length, motor branching pattern and terminal Schwann cell number in Severe SMA mice (Thomson et al., 2012). These studies suggest that the vulnerability of NMJs in SMA is not likely due to a single factor but, instead, is the result of the cumulative effects of a variety of neuromuscular factors. Determination of these factors remains a major focus of SMA research. However, recent research in the field has begun to investigate the effects of reduced Smn levels in tissues beyond the neuromuscular system.

1.3.2 Systemic Pathology in SMA

While the neuromuscular system appears particularly sensitive to reduced Smn levels, the Smn protein is ubiquitously expressed. Recent studies have identified a wide range of body tissues which display vulnerability to low Smn levels.These

investigations have encouraged the view of SMA as a multi-system rather than purely motor neuron disorder.

1.3.2.1 Muscle

Mounting evidence suggests that muscle, independent of denervation, is a key site of pathogenesis in SMA (Fidizianska & Wado, 1990; Tens et al., 1996; Stahas et al., 2008; Mutsaers et al., 2011).

High levels of apoptosis are commonly recorded in SMA skeletal muscle (Fidizianska & Wado, 1990; Tens et al., 1996; Stahas et al., 2008). Biopsies of patient muscle also show evidence of delayed development and maturation (Fidizianska & Wado, 1990; Stahas et al., 2008). These impairments of muscle development are observed in muscles where no neuromuscular pathology is evident (Lee et al., 2011). Along with defects in growth and development, intrinsic molecular pathology is found in skeletal muscles which are resistant to motor neuron pathology and NMJ dysfunction (Mutsaers et al., 2011). These studies suggest that Smn is important in the development, growth and normal cellular function of skeletal muscle.

1.3.2.2 Bone

An increased incidence of congenital bone fractures has been reported in SMA patients (Kelly et al., 1997; Felderhoff-Mueser et al., 2002). Severe SMA model mice display an osteoporotic bone phenotype with decreased mineral content and density in bones, resulting in a thin, porous cortex (Shanmugarayan et al., 2009).

Severe SMA mice also display significant reductions in key osteoblast differentiation markers and an increased rate of osteoclast formation in bone marrow (Shanmugarayan et al., 2009). These studies suggest a role for Smn in bone remodelling and skeletal pathogenesis in SMA.

1.3.2.3 Brain

The reduced levels of Smn protein found in Severe SMA mice have been found to impair perinatal brain development (Wishart et al, 2010). Morphological changes are observed in the brain of Severe SMA mice, particularly in brain regions normally associated with high Smn expression. The hippocampal dentate gyrus of Severe SMA mice was found to be 50% smaller in area than control littermates. Along with this reduction in size, a reduced cell density and proliferation was also observed in this region. Proteomic analysis of Severe SMA mice revealed widespread changes in the expression of proteins required for cellular proliferation, migration and development (Wishart et al., 2010). This study suggests that high levels of Smn are required for normal brain development.

1.3.2.4 Heart

Cardiac defects, both structural and functional, are commonly reported in SMA patients (Rudnik-Schoneborn et al., 2008) and mouse models of the disease (Shababi et al., 2010; Heier et al., 2010; Bevan et al., 2010; Gogliotti et al., 2012).

75% of Type I SMA patients carrying a single copy of SMN2 have atrial and septal defects (Rudnik-Schoneborn et al., 2008). These defects are sufficient to cause significant impairments of cardiac function (Rudnik-Schoneborn et al., 2008). The severity of these defects was associated with SMN2 copy number, with higher SMN2

copy number patients presenting less significant defects or none at all (Rudnik-Schoneborn et al., 2008). Not only does this suggest a role for Smn in normal cardiac development but it also highlights an association between SMN2 copy number and defect severity, a link which is well established in the neuromuscular system (Feldkotter et al., 2002; Wirth et al., 2006). Similar congenital cardiac defects are also reported in mouse models of SMA (Shababi et al., 2010; Heier et al., 2010; Bevan et al., 2010; Gogliotti et al., 2012).

During embryonic development, defects in interventricular septum width were observed in Severe SMA embryos. Along with this, the left ventricle, responsible for delivering blood to the body, was thin and branched in comparison to the thick and well-developed left ventricle seen in control embryos (Shababi et al., 2010). Similar septal defects were also observed in SMNΔ7 SMA pups along with a remodelling of the atrial walls and an increase in oxidative stress markers in the cardiac tissue (Shababi et al., 2010). Electrocardiogram (ECG) studies have revealed a significant bradycardia, slowing of the heart rate, in SMNΔ7 SMA pups in comparison to control littermates. This bradycardia is reported as early as P2 in SMNΔ7 SMA mice (Heier et al., 2010). This bradycardia is severe and eventually results in a progressive heart block and impaired ventricular depolarisation (Heier et al., 2010). Importantly these structural and functional defects have been observed prior to motor neuron degeneration (Shababi et al., 2010) and in the absence of motor neuron and muscle pathology (Gogliotti et al., 2012). This suggests that the defects in the heart occur independently of neuronal pathology and should be considered as an independent pathology in SMA.

1.3.2.5 Liver

Targeted deletion of SMN exon 7 in the embryonic mouse liver results in a severe impairment of liver development more commonly associated with iron overload (Vitte et al., 2004). Severe atrophy of the liver is seen before late embryonic lethality (Vitte et al., 2004). This suggests an important role for Smn in the normal development of the liver. Defects are also seen in liver function in neonatal SMA mice (Hua et al., 2011). Decreased levels of circulating hepatic insulin-like growth factor 1 (IGF-1) are recorded in neonatal SMA model mice (Hua et al., 2011). IGF-1 is a neurotrophic factor and is essential for normal post-natal growth and development. Disruption of hepatic IGF-1 production could contribute to the reduced weight seen in multiple SMA mouse modes (Monani et al., 2000; Hsieh-Li et al., 2000; Le et al., 2005).

1.3.2.6 Lung

Several defects in the structure of the lungs have been noted in Taiwanese SMA mice (Schreml et al., 2013). On gross inspection, Taiwanese SMA lungs are discoloured with large red marks mottling the surface of the lungs in comparison to the uniform pale pink colouring of control littermate lungs (Schreml et al., 2013). Histological investigation revealed ruptured alveolar septas and enlarged alveolar spaces in SMA mice (Schreml et al., 2013). Varying degrees of emphysema were also in Taiwanese SMA mice (Schreml et al., 2013). Respiration in SMA mice is already compromised due to muscle weakness. These defects will exacerbate this respiratory distress and could contribute to mortality in the mice.

1.3.2.7 Intestine

By P5 Taiwanese SMA mice display diarrhoea. Histological examination of the intestine revealed an empty, string-like structure to the organ and a reduced number of villi with the remaining villi appearing blunt and club like with large vacuoles. Severe oedema was also observed in the lamina propria of the villi (Schreml et al., 2013). This gross disruption of the intestinal epithelium and structure could contribute to the severe digestive problems reported in SMA mice.

1.3.2.8 Pancreas

Abnormalities in the cellular organisation of the pancreas are seen in SMA model mice and Type I SMA patients (Bowerman et al., 2012). While SMA mice produce insulin, cell numbers in the pancreatic islands are imbalanced, with an increased number of glucagon-producing α cells at the expense of insulin-producing β cells This imbalance is also seen in Type 1 patients. (Bowerman et al., 2012). This imbalance is accompanied by defects in glucose metabolism including hyperglycemia, hyperglucaconemia and glucose intolerance in SMA mice and evidence of glucose intolerance in SMA patients (Bowerman et al., 2012).

1.3.2.9 Metabolic Abnormalities

Type I SMA patients show problems in fatty acid metabolism which are not a consequence of immobility, illness, muscle denervation or atrophy, suggesting intrinsic metabolic defects in SMA patients (Dahl et al., 1975; Crawford et al., 1998).

Along with these systemic organ and metabolic defects, alterations to the vasculature of SMA patients (Musch et al., 1975; Rudnik-Schoneborn et al., 2008; Araujo et al., 2009) and mouse models (Naver et al., 2008; Bevan et al., 2010; Foust et al., 2010; Heir et al., 2010, Shababi et al., 2010; Gogliotti et al., 2012) is also commonly reported.

1.4 The Vasculature

The vascular network is formed by two distinct mechanisms: vasculogensis and angiogenesis (Poole et al., 1989).

The original vascular network is formed embryonically by the process of vasculogenesis which describes the initial formation of vessels from angioblasts (Risau & Flamme, 1995). Further development, growth and remodelling of this primary network is brought about by angiogenesis in which new vessels form from a pre-existing network of vessels (Risau, 1997). This growth can occur by sprouting or non-sprouting angiogenesis (Risau, 1997). In sprouting angiogenesis the extracellular matrix surrounding endothelial cells is broken down allowing for the migration of proliferating endothelial cells. These endothelial sprouts are guided to their target by specialised endothelial tip cells (Risau, 1997). These tip cells then fuse together to form functional vessel loops (Risau, 1997). In non-sprouting angiogenesis pre-existing vessels are split in two by pillars of extracellular matrix. This process is often termed intersusceptive angiogenesis (Risau, 1997). When combined these processes result in the formation of the mature, fully functional vascular network. Alterations in this vascular network have been observed in motor neuron diseases, including ALS and SMA.

1.4.1 Vascular Pathology in Motor Neuron Disease

Vascular defects and their impact on disease progression have been reported in forms of motor neurone disease. In 2004 Palencia et al., reported a reduction in the number of capillaries to muscle fibres in equine motor neuron disease (EMND). EMND is very similar in nature to another form of motor neuron disease: sporadic ALS in humans. Reports of vascular alterations have previously been made in ALS (Garbuzova-Davis et al., 2007; Zhong et al., 2008; Nicaise et al., 2009; Garbuzova-Davis et al., 2010; Miyazaki et al., 2011; Miyazaki et al., 2012).

ALS is an adult onset form of motor neuron disease characterised by degeneration of motor neurons in both the brain and spinal cord which leads to muscle atrophy and paralysis, resulting in death within three to five years of a diagnosis (Haverkamp et al 1995, Rowland and Schneider 2001). The majority of ALS cases arise sporadically with only 5-10% of cases being genetically linked, and 20% of these familial cases display miss-sense mutations in the Copper/Zinc superoxide dismutase-1 (SOD1) gene (Rosen et al., 1993).

In SOD1 mice models of ALS a reduction in the levels of the tight junction proteins Zona Ocludin-1, Claudin-5 and Occludin were reported in endothelial cells (Zhong et al., 2008). This reduction caused disruption of the blood spinal cord barrier (BSCB), resulting in haemorrhaging, reduced circulation and poor perfusion in the spinal cord. Importantly these alterations were observed prior to any motor neuron degeneration reported in this model (Zhong et al., 2008). Similarly, disruption to the association between blood vessels and neurons, the neurovascular unit, has been observed occurring prior to motor neuron degeneration in SOD1 models and ALS patients

(Miyazaki et al., 2011). Here the endothelial cells of blood vessels and the foot process of astrocytes were seen to dissociate at presymptomatic stages (Miyazki et al., 2011). Recent work has shown that interventions to correct such defects can delay disease onset and improve lifespan (Winkler et al., 2013). In 2013 Winkler et al., showed that repairing the defects in the BSCB delayed the onset of motor neuron impairment and degeneration in SOD1 model ALS mice and also increases lifespan by 25%. Taken together these studies suggest a potential role for the vascular system in the initiation of motor neuron defects and loss in ALS. Modifications to the control rather than the structure of the vascular system has also been reported to have negative effects on motor neurons (Oosthyuse et al., 2001).

Vascular Endothelial Growth Factor (VEGF) is a key angiogenic signal used for the growth and development of vascular networks (Ferrara et al., 2003). The promoter for VEGF possesses a hypoxia-response element, allowing for VEGF stimulated growth of vascular networks in response to hypoxic tissue conditions (Oosthyuse et al., 2001). When this hypoxia-response element is deleted VEGF can no longer stimulate vessel formation and growth in response to tissue hypoxia. In the spinal cord this resulted in adult-onset motor neuron degeneration similar to that found in ALS. Conversely, addition of exogenous VEGF to the spinal cord during hypoxia promoted motor neuron survival (Oosthyuse et al., 2001).

These reports from both mouse models and patients suggest that an insufficiently formed and poorly functioning vascular system can lead to motor neuron degeneration in ALS. Vascular alterations have been noted in SMA patients and mice models but their impact on disease pathogenesis has yet to be established.

1.4.2 Vascular Pathology in SMA

Defects in the vascular system have long been associated with SMA patients (Musch et al., 1975, Rudnik-Schoneborn et al., 2008, Araujo et al., 2009) and some defects have been reported in the vasculature of SMA mouse models (Naver et al., 2008, Bevan et al., 2010, Foust et al., 2010, Heir et al., 2010, Shababi et al., 2010, Gogliotti et al., 2012).

Although there is no cure for SMA, severe Type I patient lives can be extended by invasive ventilation. In case studies of such patients, defects in the vasculature have been repeatedly reported, with the digits (fingers and toes) being particularly prone to damage (Araujo et al., 2009, Rudnik-Schoneborn et al., 2010). These reports describe a progressive necrosis of the digits between four to six months of age where initially a single digit was observed to turn blue and then black. This discolouration then spread to all the digits of the foot and hand and then to more proximal body regions including the feet, knees and arms (Araujo et al., 2009). Skin biopsies of such discoloured tissue in a second case study revealed that the epidermis and upper regions of the dermis were necrotic and that the small blood vessels found within the tissue were occluded by multiple thromboses (Rudnik-Schoneborn et al., 2010), suggesting that impaired vessel perfusion may be involved in the tissue damage observed. As well as these functional impairments, alterations to the structure of small vessels in Type I SMA patients have also been reported (Musch et al., 1975).

In a case study of a young Type 1 SMA patient, the basement membrane of skeletal muscle capillaries was noted to be significantly greater in width than the basement membrane of capillaries from normal skeletal muscle (Musch et al., 1975). The main

cellular component of capillaries, the endothelial cells, also appeared abnormal in the Type I patient, containing an excessive number of vacuoles. This suggests that the structure of fine blood vessels is affected in severe SMA patients. Similar vascular defects have also been reported in multiple mouse models of SMA.

In the SMA mouse model developed by Hsieh-Li et al. in 2000, intermediate and mildly affected SMA mice developed chronic necrosis of the tail, which began at the tip and progressed retrogradely towards the base of the tail. Similar necrosis of the extremities (tail, digits and ears) has been observed in severe SMA mouse models, where the lifespan of SMA mice has been increased using therapeutic interventions (Narver et al., 2008, Foust et al., 2010).

In 2008 Narver et al., reported extensive tissue necrosis in SMN2Δ7 mice treated with the HDAC inhibitor Trichostatin A. The normal life expectancy of SMA SMNΔ7 mice is 14-16 days (Sleigh et al 2012), but treatment with Trichostatin A, along with nutritional supplementation, increased the lifespan of these mice significantly. However, mice who survived beyond 27 days began to develop tissue necrosis. A blue to black discolouration was noted at the tail tip which spread towards the base, ultimately resulting in complete loss of the tail. In some mice this necrosis spread to the pelvis and colon. The digits of the hindlimb also became necrotic and again this progressed to loss of the foot and the whole hindlimb in extreme cases. Necrosis was also observed in more proximal regions, in particular the pinnae of the ear. When examined histopathologically, thromboses were found in the small vessels of tissue from these regions, as was observed in SMA patients (Rudnik-Schoneborn et al., 2010). In addition to the thrombi observed, the walls of the blood vessels themselves appeared necrotic (Narver et al., 2008).

These studies have identified vascular defects in SMA patients and mouse models of the disease. However, whether vascular defects directly affect the key sites of pathogenesis in SMA is yet to be established.

1.5 SMA Therapeutics

At present there is no cure for SMA. However, given that the genetic basis of the disease is well understood several approaches are being developed to restore SMN levels (Avila et al., 2007; Mattis et al., 2009; Passini et al., 2011; Ling et al., 2012) and to restore the SMN1 gene (Foust et al., 2010; Valori et al., 2010). Given that motor neurons are the most established and characterised pathological target in SMA, therapies are also being developed to protect motor neurons (Haddad et al., 2003; Lesbordes et al., 2003). However, the mounting evidence of systemic pathology in SMA suggests that any effective SMA therapies will need to treat system-wide symptoms and not only motor neurons.

1.5.1 Antisense Oligonucleotides

The major product of the SMN2 gene is a truncated, non-functional, unstable version of the Smn protein (Lorson & Androphy, 2000). This arises due to alternative splicing of the SMN2 gene caused by a single nucleotide exchange which erroneously activates splicing of exon 7 from the SMN2 transcript (Monani et al., 1999; Lorson et al., 1999). Modulating this splicing activity is a direct approach to restore proper full length Smn protein production and expression. Antisense Oligonucleotides (ASOs) have been utilised to increase full length Smn expression (Hau et al., 2010; Osman et al., 2012; Passini et al., 2012).

ASOs specifically designed to bind to an intronic splicing silencer lead to the inclusion of exon 7 in the SMN2 transcript and increases the expression levels of full length Smn protein (Hau et al., 2010). Specific targeting of the ASO to this particular splicing silencer prevents unwanted off-target effects of the ASO. Infusion of the ASO into the lateral cerebral ventricle of adult mice expressing the human SMN2 transgene resulted in a robust and persistent increase in exon 7 inclusion (Hau et al., 2010) When injected neonatally, the ASO was found to reduce the tail and ear necrosis seen in Type III SMA mice (Hau et al., 2010). An ASO targeted against an intronic repressor downstream of exon 7 has also shown beneficial affects in neonatal SMA mice (Osman et al., 2012).

Intronic splicing silencer N1 (ISS-N1) lies downstream of exon 7 and when targeted by a specific ASO, increased levels of full length Smn protein were observed in the brain and spinal cord of SMNΔ7 SMA mice. This increase in Smn resulted in weight gain and an increased lifespan in SMNΔ7 SMA mice. Along with this increase in survival, ASO treatment has also been reported to improve muscle physiology and motor neuron function (Passini et al., 2011). Alongside these beneficial effects, the variety of potential delivery routes of ASOs makes them an attractive therapeutic approach to investigate. Intrathecal infusion into cynomolgus monkeys was shown to deliver ASO to all spinal cord regions, presenting a potential practical delivery route in a clinical setting (Passini et al., 2011).

1.5.2 Histone Deacetylase Inhibitors

While the major product of the SMN2 gene is the non-functional SMNΔ7 transcript, approximately 10% of SMN2 transcripts are translated into full length Smn

(Lefebvre et al., 1995). Enhancing the transcription of SMN2 is an attractive approach to increase the levels of full length Smn protein it produces. The transcriptional activity of genes is regulated by the accessibility of DNA (Johnson & Dent, 2013). The accessibility of DNA is determined by the modification of the histone proteins which promote condensation of DNA into chromatin. Histone deacetylase (HDAC) enzymes repress transcriptional activity by allowing the close association of histone proteins and DNA. Conversely, inhibition of HDACs decreases this association, freeing the DNA and increasing transcription (Johnson & Dent, 2013). HDAC inhibitor drugs have been shown to increase Smn levels, improve survival, attenuate weight loss, increase muscle fibre size and improve cardiac defects in a variety of mouse models (Avila et al., 2007; Narver et al., 2007; Riessland et al., 2010). While the effects of HDAC inhibitors are not SMN2 specific, resulting in potential off-target effects (Ling et al., 2012), the systemic nature of HDAC inhibitor activation is an attractive method for treating the variety of systemic pathologies, not just neuromuscular symptoms, that are now associated with SMA.

1.5.3 SMNΔ7 Transcript Stabilisation

The SMNΔ7 transcript produced by the SMN2 gene is not only truncated but it is also highly unstable and degenerates rapidly (Lorson & Androphy, 2000). Stabilisation of this transcript is another potential therapeutic approach in SMA.

Smn protein levels have been significantly increased by the administration of aminoglycosides (Mattis et al., 2009). Aminoglycosides induce transcriptional "read-through": continuation of translation beyond stop codons. Aminoglycoside treatment should inhibit the recognition of the translational stop codon in SMN2. Translation

would then read through the stop codon and continue on to include the normally excised exon 7 (Mattis et al., 2009). Direct daily delivery of the aminoglycoside TC007 into the CNS of SMNΔ7 SMA mice increased full length Smn levels in the brain and spinal cord. TC007 treatment has also been shown to increase full length Smn protein levels in induced pluripotent stem-cell derived SMA motor neuron cultures and patient fibroblasts (Mattis et al., 2009).

1.5.4 Gene Therapy

Depleted Smn levels have also been increased using viral gene therapy strategies to reintroduce the missing SMN1 gene into SMA cells and tissues (Azzous et al., 2004; Bevan et al., 2010; Foust et al., 2010, Valori et al., 2010, Dominguez et al., 2011).

Viral SMN1 delivery has been shown to increase Smn levels in Type I SMA patient fibroblasts (Azzous et al., 2004; Bevan et al., 2010; Foust et al., 2010, Valori et al., 2010, Dominguez et al., 2011) and similar studies in SMNΔ7 SMA mice have shown a restoration of motor neuron Smn levels, reduced motor neuron death and increased life span (Azzous et al., 2004). Investigations using self-complimentary adeno-associated virus serus number 9 (scAAV9), which crosses the blood brain barrier (BBB), have reported rescue of motor neuron function, improved neuromuscular pathology and increased lifespan in SMA model mice (Foust et al., 2010; Valori et al., 2010; Dominguez et al., 2011). Improvements of structural and functional cardiac defects have also been reported following scAAV9 SMN1 delivery (Bevan et al., 2010). While these results identify SMN1 replacement as a promising therapeutic, effective gene therapy in human patients has yet to be reported.

1.5.5 Neurotrophic and Neuroprotective Agents

To develop properly, motor neurons require trophic support from their target skeletal muscle. Several factors are implicated in the trophic support of motor neurons, including Cardiotrophin-1 (CT-1) (Oppenheim et al., 2001). Secreted by embryonic myotubes, CT-1 is expressed in high levels in embryonic skeletal muscle and increases the survival of embryonic motor neurons (Oppenheim et al., 2001). Systemic adenoviral delivery of CT-1 has been shown to delay motor defects and improve survival in mutant mice which lack SMN exon 7 in their neurons (Lesbordes et al., 2003). CT-1 delivery was also noted to protect against motor axon loss and NMJ defects (Lesbordes et al., 2003).

1.6 Aims

From the above introduction covering the current literature available, is it clear that there is a rationale and requirement for studies on vascular pathology in SMA. This thesis will therefore aim to address the following questions;

1) Is the vasculature altered in the primary pathological targets of SMA?
2) What effect, if any, do these defects have on the tissue they are found in?
3) Are these defects amenable to current SMA therapeutics?
4) Are these defects the result of intrinsic defects in the main cell type of the vasculature?
5) How should future studies seek to determine the mechanism underlying these defects?

In order to answer these questions, the incidence of vascular defects in the skeletal muscle and spinal cord will be investigated in a variety of established mouse models of SMA (Chapter 2, 3). The implication of these defects will be examined using an *in vivo* marker of tissue hypoxia (Chapter 3). The amenability of these defects to current SMA therapeutic strategies will be investigated using HDAC inhibitor treatment (Chapter 4). The viability of SMA endothelial cells will be investigated using cell culture techniques, to identify any potential cellular cause of the defects (Chapter 5). Finally, experimental approaches for the future investigation of the mechanisms underlying the defects observed, will be established (Chapter 5).

Chapter 2: Skeletal muscle capillary defects in mouse models of SMA

2.1 Introduction

SMA displays the hallmark characteristics of a motor neurone disease with patients exhibiting a loss of motor neurons in the ventral horn of the spinal cord, followed by weakening and wasting of skeletal muscle which in turn leads to paralysis and death. However, given the ubiquitous expression of survival motor neuron (Smn) protein, the SMA gene product, it seems unlikely that the neuromuscular system alone is affected by the depleted levels of Smn found in SMA. Recent work has begun to emphasise the systemic nature of SMA, identifying a variety of tissues beyond the neuromuscular system which show alterations in SMA. These include the brain (Wishart et al 2010), the bone (Hseih-Li et al., 2000; Felderhoff-Mueser et al., 2002; Shanmugarajan et al., 2009), the liver (Ville et al., 2004; Hua et al., 2011), the intestine (Schreml et al, 2013), the lung (Schreml et al., 2013), the pancreas (Bowerman et al., 2012) the heart (Rudnik-Schoneborn et al., 2008; Bevan et al., 2010; Heier et al., 2010; Shababi et al., 2010; Palladino et al., 2011; Gogliotti et al., 2012) and the vasculature (Hsieh-Li et al., 2000; Narver et al., 2008; Araujo et al., 2009; Foust et al., 2010; Rudnik-Schoneborn et al., 2010).

Defects in the vascular system in particular have long been associated with SMA patients (Musch et al., 1975; Rudnik-Schoneborn et al., 2008; Araujo et al., 2009) and similar defects have been reported in the vasculature of SMA mouse models (Naver et al., 2008; Bevan et al., 2010; Foust et al., 2010; Heir et al., 2010; Shababi et al., 2010; Gogliotti et al., 2012).

While there is no cure for SMA, the lifespan of Type I SMA patients can be extended by invasive ventilation. In these longer surviving patients,defects in the structure and

function of the vasculature were aparent. The extremities of ventilated patients display a progressive necrosis, beginning at the digits and spreading to the arms and knees (Araujo et al., 2009). Biopsies of these necrotic tissues show alterations to the blood vessels including thromboses (Rudnick- Schoenebon et al., 2010) and thickened capillary basement membranes (Musch et al., 1975). These studies suggest that the perfusion of peripheral tissues is compromised in severe SMA patients and that this could be a result of alterations to fine vessel structure in SMA. Such defects are also commonly reported in mouse models of SMA.

Intermediate and mildly affected SMA mice develop chronic, progressive necrosis of the tail (Hseih-li et al., 2000). Similar necrosis of the tail, ear and digits is seen to develop in more severe SMA mouse models where the lifespan of SMA mice has been extended as a result of therapeutic intervention.

Extensive necrosis is seen in SMNΔ7 SMA mice which survived an additional 10-11 days as a result of HDAC inhibitor treatment (Narver et al., 2008). This necrosis began at the tail and spread to the colon. As observed in patients, vessels form these necrotic regions housed multiple thromboses and even displayed necrosis of their own walls (Narver et al., 2008). How these vascular defects arise and their contribution to SMA pathogenesis has yet to be investigated. However, the involvement of vascular defects in other motor neuron diseases has been readily investigated.

Capillary to muscle fibre ratios reduced in equine motor neuron disease (EMND) (Palencia et al., 2004) and a variety of vascular alterations are observed in ALS patients and animal models of the disease (Garbuzova-Davis et al., 2007; Zhong et

al., 20008; Nicaise et al., 2009; Garbuzova-Davis et al., 2010; Miyazaki et al., 2011; Miyazaki et al., 2012). In ALS, the blood spinal cord barrier (BSCB) is particularly affected.

The expression of tight junctional proteins are reduced in ALS endothelial cells causing a disruption of the BSCB (Zhong et al., 2008). This BSCB disruption causes haemorrhaging and reduced circulation and perfusion in the spinal cord. Importantly, these defects are observed prior to motor neuron degeneration (Zhong et al., 2008). Further disruption to the neurovascular unit, including disassociation of endothelial cells and astrocytes, is seen before motor neuron degeneration in SOD 1 mutant mice and ALS pateints (Miyazaki et al., 2011). Importantly, correction of these vascular defects has been shown to delay disease onset and increase lifespan (Winkler et al., 2013). While adult onset motor neuron degeneration, reminiscent of ALS, can be initiated by preventing proper formation of the spinal cord vasculature (Oosthyuse et al., 2001).

These reports from both mouse models and patients suggest that an insufficiently formed and poorly functioning vascular system can lead to motor neuron degeneration in ALS. Vascular alterations have been noted in SMA patients and mice models but their impact on disease pathogenesis has yet to be established. A key site of pathogenesis in SMA is the skeletal muscle where intrinsic pathology has been reported in both SMA patient tissue (Fidzianska and Wado 1990; Tens et al., 1996; Stahas et al., 2008; Mutsaers et al., 2011) and mouse models of the disease (Mutsaers et al., 2011).

High levels of apoptosis in skeletal muscle (Fidzianska and Wado 1990; Tens et al., 1996; Stahas 2008), is a well-characterised hallmark of SMA. Along with increased levels of cell death, the development and maturation of skeletal muscle has also been reported to be affected in SMA (Fidzianska and Wado, 1990). Muscle biopsies from an eight-month-old SMA patient displayed prenatal-like organisation of muscle fibres (Fidzianska and Wado, 1990). In another study postnatal muscle biopsies from SMA patients expressed high levels of fetal muscle protein markers (Stahas et al., 2008). These findings suggest retardation in the development of SMA skeletal muscle. Similar impairments in muscle development have also been reported in muscles which do not show signs of neuromuscular pathology in SMA (Lee et al., 2011).

In the SMNΔ7 mouse model of SMA, impaired postnatal growth of skeletal muscle is observed in SMA mice where no evidence of motor neuron loss or altered neuromuscular transmission was observed (Lee et al., 2011). Intrinsic molecular pathology, including alterations in expression of proteins involved in muscle function, cell death pathways and morphological development, is found in skeletal muscle resistant to motor neuron pathology and neuromuscular junction dysfunction (Mutsaers et al., 2011). This suggests that Smn is important in the development and function of healthy skeletal muscle. This role of Smn in normal skeletal muscle is emphasised by work examining the effects of Smn knockdown in muscle cells (Shafey et al., 2005).

Myoblast C2C12 lines with reduced levels of Smn protein have shown reduced cell proliferation and defective myoblast fusion resulting in malformed myotubes (Shafey et al., 2005). Importantly the severity of these defects in muscle cell development

was linked to the level of Smn protein present in the cells: the less Smn present, the more severe the defect (Shafey et al., 2005). This work further suggests a key role for Smn in the normal development and function of skeletal muscle cells. While the presence of Smn in the sarcomere of both *Drosophila* and mice (Rajeda et al., 2007) along with the localisation of the Smn-complex to the sarcomere, in both cardiac and skeletal muscle (Walker et al., 2008), suggest that the function of Smn in muscle is conserved across species and muscle type.

Given that reduced Smn levels result in defects in the molecular composition of skeletal muscle as well as its development and growth, it is possible that other systems within skeletal muscle are also affected by Smn depletion in SMA. The vasculature of skeletal muscle in particular provides an interesting topic of investigation. Not only has the vascular system been reported to show alteration in SMA patients (Araujo et al., 2009; Rudnik-Schoneborn et al., 2010) and mouse models (Narver et al., 2008; Foust et al., 2010), as previously described, it also particularly sensitive to alterations in other myopathies (Norton et al., 1968; Kobayashi et al., 1983; Visser et al., 1989; Estruch et al., 1992; Authier et al., 1996) and neuropathies (Malik et al., 1992; Borisov, 2000; Dedkov, 2002).

Alteration to the form and composition of skeletal muscle capillaries has been reported in a variety of childhood myopathies (Norton et al., 1968; Kobayashi et al., 1983; Visser et al., 1989; Estruch et al., 1992). Capillaries from patients with Duchene's muscular dystrophy and mitochondrial myopathy have been reported to show an enlargement of the endothelial cells in the walls of vessels and consequently a narrowing of capillary lumens (Kobayashi et al., 1983). Similarly, alterations to

capillary structure are a commonly reported feature of inflammatory myopathies (Norton et al., 196; Visser et al., 1989; Authier et al., 1996).

The basal lamina of capillaries is altered in SMA patients (Musch et al., 1975) and thickens in two inflammatory muscle disorders: scleroderma and systemic lupus erythematosis (SLE) (Norton et al., 1968). Together with changes in capillary width, a reduction in the number of capillaries in skeletal muscle has been reported in SLE (Norton et al., 1968). This loss of capillaries in skeletal muscle has also been reported in inflammatory myopathies such as dermatomyositis (Estruch et al., 1992) and in necrotising myopathies (Authier et al., 1996). In these myopathies the basal lamina was found to be duplicated, a feature often reported in SLE as well (Norton et al., 1968). Interestingly, similar alterations to capillary structure have been reported to occur prior to muscle fibre damage in dermatomyositis (Visser et al., 1989).

Electron microscopy of skeletal muscle biopsies from early stage dermatomyositis patients showed alterations to the capillary bed of muscles. Patients who displayed mild muscle weakness showed no evidence of structural alteration to muscle samples but capillaries within the muscle showed numerous defects. The endothelial cells of capillary walls showed microtubule inclusions and macrovacuoles while a number of capillaries were found to be necrotic (Visser et al., 1989). Observing such structural changes in the capillaries of skeletal muscle while the muscle fibres themselves appear healthy suggests that damage to the vascular network in these muscles occurs prior to muscular pathology. Vascular changes prior to muscle atrophy are also observed in denervated skeletal muscles (Borisov et al., 2000,).

In denervated rat *extensor digitorum longus* muscles, the number of capillaries to muscle fibres, the capillary-to-fibre ratio, was reduced by 88% in the months following denervation. The loss of capillaries was found to begin before any muscle fibre atrophy was observed (Borisov et al., 2000). This reduction in capillary number within the muscle resulted in an increase in diffusion distance between capillaries and muscle fibres of up to 400% and 18 months after the denervation was performed, 40% of muscle cells were found to be avascular (Borisov et al., 2000). As well as this profound reduction in extent, skeletal muscle capillary beds have been reported to respond to denervation in a more dynamic fashion (Chernukh and Alekseeva 1975; Dedkov et al., 2002).

A nine-fold reduction in the capillary-to-fibre ratio was reported in the hindlimb muscles of rats following denervation (Dedkov et al., 2002). While the number of capillaries within the muscle was reduced, the vessels themselves showed evidence of regenerative structures, in particular, an increase in the number of growing endothelial cells (Dedkov et al., 2002). This suggests that even though the capillary bed was reduced in density by denervation, the remaining vascular network retained its ability to generate new vessels. Similarly following a reduction in the total number of capillaries and a reduction in the number of functioning capillaries during denervation, an increase in capillary number was observed during reinervation of the gastrocnemius muscle in rats (Chernukh and Alekseeva 1975). These investigations of the skeletal muscle capillary bed suggest that capillaries within skeletal muscle are highly sensitive to alterations in muscle, be this change within the muscle tissue itself or damage to the nervous supply of the muscle. As both skeletal muscle and lower motor neurons innervating skeletal muscle show pathology in SMA it is possible that

the capillary bed in skeletal muscle is altered in response to one, either or both of these factors.

Based on the evidence that the vasculature is altered in SMA and other forms of motor neuron disease and that the form and extent of the skeletal muscle capillary bed is altered in denervation and pathological myopathies, we hypothesised that the capillary bed of skeletal muscle could show similar alterations in SMA. To investigate this hypothesis a novel means of measuring capillary density in skeletal muscle is required.

Skeletal muscle capillary density has historically been measured in muscles of the hindlimb. While these muscles are easy to locate and dissect from experimental animals, they present difficulties from an analytical perspective. Given their large bellied nature hindlimb muscles must be sectioned for immunological processing and analysis. This results in the quantification of two dimensional relationships between capillaries and muscle fibres, the most commonly used being the capillary-to-muscle fibre (CF) ratio. Recent stereoscopic analysis has discredited the use of the CF ratio as a means of measuring capillary density, reporting that the method underestimates capillary density in muscle by up to 75% (Cebasek et al., 2009). While 3D stereoscopic reconstruction techniques such as that described by Cebasek et al., provide a more accurate measure of capillary density in skeletal muscle, reconstruction of a single muscle fibre requires ten hours of microscopic work. This clearly emphasises the need for an accurate and efficient means of investigating and quantifying skeletal muscle capillary density.

Here a novel means of investigating capillary density in skeletal muscle was developed using a selection of thin, flat muscles from the cranial region and body wall. Capillary density in these muscles was quantified using immunohistochemical staining and fluorescent microscopy. Morphological aspects of the skeletal muscle capillary bed, such as the ramification of capillaries through skeletal muscle, as well as the calibre of capillaries were analysed using confocal and fluorescent microscopy. The capillary bed of SMA skeletal muscle was found to be dramatically altered at a late symptomatic time point in Severe SMA mice. Capillary density, when measured via immunofluorescence, was significantly decreased in SMA mice when compared to control littermates. The calibre of capillaries in SMA skeletal was significantly larger than that of control littermates while the ramification of capillaries through muscle was reduced in SMA mice. Timeline analysis of capillary density showed no difference in the extent of the capillary bed between SMA and control littermates at birth. Similar levels of reduction in capillary density in SMA mice was also observed in the Taiwanese and SMN2Δ7 models of SMA at late symptomatic timepoints. Time line analysis of capillary density in the Taiwanese model showed a similar pattern of postnatal development of the capillary defect as that seen in the Severe model.

2.2 Methods

2.2.1 Ethics Statement

All animal experiments were approved by a University of Edinburgh internal ethics committee and were performed under license by the UK Home Office (Project License number 60/3891).

2.2.2 Animal Husbandry

Smn$^{+/-}$*;SMN2*$^{+/+}$ (Severe) mice (Jackson Labs strain no. 005024) on a congenic FVB background were maintained as heterozygous breeding pairs under standard SPF conditions in animal care facilities in Edinburgh. All animal procedures and breeding were performed in accordance with Home Office and institutional guidelines. *(SMN2)2Hung Smn1*^{tm1Hung}*/J* mice (Taiwanese) (originally received from Brunhilde Wirth in Koln) on a congenic FVB background were maintained as heterozygous breeding pairs under standard SPF conditions in animal care facilities in Edinburgh. All animal procedures and breeding were performed in accordance with Home Office and institutional guidelines. Retrospective genotyping for both strains was carried out using standard PCR protocols detailed below. *Smn+/-;SMN2;Δ7* (SMNΔ7) (Jackson labs strain no. 005025) breeding pairs were maintained in animal care facilities in Oxford. For this strain, basic dissection of the chest and abdominal wall were performed in Oxford by James Sleigh and shipped to Edinburgh. All genotyping of this colony was performed in Oxford by James Sleigh.

Neonatal SMA mice and control littermates up to the age of P5 were sacrificed by immersion in ice/ water followed by decapitation. Pups above the age of P5 were sacrificed by an overdose of anaesthetic administered via *intraperitoneal* (IP)

injection of sodium pentabarbitol (Euthenal). Care was taken to ensure both methods of sacrifice were performed in such a manner as to protect the integrity of the muscles of interest: decapitations were performed inferior to cranial muscle attachments and IP injections were placed out with the boundaries of the transverses abdominus (TVA) muscle.

2.2.3 Genotyping of Severe mice

After death 10mm tails tips were collected from all mice for retrospective genotyping. The tips were digested overnight in tail tip lysis buffer plus 5µl proteinase K at 55ºC. The following day the digested tail tips were vortexed, to ensure complete digestion, and centrifuged at 14000K for 15 mins. The supernatant was added to 500µl of iso-propanol and gently inverted to precipitate the DNA, as was evident by the formation of thin white strands. The samples were centrifuged at 14000K for 10 minutes to pellet the DNA. The DNA pellet was washed twice with 70% ethanol. After the second wash any remaining ethanol was allowed to evaporate before the pellet was resuspended in 200µl of autoclaved, filtered, de-ionised water.

To genotype Severe mice two separate PCR reactions were needed: one to identify the presence of the endogenous mouse Smn gene and a second to identify the presence of the neomycin cassette used to insert the human SMN2 gene into the mouse genome. The presence, absence or combination of endogenous mouse Smn and the neomycin cassette determined the genotype of the mice. A sample where only endogenous mouse Smn was present indicated that the corresponding mouse was a wildtype. A sample where only the neomycin cassette was present indicated a knockout. Possessing both endogenous Smn and the cassette indicated a

heterozygous mouse. These heterozygous mice were phenotypically indistinguishable from their wildtype littermates and so, were considered control mice along with wildtypes.

PCR reaction mixes were made using the following standards:

Reagent	Volume (µl)
Water	11.7
Buffer	4
$MgCl_2$	1.6
Forward Primer WT	0.1
Reverse Primer WT	0.1
Forward Primer NEO	0.2
Reverse Primer NEO	0.2
dNTPs	0.4
Taq	0.1

Table 1: Details of the standard PCR reagent volumes per sample.

Primer sequences were as follows:

Primer	Sequence
Forward WT	TTTTCTCCCTCTTCAGAGTGAT
Reverse WT	CTGTTTGAAGGGAGTTGTGGC
Forward NEO	CTTGGGTGGACAGGCTATTC

Reverse NEO	AGGTGAGATGACAGGAGATC

Table 2: Details of the primer sequences for Severe model genotyping

1µl of extracted DNA was added to each reaction mix. Positive and negative controls were ran with every experimental litter genotyped. For negative controls 1µl of auto-claved, filtered water was added in the place of DNA. All reactions were ran with a previously identified heterozygous sample and a positive control. The reactions were conducted in a PCR machine using the following programme:

Step	**Temperature (°C)**	**Time (seconds)**
1	94	120
2	94	30
3	*61*	30
4	72 (27 cycles)	45
5	72	120
6	4	Indefinite

Table 3: Details of the PCR programme used for Severe model genotyping

The PCR reaction products were separated by gel electrophoresis. Samples were run on a 1.5% agarose gel (1.5g Agarose, 100ml 0.1M TAE buffer and 10 µl Sybersafe DNA stain (Invitrogen)) at 100v for 30 minutes and visualised. Specific bands were identified by their molecular weight.

2.2.4 Genotyping of Taiwanese mice

The Taiwanese experimental mice are generated from the crossing of two separate parent lines. One parent strain possess two copies of murine Smn, one of which is

complete and produces full length Smn. The other contains a neomycin cassette which has been inserted into the Smn gene, interrupting it, producing a shorter, non-functional Smn product. These heterozygous mice have no additional human SMN2. This parent strain is crossed with a second line of mice which possess multiple copies of human SMN2 but have no full length endogenous Smn. These homozygous mice have four copies of human SMN2 (2 copies on each allele) but only possess a copy of the interrupted Smn gene and not the full length endogenous murine Smn gene. When these two parent lines are bred the resulting experimental Taiwanese mice retain four copies of human SMN2 and a combination of endogenous full length and interrupted murine Smn genes. It is this combination that determines the genotype. A single PCR reaction is used to determine these genotypes.

In the PCR reaction there are three primers; one forward and two reverse. These primers are used to identify the condition of the murine Smn. The forward primer and the first reverse primer identify full length murine Smn (1050bp), while the second reverse primer recognises the neomycin insert and so produces the shorter, interrupted Smn (950bp) product. Presence of both the full length and interrupted Smn product identifies a pup as heterozygous. These heterozygous mice are healthy, gain weight and develop normally with no sign of motor deficiencies. These mice are considered as control littermates in all experiments described. Presence of only the shortened interrupted Smn product identifies the pup as homozygous. These homozygous pups lag behind control mice in weight gain by 2-3 days after birth and are SMA symptomatic by P5.

To genotype the Taiwanese mice 10mm tails tips were collected from all mice after death for retrospective genotyping. Tail tip digestion and DNA extraction was performed as described for the Severe model mice.

PCR reaction mixes were made up using the following standards;

Reagent	Volume (µl)
Water	6.25
Buffer	3
$MgCl_2$	0.9
Forward Primer	1.5
Reverse Primer 1	1
Reverse Primer 2	1
dNTPs	0.15
Taq	0.2

Table 4: Details of the standard PCR reagent volumes

The sequence of the forward and two reverse primers were as follows:

Primer	**Sequence**
Forward	ATAACACCACCACTCTTACTC
Reverse 1	GTAGCCGTGATGCCATTGTCA
Reverse 2	AGCCTGAAGAAGATCAGC

Table 5: Details of the primer sequences used for Taiwanese model genotyping

1µl of extracted DNA was added to each reaction mix. Positive and negative controls were ran with every experimental litter genotyped. For negative controls 1µl of auto-claved, filtered water was added in the place of DNA. All reactions were ran with a previously identified heterozygous sample and a positive control. The reactions were conducted in a PCR machine using the following programme:

Step	**Temperature (°C)**	**Time (seconds)**
1	95	180
2	94	30
3	*59*	30
4	68 (35 cycles)	60
5	68	300
6	4	Indefinite

Table 6: Details of the PCR programme used for Taiwanese genotyping

The PCR reaction products were separated by gel electrophoresis. Samples were run on a 1.5% agarose gel (1.5g Agarose, 100ml 0.1M TAE buffer and 10 µl Sybersafe DNA stain (Invitrogen) at 100v for 30 minutes. Gels were visualised and specific bands were identified by their molecular weight against a DNA ladder (Promega Express, g2101).

2.2.5 Quantitative Fluorescent Western Blotting

The aortas from P5 SMA and control littermates were collected and pooled into a single sample for each condition. Total protein was isolated from the aortas by homogenisation in RIPA buffer (Pierce, 89900). Proteinase inhibitor cocktail

(Thermo Scientific, 1861278) was added to the RIPA buffer at a concentration of 5µg/ml. 30µl of RIPA buffer was added to each sample. Following homogenisation the samples were centrifuged at 14000rpm for 20 minutes. A BCA assay was then conducted to determine protein concentration in the samples, using a micro BCA Assay kit (Pierce, 23235). A master mix was made up using the following volumes per sample and standard; 500µl reagent A, 480µl reagent B and 20µl reagent C. Enough master mix was made to analyse each sample and standard in duplicate (1ml per sample). A protein standard curve was produced by adding increasing volumes of 2mg/ml of BSA albumin protein standard (Pierce, 23209) to the master mix. 1ml of mix was transferred to appropriately labelled 1.5ml Eppendorf tubes to which 1µl of corresponding sample was added. The samples were briefly vortexed and then incubated at 60°C for one hour. Following incubation samples were transferred to cuvettes and their absorbance measured at 562nm on a Thermo Scientific spectrophotometer. The absorbance readings from the standard samples were used to produce a standard curve. Using the equation of the line $y = mx + c$ the concentration of the experimental samples was calculated. After doing so, 15mg of protein per lane was chosen as the optimum loading concentration for western blotting. Samples were diluted with the appropriate volume of autoclaved, deionised water to prepare 10µl for loading. To aid loading 5µl of NuPAGE LDS Sample Buffer (Novex, NP0007) was added to each sample. The samples were then incubated at 98°C for 2 minutes before loading into 4-12% precast NuPageBisTris gradient gels (Novex, NP0323BOX) along with 5µl of Sharp Pre-stained protein standard (Novex, LC5800). Samples were run at 80V for 5 minutes, to ensure even entry of the samples into the gel, and then at 170V for 45 minutes. The gels were then removed

from their precast casing and trimmed. The gels were then transferred to PVDF membranes (NuPAGE,) in transfer buffer (NuPAGE,) at 24Mv 16 hours. Following overnight transfer, the membranes were moved to 50ml falcon tubes and incubated with 5mls Odyssey blocking buffer (Licor, 402-467-0700) at room temperature, on a rolling platform for at 30 minutes. After this initial blocking, a fresh 5ml of blocking buffer was added to the membranes along with Tween-20 at a concentration of 1:1000. Primary antibodies were added to the blocking buffer and tween solution, SMN (BD Biosciences, 610646) was added at a concentration of 1:1600. β Actin (Abcam, ab8226, 42 kDa) at a concentration of 1:1600 was added as a loading control. The membranes were then incubated overnight at 4°C on a rolling platform. Following incubation with the primary antibodies, the membranes were washed for 6x5 minutes in 0.1M PBS. Corresponding Odyssey secondary antibodies were then applied to the membranes along with fresh blocking buffer and Tween-20 for an incubation period of 90 minutes, at room temperature, on a rolling platform. Both Goat anti rabbit 680 (Odyssey) and Rabbit antimouse IRDye 800 (Odyssey) were used at a concentration of 1:1600. The membranes were washed again for 6x5 minutes in 0.1M PBS before being dried and scanned at 600 and 800 nm on a Licor Odyssey scanner. Quantification of the blots was performed on single channel scans. Bands were identified according to their molecular weight and their arbitrary fluorescence intensity calculated by Odyssey software.

2.2.6 Dissection

All pre-fix dissections were performed in oxygenated mammalian physiological ringer (mM: NaCl 120, KCl 5, $CaCL_2$ 2, $MgCl_2$ 1, NaH_2PO_4 0.4, $NaHCO_3$ 23.8, Glucose 5.6). All post-fix dissections were performed in 0.1M PBS.

2.2.6.1 Cranial Muscles

The cranial muscles of the mouse are located on the posterior aspect of the neck, at the base of the skull. To remove these muscles intact, the whole muscle mass covering the skull, along with the skin and ears of the mouse was removed. The resulting preparation was pinned out flat, using insect pins, in a Sylgard lined petri dish. The preparation was orientated so that the skin and ears were flat on the Sylgard and the deepest muscle layer faced upwards towards the dissector. Excess muscle tissue and fat was carefully cleaned from the preparation until the cranial muscles and their midline raphe was visible. The preparation was then fixed in 4% paraformaldehyde (PFA) for 10 minutes, at room temperature, on a rocking platform. Following fixation the preparation was repeatedly rinsed in 0.1M PBS to remove excess fixative. At this point any remaining overlaying muscles, fat, connective tissue and skin covering the cranial muscles was removed. The cranial muscles were dissected individually, starting with the most superficial the interscutilaris (IS), followed by the abductor auris longus (AAL), the auricularus superior (AS) and finally the levator auris longus (LAL). The muscles were cut from their midline raphe before being reflected laterally towards their insertion at the pinnae of the ear and cut flush. Once removed from the preparation the individual muscles were gently cleaned of any remaining connective tissue by blunt dissection.

2.2.6.2 Transversus Abdominus

The skin on the front and back of the mouse was carefully removed to expose the intact underlying musculature and peritoneum. A horizontal, suprapubic incision was

made into the peritoneum and was extended bilaterally to reach the spine. Here the incision was extended proximally on the back of the mouse, by cutting through the ribs at their costovertebral attachment, freeing the ribcage from the spine. These ascending incisions were then extended medially on the front of the mouse, through the clavicle and sternum to free the ribcage from its superior attachment to the axial skeleton. The abdominal organs and diaphragm were gently removed from the preparation allowing the thoracic cage and the inferiorly attached abdominal musculature to be removed from the mouse. The preparation was then pinned flat in a Sylgard lined dish using insect pins. The superficial abdominal musculature was removed by cutting down the midline of the chest from the sternum to the cut edge of the abdominal wall. This midline incision was extended laterally to reach the ribs and then diagonally back towards the sternum, along the medial border of the ribcage, to remove a triangular flap of muscle, exposing the underlying TVA. The superior epigastric vessels, running the length of the midline, were gently dissected from the surface of the TVA. The preparation was then fixed in 4% PFA for 10 minutes, at room temperature, on a rocking platform. Following fixation the preparation was repeatedly rinsed in 0.1M PBS to remove excess fixative. After washing, ribs attached to the TVA were gently removed one at a time. Overlying fibres of the oblique muscles, identified by their diagonal arrangement, were gently removed by blunt dissection. At this point the TVA was removed from the ribcage by repeating the triangular dissection pattern used to remove the superficial abdominal musculature. Any remaining connective tissue was removed by gentle blunt dissection.

2.2.7 Immunohistochemistry

Two staining approaches were utilised to label the skeletal muscle capillary bed; one an antibody based protocol and a second more rapid labelling technique involving a fluorescently conjugated isolectin.

2.2.7.1 Platelet cell adhesion molecule 1 (PECAM 1) capillary staining

Intact muscles were blocked in immunoglobulin G protease-free standard blocking solution (0.2% bovine serum albumin (BSA), 0.5% Triton-X-100 (TX100) made up in 0.1M PBS) for 30 minutes, at room temperature on a rocking platform. Muscles were then incubated overnight, at 4°C, on a rocking platform with goat anti-mouse PECAM 1 primary antibody (R&D Systems, AF3628) at a concentration of 1:1000 made up in blocking solution. The following day muscles were washed for 6x5 minutes in 0.1M PBS at room temperature, on a rocking platform. After washing, the muscles were incubated with donkey anti-goat Cy 3 conjugated secondary antibody (Jackson ImmunoResearch Laboratories Inc) at a concentration of 1:250 made up in fresh that day standard blocking solution. Muscles were incubated with the secondary antibody for 1 hour, at 4°C in the dark, on a rocking platform. From this point on the muscles were kept in the dark. Following the secondary incubation muscles were washed again for 6x5 minutes in 0.1M PBS at room temperature, on a rocking platform. Muscles were then exposed to 5µg/ml FITC conjugated α-bungarotoxin (α-BTX) to label post-synaptic acetylcholine receptors. The muscles were washed for the final time for 3x5 minute washes in 0.1M PBS before being whole mounted on glass slides, with glass coverslips. Muscles were mounted in

Mowiol (10%Mowiol, Polyscience Inc., 20%Glycerol, 50%0.2M Tris buffer pH8.5, 3%1,4-diazobicyclooctane made up in distilled water) with the diazobicylooctance (DABCO) acting as an anti-fade reagent. The resulting slides were left overnight, in the dark, at room temperature to set before visualisation and imaging the following day.

2.2.7.2 Griffonia Simplicifolia Lectin -1 (GSL-1) capillary staining

Whole muscles were incubated with Rhodamine conjugated Griffonia Simplicifolia Lectin-1 (GSL-1) (Vector Laboratories) at a concentration of 1:100 made up in 0.1M PBS for one hour, in the dark, at room temperature, on a rocking platform. From this point on muscles were kept in the dark. Following GSL-1 incubation the muscles were washed for 6x5 minutes in 0.1M PBS before being exposed to FITC conjugated α-BTX as standard to label post-synaptic acetylcholine receptors. Muscles were then washed for the final time for 3x5 minutes in 0.1M PBS before being mounted in Mowiol on glass slides, with glass coverslips. The resulting slides were left overnight, in the dark, at room temperature to set before visualisation and imaging the following day.

2.2.8 Imaging

Micrographs for the calculation of capillary density and calibre were captured using a standard inverted epifluorescence microscope (Olympus 1X71) combined with a chilled CCD camera (Hammamatsu C4742-95) and OpenLab (Improvision) image capture software. Cy3 and rhodamine labelled capillaries were imaged using 550nm excitation and 570nm emission optics. FITC post-synaptic acetylcholine receptors were imaged using 494nm excitation and 520nm emission optics.

Micrographs for the analysis of capillary ramification were captured using a Zeiss LSM 710 laser scanning confocal microscope (20 x objective/ 0.4 NA; 40 x objective/ 1.3 NA oil objective). 488nm and 543nm laser lines were used for excitation. Confocal z-series images were merged into stacks using Zen software.

2.2.9 Quantification and Analysis

Any muscles with poor quality staining or those that had been damaged during dissection were excluded from analysis. For capillary density calculations a minimum of 40 fields of view per muscle were taken with 40 x objective, 0.8 NA) Any fields of view where excessive overlying connective tissue interfered with imaging were excluded from further analysis. If excluded fields of view amounted to five or more in an individual muscle the entire muscle in question was discarded from further analysis. The cranial muscles were systematically samples and images were captured in every field of view (40x objective, 0.8 NA) across the entire muscle. For the larger, segmentally innervated TVA images were captured in every third field of view across the entirety of the muscle. For initial analysis images from the regions of the muscles; medial, endplate and lateral, were quantified separately to determine any regional variation in skeletal muscle capillary density. These regions could be identified by following the well defined endplate banding pattern in the muscles along with the characteristic shape of the origin and insertions of each of the muscles.

2.2.9.1 Quantifying capillary density

Images were first enhanced in Adobe Photoshop (CS4) for contrast and brightness. This ensured that definite vessel borders were visible and also prevented any fine

capillary structures from being lost and discounted. Any out of focus images where capillaries appeared blurred or those where background was too high to completely isolate capillary structures were excluded from further analysis. Using Image J (NIH) the enhanced images were converted to binary. In the resulting binary images capillaries were assigned black and muscle background white, allowing for the ratio of black to total white pixels to be calculated. This produced a value for capillary area per field of view. By calculating the area of a x40 field of view, it was then possible to calculate the area of capillaries in mm^2 per mm^2 of muscle.

2.2.9.2 Quantifying capillary calibre

Measurements were taken from the same images used to quantify capillary density. A grid was overlain onto the images using Image J (NIH) and the diameter of capillaries found at the intersection of gridlines was measured. The shortest distance across each capillary was measured and measurements were not taken at capillary bifurcations. To prevent repeated measurement of the same capillary across an image, any capillaries which crossed multiple gridline intersections were excluded from measurement.

2.2.9.3 Analysis

All data were collected using Microsoft Excel software and were graphed and analysed using GraphPad Prism software. Charts shown are mean ± s.e.m. In all analyses statistical significance was considered to be $p < 0.05$. Tests used are detailed in figure legends.

2.3 Results

2.3.1 SMN protein is present in endothelial cells and is reduced in SMA mice

Having identified the vascular system as a key area of interest in SMA we initially determined if the Smn protein, the reduction of which results in the SMA phenotype, was present in the cells of the vascular system. Western blots for the Smn protein in the aortas of P5 Severe SMA mice and control littermates show abundant levels of Smn in control aortas and reduced levels in SMA mice. Adding this result to our knowledge of muscular pathology and vascular defects in both animal models of the capillary network supplying SMA skeletal muscle. In order to do this we developed a novel method to measure skeletal muscle capillary density using thin, flat muscles which can be viewed in a 2D planar manner.

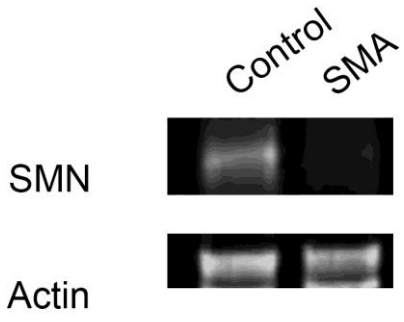

Figure 1- Smn protein is present in the cells of the vasculature. *Western blot of Smn (~42kDa) and β Actin (~42kDa) of P5 Control and SMA aortas. A western blot was carried out to determine the presence of the Smn protein in cells of the vasculature. An antibody against Smn was used to probe protein samples extracted from P5 aortas. In the control sample a strong band was detected at approximately 42kDa, the molecular weight of Smn protein. In the SMA sample a very faint band was present at 42kDa. β Actin was used as a loading control, with bands of similar intensity and weight present in both control and SMA samples.*

2.3.2 Novel Capillary density quantification technique

2.3.2.1 Muscle selection, preparation and staining

In order to examine the skeletal muscle capillary bed flat, thin muscles form the cranial region (Fig 2 Cranial muscles) and the abdominal wall (Fig 3 TVA) were selected. These muscles have the advantage of being only a few muscle fibres thick allowing for the examination of the entire capillary bed in a whole mount preparation, removing the need for sectioning. Classical capillary density quantification has relied upon the counting of capillary to muscle fibre ratios in sectioned muscle, which can underestimate capillary density by up to 75% (Cebasek et al., 2009). By analysing the intact capillary bed a more accurate measure of capillary density should be produced. The selected muscles also encompass a range of developmental phenotypes, fibre types, body position and susceptibility to pathology in SMA (Murray et al., 2008, Murray et al., 2010), allowing for the investigation of the nature of the capillary bed in a range of phenotypically distinct muscle. For initial investigations the well characterised LAL muscle was chosen. In particular the caudal band of the LAL muscle (LALc), as it is known to be susceptible to neuromuscular pathology and is severely affected in SMA (Murray et al., 2008).

The cranial muscles of the mouse are located on the posterior aspect of the neck, at the base of the skull. The muscles are responsible for independent movement of the ears. The most superficial of these muscles, the *levator auris longus* (LAL) muscle has been chosen muscle for this investigation. (A) To remove the entire muscle mass at the base of the skull a vertical incision was made through the skin between the eyes of the mouse. This incision was then extended caudally along the skull to the

midpoint between the scapulae of the mouse (Figure 2A). This incision was extended bilaterally underneath the ears to reach the original incision between the eyes. To remove the skin, ears and attached muscles, the skin at the cut edge underneath the ear was lifted to expose the ear canal. Keeping the dissecting scissors flat to the roof of the skull the ear canal was cut away from the skull. Keeping the scissors flat to the skull this cut was extended medially towards the original midline incision. This was then repeated on the opposite side of the skull (Figure 2B). The resulting preparation contains the ears, skin and underlying muscle mass (Figure 2C). The preparation was then pinned out in a Sylgard lined petri dish using insect pins. The preparation was pinned so that the most superficial layer of muscles became the deepest layer (Figure 2D). The overlying large muscles were gently dissected until the cranial muscles and their midline raphe, highlighted with an arrow, were visible (Figure 2E). The preparation was now fixed for 10 minutes in 4% PFA, at room temperature on a rocking platform. Following fixation the superficial cranial muscles were dissected to reach the muscles of interest, the LAL, which forms the deepest layer of cranial muscle group when the preparation is pinned in this fashion. Individual cranial muscles were removed one at a time from the preparation by locating and cutting through their individual sites of attachment at the pinae of the ears and reflecting the muscle medially towards the midline where they were cut flush. Once removed from the preparation the muscles were cleaned of any remaining fat or connective tissue by gentle blunt dissection. Here the muscles are shown in their order of removal starting with the most superficial IS, followed by the AS, the AAL and then the LAL. After being removed intact the LAL was then separated into its two distinct bands: the larger rostral band and the smaller caudal

band, highlighted with arrows and labelled (Figure 2F). Along with the distinct bands of the LAL, the TVA was also chosen for analysis (Figure 3).

Figure 2 – Cranial muscle dissection. *Step by step images depicting the cranial muscle dissection procedure.*

The TVA muscle forms the deepest layer of the abdominal musculature. To expose the abdominal musculature the skin on the front and back of the mouse was removed (Figure 3A). A horizontal incision was then made in the body wall (Figure 3B). This incision was first extended bilaterally to reach the spine and then proximally by cutting through the ribs to remove the rib cage and attached abdominal musculature (Figure 3C). The preparation was thinned pinned out in a Sylgard lined petri dish using insect pins (Figure 3D). A triangular flap of overlying abdominal musculature was removed, along with the overlying blood vessel to expose the underlying TVA (Figure 3E). The preparation was then fixed in 4% PFA for 10 minutes, at room temperature, on a rocking platform. The overlying fibres of the oblique fibres, the

ribs and sternum were removed from the TVA allowing it to be freed from the rib cage. The muscle was then cleaned of any remaining fat or connective tissue in preparation for staining (Figure 3F).

Figure 3 – Transversus Abdominus (TVA) dissection. *Step by step images depicting the TVA dissection procedure.*

In these muscles the capillary bed was visualised by staining with an antibody against Platelet Cell Adhesion Molecule 1 (PECAM 1) (R&D Systems), the major component of endothelial cell-to-cell junctions (Newman 1997) (Figure 4). PECAM 1 functions in the cell adhesion cascade which results in the extravasation of immune cells during inflammatory responses (Newman 1997).PECAM 1 has been used

extensively in other studies to reliable label muscle capillary beds. The motor endplates of muscles were visualised using FITC-conjugated α bungarotoxin. α bungarotoxin is a naturally occurring toxin, isolated from the venom of the Banded Krate. The toxin specifically binds to the α subunit of the nicotinic acetylcholine receptor (Figure 4). After staining images were captured using either a standard epifluorescent microscope or a laser scanning confocal microscope, depending on the type of analysis to be performed. Confocal microscopy was used to obtain Z-stacks for the analysis of capillary ramification.

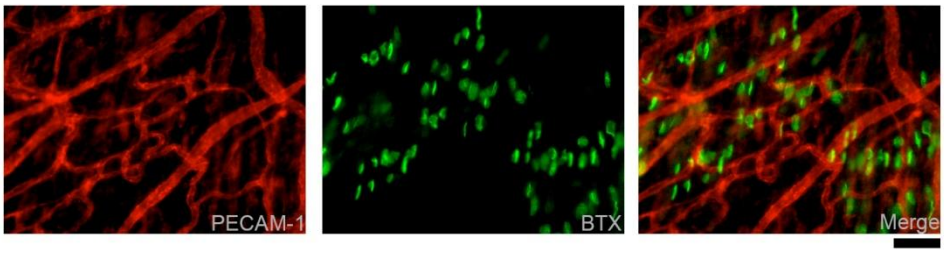

Figure 4 – Skeletal muscle capillary bed staining*. The capillary bed was stained using immunohistochemistry to label capillaries and bungarotoxin staining to label motor endplates. (A) Capillaries were visualised using an antibody against Platelet Cell Adhesion Molecule 1 (PECAM 1) (R&D Systems) and a corresponding Cy 3 secondary antibody (Jackson Research Laboratories Inc). (B) Motor endplates were visualised using an FITC-conjugated α bungarotoxin (Molecular Probes)which binds specifically to acetylcholine receptors (C) Merged images of the PECAM 1(A) and FITC-conjugated α bungarotoxin (B) staining. Images were captured at 20 x magnification. Scale bar equals 50μm.*

A second staining technique, involving a rhodamine conjugated lectin, was also utilised to stain the skeletal muscle capillary bed (Figure 5B). Lectins are naturally occurring sugar agglutinating molecules which are found in plants, seeds and legumes. Individual lectins have highly specific binding for a variety of sugar moieties in specific cell types and regions. In this investigation, GSL-1 was used. GSL-1 is derived from the seeds of the Griffonia Simplicifolia (Bandeiraea) plant. It

is a four-subunit 114kDa glycoprotein which has specific binding affinity for the galactose sugar group present in the glycoproteins of endothelial cells (Vector Laboratories). GSL-1 staining of the skeletal muscle capillary bed was found to be identical to the labelling of the capillary bed achieved by PECAM 1 antibody staining (Figure 5A). Given that GSL-1 labelled the capillary in an identical manner to PECAM 1 antibody staining it was preferentially chosen as the main means to label the skeletal muscle capillary bed. This was due to the many advantages of GSL-1 labelling over antibody staining.

As lectins are not antibodies they do not require many of the stages required in standard antibody staining protocols. Given the high affinity of GSL-1 for its target glycoproteins, the muscles did not need to be incubated in blocking solution to prevent non-specific binding. By using a fluorescently conjugated lectin, capillaries could be visualised in a single incubation without the need for additional fluorochrome incubation stages. This allowed the capillary bed to be reliably labelled more efficiently than conventional antibody staining.

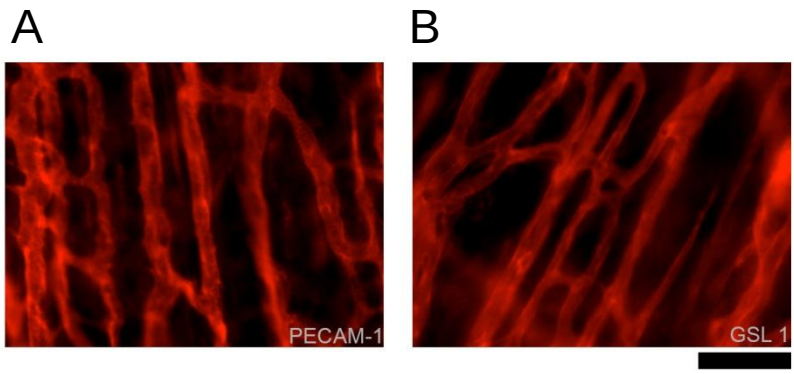

Figure 5 – Comparison of PECAM 1 antibody and GSL-1 lectin staining of the skeletal muscle capillary bed*. (A) Capillaries were visualised using the standard PECAM 1 primary and Cy 3 secondary antibody protocol. (B) Capillaries were visualised using the rhodamine conjugated Griffonia Simplicifolia Lectin-1 (GSL-1). PECAM 1 (A) and GSL-1 (B) label skeletal muscle capillaries in an identical fashion. Images were captured at 40 x magnification. Scale bar equals 50µm.*

2.3.2.2 Quantification of Capillary Density

Once stained the capillary bed was imaged for analysis. The thin, flat muscles selected for investigation can be viewed as whole mount preparations in plan-view. This presents a unique opportunity to view, image and assess the form and extent of the entire capillary bed of skeletal muscle in an intact and uninterrupted state. The initial assessments performed examined the extent of the capillary bed in skeletal muscle of Severe SMA model mice and control littermates. To generate values for capillary density from the images of the capillary bed a novel system of area based measurements was used.

40 x magnification images of the capillary bed were converted from their RGB colour format (Figure 6A) into binary using Image J (NIH) software. In doing so the capillaries were assigned black and the background of underlying skeletal muscle was assigned white (Figure 6B). The form and extent of capillaries within the image were not altered, merely their colouring. It was now possible to measure the ratio of black pixels to white pixels using Image J (NIH). This generated a percentage value for the area of the image inhabited by black pixels and so gave a value for the percentage area of the image occupied by capillaries. This could then be presented as the percentage area of capillaries per 40 x magnification field of view of muscle. By calculating the area of a 40 x magnification field of view in mm^2 it was possible to present the data as capillary area per mm^2 of muscle. Using this method the capillary density for the selected muscles of interest was calculated.

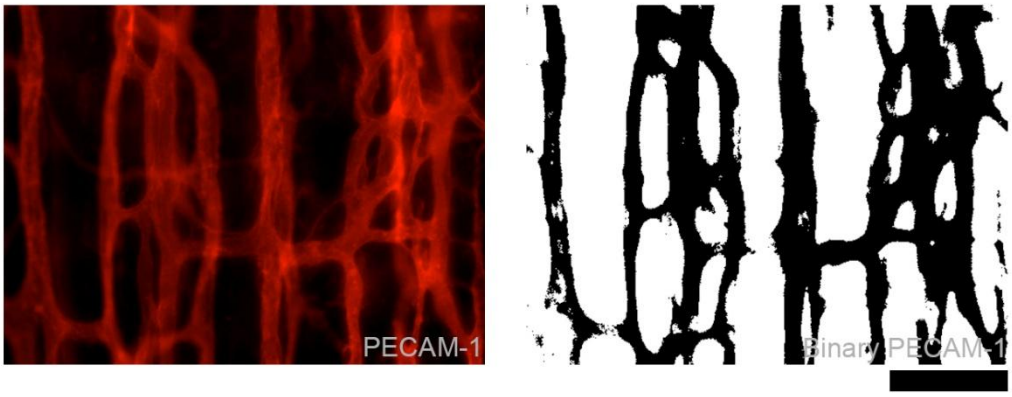

Figure 6 – ImageJ binary conversion of labelled skeletal muscle capillaries. *(A) Representative image of PECAM 1 labelled capillary bed. (B) The same representative image converted into binary using ImageJ software. Image was captured at 40 x magnification. Scale bare equals 50µm.*

2.3.3 Alterations to skeletal muscle capillary bed of the LALc muscle in late symptomatic Severe SMA mice

Initial inspection of capillary bed staining in the LALc muscle showed a dramatic difference in the architecture of the capillary bed in Severe SMA mice (Figure 7B) when compared to control littermates (Figure 7A). The arrangement, organisation and size of Severe SMA capillaries appeared altered but most striking alteration was the apparent reduction in muscle capillary density. In control littermate LALc muscles, a densely packed, well organised capillary bed with evenly-spaced capillaries was observed (Figure 7A). In contrast the capillary bed of the LALc in Severe SMA mice was sparse, with large spaces between adjacent capillaries, resulting in a loose open loop arrangement (Figure 7B). As this apparent difference in capillary density was the most striking and dramatic alteration to the capillary bed of Severe SMA mice it was chosen as the principal feature to measure.

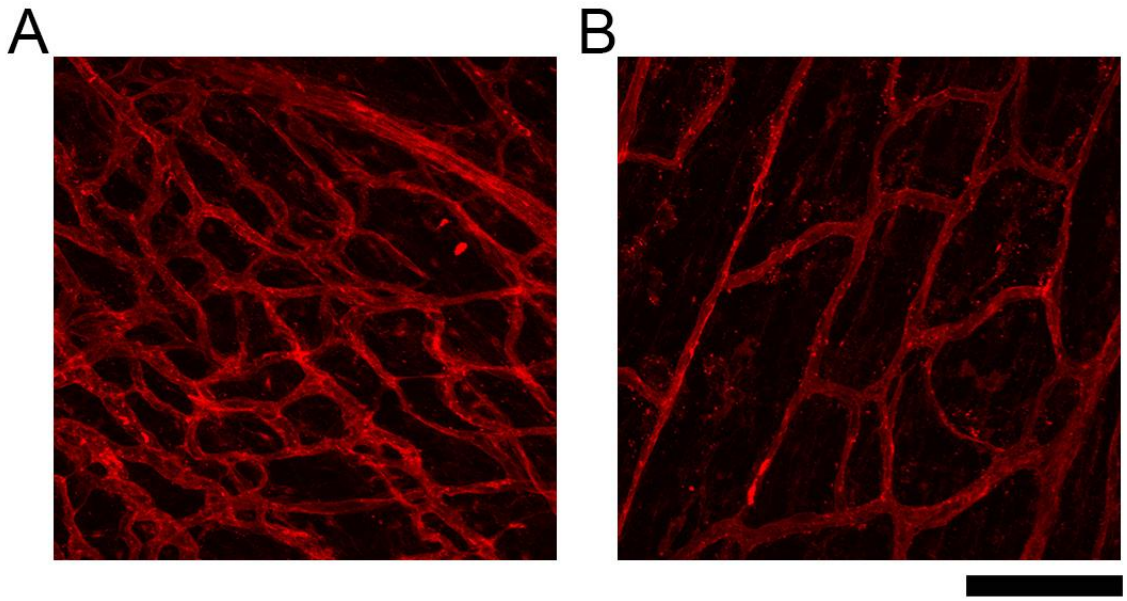

Figure 7 – Altered skeletal muscle capillary bed architecture in Severe SMA mice. *Representative confocal micrographs of control (A) and SMA (B) LALc muscles visualised with PECAM 1. Images are 40 x magnification. Scale bar equals 50µm.*

2.3.3.1 There is a significant, consistent reduction in capillary density across the entire LALc muscle in Severe SMA mice

For analysis of capillary density, the LALc muscle was split into three regions, shown in schematic form in Figure 8A. Firstly, the lateral region of the muscle, closest to the muscles attachment at the pinae of the ear (Figure 1), where the main blood supply of the LALc enters the muscle. Secondly, the endplate region, which has been previously defined (Murray et al., 2008), houses the motor endplates of the muscles and traverses the majority of the belly of the muscle. Finally, the medial region of the muscle, which is furthest from the arteriolar entry point and closest to the attachment of the LALc to the midline raphe (Figure 1). Images were captured in each of three regions and the capillary density for each quantified.

In P5 control mice, no significant difference in capillary density was observed between the three muscle regions. The lateral region, closest to the arteriolar entry point, had a comparable capillary density to the medial region of muscle, which is furthest from the initial blood supply to the muscle. A similar density of capillaries at either end of the muscle suggests that by P5, the capillary bed of the LALc has extended across the full length of the muscle. Interestingly, the density of capillaries in the endplate region was not significantly different from the regions of the muscle which lack motor endplates. It could have been expected that given the high energy status of motor endplates and neuromuscular transmission, capillary density in this region would be increased to meet greater oxygen and nutrient delivery demands. This data instead suggests that the skeletal muscle capillary density is uniform across the muscle, regardless of distance from primary blood supply or local specialisations of the tissue. A similar uniformity was observed in the capillary density of LALc muscles of SMA mice.

A significant reduction was seen in the capillary density of the P5 Severe SMA LALc muscles when compared to their control littermates. This reduction was seen in all three regions of the muscle. Again, as in the control LALc muscle, the capillary density in each of the three regions was comparable. This suggests that capillary density is not preferentially reduced in a specific region of the muscle.

With no significant difference in capillary density between the muscle regions within the LALc muscle, the individual data sets were pooled giving one total muscle value for each condition. This allowed the relative capillary density of control and Severe SMA LALc muscles to be compared. The capillary density of Severe SMA LALc

muscles was significantly reduced ($P<0.0001$, unpaired two-tailed t-test) in comparison to control littermate muscles by 36%.

The uniform reduction in density observed across the LALc muscle suggests that the Severe SMA capillary bed, however altered, is capable of extending across the entire muscle. The presence of other noticeable defects in the structure of the capillary bed suggests that the capillary network in Severe SMA mice, while capable of expanding with a growing muscle, is not as fully developed as the capillary bed observed in control mice of the same age.

Immature skeletal capillary networks have a polygonal arrangement which contracts and lengthens with the growing muscle fibres, to form a parallel ladder-like association between the capillaries and underlying muscle fibres (Wolffe et al. 1975,). In the P5 control LALc muscles this arrangement is evident, while the P5 Severe SMA muscles retain their large, extended, open, polygonal loops described in early stages of skeletal muscle vascular development (Wolffe et al., 1975). Along with this loose and disorganised structure on the surface of the muscle, the capillary bed of the Severe SMA LALc also appeared to differ in its penetration into the belly of the muscle.

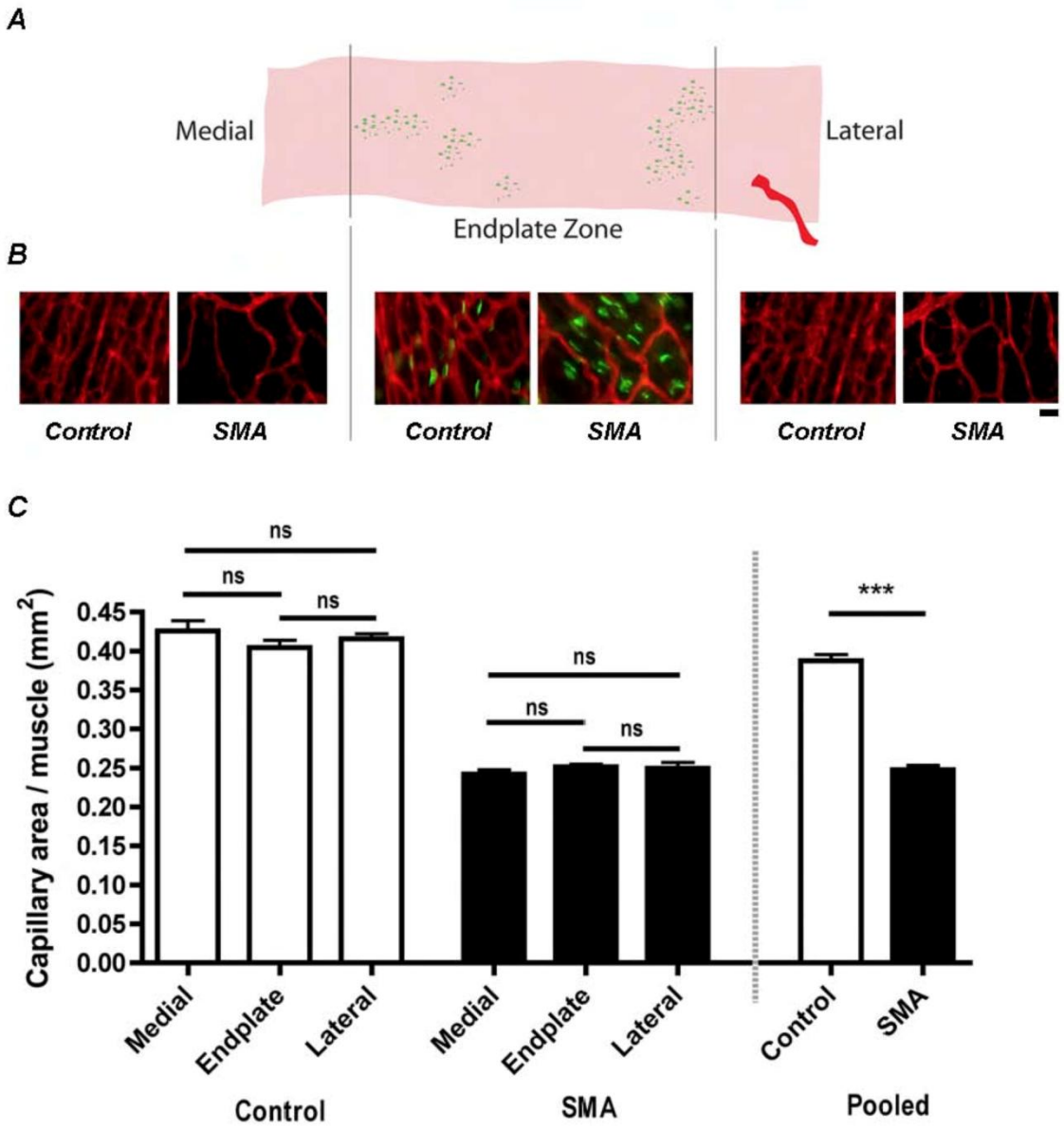

Figure 8- Uniform reduction in capillary density across the LALc in Severe SMA mice*. (A) Schematic representation of the LALc muscle indicating the entry site of the main muscle artery (red), the location of the motor endplate band (green dots) and the three muscle regions sampled (medial, endplate zone and lateral). (B) Representative micrographs of the capillary be visualised with GSL-1and motor endplates visualised with FITC-conjugated α bungarotoxin in control and Severe SMA LALc muscles from the three muscle regions sampled. Images are 40 x magnification. Scale bar equals 25µm. (C)Bar chart (mean ± s.e.m) quantifying capillary density in muscle regions of P5 control and Severe SMA mice. One Way ANOVA with Tukey post-hoc test, ns = no significance, P>0.05. Bar chart (mean ± s.e.m) quantifying pooled data from the three sampled regions. Unpaired, two-tailed t-test, *** P<0.0001. N≥3 mice and n≥6 muscles for each bar.*

2.3.3.3 The ramification of capillaries through the skeletal muscle bed is altered in late symptomatic Severe SMA mice

From the original confocal images it appeared that the capillary bed of the Severe SMA LALc lay in monolayer on the surface of the muscle (Figure 7). In comparison, the capillary bed in the control LALc muscle appeared to extend from the surface into the belly of the muscle. To assess the three dimensional relationship of the capillary bed in the muscle confocal Z-stack images were captured and extended orthogonal slices were taken through the stacks. When compared these slices through the full thickness of the LALc muscle belly revealed a difference in the ramification of the capillary bed between control and Severe SMA muscles. In control muscle (Figure 9A) multiple capillary loops could be seen extended throughout the full thickness of the muscle. In comparison the Severe SMA capillary bed appeared to form a monolayer which, rather than penetrating through the muscle, appeared to lie on its surface. This again suggests that the capillary bed in Severe SMA mice is capable of forming an initial simple network on the surface of the muscle, but the further development and growth required to extend this monolayer through the depth of the muscle is not occurring. This decreased ramification of capillaries through the muscle and the reduction in capillary density is further compounded by a structural alteration to the capillaries themselves observed in Severe SMA muscles.

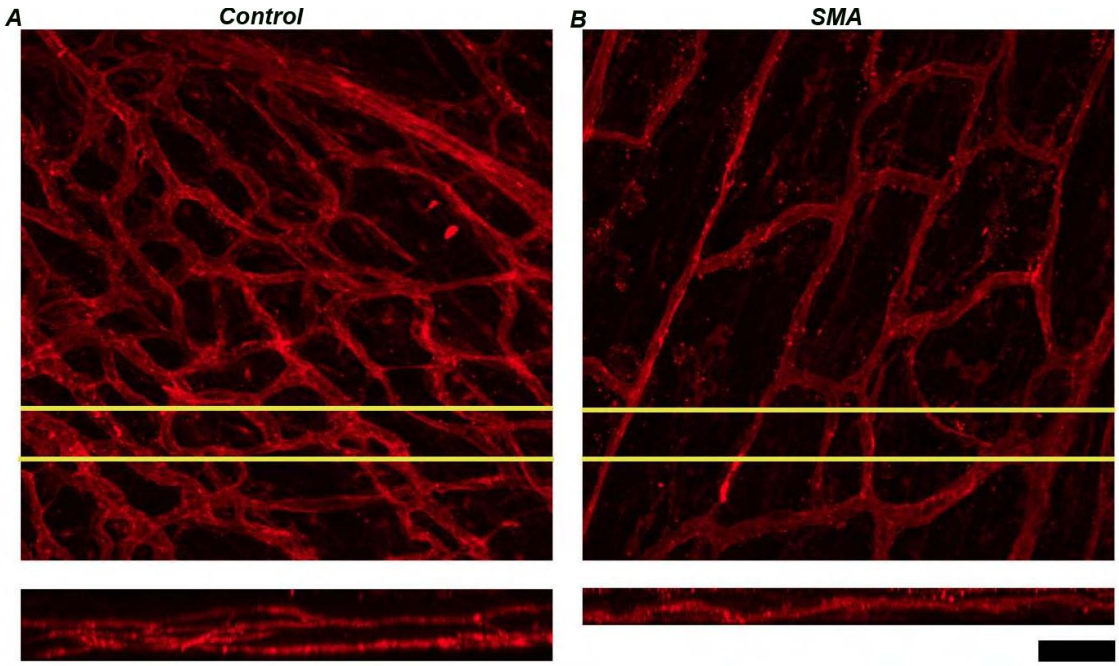

Figure 9 – Altered ramification of capillaries in Severe SMA muscle. *(A) Maximum intensity projections of confocal Z-stacks of LALc skeletal muscle capillary bed, visualised with GSL-1, from P5 control and Severe SMA mice. Yellow bars on these confocal micrographs indicate the position from where orthogonal slices were taken.(B) Extended, orthogonal slices of the capillary bed taken through Z-stacks. Images are 10 x magnification. Scale bar equals 25µm.*

2.3.3.4 Capillary calibre is increased in late symptomatic Severe SMA mice

When first observing the capillary bed the most striking difference between control and Severe SMA LALc muscles, was the extent of capillaries covering the muscle. On closer inspection, subtle differences in the structure of the capillaries themselves, beyond their number and arrangement, seemed apparent, in particular, the calibre (diameter) of the capillaries themselves. To assess this, the calibre of capillaries from across all regions of the LALc muscle were measured in both control and Severe SMA mice. In comparison to control littermates, the calibre of Severe SMA capillaries was significantly increased ($P<0.0001$, unpaired, two-tailed students t-test). On average control capillaries were approximately 4µm in diameter, while the average diameter of Severe SMA capillaries in the LALc muscle was approximately

6µm (Figure 10A). Representing an average 50% increase in capillary calibre in Severe SMA mice. When individual capillary calibres were presented in scatter plot format a far wider distribution of capillary calibres was seen in Severe SMA muscle. The tail of larger calibre capillaries was positively skewed, with 3.5% (62/1826) of capillaries lying in this tail (Figure 10B). In addition to a poorer ramification through the muscle the capillaries present in the Severe SMA capillary bed were much larger.

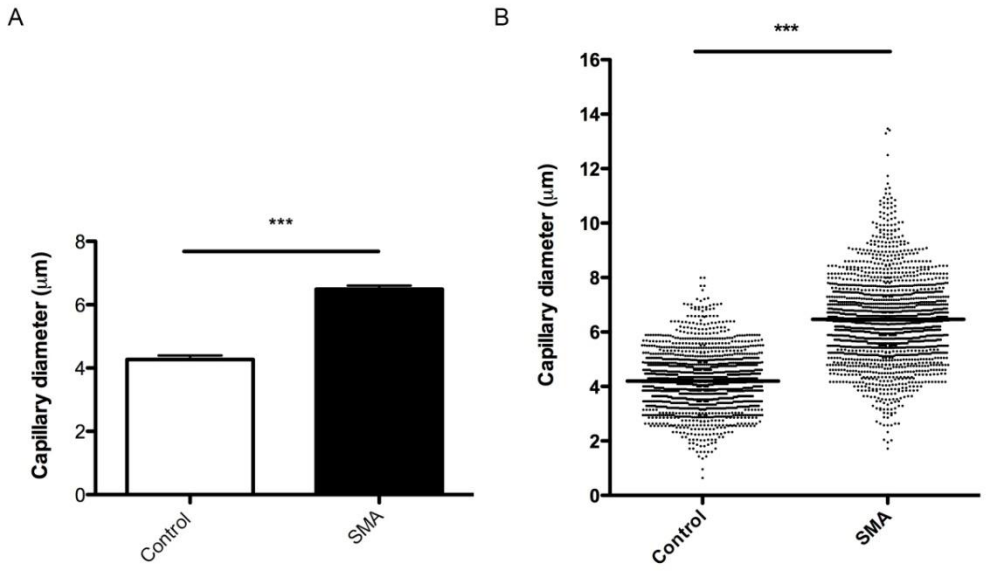

Figure 10 – Increased capillary calibre in Severe SMA skeletal muscle. *(A) Bar chart (mean ± s.e.m) quantification of capillary calibre in the LALc muscle of P5 Severe SMA mice (black bar) and control littermates (white bar). Unpaired, two-tailed t-test, *** = P<0.0001. N≥1650 profiles from ≥6 muscles from ≥3 mice for each bar. (B) Scatter plot of capillary calibres showing a wider distribution of diameters in Severe SMA mice with a positively skewed tail towards larger diameters.Black lines indicate mean capillary diameter.*

2.3.4 Consistent loss of capillary density in skeletal muscle, regardless of muscle position, fibre type, developmental sub-type or susceptibility to neuromuscular pathology in SMA

Having analysed the form and extent of the capillary bed in the LALc muscle in detail, the extent of the capillary bed in two other muscles was analysed. First the rostral band of the LAL (LALr) and then the abdominal *Transversus Abdominus* (TVA) muscle.

Despite being closely related anatomically and sharing the same innervation the two bands of the LAL muscle show varying susceptibility to pathology in SMA (Murray et al., 2008). The LALc muscle is vulnerable to pathology and shows high levels of denervation at late symptomatic time points with more than 95% of motor endplates denervated at P5 (Murray et al., 2008). The LALr however, is resistant and shows very little, to no pathology at P5 with less than 5% of motor endplates being denervated at this late symptomatic time point (Murray et al., 2008). The capillary density of the LALr muscle showed a 38% reduction in capillary density, closely mirroring the 36% reduction that was found in the LALc muscle (Figure 11). Observing a reduction in capillary density in skeletal muscle irrespective of the whether profound denervation of the muscles fibres is present or not is a key finding. The data suggests that the capillary phenotype we observed in Severe SMA skeletal muscle is not a result of muscle denervation. As well as their differing denervation status, the LALc and LALr are also of different developmental subtypes.

Muscles can be classed into differing developmental phenotypes on the basis of the rate at which mature neuromuscular junction (NMJ) formation occurs in the muscle (Pun et al., 2002). A mature NMJ will display clustered acetylcholine receptors to

which the presynaptic motor nerve and surrounding Schwann cells will be well aligned (Pun et al., 2002). In Fast Synapsing (FaSyn) muscles this process will take place over one day of embryonic development. In Delayed Synapsing (DeSyn) muscles this process can take up to five days of development (Pun et al., 2002). It has been suggested that this developmental phenotype could pre-determine muscle susceptibility to disease (Pun et al., 2002). The LALc muscle is of FaSyn while the LALr is of DeSyn developmental phenotype (Frey et al.,2000; Pun et al., 2002). Again, observing an almost identical reduction in capillary density in both the LALc and LALr suggests that developmental phenotype of a muscle does not affect the capillary defect. Another key difference between skeletal muscles, which could influence their capillary density, is their fibre type.

Muscles can be classified on the basis of their fibre contraction responses (Close 1964). Slow muscle fibres contract for long periods of time with little force, while fast fibres contract more rapidly and powerfully but fatigue more readily (Denny-Brown, 1929; Eccles and Eccles et al., 1960; Close, 1964). After examining the bands of the LAL, both of which are of a fast fibre nature, the slow fibre, abdominal *Transversus Abdominus* (TVA) muscle was analysed.

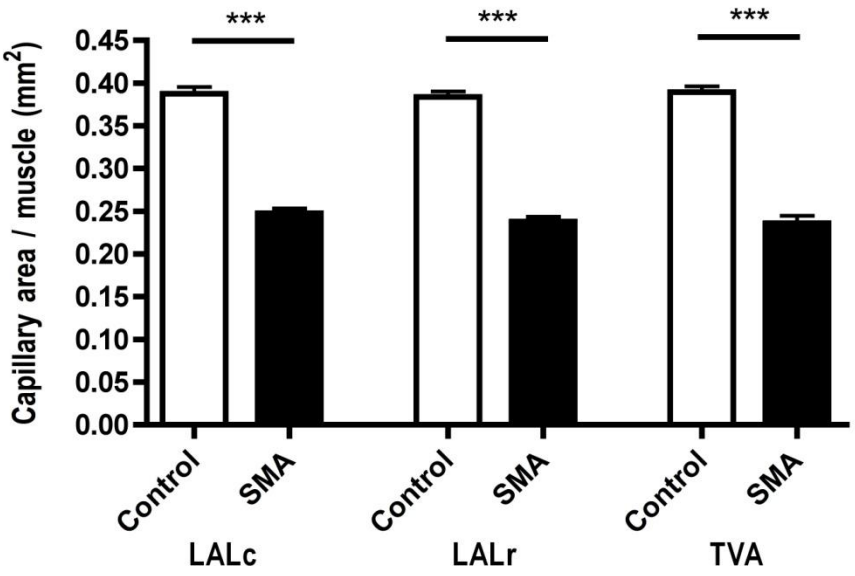

Figure 11 – Consistent reduction in Severe SMA skeletal muscle regardless of muscle position, developmental or fibre type*. Bar chart (mean ± s.e.m) quantification of capillary density in LALc, LALr and TVA muscles of Severe SMA mice (black bars) and control littermates (white bars). Unpaired, two-tailed t-test, *** =P<0.0001. N≥3 mice and n≥6 muscles for each bar.*

As well as being of a slow twitch fibre type the TVA is also susceptible to pathology in SMA (Murray et al., 2008). While analysing the two bands of the LAL muscle already allowed for the comparison of capillary density between pathologically vulnerable and resistant muscles, analysis of the TVA incorporates an important factor in the susceptibly of muscles to pathology in SMA: position in the body. In SMA, the upper and proximal muscles of the body are preferentially targeted, in particular the respiratory muscles and muscles of the upper limb (Lunn & Wang, 2008). The TVA is located in the abdominal and thoracic regions of the body, much more caudally positioned than the LAL muscles in posterior aspect of the neck. Here the capillary density of Severe SMA TVA muscle showed a 40% reduction in comparison to control littermates, again in line with the reduction that was observed

in both LAL muscles (Figure 11). This suggests that capillary density is reduced in Severe SMA muscles, regardless of their position in the body.

From the analysis of the LALc, LALr and TVA muscles, it can be suggested that capillary density is significantly reduced in Severe SMA skeletal muscle, regardless of muscle position in the body, muscle fibre type, developmental phenotype and of key interest, regardless of the level of denervation present in the muscle. The denervation which occurs in vulnerable muscles in the Severe SMA mouse model occurs postnatally (Monani et al., 2009; Murray et al., 2010). To address when this reduction in skeletal muscle capillary density occurred, the same selection of muscles were analysed in the same manner at two earlier time points; the early symptomatic P3 and pre-symptomatic P1 ages.

2.3.5 Reduction in capillary density is a postnatal event which occurs in parallel with motor neuron loss

The LAlc, LALr and TVA muscles were collected, stained, imaged and quantified in an identical manner to the previously described experiments, from neonatal P3 and P1 Severe SMA mice and their control littermates. In the Severe SMA model day of birth is considered to be P1. At the early symptomatic P3 time point, a reduction of 30-33% was observed in all three of the Severe SMA skeletal muscles when compared to their control littermates (Fig 12). This reduction is in line with the reduction previously found at the late symptomatic P5 time point. However, at the earlier P1 (birth) pre-symptomatic time point a similar reduction was not observed. Here, instead, the capillary density of all three Severe SMA muscles did not differ from their control littermates ($P>0.05$, One Way ANOVA). With Severe SMA

muscles retaining 96-99% of the capillary density observed in control littermates. Seeing no difference in the capillary density of Severe SMA and control muscles suggests that the capillary bed of Severe SMA skeletal muscle is normal at birth. The capillary beds of control and Severe SMA mice are comparable when imaged (Fig 12B) showing a similar structure and organisation. By P3 this similarity is lost, with control capillary beds already displaying a more compact and parallel network while Severe SMA capillaries retain the more loose, open looped arrangement. It is around this same time that the neuromuscular pathology found in the Severe SMA mice becomes apparent with SMA affected mice displaying NMJ defects in the TVA muscle (Sleigh et al., 2011). Observing the reduction in capillary density at this time, but not at birth, suggests that the defect is an early postnatal event which occurs in parallel with the neuromuscular pathology in this model, rather than as a consequence of it.

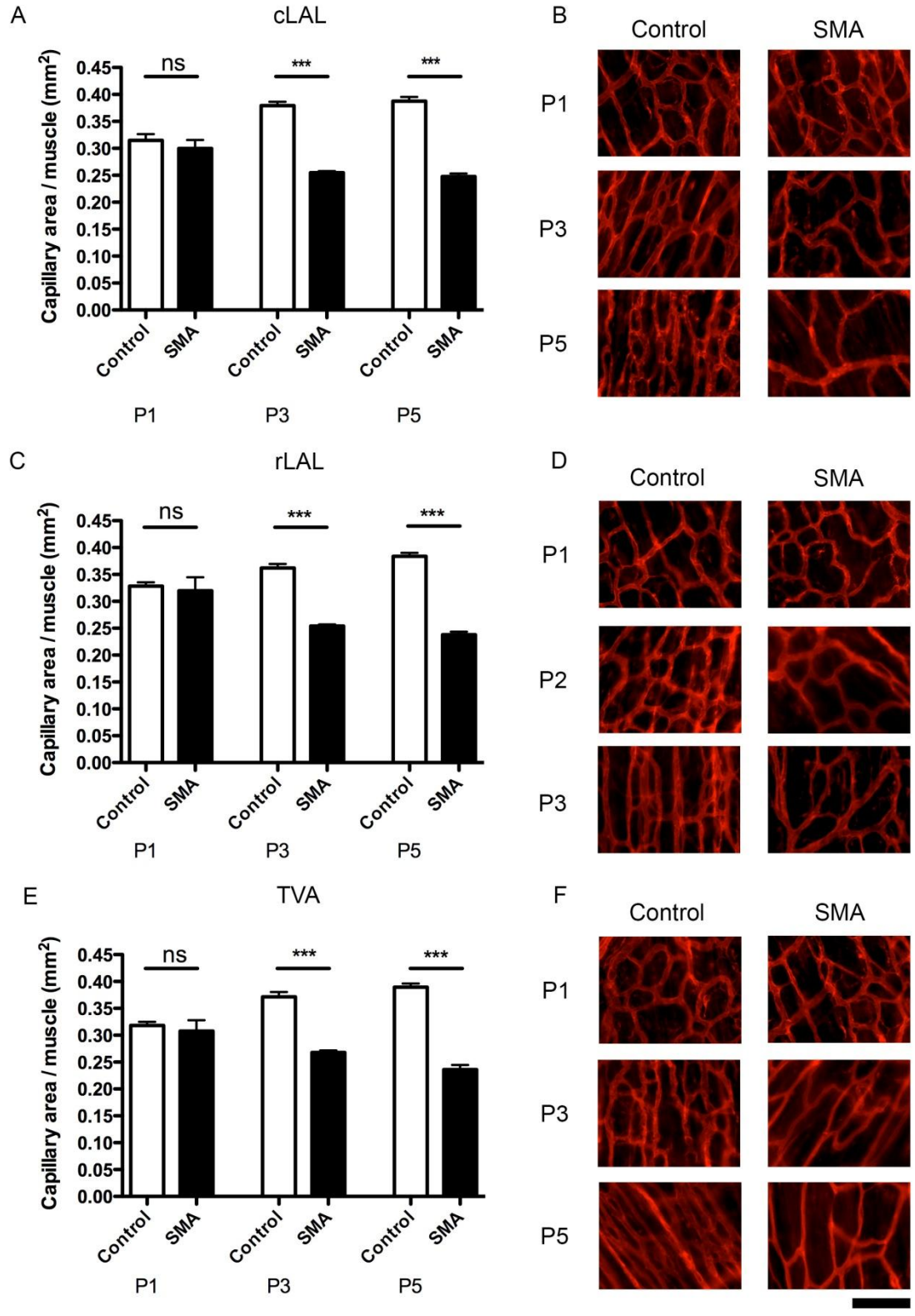
A
cLAL
Capillary area / muscle (mm²)
0.45
0.40
0.35
0.30
0.25
0.20
0.15
0.10
0.05
0.00
ns
***
***
Control
SMA
Control
SMA
Control
SMA
P1
P3
P5
B
Control
SMA
P1
P3
P5
C
rLAL
Capillary area / muscle (mm²)
ns
***
***
Control
SMA
Control
SMA
Control
SMA
P1
P3
P5
D
Control
SMA
P1
P2
P3
E
TVA
Capillary area / muscle (mm²)
ns
***
***
Control
SMA
Control
SMA
Control
SMA
P1
P3
P5
F
Control
SMA
P1
P3
P5

Figure 12 – Capillary density is reduced in P3 but P1 Severe SMA skeletal muscle. *(A) Bar chart (mean ± s.e.m) quantification of capillary density in the LALc muscle from pre-symptomatic (P1), early symptomatic (P3) and late symptomatic (P5) Severe SMA mice and control littermates. (B) Representative micrographs of GSL-1 labelled capillary bed of the LALc muscle in P1, P3 and P5 Severe SMAmice and control littermates. (C) Bar chart (mean ± s.e.m) quantification of capillary density in the LALr muscle from pre-symptomatic (P1), early symptomatic (P3) and late symptomatic (P5) Severe SMAmice and control littermates. (D) Representative micrographs of GSL-1 labelled capillary bed of the LALr muscle in P1, P3 and P5 Severe SMAmice and control littermates. (E) Bar chart (mean ± s.e.m) quantification of capillary density in the TVA muscle from pre-symptomatic (P1), early symptomatic (P3) and late symptomatic (P5) Severe SMAmice and control littermates. (F) Representative micrographs of GSL-1 labelled capillary bed of the TVA muscle in P1, P3 and P5 Severe SMAmice and control littermates. One Way ANOVA with Tukey post-hoc test, ns = no significance P>0.0, ***=P<0.0001. N≥3 mice and n≥6 muscles for each bar. Images are 40 x objective. Scale bar equals 50µm.*

2.3.6 A similar reduction in capillary density is observed in other mouse models of SMA

Having assessed the capillary defect in detail in the Severe SMA mouse model of SMA we sought to determine if a similar defect was present in other mouse models of SMA. In particular, the Taiwanese and 2Δ7 mouse models of SMA, both of which have an extended postnatal lifespan in comparison to the Severe SMA model.

2.3.6.1A significant reduction in skeletal muscle capillary density is observed in Taiwanese SMA model mice

The first model that was chosen to investigate was the Taiwanese. In comparison to the Severe SMA mice, Taiwanese SMA mice live for up to 11 days and develop an SMA phenotype at P6-7 when weight loss and motor deficits are apparent (Hsieh-li et al.,2000; Riessland et al 2010). From these mice the TVA muscle was collected and the capillary bed stained, imaged and quantified in the same manner as previous experiments. Here again, at a late symptomatic time point (P11) there was a

significant (P<0.0001, One Way ANOVA with post hoc Tukey) 45% reduction in capillary density in SMA muscle when compared to control littermates (Figure 13A, 13B). This confirmed the initial finding of the capillary defect in P5, late symptomatic Severe SMA mice in a second mouse model of SMA. As with the Severe SMA model a timeline analysis of capillary density was conducted.

As was seen in the Severe SMA mice, at birth the capillary beds of Taiwanese SMA and control littermates were indistinguishable (Figure 13B) and, when quantified, the capillary density in both conditions was comparable (P>0.05, One Way ANOVA with post hoc Tukey). The similarity between control and capillary density was present at postnatal day 3, when Taiwanese SMA mice are described as pre-symptomatic (Hsieh-li et al., 2000, Riessland et al., 2010). Again no significant difference was fond between the capillary density of control and Taiwanese SMA mice (P>0.05, One Way ANOVA with post hoc Tukey). When TVAs from P5 animals were analysed, a visible difference was present in the form and extent of the capillary beds (Figure 13B) of control and Taiwanese muscle. Capillary density of P5 Taiwanese SMA TVA muscle was reduced by 30 %, in comparison to control littermates. At this time Taiwanese SMA mice begin to display a distinguishable phenotype, lagging behind their control littermates in weight gain, suffering diarrhoea and displaying neuromuscular junction (NMJ) defects (Hsieh-Li et al.,2000; Riessland et al., 2010; Schreml et al.,2013). Here, as was seen in the Severe SMA model, defects in the capillary bed are not present at birth but develop postnatally.

As the timeline progressed, a more pronounced difference between the organisation of capillary beds was evident and by late symptomatic P8 and P11 time points the

difference in the form and extent of the capillary bed between Taiwanese and control littermates was drastic (Figure 13B). A 39% reduction in capillary density at P8 and 45% at P11 was seen between Taiwanese SMA and control skeletal muscle (Figure 13A). Which is similar to the 36% late symptomatic reduction observed in the shorter lived Severe mouse model. This not only confirms the initial finding of a significant reduction in capillary density in SMA skeletal muscle in a second mouse model of the disease, but also confirms the postnatal time line development of the capillary defect in a second model of the disease. Another commonly used mouse model of SMA is the 2Δ7 model, which has an increased lifespan in comparison to the Taiwanese model.

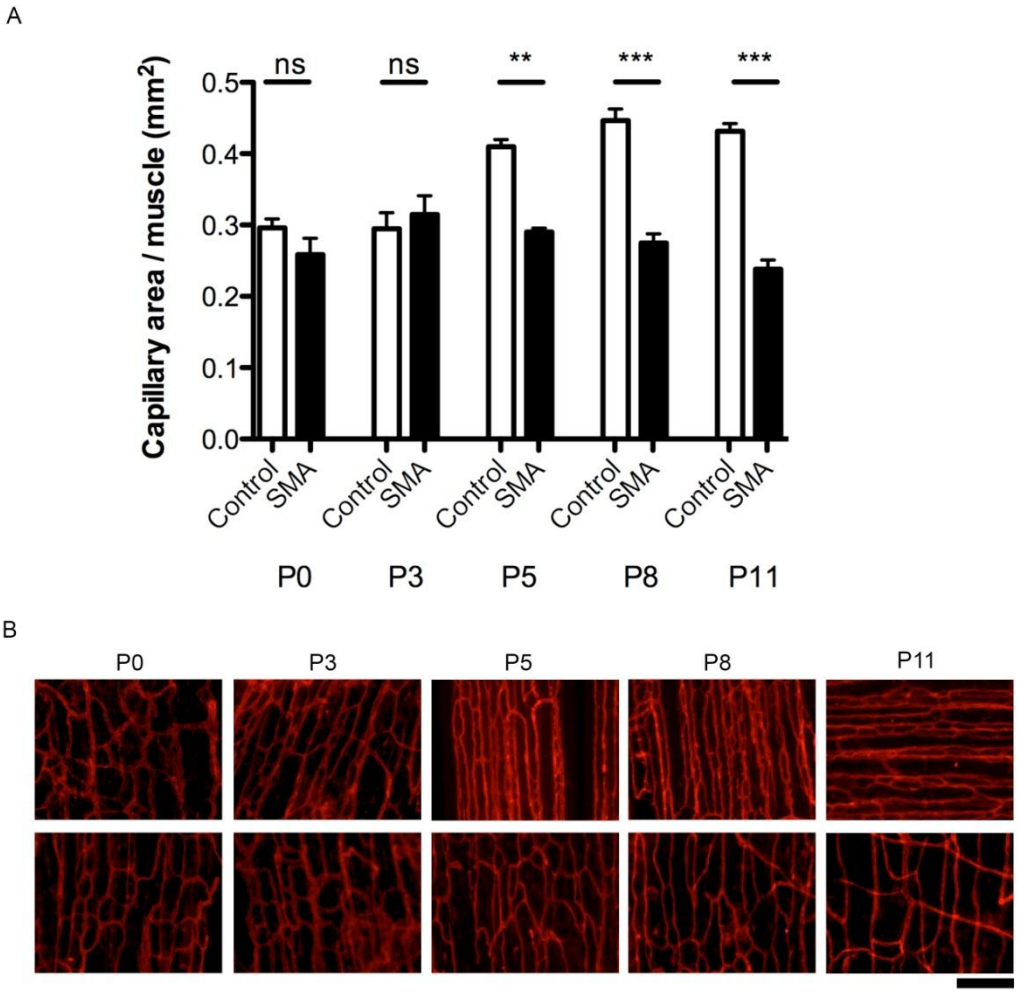

Figure 13 – Reduction in capillary density is evident by P5 in Taiwanese SMA skeletal muscle. *(A) Bar chart (mean ± .e.m) quantification of capillary density in the TVA muscle of pre symptomatic (P0, P3), early symptomatic (P5) and late symptomatic (P8,P11)* Taiwanese SMA mice *(black bars) and control littermates (white bars). One Way ANOVA with Tukey post-hoc test, ns = no significance P>0.0, **=P<0.001, ***=P<0.0001. N≥3 mice and n≥6 muscles for each bar. (B) Representative micrographs of GSL-1 labelled capillary beds of TVA muscle from P0,P3,P5,P8 and P11 Taiwanese SMA mice and control littermates. Images are 10x objective. Scale bar equals 50μm.*

2.3.6.2 A significant reduction in skeletal muscle capillary density is observed in SMNΔ7 SMA mice

SMNΔ7 SMA mice survive on average 14 days and develop an SMA phenotype by P6-7 (Kerr et al., 2000). These mice differ from the Severe and Taiwanese SMA models in that while possessing a copy of the incorrectly spliced human SMN2 the SMNΔ7 mice also carry a copy of the missing exon 7 transcript (Kerr et al., 2000). Again the TVA muscle was collected and the capillary bed stained for imaging and analysis.

The capillary bed of late symptomatic P14 SMNΔ7 SMA mice displayed a significant 37% reduction in capillary density in comparison to control littermates (P<0.001, One Way ANOVA with post hoc Tukey) (Figure 14B). This confirmed the initial finding of a reduced capillary density in SMA skeletal muscle when compared to control tissue in a third mouse model of the disease. When an earlier, pre-symptomatic time point (P6) was analysed (Figure 14B), a similar significant 31% reduction in SMA skeletal muscle capillary density was also observed (P<0.001, One Way ANOVA) (Figure 14A). This again confirming the development of the capillary defect is a postnatal phenomenon, in a third mouse model of the disease.

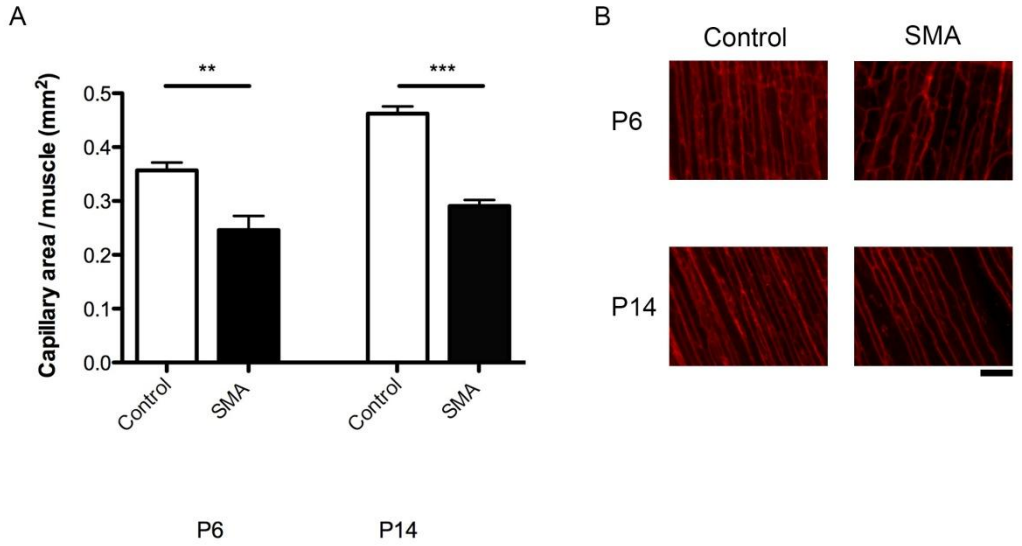

Figure 14 – Significant reductions in P6 and P14 SMNΔ7 capillary density. *(A) Bar chart (mean ±s.e.m) quantification of capillary density in the TVA muscle of early (P6) and late symptomatic (P14) SMNΔ7 mice (black bars) and control littermates (white bars). One Way ANOVA with Tukey post-hoc test, **=P<0.001, ***=P<0.0001. N≥3 mice and n≥6 muscles for each bar. (B) Representative micrographs of GSL-1 labelled capillary beds of TVA muscle from P6 and P14 SMNΔ7 SMA and control littermates. Images are 10 x objective. Scale bar equals 50µm.*

2.3.7 Post natal appearance and progression of the capillary defect

In the three mouse models of SMA examined, the capillary defect arises postnatally (Figure 12, Figure 13) and is first observed in line with the appearance of NMJ pathology reported in each model (Figure 15). As the disease progresses in each model, the reduction in capillary density becomes more pronounced (Figure 12, Figure 13). By examining tissue from three models of varying lifespan this progression of the capillary defect can be followed in comparison to normal skeletal muscle capillary bed development.

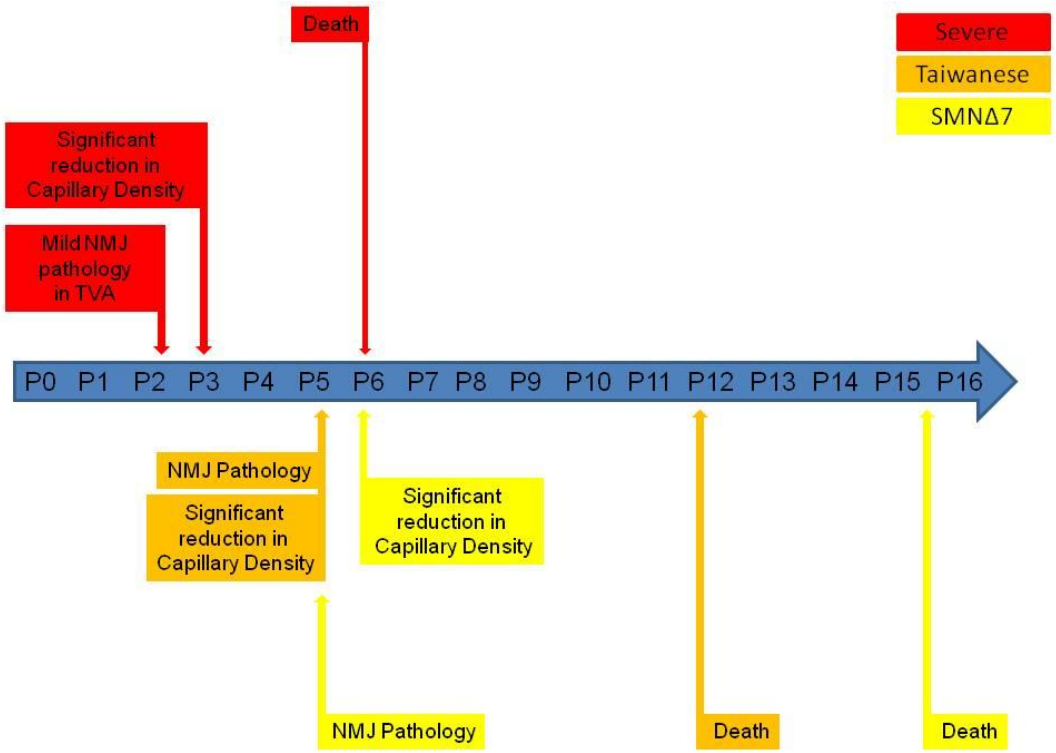

Figure 15 – A schematic showing the appearance of neuromuscular pathology and skeletal muscle capillary defects in the Severe-SMA, Taiwanese-SMA and SMNΔ7 mouse models of SMA.

When examined there are subtle morphological differences between the capillary beds of control skeletal muscles from the three models. The older P11 Taiwanese (Figure 16B) and P14 SMNΔ7 (Figure 16C) display a more compact and parallel capillary bed than the younger P5 control Severe model TVA muscle (Figure 16A). This follows the normal pattern of capillary development in skeletal muscle, where capillaries are seen to lengthen with the muscle and become rectangular in arrangement and parallel to the underlying muscle fibres (Wolffe et al., 1975). This pattern is still observed, but to a lesser extent, in the corresponding SMA TVA muscles.

When compared to the P5 Severe model muscle (Figure 16D), the capillary beds of the longer surviving P11 Taiwanese (Figure 16E) and P14 SMNΔ7 (Figure 16F) muscles show a more mature organisation. While the younger P5 Severe SMA muscle displays an open, loosely looped capillary network structure (Figure 16E), the P14 SMNΔ7 SMA skeletal muscle in particular displays a more parallel, rectangular arrangement of capillaries (Figure 16F). While the organisation of the capillary bed is somewhat improved in the longer surviving SMA muscle, capillary density is not (Figure12, Figure 13, Figure 14). This suggests that while an increased lifespan allows the SMA muscle to enhance the initial primary structure of the capillary bed the further angiogenesis required to develop the mature capillary bed does not occur.

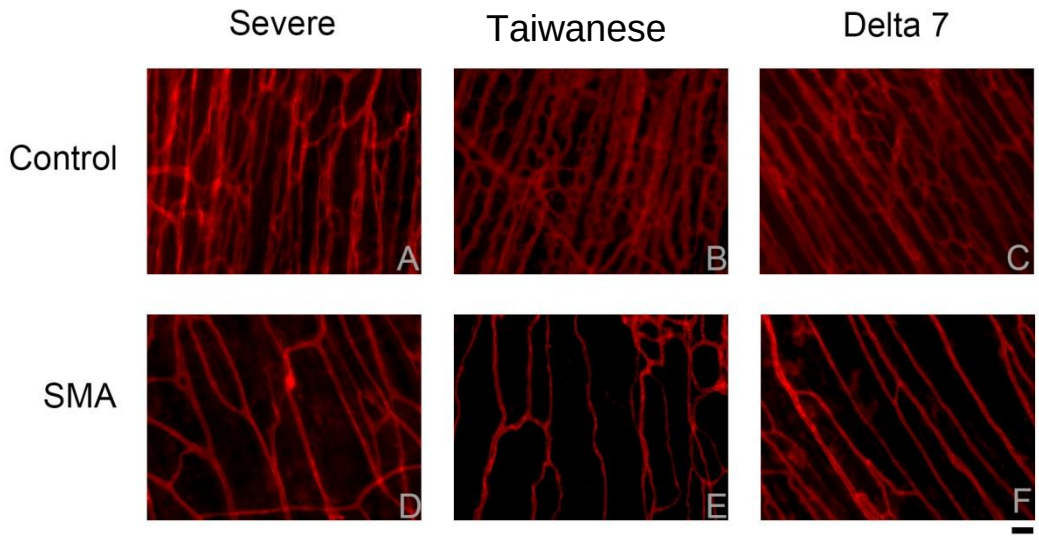

Figure 16 – Comparative capillary network maturity in the three mouse models examined. *Representative GSL-1 labelled skeletal muscle capillary beds from the TVA muscle at a late symptomatic time point in the Severe, Taiwanese and SMNΔ7 mouse models of SMA show almost identical late-stage pathology. Images are 10x magnification. Scale bar equals 50μm.*

2.4 Discussion

In this chapter a novel means of assessing the skeletal muscle capillary bed is presented. This simple and efficient method takes advantage of the almost two-dimensional capillary bed found in the small, thin, flat cranial and TVA muscles, which allows these muscles to be visualised and analysed in plan-view. The findings of this chapter show that the measurements obtained from this plan-view analysis were robust and repeatable across all regions of muscle, between phenotypically and regionally distinct muscles from the same animal and between muscles from different animals. Examining muscle in plan-view also allowed for the analysis of vessel structure, in particular, capillary calibre (diameter), a key component in determining the surface area of vessels. These finding suggest the method presented is a reliable means of assessing the form and extent of skeletal muscle capillary beds. It should be noted that the values presented in this study are relative and not absolute capillary density.

The findings of this chapter show that the capillary bed of skeletal muscle is altered in SMA mice. Initially the results of this chapter show that the form and extent of the skeletal muscle capillary bed is altered in late symptomatic (P5) Severe SMA Severe model SMA mice. These alterations in SMA muscle include a reduction in capillary density, an increase in capillary calibre and a decrease in the penetration of vessels through the muscle belly, when compared to control littermates.

Second, these findings show that the most striking alteration to the capillary bed, the reduction in its density was observed in a selection of phenotypically distinct muscles. Significant levels of capillary density reduction were observed in the cranially located fast twitch FaSyn LALc and DeSyn LALr and the abdominal slow

twitch TVA muscle. This suggests that the occurrence of the capillary defect is unaffected by the developmental phenotype, fibre twitch type and body position of the skeletal muscle examined.

Thirdly this work showed an almost identical reduction in capillary density in the LALr muscle which is resistant to neuromuscular pathology in the Severe model and the LALc muscle which is particularly susceptible to pathology in this model, displaying denervation of >95% of motor endplates (Murray et al., 2008). The finding that the capillary bed is altered irrespective of the level of denervation present in the muscle suggests that the capillary defect is the result of intrinsic defects in the skeletal muscle rather than neuronal pathology.

Fourthly this investigation revealed that while dramatically reduced at a late symptomatic (P5) timepoint, the capillary density of Severe SMA muscle was not significantly different from control littermates at birth (P>0.5, One WayANOVA, with post hoc Tukey). At birth Severe SMA mice are pre-symptomatic and show no neuromuscular pathology (Murray et al., 010). By P3 Severe SMA mice show neuromuscular pathology and are regarded as early symptomatic. At this early symptomatic stage the capillary beds of control and SMA skeletal muscle were observed to be significantly different (P>0.5, One Way ANOVA, with post hoc Tukey). These findings suggest that the capillary defect observed in SMA skeletal muscle is a postnatal phenomenon which occurs in line with the appearance of neuromuscular pathology.

Lastly it was observed that the capillary defect seen in the Severe model was also present in a second and third mouse model of SMA. Full time line analysis in the Taiwanese mouse model revealed a similar developmental pattern of the capillary

defect as was observed in the Severe model. At birth and pre-symptomatic time points no significant difference was observed between control and SMA capillary density ($P>0.5$, One Wan ANOVA, with post hoc Tueky). Again the capillary defect was first observed at an early symptomatic (P5) time point when neuromuscular pathology is first observed in this model (Schreml et al., 2013). This again suggests that the development of the capillary defect parallels that of neuromuscular pathology rather than occurring as a consequence of it. Analysis of a late (P14) and early symptomatic (P6) time point in the SMNΔ7 model confirms the presence of significant reductions in skeletal muscle capillary density at these stages of disease progression in a third mouse model of SMA

2.4.2 Effects of denervation on skeletal muscle capillaries

These results suggest that the decrease in capillary density observed in SMA skeletal muscle is a postnatal phenomenon which occurs in parallel with the neuronal pathology observed in the mouse models examined and not as a consequence of the denervation which occurs during disease progression.

An almost identical reduction in capillary density was observed in the LALr muscle, which is spared from neuronal pathology, as was seen in the LALc muscle which shows dramatic denervation and neuronal pathology in the Severe SMA mouse model of SMA (Murray et al., 2008). Both the LALr and LALc are fast twitch fibre type muscles (Erzen et al., 2000). While multiple studies have reported a reduction in capillary to muscle fibre ratio in response to denervation (Chernukh and Alekseeva, 1975, Borisov et al., 2000; Dedkov et al., 2002; Cebasek et al., 2006), experimental denervation of the *Extensor Digitorum Longus* (EDL), a fast twitch fibre type

muscle, did not result in capillary loss (Cebasek et al., 2006). As well as maintaining capillary number following denervation, the organisation and arrangement of capillaries within the EDL was also retained, with capillaries seen to be running parallel to muscle fibres before and after denervation (Cebasek et al., 2006). While the slow twitch fibre Soleus muscle showed a significant reduction in capillary number and perturbations of vessel organisation when subjected to denervation (Cebasek et al., 2006). This suggests that the capillary bed of fast twitch fibre muscles are unaffected by denervation. In contrast to this, the findings within this chapter report a dramatic alteration in the form and extent of the denervated fast twitch fibre type LALc muscle and also in the innervated fast twitch fibre type LALr. Observing such alterations in both muscles suggests that the capillary defect is not a consequence of denervation but that it occurs independently as a result of changes in the vascular system or the muscle, both of which have been described as being affected in SMA (Fidzianska and Wado, 1990; Tens et al., 1996; Stahas et al., 2008; Araujo et al., 2009; Rudnik-Schoneborn et al., 2010; Mutsaers et al., 2011) or as a failure of the capillary bed to develop properly.

2.4.3 Development of skeletal muscle capillaries

The initial vascular network is formed by the process of vasculogenesis, which describes the formation of vessels from angioblasts (Risau and Flamme, 1995). This primitive network is further developed by angiogenesis, the process by which new vessels form from a pre-existing network (Risau, 1997). The formation of capillaries in tissue is described by the classical studies of Clark who investigated vasculogenesis and angiogenesis in the tadpole tail (Clark, 1918; Clark, 1939).

Clark reported that following a period of primary differentiation the vascular system of the tadpole developed by sending out endothelial sprouts which were seen to anastomose with other nearby sprouts to form a putative capillary network (Clark, 1918). Growth of new capillaries in adult tissue was found to occur in the same manner, with sprouts anastomosing to form capillary loops (Clark, 1939). Later studies by Wolff et al describe the further development of the primary capillary network in skeletal muscle.

In their investigation Wolff et al injected India Ink into the hearts of rats ranging in age from embryonic to adult. Circulation of the dye allowed for the visualisation of the vascular network throughout the body, with the limb muscles in particular being examined in detail. In E17 skeletal muscles, a wide mesh of terminal vessels arranged in a polygon-shaped plexus reaching across the entire surface of the muscles were observed. As the animal age increased these meshes were seen to lengthen with the muscle, becoming rectangular in shape and parallel to muscle fibre direction (Wolff et al., 1975).

As was observed in the work of Wolff et al., the present study shows that the vascular network of both control and SMA Severe and Taiwanese mice is well established by birth, with the capillary network covering the entire muscle. Observing that the capillary bed of control and SMA skeletal muscle is indistinguishable at birth suggests that the initial development of the vascular network (vasculogenesis) is not impaired in SMA skeletal muscle. As the age of animals increased, capillaries in control skeletal muscle followed the pattern of development described by Wolff becoming more rectangular and parallel in arrangement (Figure 12, Figure 13) while capillaries in SMA tissue retained a more

loose open loop arrangement similar to that seen at birth (Figure12, Figure 13). Maintaining a more immature capillary bed suggests that while the vascular network is able to form in SMA skeletal muscle, the ability to develop beyond the primary capillary network is impaired. Formation of a mature vascular network is the result of complex angiogenic signalling involving multiple pathways and molecules (Rissau 1997). Given the knowledge that intrinsic molecular pathology is present in SMA skeletal muscle, which is found independently of denervation (Mutsaers et al., 2011), it is possible that angiogenic signalling pathways are also affected in SMA, resulting in the defective capillary bed observed in this chapter.

2.4.4 The Neurovascular Link

The patterning of blood vessels and nerves in peripheral tissues is shared (Mukouyama et al., 2002). In the skin arterioles and nerves are aligned as a result of nerve derived vascular endothelial growth factor (VEGF) directing the path of arteriolar growth (Mukouyama et al., 2002). In other tissues it is the nerves that rely upon vessels for development and differentiation (Shen et al., 2004). In the central nervous system neural stem cell neurogenesis is stimulated in regions where high levels of endothelial cell-derived growth factors are found (Shen et al., 2004). Not only is the development of the neural and vascular system closely related, the systems share regulatory and guidance signals (Eichman et al., 2005).

Neuronal axons are guided to their target by the growth cone, the highly motile distal tip of the axon (Tessier-Lavigne and Goodman, 1996; Dickson, 2002). Similarly, the distal region of capillaries display highly motile tip cells which function in a similar manner to growth cones, guiding capillaries. These tip cells are guided by VEGF

(Ruhrberg et al., 2002, Stalmans et al., 2002) but also by many signals used by the neural system to guide axons.

Neuropilin receptors along with semaphoring signals are known to function in repulsive axon guidance (Kolodhin et al., 1997; He and Tessier-Lavigne, 1997). The neuropilin 1 receptor is expressed in endothelial cells and neuropilin 1 mutant mice show multiple vascular defects, including impaired angiogenesis and insufficient vascular network development (Kawaksi et al., 1999). The neuropilin receptors have also been reported to be involved in vessel guidance (Herzog et al., 2001; Moyon et al., 2001; Yuan et al., 2002). Other notable pathways including PlexinD1 - Semaphorin (Gitler et al., 2004; Torrez-Vazquez et al., 2004; Gu et al., 2004) and netrin (Dickson and Keleman, 2004; Lu et al., 2004) signalling have been shown to have roles in guiding vessels.

These studies suggest a conservation of molecular mechanisms between the neural and vascular networks. In such shared systems perturbation of one network could highlight a potential area of defect in the other. Axon growth and guidance has been reported to be disturbed in SMA. A reduction in axon outgrowth is observed in SMA motor neurons in culture (Rossoll et al., 2003). This impaired growth was attributed to a reduction in β-actin mRNA in the growth cones of developing motor neurons (Rossoll et al.,2003) suggesting defects in the machinery required for axon growth in SMA. Along with this impairment in growth, defects in axon path finding have been reported in SMA (McWhorter et al., 2003). Knock-down of Smn in zebra fish resulted in axon pathfinding defects (McWhorter at al., 2003). If the growth and pathfinding ability of axons is affected by low levels of Smn, it is reasonable to suggest that the growth and organisation of blood vessels, which share angio-

neurogenic signals and guidance cues, could also be negatively impacted by the Smn reduction found in SMA. Such disturbances of the neurovascular link have been reported in neurodegenerative diseases such as Alzheimers Disease (Zlokovic, 2005; Zlokovic, 2008; Ruiz de Almodovar, 2009) and importantly, another form of motor neuron disease: ALS (Azzouz et al., 2004; Storkebaum et al., 2005; Zacchinga et al., 2008; Ruiz de Almodovar 2009; Hwang et al 2009).

2.4.5 Weaknesses of Study

Although every attempt was made to ensure that this study was as robust as possible, there is an area of weakness that should be noted: the lack of clinically relevant muscles selected for analysis, such as the proximal limb muscles.

Upper limb muscles show significant atrophy in SMA patients. While the vasculature of such large bellied muscles has been routinely analysed in previous studies of skeletal muscle, the measurements of capillarity obtained rely on the quantification of the capillary-to-muscle fibre ratio, which has been shown to underestimate capillary density by up to 75% (Cebasek et al 2010). In order to obtain a more accurate and reliable measurement of skeletal muscle capillary density the decision was made to analyse the capillary bed of the thin, flat LALc and LALr cranial muscles and the TVA of the abdomen. While the LAL muscles, which are responsible for independent ear movement in the mouse, have no corresponding human analogue they are a useful preparation to investigate skeletal muscle vasculature in SMA. As well as being a more anatomically appropriate preparation for the visualisation and analysis of the capillary bed, the pathology of the cranial muscles in SMA is well characterised and understood (Murray et al., 2008, Murray et

al., 2010). The decision was made to include the TVA muscle in this investigation to complement the LAL muscles as while also being a thin, flat muscle it is present in humans and is affected in SMA. However, work conducted by an honours project student under my supervision has revealed a similar reduction in proximal limbs muscles as that seen in the LAL and TVA muscles.

In brief, proximal limb muscles from P8 symptomatic Taiwanese SMA and control littermate mice were examined. A 63% reduction in capillary density was seen in Taiwanese SMA mice when compared to control littermates, along with a 57% reduction in the number of intramuscular arterioles in SMA muscle. These findings suggest that a similar level of capillary reduction occurs in both the thin, flat muscles used in this investigation and the clinically relevant proximal limb muscles.

4.4.4 Conclusion

From these results we can conclude that the form and extent of the skeletal muscle capillary bed is dramatically altered in mouse models of SMA. A substantial reduction in the density of the capillary bed was observed in all muscles examined, at early and late symptomatic time points, in three genetically distinct models of SMA. This reduction in capillary density is a postnatal phenomenon which occurs independently of denervation. The organisation of the capillary network within SMA skeletal muscle is also impaired, including an increase in capillary calibre and a reduction in the ramification of capillaries into muscle.

Chapter 3: Spinal cord capillary defects in mouse models of SMA

3.1 Introduction

In the previous chapter a significant vascular defect was identified and characterised in skeletal muscle, a key site of pathogenesis in SMA. The other principal pathogenic target being the spinal cord. Both of these tissues house key elements of the motor neuron: motor nerve terminals are found in skeletal muscle while motor neuronal cell bodies are located in the spinal cord. If capillary defects are present in skeletal muscle, the nerve terminal field of the motor neuron, could similar defects be found in the spinal cord where motor neurons originate? Alterations to the vasculature in either or both of these regions could contribute to the motor neuron pathology seen in SMA.

The term Motor Neuron Disease encompasses a variety of disorders which result from the degeneration of motor neurons and the atrophy of their associated muscles. Motor neuron diseases can be classified on the basis of the motor neuron populations affected in the disorder and these populations can be identified depending on their location within the nervous system. Upper motor neurons project from the motor cortex to the spinal cord, while lower motor neurons project from the spinal cord to skeletal muscle. In Primary Lateral Sclerosis (PLS) a progressive dysfunction of upper motor neurons is observed (Singer et al., 2006) while Amyotrophic Lateral Sclerosis (ALS) is characterised by progressive paralysis resulting from the death of upper and lower motor neurons (Cleveland & Rothstein, 2001). Spinal Muscular Atrophy (SMA) is characterised by the specific loss of lower motor neurons in the ventral horn of the spinal cord (Monani et al., 2005). In contrast to the adult onset PLS and ALS, SMA is a childhood form of motor neuron disease with motor neuron

loss occurring prenatally in the severest forms of the disease (Soler-Botija et al., 2002). Studies of control and Type I SMA foetuses have identified enhanced neuronal death from as early as 12 weeks of gestation, resulting in a progressive loss of motor neurons towards the neonatal period (Soler-Botija et al., 2002). This prenatal loss of motor neurons in the ventral horn identifies the spinal cord as a key site of pathogenesis in SMA.

The scarcity of large motor neurons in the spinal cord has long been established as the primary neuropathology in SMA (Chou & Fakadej 1971; Robertson et al., 1978, Steiman et al. 1980; Araki et al., 2003). In 1971 Chou & Fakadej reported a marked loss of large motor neurons in the spinal cord and brainstem of a Type I SMA patient. In a later study by Robertson et al., this loss was quantified in more detail, with SMA patient cords exhibiting a 95% reduction in large motor neuron cell bodies when compared to age matched controls (Robertson et al., 1978). While the level of neuronal loss reported is high, some motor neurons do remain, even in the most severe form of the disease. However, of the few remaining motor neuron cell bodies the vast majority are found to be structurally compromised (Chou & Fakadej 1971; Lippa & Smith 1988; Murayama et al., 1990; Matsumoto et al., 1992; Araki 2003).

Electron microscopy analysis of Type I patient spinal cord revealed the remaining SMA motor neuron cell bodies to be uncharacteristically rounded and distended with a swollen cytoplasm housing large numbers of mitochondria (Chou & Fakadej, 1971, Murayama et al., 1990). Further ultrastructural analysis highlighted the fragmentation of the rough endoplasmic reticulum and the accumulation of vesicles in the remaining cell bodies (Murayama et al., 1990). Immunohistochemical studies also revealed the accumulation of phosphorylated neurofilaments in the cell body

(Lippa & Smith, 1988; Murayama et al., 1990) along with granular ubiquitin deposits, while only occasional ubiquitin positive nuclei were observed in control cell bodies (Murayama et al., 1990; Matsumoto et al., 1992). Along with these accumulations in the cell body, chromatolysis, the disintegration of Nissl bodies, is commonly reported in SMA motor neurons (Chou & Fakadej, 1971; Robertson et al., 1978; Lippa & Smith 1988; Murayama et al., 1990; Araki et al., 2003). Importantly, when tissue from Type II patients was analysed the same severe motor neuron loss was observed but less structural perturbations were noted (Araki et al., 2003). Fewer swollen and chromalytic neurons were present, but no evidence of neurofilament accumulation (Araki et al., 2003), suggesting a link between neuronal defects and disease severity. Along with these changes to motor neuron number and structure, the glial population of the spinal cord was also affected in both patients (Chou & Fakadej 1971; Steiman, 1980; Brock et al., 1984; Araki et al., 2003; Garcia-Cabezas et al., 2004; Kuru et al., 2009) and SMA mouse models (Dahs et al., 2011; Caraballo-Miralles et al., 2013).

In histological analysis of Type I patient spinal cords intricate glial bundles were observed encasing motor neuron cell bodies and their atrophied terminal nerve endings (Chou & Fakadej, 1971). These glial bundles were seen to protrude into both the ventral and dorsal spinal roots in SMA patients (Chou and Fakadej, 1971) where aberrant expression of the astrocyte marker glial fibrillary acidic protein (GFAP) and its breakdown products were also reported (Brock et al., 1984). More recent studies have reported extensive gliosis in the ventral horn of Type I, II and III patient spinal cords (Araki et al., 2003, Garcia-Cabezas et al., 2004, Kuru et al., 2009) and in several mouse models of the disease (Dachs et al., 2011, Caraballo-Miralles et al.,

2013). An increase in astroglial number in the ventral horn was reported in symptomatic P11 SMNΔ7 SMA mice when compared to control mice (Caraballo-Miralles et al., 2013). A similar increase in astroglia number was found in newborn Severe SMA mice, but in the absence of high levels of motor neuron loss (Dachs et al., 2011). Taken together these findings suggest that cell populations in the spinal cord, beyond motor neurons alone, are affected in SMA. Similar spinal cord defects are noted in other pathologies including other forms of motor neuron disease, in particular Amyotrophic Lateral Sclerosis.

Loss of spinal motor neurons is reported in ALS patients (Boillee et al., 2006; Ravits et al., 2006) and mouse models of the disease (Gurney et al., 1994; Wong et al., 1995; Bruijn et al., 1997; Wang et al., 2003; Jonsson et al., 2004). As is observed in SMA, the surviving motor neurons also display abnormalities, in particular the accumulation of neurofilaments, once again seen in ALS patients (Hirano et al., 1984a; Hirano et al., 1984b) and mouse models (Gurney et al., 1994; Bruijn et al., 1997; Dal Canto & Gurney 1994). These similar defects in both ALS and SMA, emphasises the importance of the spinal cord in the pathogenesis of motor neuron diseases.

Having previously established alterations to the vasculature of SMA skeletal muscle, a key site of disease pathogenesis, we sought to examine the vasculature of the spinal cord, which is known to be altered in response to injury (Bartholdi,1997; Imperato, 1997) and in ALS (Zhong et al., 2008; Zhong et al., 2009; Miyazaki et al., 2011). Before examining the vasculature of the cord in pathological circumstances it is imperative to understand the development and structure of the cord vasculature in both human and murine systems.

The vasculature of the spinal cord is complex, with a network of extrinsic and intrinsic vessels supplying the neural tissue of the cord. In humans, 31 pairs of segmental vessels grow from the dorsal aspect of the aorta early in gestation. Beginning cranially and working caudally down the length of the cord these paired vessels begin to fuse, forming the midline anterior spinal artery (Roth & Zonenshayn, 2003). Along the length of the anterior spinal artery approximately 200 to 300 Central Arteries arise which enter the cord in the midline, to supply the anterior two thirds of the cord, including the ventral horns, with blood (Brockstein, 1994). On the posterior aspect of the cord two posterior spinal arteries are formed which supply the posterior third of the cord (Brockstein, 1994). These two sets of arteries and their resulting capillaries remain functionally and anatomically distinct. There are no anastomoses between the capillaries of the anterior and posterior spinal cord (Roth & Zonenshayn, 2003). This anatomical distinction in also found in murine spinal cord vasculature (Sturrock, 1990).

In humans the spinal cord is supplied by a single anterior and two posterior spinal arteries, while only a single posterior artery is observed in mice (Sturrock, 1990). The smaller number of posterior arteries is the major difference between human and murine cord vasculature. The murine vasculature develops prenatally as does its human counterpart. A dense network of vessels can be seen surrounding the cord by E10, with the anterior artery evident by E13 and a distribution of vessels throughout the cord tissue by E15 (Sturrock, 1990). Close examination of the murine cord revealed differences in the vessel density between the grey and white matter (Sturrock, 1990) a phenomenon also observed in the human cord (Brockstein, 1994).

The grey and white matter of the spinal cord receive their blood supply from distinct vessels. The end capillaries of the anterior and posterior spinal arteries supply the grey matter of the cord while the white matter is supplied by perforating branches of the pial plexus, an irregular network of vessels found within the pia mater (Brockstein,1994). In both humans and mice the white matter has a less dense capillary network than the grey mater (Sturrock, 1990; Brockstein, 1994). This reflects the greater metabolic needs of the grey in comparison to the white matter. The blood supply to the grey matter itself is variable with regions of the cord with larger areas of grey matter (such as those supplying limb musculature) possessing larger diameter vessels than regions with smaller grey matter areas (such as those supplying trunk musculature) (Brockstein, 1994). Although these changes in supply reflect the high metabolic needs of neuronal tissue, the spinal cord itself has a relatively sparse blood supply (Dommusse, 1974).

Classical studies describe the sparse nature of the spinal cord vasculature with Feeney &Watterson (1946) stating that "the nervous system is supplied with blood supply just enough for its minimum needs" and Woollam & Millen's (1958) observation that "man has just as much nervous system as he can supply with oxygen and no more". Taking the sparse nature of the spinal cord vasculature into consideration, any defect in the already limited supply could have dramatic consequences for the spinal cord. Such alterations to the cord vasculature are reported in variety of pathological conditions including multiple injury models and forms of motor neuron disease.

The vasculature of the spinal cord shows a dynamic response to injury (Bartholdi, 1997; Imperato, 1997). The initial response to compression of the cord is a reduction

in blood vessel number (Imperato, 1997). This is followed by an increase in vessel number at the site of injury. However, these new vessels often lack the astrocyte coating found surrounding central nervous system capillaries and these vessels soon disappear with the tissue debris as the site is cleared by macrophages. Devoid of vessels the resulting space becomes a fluid filled cavern (Imperato, 1997). This suggests that though neovascularisation occurs after injury, the new vessels formed are unstable and when the other cell types required to stabilise the new capillary network do not regenerate, the vasculature will be lost. While these compression injury studies prompt neovascularisation, X-ray irradiation injury paradigms result in a reduction in vessel density (Barthaldi et al., 2006). The spinal cord of neonatal rats was subjected to a single bout of x-ray irradiation. In comparison to control rats, the spinal cords of x-rayed rats showed a reduction in vessel density. When the rats were examined at later timepoints the density of vessels in control rat spinal cords increased. In comparison the vessel density in the x-rayed rats remained at the same low level observed in the animals sacrificed at earlier timpoints (Barthaldi et al., 2006). Not only was vessel number affected by x-ray, the structure of vessels themselves also altered. The vessels which remained in x-rayed spinal cords were found to be shorter and appeared swollen when compared to control vessels (Barthaldi et al., 2006). Impact injury to adult rat spine causes multiple alterations to endothelial cells which became swollen, with excessive ribosomes and Rough ER found in the cytoplasm (Barthaldi, 1997). Both the decrease in vessel density and alterations to the vessel cellular architecture had functional consequences. Reductions in grey and white matter perfusion were recorded 30 minutes after impact injury and perfusion continued to decline until severely low levels were recorded 8

hours post injury (Bartholdi, 1997). These investigations highlight how important vessel number and structure is for the normal functioning of the spinal cord vasculature.

Reductions in vessel number, alterations in vessel structure and reduced blood flow in the spinal cord have all been reported in SOD1 mutant ALS mice (Zhong et al., 2008, Zhong et al., 2009, Miyazaki et al., 2011). A 10-15% reduction in spinal cord total capillary length has been recorded in G93A SOD mutant mice (Zhong et al., 2008). Importantly, this reduction in overall capillarity was found to occur before any loss of motor neurons. Functionally this decrease in capillarity resulted in a 30-45% reduction in blood flow through the cord. Again this decrease in blood flow was recorded prior to motor neuron degeneration (Zhong et al., 2008). Observing such changes in the blood flow of the spinal cord before the onset of motor neuron degeneration suggests that impaired blood supply could be a contributing factor in motor neuron loss in the disease.

A reduction in spinal cord capillary density in SOD1 mutant mice when compared to control mice was noted by Miyazaki et al., 2011. This reduction was observed presymptomatically and became more pronounced as the disease progressed. The diameter of capillaries in the mutant mice was also found to decrease with age. This suggests that the architecture of the capillary bed as a whole is significantly altered as the disease progresses. As well as gross changes in capillaries, the association between capillaries and neurons, the neurovascular unit, was also disrupted in mutant mice. The expression levels of key tight junction proteins responsible for maintaining the close association between astrocytes and capillaries was decreased while a key component of the endothelial cell basement membrane, Collagen IV, was increased

(Miyazaki et al., 2011). These alterations were found throughout the cord, including the ventral horn where large motor neurons are housed. Again these changes were recorded before the degeneration or loss of motor neurons in the cord and importantly, similar alterations in key components of the neurovascular unit were found in human ALS patients (Miyazaki et al., 2011). These findings identify the disruption of the neurovascular unit as a consistent phenotype in both patients and mouse models of ALS and suggest that the breakdown of the neurovascular unit may contribute to motor neuron degeneration and loss in ALS. Another key neurovascular association, the blood spinal cord barrier (BSCB), is also compromised in both ALS patients (Leonardi, 1984; Donnenfeld, 1984; Engelhardt,1993; Henkel, 2004; Garbuzoa-Davis et al., 2012; Winkler, 2013) and mouse models of the disease (Garbuzo-Daiz et al., 2007; Zhang et al., 2008; Nicaise et al., 2009; Zhang et al., 2009; Garbuzova-Davis et al., 2011; Miyazaki et al., 2011).

The BSCB along with the blood brain barrier (BBB) are vital to prevent the entry of erythrocytes and plasma molecules into the central nervous system (CNS). Breakdown in these barriers can lead to penetration of toxic substances into the CNS. Early investigations of cerebrospinal fluid (CSF) reported significantly higher levels of total protein in ALS patient CSF when compared to age matched controls (Leonardi et al., 1984), suggesting that unwanted proteins are able to leak through these barriers in ALS patients. Post-mortem analysis also revealed a build up of non CSF proteins in ALS patient spinal cords, in particular inflammatory and immune cell infiltration (Donnenfeld 1984, Engelhardt 1993, Henkel 2004). Build up of these proteins suggests impaired barrier permeability in ALS. Along with this accumulation of unwanted cells and proteins in the CNS of ALS patients, studies

have also reported a decrease in the expression of proteins key in maintaining CNS barrier integrity (Henkel et al., 2009).

Quantitative-reverse transcriptase PCR analysis of ALS patient spinal cord samples showed a decrease in the mRNA expression of tight junctional proteins (Henkel et al., 2009). A similar reduction in tight junction marker expressions is also observed in mutant SOD ALS rats (Nicaise et al., 2009). These proteins including Zona-Occludens 1, Occludin and Claudin-5, are essential to maintain the integrity of the CNS barriers. Reduction in the expression of these proteins suggests that the BBB and BSCB associations are compromised in ALS. This breakdown of the BBB and BSCB is a commonly reported feature of mutant SOD mice (Garbuzova-Davis et al., 2007; Zhong et al., 2008; Zhong et al., 2009; Miyazaki et al., 2011).

Electron microscopy studies of G93A SOD1 mutant ALS mouse spinal cord showed significant alterations to all components of the BBB and BSCB (Garbuzoa-Davis et al., 2007). Disorganised and degenerating mitochondria were seen in endothelial cells and the neuropill. Cells, including endothelial cells, astrocytes and their foot processes along with motor neurons, were swollen and a number of degenerating endothelial cells were also observed (Garbuzova-Davis et al., 2007). Importantly, these alterations were observed at early stages in the disease process as well as with disease progression. This suggests that impairment of the CNS barriers could contribute to disease progression. When analysed functionally the integrity of the BSCB was found to be compromised, with leakage from spinal cord microvessels observed from the earliest disease stages analysed (Garbuzova-Davis et al., 2007). Similar barrier leakage is also observed in mutant SOD1 ALS rats (Nicaise et al., 2009). Again, highlighting the importance of CNS barrier integrity in motor neuron

health, many studies have the revealed the presence of BSCB defects prior to motor neuron degeneration (Zhong et al., 2008; Zhong et al., 2009; Miyazaki et al., 2011).

In 2008 Zhong et al., reported micro-haemorrhaging, reductions in microcirculation and hypoperfusion in SOD 1 mutant mice before any motor neuron degeneration was observed. Disruptions to the endothelium, tight junction and basement membrane components of the neurovascular unit have been noted presymptomatically in the same mouse model of ALS (Miyazaki et al., 2011). This damage to the spinal cord vasculature was shown to be one of the earliest pathological events in SOD 1 mutant mice (Zhang et al., 2008), suggesting that alterations to the spinal cord vasculature could contribute to the degeneration of motor neurons in ALS.

Based on our finding in skeletal muscle and the evidence that spinal cord vasculature is altered in other forms of motor neuron disease, we hypothesised that the capillary bed of spinal cord could be altered in SMA. We also hypothesised that any alteration to the spinal cord capillary bed would affect the ability of the network to supply oxygen to the cord tissue. To examine this, we looked for evidence of hypoxia in the spinal cord using an *in vivo* marker of tissue hypoxia: Pimonidazole Hydrochloride (Hypoxyprobe $^{TM-1}$).

Pimonidazole Hydrochloride (Hypoxyprobe $^{TM-1}$) in a nitroimidazole compound. Nitroimidazole compounds are derivatives of the organic, ring compound imidazole which contain a nitro functional group ($-NO_2$) (Carreauet et al., 2011). Nitroimidazoles, including Pimonidazole Hydrochloride, are reductively activated in cells with a oxygen concentration less than 14 micromolar. This oxygen concentration is equivalent to an oxygen tension of 10mmHg at 37°C. Physiologic

oxygen tension differs depending on the body tissue and ranges between 35mmHg in the brain to 70mmHg in the kidney (Carreau et al., 2011). The activation of Pimonidazole Hydrochloride therefore only occurs in hypoxic cells. This activation allows Pimonidazole Hydrochloride to bind to thiol groups in proteins, peptides and amino acids. Primary antibodies targeted against these Pimonidazole Hydrochloride-thiol adducts allows for the detection of tissue hypoxia by immunochemical means. By administrating Pimonidazole Hydrochloride to SMA mice and control littermates the presence or absence of hypoxia in key elements of the spinal cord was evaluated.

Here the novel means of measuring capillary density described in Chapter 2 was modified and applied to sections of spinal cord. Capillary density in these sections was quantified using immunohistochemical staining and fluorescent microscopy. The integrity of the blood spinal cord barrier was also analysed using immunohistochemical staining and fluorescent microscopy. Capillary density, when measured via immunofluorescence, was significantly decreased in Taiwanese SMA mice when compared to control littermates. Timeline analysis of capillary density showed no difference in the extent of the capillary bed between SMA and control littermates at birth. A reduction in capillary density is also observed in the less severe SMN2Δ7 model of SMA at late symptomatic time point. Investigation of tissue hypoxia using Piminodizole Hydrochloride showed an increase in the number of hypoxic neurons in the ventral horn of Taiwanese SMA spinal cords when compared to control littermates.

3.2 Methods

3.2.1 Ethics Statement

All animal experiments were approved by a University of Edinburgh internal ethics committee and were performed under license by the UK Home Office (Project License number 60/3891).

3.2.2 Animal Husbandry

(SMN2)2Hung Smn1^{tm1Hung}*/J* mice (originally received from Brunhilde Wirth in Koln) on a congenic FVB background were maintained as heterozygous breeding pairs under standard SPF conditions in animal care facilities in Edinburgh. All animal procedures and breeding were performed in accordance with Home Office and institutional guidelines. Retrospective genotyping this strain was carried out using standard PCR protocols detailed in previous chapters. *Smn+/-;SMN2;Δ7* (Jackson labs strain no. 005025) breeding pairs were maintained in animal care facilities in Oxford. For this strain dissection of the vertebral column was performed in Oxford by James Sleigh and shipped to Edinburgh. All genotyping of this colony was performed in Oxford by James Sleigh.

SMA mice and control littermates were sacrificed by an overdose of anaesthetic administered via intraperitoneal (IP) injection of sodium pentabarbitol (Euthenal). The mice were monitored closely following injection.

3.2.3 Genotyping

Retrospective genotyping of Taiwanese SMA and control littermate mice was performed as per the Genotpying protocol described in earlier chapters (Chapter 2)

3.2.4 Administration of Pimonidazole Hydrochloride 1

Whole Taiwanese litters aged P5 were injected with the hypoxia marker Piminodizole HCL 1 (PIMO). The P5 timepoint was selected as this is the earliest timpoint in the Taiwanese SMA mice that a reduction in blood vessel density is observed in the spinal cord. A single 60m g/kg dose of PIMO was administered via intraperitoneal (IP) injection. After injection mice were returned to their cage with their parents for an hour, during which time the mice were closely monitored. During this time PIMO was delivered to the body tissue via the bloodstream. In mice, PIMO has a plasma half of 25 minutes. This hour long period between injection and removal from the animal facility allows for the distribution of PIMO and its clearance from the plasma.

3.2.5 Tissue Collection

3.2.5.1 Pimonidazole Hydrochloride 1 injected mice

90 minutes after injection with PIMO, Taiwanese SMA mice and control littermates were sacrificed by an overdose of anaesthetic administered via intraperitoneal (IP) injection of sodium pentabarbitol (Euthenal). Mice were sacrificed in the order they were initally injected with PIMO. Each injection was timed to ensure that each animal was exposed to PIMO for the same amount of time and given the same time to clear residual unbound PIMO from the plasma. At the time of tissue collection

PIMO will already be bound to any hypoxic cells in the body tissues. During harvesting, tissue becomes anoxic. The very low levels of PIMO remaining in the plasma at the time of collection should prevent any PIMO binding as a result of dissection anoxia. To further ensure this, dissections were performed rapidly with tissues being collected and fixed in under five minutes.

3.2.6 Dissection

All pre-fix dissections were performed in oxygenated mammalian physiological ringer (mM: NaCl 120, KCl 5, $CaCL_2$ 2, $MgCl_2$ 1, NaH_2PO_4 0.4, $NaHCO_3$ 23.8, Glucose 5.6). All post-fix dissections were performed in 0.1M PBS.

3.2.6.1 Vertebral Column

Following injection with anaesthetic, the mice were monitored closely. When no breathing was observed for a full minute and neither footpad or tail stimulation evoked a response, the mice were decapitated. Following decapitation the skin ws removed from the abdomen of the mice and the forelimbs were removed. The chest wall and abdominal musculature was then removed as if performing a TVA muscle dissection. The contents of the thoracic, abdominal and pelvic cavities were removed, leaving the intact vertebral column attached to the hindlimbs. Finally, the hindlimbs were removed leaving the full length of the vertebral column with the spinal cord intact within. This preparation was then transferred to a bijou tube containing approximately 5mls of 4% PFA and was left to fix overnight, at 4°C on a rocking platform. The following day the preparation was washed repeatedly in 0.1M PBS to remove excess fixative.

3.2.7 Tissue preparation

3.2.7.1 Cryopreservation

Before being sectioned with a cryostat the vertebral columns were cryoprotected. Columns were added to 15ml Falcon tubes filled with a 30% sucrose solution (made up in 0.1M PBS) and left until they had sunk to the bottom of the tubes. The columns were then embedded in a 50:50 solution of OCT (Cell Pathology) and 30% sucrose solution. The columns were transferred to tapered easy peel plastic embedding moulds filled with the OCT-sucrose solution and were left for one hour, at room temperature, on a rocking platform. After this acclimatisation period the columns and their surrounding embedding solution were frozen on dry ice. The resulting solid blocks were stored at -80°C until sectioning. Columns from very young neonates (P0) were embedded whole with the cervical region (cranial end of the vertebral column) flat on the base of the mould – so it would be cut first. Columns from older mice (P5 and P11) were split into cervical, thoracic and lumbar regions and embedded in three individual moulds. In each case the superior cut edge of each vertebral/cord unit was embedded flat to the base of the mould.

3.2.7.2 Tissue Processing for wax embedding

Following fixation the P5 vertebral columns were dehydrated in the Centre for Integrative Physiology histology department tissue processor, using standard protocols. The columns were then cut in half at the mid point of the thoracic region and were embedded in paraffin wax. As above, the cervical region and most superior cut edge of the column were embedded flat to the base of the mould. The blocks were stored at 4°C until sectioning.

3.2.8 Cryostat Sectioning of Vertebral Column

P0, P5 and P11 columns were sectioned at a thickness of 10µm on a Leica cryostat. Ten to twelve individual sections were collected onto each superfrost slide. Slides were stored at -20°C until staining.

3.2.9 Microtome Sectioning of Vertebral Column

P5 columns were sectioned at a thickness of 16µm on a Leica microtome. Adjacent sections from the beginning, middle and end of tissue ribbons were floated out in a water bath at 42°C and were mounted on superfrost slides. The resulting slides were stored at 4°C until staining.

3.2.10 Immunohistochemistry of Frozen Sections

3.2.10.1 PECAM 1 Capillary Staining

Before staining slides were removed from -20°C storage and were left at room temperature to defrost. Once defrosted the slides were blocked in immunoglobulin G protease-free standard blocking solution (0.2% BSA, 0.5% Triton-X 100 (TX100) in PBS, for 30 minutes at 4°C. To visualise the spinal cord capillary bed, slides were then incubated overnight with goat anti mouse PECAM-1 primary antibody (R&D Systems Cat. No. AF3628) at a concentration of 1:750 in standard blocking solution at 4°C. The following day slides were washed for 6x5 minutes in 0.1M PBS at room temperature on a rocking platform. After washing slides were incubated with donkey anti goat Cy3 conjugated secondary antibody (Jackson ImmunoResearch Laboratories Inc) made up in standard block at a concentration of 1:250, for 1 hour at 4° C in the dark. Slides were washed for the final time for 6x5 minutes in 0.1M PBS,

at room temperature on a rocking platform. At all times slides were protected from exposure to light. Following this final washing series, slides were mounted with glass coverslips in Mowiol (10% mowiol, Polyscience Inc, 20% glycerol, 50% 0.2M Tris buffer pH 8.5, 3% 1,4-diazobicyclooctane made up in distilled water), the added 1,4-diazobicyclooctane acting as an anti-fade reagent. The mounted slides were left overnight in the dark, at room temperature to set before visualisation and imaging the following day.

3.2.10.2 Blood Spinal Cord barrier Double Labelling Staining

As with PECAM 1staining, frozen sections were defrosted and then blocked for 30 minutes. To visualise key components of the blood spinal cord barrier, slides were then incubated overnight at 4°C with rabbit anti mouse Aquaporin 4 (Abcam ab125049), rabbit anti mouse Claudin 5 (Abcam ab59720 and rabbit antimouse Zona-Occludin 1 (Abcam ab53765) primary antibodies at a concentration of 1:100 in standard blocking solution. The following day slides were washed for 6x5 minutes in 0.1M PBS at room temperature on a rocking platform. After washing slides were incubated with swine anti rabbit FITC conjugated secondary antibody (Dako) made up in standard block at a concentration of 1:40, for 1 hour at 4° C in the dark. Slides were then washed for 6 x 5 minutes in 0.1M PBS at room temperature, on a rocking platform. To visualise the spinal cord capillary bed, slides were then incubated with rhodamine conjugated Griffonia Simplicifolia Lectin 1 (GSL-1) at a concentration of 1:100, made up in 0.1M PBS, for 1 hour at 4°C in the dark. GSL-1 was selected as the means of visualising the capillary bed in double labelling experiments as it is not an antibody and could therefore not cross-react with the antibodies used to label the

blood spinal cord barrier. Slides were then washed and mounted as previously described.

3.2.10.3 Capillary and Motor Neuron Double Labelling Staining

The capillary bed was labelled with PECAM 1 as previously described. To visualise motor neurons in the spinal cord, slides were then incubated overnight in anti mouse SMI-32 primary antibody (a gift from Professor Siddharthan Chandran, University of Edinburgh) at a concentration of 1:500 in standard blocking solution at 4°C. The following day slides were washed for 6 x 5 minutes in 0.1M PBS at room temperature on a rocking platform. After washing slides were incubated with donkey anti mouse Alexalfuor 488 conjugated secondary antibody (Dako) made up in standard block at a concentration of 1:250, for 90 minutes at room temperature in the dark. Slides were then washed and mounted as previously described.

3.2.10.4 Cresyl Fast Violet Staining

Nissl staining, to identify the grey and white matter regions of the spinal cord, was performed using cressyl fast violet (CFV) staining. Again frozen sections slides were allowed to defrost and were rinsed in tap water before incubation in 0.2% CFV solution for 10 minutes. Slides were then rinsed in tap water and the intensity of staining checked under a Zeiss light microscope. Slides were further incubated with CFV if required, with staining checked at the end of every additional minute. When the distinction between grey and white matter was clearly evident slides were mounted in DPX, mounted and left overnight at room temperature in a fume hood to set.

3.2.11 Immunocytochemistry of Paraffin Sections

Slides of sectioned spinal cord were deparaffinised in xylene for 20 minutes (two separate xylene solutions for 10 minutes each). After dewaxing the slides were rehydrated in a descending ethanol series (100% x2, 90%, 70% and 50%) for 5 minutes in each ethanol percentage. Slides were then washed in 0.1% Tween in distilled water for 2 minutes followed by a further 2 minutes washing in 0.1% Tween in Tris-buffered saline (TBS), both washes performed on a rocking platform. Slides were then incubated for 5 minutes in 3% Hydrogen Peroxide solution to quench tissue peroxidise. Slides were washed again for 2 minutes in 0.1% Tween-TBS on a rocking platform. Antigen retrieval was performed by heating slides in sodium citrate buffer for 20 minutes in a water bath heated to 90°C. Following heating slides were removed from the water bath and left in the sodium citrate buffer for at least 20 minutes to cool to room temperature. Slides were blocked in immunoglobulin G protease-free standard blocking solution (0.2% BSA, 0.5% Triton-X 100 (TX100) in PBS) for 10 minutes at room temperature. Slides were then incubated with FITC anti MAb1 primary antibody (Hypoxyprobe, Catalog Number: HP2-100Kit) at a concentration of 1:50 made up in standard blocking solution, for one hour at room temperature. Slides were washed 3 x 2 mins in 0.1% Tween-TBS on a rocking platform. After washing, slides were incubated with HRP linked rabbit anti-FITC secondary antibody (Hyproxyprobe, Catalog Number: HP2-100Kit) at a concentration of 1:50 made up in standard blocking solution, for 30 minutes at room temperature. Slides were washed 3 x 2 mins in 0.1% Tween-TBS on a rocking platform. Slides were then incubated with DAB (Vector Laboratories, SK-4100) for 7 minutes before being flushed with distilled water to end the DAB reaction. Slides

were then stained with CFV as previously described. When the desired intensity of staining was achieved slides were dehydrated in an ascending ethanol series (50%, 70%, 90%, 100% x2) for 5 minutes in each ethanol percentage. Slides were then briefly dipped in xylene before being mounted in DPX and left overnight, at room temperature, in a fume hood to set.

3.2.12 Imaging

Micrographs for the reconstruction of spinal cord sections, calculation of capillary density, for the analysis of blood spinal cord barrier integrity and of double labelled capillary bed and motor neurons were captured using a standard inverted epifluorescence microscope (Olympus 1X71) combined with a chilled CCD camera (Hammamatsu C4742-95) and OpenLab (Improvision) image capture software. Cy3 and rhodamine labelled capillaries were imaged using 550nm excitation and 570nm emission optics. FITC labelled blood spinal cord barrier components were imaged using 494nm excitation and 520nm emission optics. Alexafluor 488 labelled motor neurons imaged using 494nm excitation and 520nm emission optics. Micrographs of CFV and DAB stained spinal cord sections were captured using a standard upright light microscope (Leica DM LB) combined with a Leica DFC480 camera and LAS AF Lite image capture software.

3.2.13 Quantification and Analysis

3.2.13.1 Quantifying capillary density

Any section with poor quality staining, folding or those that had been damaged during sectioning were excluded from analysis. For capillary density calculations three sections per slide from a minimum of three slides for each mouse were imaged.

To calculate capillary density the spinal cord was divided into four regions; dorsal left, dorsal right, ventral left and ventral right. Within each quadrant three radial lines of 40x images, originating from the central canal and extending to the edge of the cord, were captured. Using adjacent CFV stained slides to distinguish between white and grey matter each of these lines could be divided into grey and white matter, resulting in images from the following regions; dorsal left grey and white, dorsal right grey and white, ventral left grey and white and ventral right grey and white. All images were analysed blind. Images from all spinal cord regions were first enhanced in Adobe Photoshop (CS6) for contrast and brightness. This ensured that definite vessel borders were visible and also prevented any fine capillary structures from being lost and discounted. Any out of focus images where capillaries appeared blurred or those where background was too high to completely isolate capillary structures were excluded from further analysis. Using Image J (NIH) the enhanced images were converted to binary. These binary images were produced solely for quantification. In the resulting binary images capillaries were assigned black and spinal cord background white, allowing for the ratio of black to total white pixels to be calculated. This produced a value for capillary area per field of view. Knowing the area of a 40x field of view the results could be presented per unit area of spinal cord.

3.2.13.2 Spinal Cord Reconstructions

Reconstructions of spinal cord sections in their entirety were created using Adobe Photoshop (CS6). Overlapping 10x magnification images covering whole sections were captured and then enhanced in Adobe Photoshop for contrast and brightness. By reducing the opacity of the images common features between individual images

could be identified and matched. This allowed for individual images to be stitched together to create a montage of the whole section. To achieve a more uniform image the resulting montages were converted to black and white. In these montage images spinal cord background is black and capillaries are white.

3.2.13.3. Quantification of Hypoxic Cells

Any section with poor quality staining, folding or those that had been damaged during sectioning were excluded from analysis. Using CFV staining as a guide the spinal cord was divided into four regions; dorsal left, dorsal right, ventral left and ventral right. Within each quadrant a single x40 magnification image was captured at the boundary between grey and white matter. Three sections per slide from a minimum of three slides for each mouse were imaged. All images were analysed blind. The automated Image J (NIH) Huang setting was then used to threshold the images. Cells below the defined intensity were removed from the image, while cells above the set threshold remained. The remaining cells having been DAB labelled in the PIMO reaction. The number of these DAB and CFV Nissl labelled cells present after the threshold step was then counted using the cell counter plug-in in Image J (NIH).

3.2.13.4 Analysis

All data were collected using Microsoft Excel software and were graphed and analysed using GraphPad Prism software. Charts shown are mean ± s.e.m. In all analyses statistical significance was considered to be $p < 0.05$. Tests used are detailed in figure legends.

3.3 Results

3.3.1 Quantification of Spinal Cord Capillary Density

In the previous chapter a novel method of measuring capillary density was presented. This technique calculated the area of skeletal muscle covered by capillaries. In this chapter an adapted version of this capillary density measurement is applied to sections of spinal cord.

When calculating capillary density in skeletal muscle the muscles were sampled systematically, with 40x magnification images captured in the medial, endplate and lateral regions of the muscle at a stipulated number of fields of view apart. The structure of the spinal cord is comparatively more complex than skeletal muscle, containing a variety of cell types, structures and regions. This means the cord can be segregated in a variety of ways either on the basis of body axis position (dorsal/ ventral) or cell type (grey/white matter). To ensure that capillary density was measured across entire spinal cord sections, the cord was divided into identifiable regions using CFV staining of Nissl bodies (Figure 1).

Initially, the cord was divided into quadrants through the central canal, creating the following zones; dorsal right, dorsal left, ventral right and ventral left. Within these for zones radial lines of 40 x magnification images extending from the central canal to the edge of the edge of the cord were captured. Images were taken in every field of view available. To ensure each zone was sampled thoroughly, three equidistant, radial sets of images at approximately 25°, 45° and 65° from the origin in each segment were captured. CFV staining highlighted the boundary between grey and white matter in each radial set, allowing for the capillary density for grey and white

matter to be collected and analysed separately. This division is denoted by the dotted blue line in Figure 1. This resulted in eight separate zones from which images were captured; dorsal right grey, dorsal right white, dorsal left grey, dorsal left white, ventral right grey, ventral right white, ventral left grey and ventral left white. Upon analysis, no significant difference in capillary density was found between the right and left sides of the cord in P11 control mice ($P>0.05$ One Way ANOVA with post hoc test Tukey) (Figure 2) and P11 Taiwanese SMA mice ($P>0.05$ One Way ANOVA with post hoc test Tukey) (Figure 3). Data from the right and left sides were therefore pooled to give the four final regions of the cord presented in all further analysis; Dorsal Grey, Dorsal White, Ventral Grey and Ventral White. This method of sampling was applied to every section of cord analysed. Having designed and tested the sampling technique, careful consideration was given to the region of cord selected for analysis.

Historically, the lumbar region of the spinal cord has been the preferred cord region examined in SMA investigations. This is due to the greater number of motor neurons present in the ventral horn of the grey matter supplying the musculature of the lower limb. However, areas of the spinal cord with increased grey matter volumes have been shown to have the most variable capillary density and diameter (Brockstein, 1993). In our initial investigation of the vasculature in SMA (Chapter 2 of this thesis), we reported alterations in both the density and diameter of capillaries in SMA skeletal muscle. To prevent any inherent differences in vessels masking potential alterations in the cord vasculature in SMA, the thoracic region of the cord was selected for analysis. All of the results presented in this chapter are from the thoracic region of the spinal cord. The thoracic spinal cord, lacking increased

projections for upper and lower limbs, contains the most consistent grey matter area in the cord and should therefore contain the most consistent vessel density and diameter. Examining the thoracic region of the cord increases our confidence that any potential alterations observed in the spinal cord vasculature are due to the disease mutation and not inherent differences caused by variation between different regions of the cord.

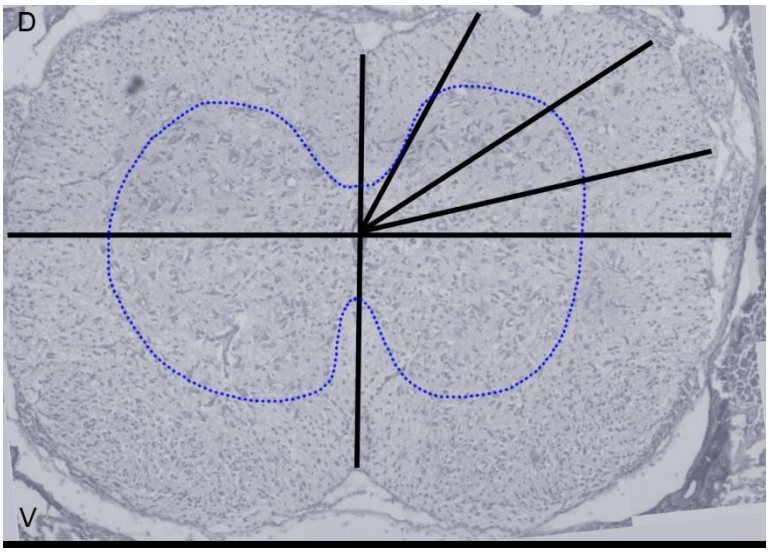

Figure 1 – Schematic representation of spinal cord sampling method.
Representative micrograph of P11 control spinal cord visualised with cressyl fast violet. Horizontal and vertical lines through the central canal indicate the four initial regions into which the cord was divided; Dorsal Right, Dorsal Left, Ventral Right and Ventral Left. Diagonal lines represent the tracks along which 40 x magnification sample images were collected in each quadrant. Dotted blue line highlights the distinction between grey and white matter. 10x magnification.

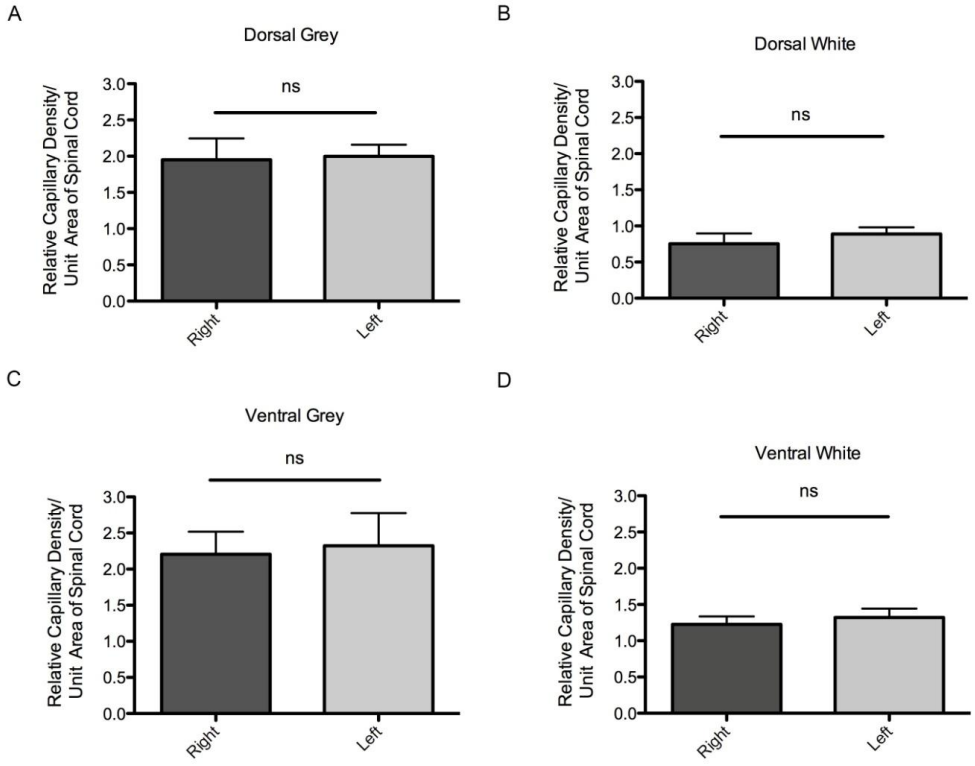

Figure 2 – Comparison of capillary density in right and left regions of P11 control Taiwanese mice*. Bar chart (mean ± s.e.m) quantification of capillary density in the right (dark grey bars) and left (light grey bars) sides of the four regions of the spinal cord of P11 control mice. Unpaired, two-tailed t-test, ns = no significant difference, P>0.05. N≥3 mice and n≥3 cords for each bar.*

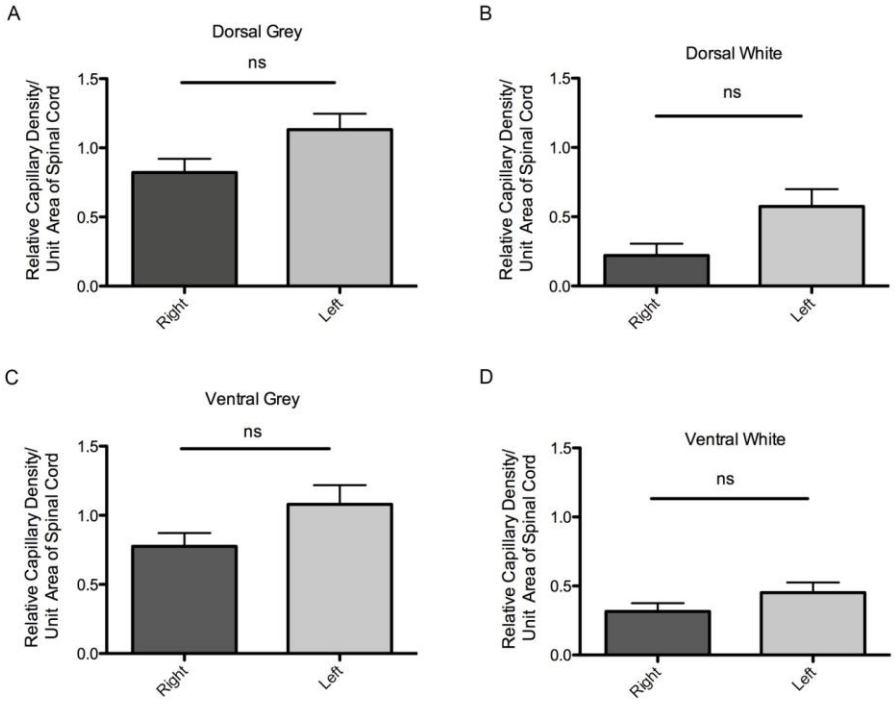

Figure 3 - Comparison of capillary density in right and left regions of P11 Taiwanese SMA mice*. Bar chart (mean ± s.e.m) quantification of capillary density in the right (dark grey bars) and left (light grey bars) sides of the four regions of the spinal cord of P11 Taiwanese SMA mice. Unpaired, two-tailed t-test, ns = no significant difference, P>0.05. N≥3 mice and n≥3 cords for each bar.*

3.3.2 Significant reduction in spinal cord capillary density in late symptomatic Taiwanese SMA mice

Along with the individual images captured for capillary density measurement, example cord sections were imaged in their entirety. Overlapping 10x magnification images were captured across whole sections and then stitched together using Photoshop to create low magnification montages of whole spinal cord sections. Initial inspection of these montage images revealed a dramatic reduction in the capillary density of late symptomatic P11 Taiwanese SMA spinal cords (Figure 5) when compared to control spinal cord montages (Figure 4).

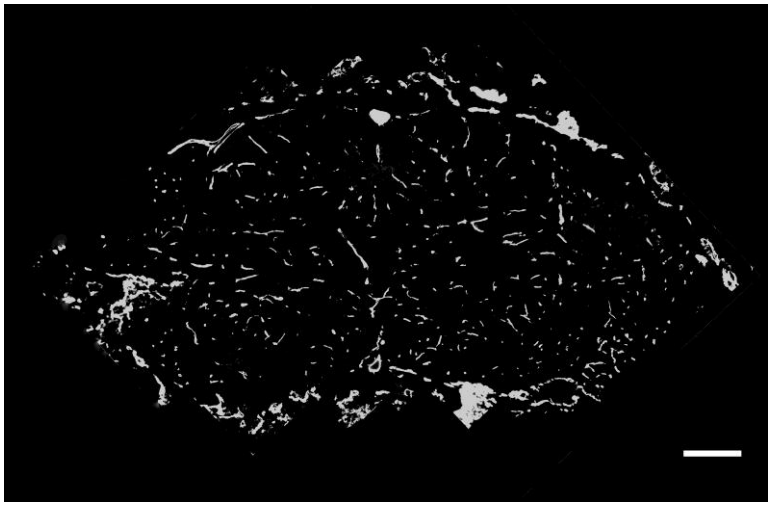

Figure 4 – P11 Control Taiwanese spinal cord capillary bed. *Representative montage micrographs of P11 control spinal cord visualised with PECAM 1. Individual images used to construct montage of entire section are 10 x magnification. Scale bar equals 200µm.*

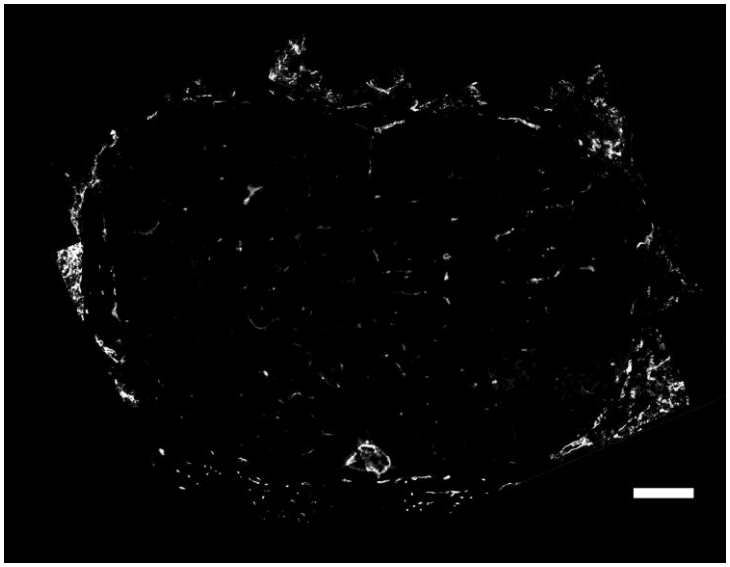

Figure 5 – P11 Taiwanese SMA spinal cord capillary bed. *Representative montage micrographs of late symptomatic P11 Taiwanese SMA cord visualised with PECAM 1. Individual images used to construct montage of entire section are 10 x magnification. Scale bar equals 200µm.*

From the montage images, capillary density in both P11 Taiwanese SMA and control spinal cords appeared to be greater in the more central grey matter regions than the

white matter cord periphery. When measured, the capillary density of P11 control spinal cord grey matter was found to be significantly greater than that of the white matter (unpaired, two-tailed, t-test) (Figure 6). A similar significant difference was also seen in P11 Taiwanese SMA cords, with capillary density in the grey matter again being significantly greater than the white matter (unpaired, two-tailed, t-test) (Figure 7). These findings are consistent with studies of both human and mouse spinal cord vasculature which describe higher capillary numbers in the grey matter to cope with higher metabolic demands (Sturrock, 1980; Brockstein, 1993). Having confirmed the internal differences between grey and white matter within the cord, the vasculature of Taiwanese SMA and control spinal cords was compared in detail.

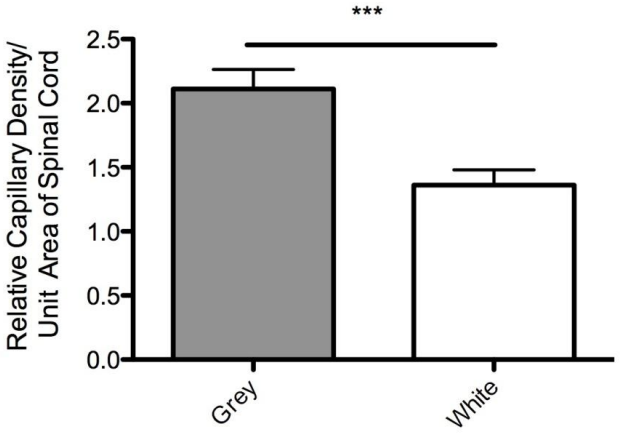

Figure 6 – Comparison of Grey and White matter capillary density in P11 control Taiwanese mice. *Bar chart (mean ± s.e.m) quantification of capillary density in P11 control mice in the grey matter (grey bar) and white matter (white bar) of the spinal cord. Unpaired, two tailed t-test, ***= P<0.001.*

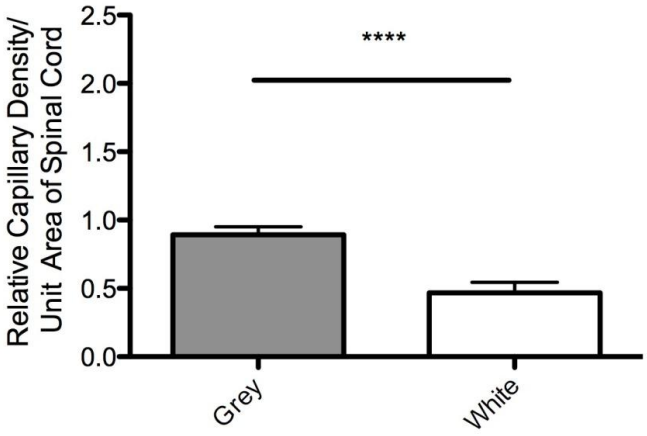

Figure 7 - Comparison of Grey and White matter capillary density in P11 Taiwanese SMA mice *Bar chart (mean ± s.e.m) quantification of capillary density in P11 Taiwanese SMA mice in the grey matter (grey bar) and white matter (white bar) of the spinal cord. Unpaired, two tailed t-test, ****= P<0.0001.*

In control cords capillaries can be seen throughout the section, extending from the centre to the edges of the cord. While the distinction between grey and white matter cannot clearly be identified without CFV stained adjacent sections, capillaries do appear more dense in the central regions of the cord in comparison to the periphery (Figure 4). In comparison to skeletal muscle, the capillaries of the spinal cord do not appear in a particular pattern of organisation. The capillaries are not tightly packed into a neat arrangement but appear scattered throughout the cord. Although scattered, the capillaries appear to be equally distributed and separated from one another (Figure 4). In contrast, considerable portions of the Taiwanese SMA cord appear completely devoid of capillaries, with large gaps between neighbouring vessels (Figure 5). As was seen in the control cords, more capillaries are seen in the centre of the cord than the periphery, although far fewer capillaries are seen in each of these areas in P11 Taiwanese SMA cords than control cords (Figure 4, Figure 5) and

almost no capillaries can be seen around the periphery of P11 Taiwanese SMA cords (Figure 5). After examining the appearance of the overall cord vasculature the capillary density in the individual regions of the cord was measured.

For analysis, the data from the four spinal cord regions detailed in Figure 1 were graphed and compared. In each of the four regions capillary density was significantly reduced in P11 Taiwanese SMA cords when compared to control littermates ($P<0.0001$,unpaired two-tailed, t-test) (Figure 8). Specifically, over the four regions capillary density was reduced by: Dorsal Grey 53%; Dorsal White 60%; Ventral Grey 62%; Ventral White 70 % (Figure 8). This represents an overall average reduction in spinal cord capillary density of approximately 61% in P11 Taiwanese SMA mice when compared to control littermates (Figure 9). Observing a significant reduction in capillary density in the Ventral Grey region is particularly pertinent as this is the region of the cord where the lower motor neuron cell bodies affected in SMA are located.

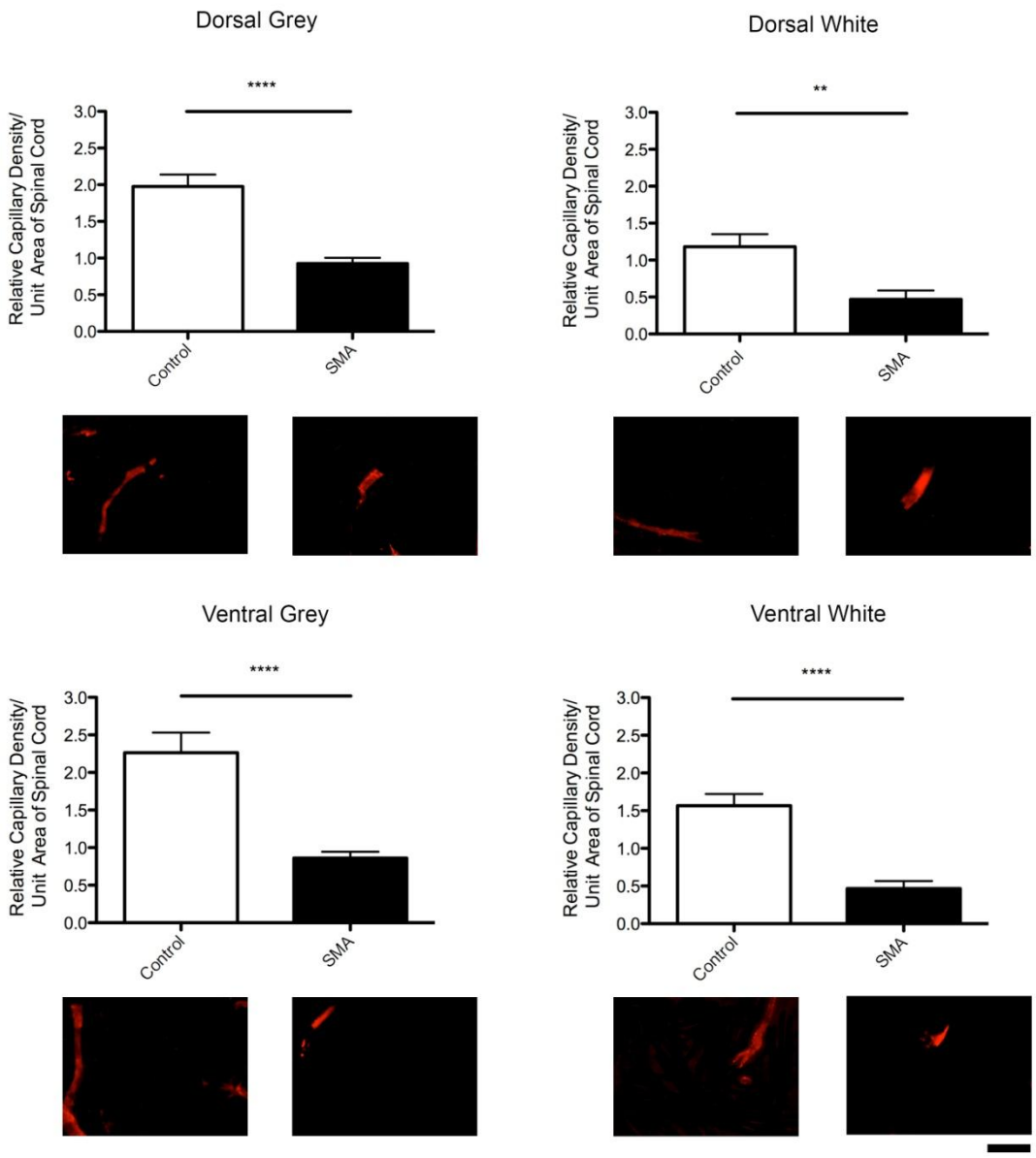

Figure 8 – Reduced capillary density in all four spinal cord regions in P11 Taiwanese SMA mice*. Bar chart (mean ± s.e.m) quantification of capillary density in the four regions of the spinal cord of P11 Taiwanese SMA mice (black bars) and control littermates (white bars). Unpaired, two-tailed t-test,**P<0.01,**** =P<0.0001. N≥3 mice and n≥3 cords for each bar. Representative micrographs of PECAM 1 stained capillaries (seen in white) in each cord region in Taiwanese SMA and control littermates. PECAM 1 staining was converted to binary to show vessels of the white matter clearly. 40 x magnification. Scale bar equals 50µm.*

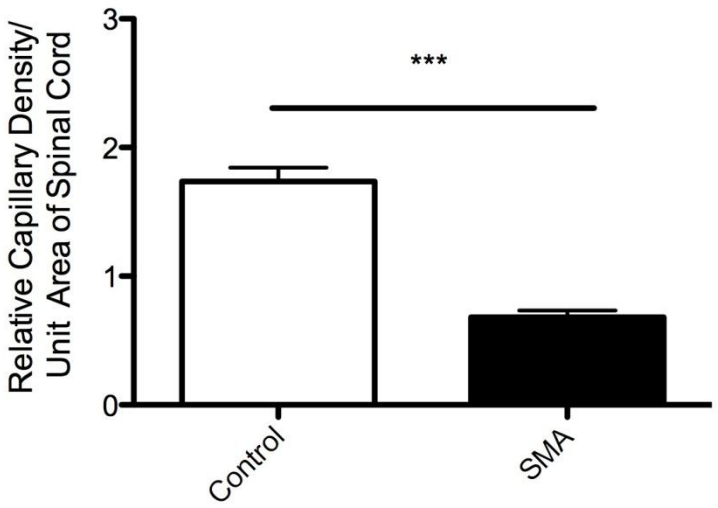

Figure 9 – A significant difference overall spinal cord capillary density in P11 Taiwanese SMA mice and control littermates. *Bar chart (mean ± s.e.m) quantification of overall spinal cord capillary density in P11 Taiwanese SMA mice (black bar) and control littermates (white bar). Unpaired, two tailed t-test, ***= P<0.001.*

3.3.3 Spinal cord capillary density defects occur postnatally in parallel with motor neuron loss

Examination of P11 late symptomatic Taiwanese SMA spinal cord revealed a very similar degree of capillary reduction to that which was found in P11 Taiwanese SMA skeletal muscle (Chapter 2, Figure 13). Timeline analysis of Taiwanese skeletal muscle highlighted that this reduction in capillary density was a post natal phenomenon which occurred in parallel with the neuromuscular pathology present in the Taiwanese mouse model. To determine if a similar pattern occurs in the spinal cord two younger ages of mice were examined; the presymptomatic day of birth (P0) and the symptomatic P5 age.

As with the late symptomatic P11 time point, montage images of entire cross-sections of Taiwanese SMA and control spinal cords were created. At the presymptomatic P0 timepoint Taiwanese SMA and control montages were indistinguishable from one another (Figure 10). Capillaries were present throughout cord sections consistent with previous studies of murine spinal cord vasculature, which show capillaries dispersed throughout the cord by E15 (Sturrock, 1980). While capillaries are present in both Taiwanese SMA and control cords there appear to be fewer vessels than were observed at the P11 time point. Again, this is consistent with previous studies of the cord which describe a rapid period of vascularisation occurring later in postnatal development at P5, (Sturrock, 1980). After these initial general observations the capillary density of each region of the cord was investigated in more detail.

Figure 10 –

P0 spinal cord capillary bed. *Representative montage micrographs of P0 spinal cord visualised with PECAM 1. Individual images used to construct montage of entire section are 10 x magnification. Scale bar equals 200µm.*

In each of the four spinal cord regions at P0, no significant difference was found between the capillary density of Taiwanese SMA mice and control littermates ($P>0.05$, un-paired, two-tailed, t-test) (Figure 11). When these regional measurements were combined to generate a value for overall cord capillary density, again, no significant difference was observed between Taiwanese SMA and control mice ($P>0.05$, up-paired, two-tailed, t-test) (Figure 12). Seeing no difference in capillary density between Taiwanese SMA and control mice suggests that the capillary bed of Taiwanese SMA spinal cord is normal in its extent at birth. By P11 however the capillary density of Taiwanese SMA spinal cords is dramatically lower

than control littermates. To determine at which stage of the disease this disparity in density occurs, spinal cords from symptomatic P5 Taiwanese SMA and control littermates were analysed.

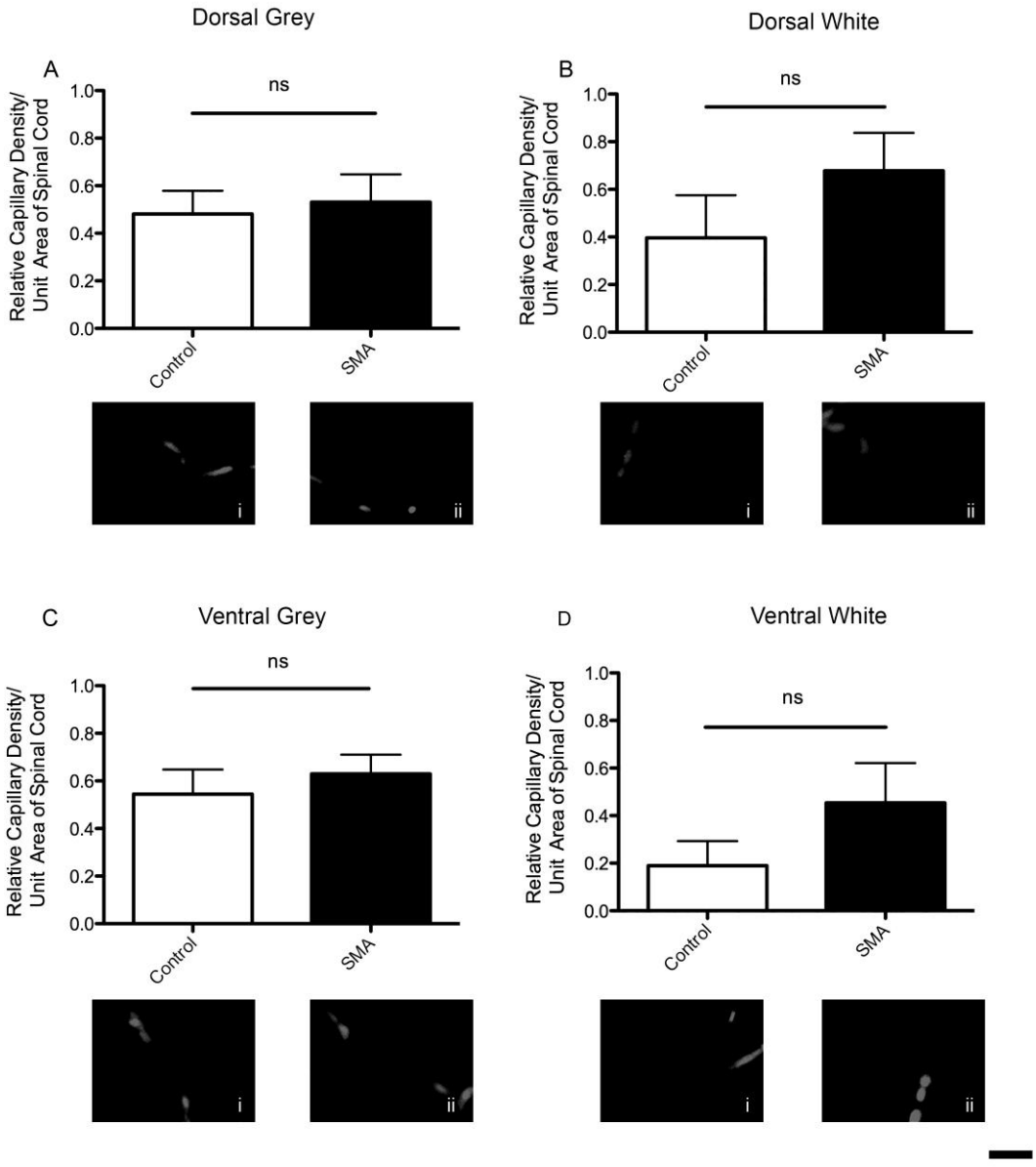

Figure 11 - No significant difference in capillary density between control and Taiwanese SMA mice at birth. *Bar chart (mean ± s.e.m) quantification of capillary density in the four regions of the spinal cord of P0 Taiwanese SMA mice (black bars) and control littermates (white bars). Unpaired, two-tailed t-test, ns= no significant difference, P>0.05. N≥3 mice and n≥3 cords for each bar. Representative micrographs of PECAM 1 stained capillaries in each cord region in Taiwanese SMA and control littermates. 40 x magnification. Scale bar equals 50μm.*

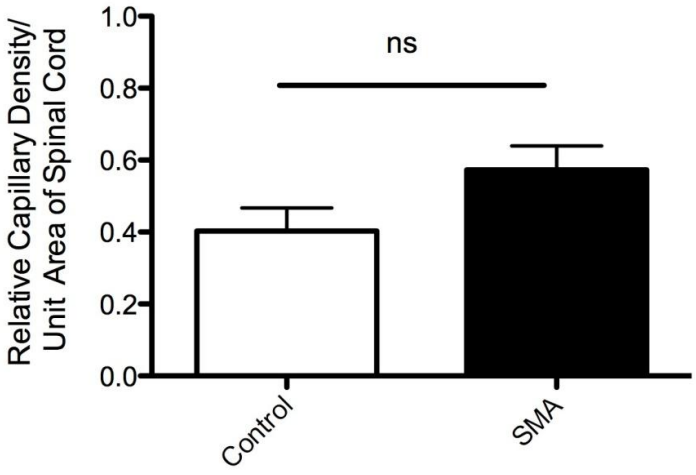

Figure 12 - No significant difference in overall spinal cord capillary density in P0 control and Taiwanese SMA mice. *Bar chart (mean ± s.e.m) quantification of overall spinal cord capillary density in P0 Taiwanese SMA mice (black bar) and control littermates (white bar). Unpaired, two tailed t-test, ns= no significance, P>0.05. N≥3 mice and n≥3 cords for each bar.*

When the spinal cords of P5 Taiwanese SMA and control littermates were examined, a difference in capillary density was observed, but only reached significance in three out of the four defined regions; Dorsal Grey 27% ($P<0.01$) Dorsal White 75% ($P<0.001$), Ventral Grey 51% ($P>0.05$) and Ventral White 69% ($P<0.01$). The accompanying P values were generated from individual unpaired, two-tailed, t-tests of each region (Figure 13). On average this amounts to an overall reduction in spinal cord capillary density of approximately 68% (Figure 14). Capillary density was decreased by 51 % in the Ventral Grey region of Taiwanese mice in comparison to controls, this was not found to be a significant reduction ($P = 0.1508$, unpaired, two-tailed, t-test). However the Ventral Grey region does maintain the same trend as the three other regions of the cord, displaying fewer capillaries than the control counterpart region (Figure 13).

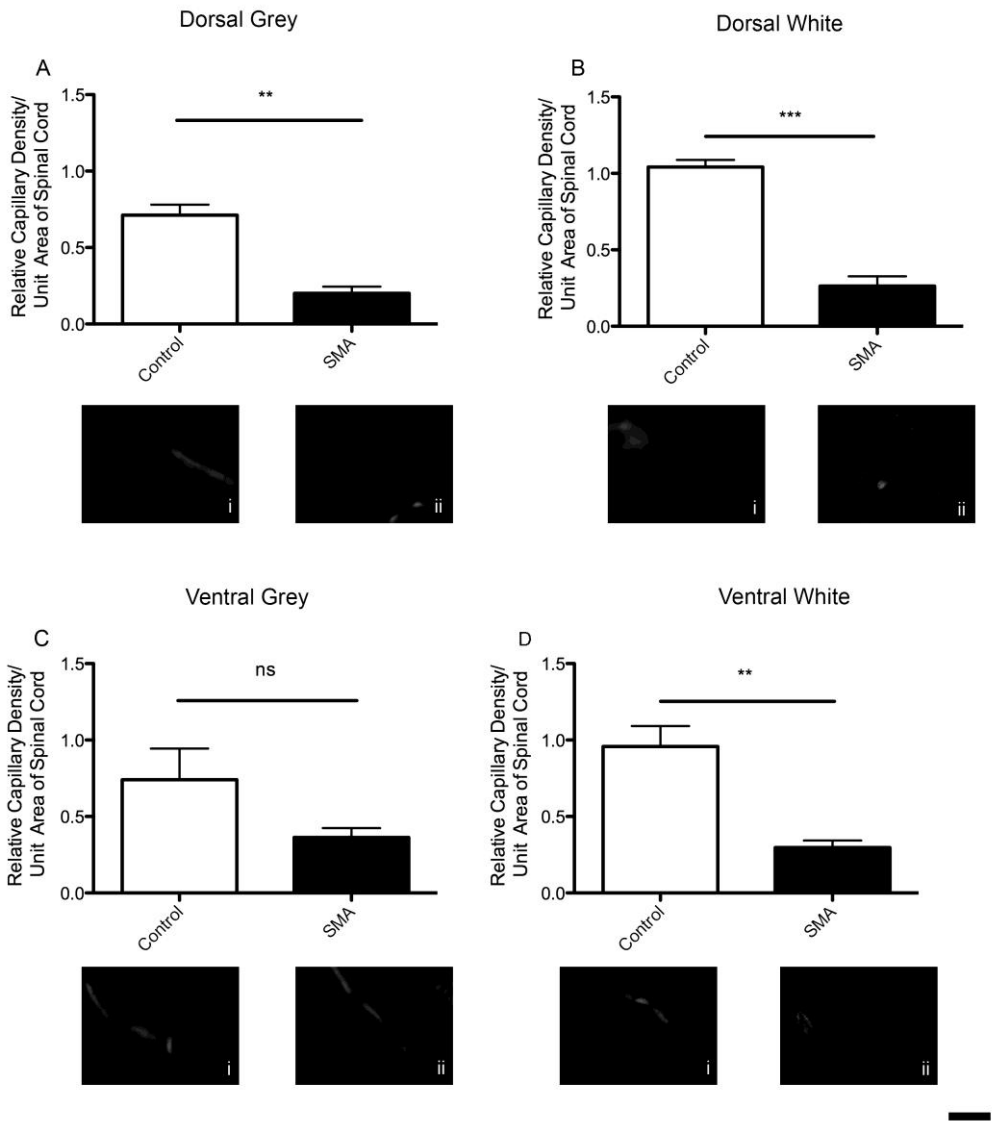

Figure 13 – Significant difference in capillary density in three of the four spinal cord regions in P5 Taiwanese SMA mice*. Bar chart (mean ± s.e.m) quantification of capillary density in the four regions of the spinal cord of P5 Taiwanese SMA mice (black bars) and control littermates (white bars). Unpaired, two-tailed t-test, ns = no significance P>0.05, ** =P<0.01, ***P<0.001 N≥3 mice and n≥3 cords for each bar. Representative micrographs of PECAM 1 stained capillaries in each cord region in Taiwanese SMA and control littermates. 40 x magnification. Scale bar equals 50µm.*

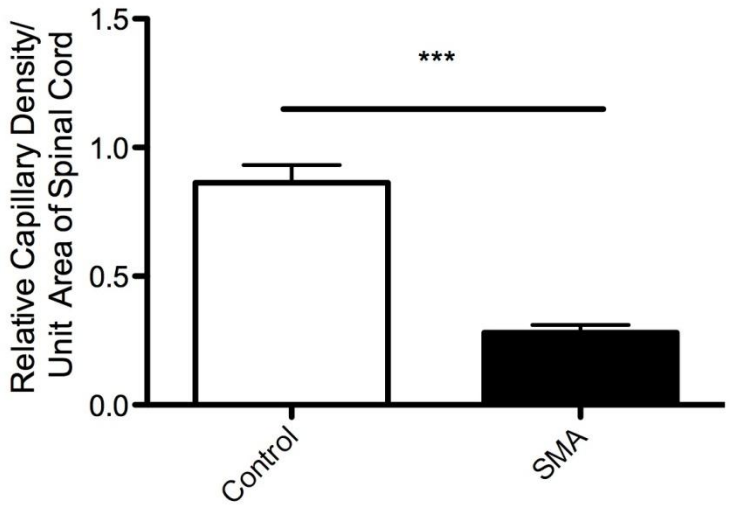

Figure 14 – Significant difference in overall spinal cord capillary density in P5 control and Taiwanese SMA mice. *Bar chart (mean ± s.e.m) quantification of overall spinal cord capillary density in P5 Taiwanese SMA mice (black bar) and control littermates (white bar). Unpaired, two tailed t-test, ***=P<0.001. N≥3 mice and n≥3 cords for each bar.*

These findings suggest that the reduction in capillary density observed in the Taiwanese SMA spinal cord follows similar post natal pattern of development to that seen in Taiwanese SMA skeletal muscle (Chapter 2, Figure 13). Here, as was seen in SMA skeletal muscle, the spinal cord capillary beds of presymptomatic (P0) mice are indistinguishable but by symptomatic (P5) stages a significant defect is observed, which is maintained to late symptomatic (P11) stages (Figure 15). When overall spinal cord capillary density values for the three ages analysed are presented together, control capillary density can be seen to increase steadily with age (Figure 15). In Taiwanese SMA spinal cords a less regular pattern is observed (Figure 15). For a more detailed discussion of this please refer to the Weaknesses Of Study section within the Discussion portion of this chapter. Importantly, by the symptomatic stage capillary density of Taiwanese SMA spinal cords is markedly decreased in comparison to controls and the disparity in densities between the two conditions is never bridged (Figure 15).

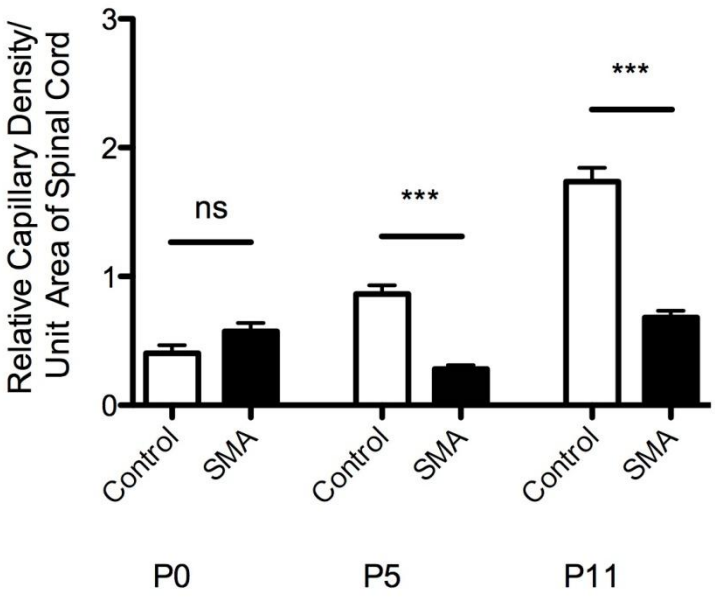

Figure 15 – Difference in capillary density between control and Taiwanese SMA mice is evident by P5 and persists until late symptomatic P11 time point. *(A) Bar chart (mean ± s.e.m) quantification of capillary density in the spinal cord from presymptomatic (P0), symptomatic (P5) and late symptomatic (P5) Taiwanese SMA mice(black bars) and control littermates (white bars). One Way ANOVA with Tukey post-hoc test, ns = no significance P>0.05 ***=P<0.0001. N≥3 mice and n≥3 cords for each bar.*

3.3.4 A significant reduction in spinal cord capillary density is observed in the SMNΔ7 mouse model of SMA

Having assessed the spinal cord capillary defect in detail in the Taiwanese mouse model of SMA, we sought to determine if a similar defect was present in another mouse model of the disease, the SMNΔ7 model. SMNΔ7 mice survive on average 14 days and develop an SMA phenotype by P6-7 (Kerr et al., 2000). Along with the incorrectly spliced human SMN2 gene found in the Taiwanese model, SMNΔ7 also carry a copy of the missing exon 7 transcript (Kerr et al., 2000). Here, spinal cords from P14 late symptomatic SMNΔ7 SMA mice and control littermates were

collected and the capillary bed stained and imaged for analysis. Analysis of P0 and an earlier disease timepoints was not possible as the SMNΔ7 colony became unavailable to us.

Again for initial examination of general capillary bed architecture low magnification montage images of SMNΔ7 SMA (Figure 17) and control thoracic regions of spinal cords (Figure 16) were created. In these older control mice the distinction between grey and white matter is clearly evident (Figure 16). This creates a more organised capillary bed appearance in these P14 mice than the younger P11 Taiwanese mice, where this boundary was not readily identifiable with PECAM 1 staining alone. In comparison to this relatively organised control capillary bed, SMNΔ7 spinal cords appeared markedly different, with a striking reduction in the number of observable capillaries within the cord (Figure 17). When capillary density was measured a significant reduction was found in each of the four spinal cord regions; Dorsal Grey 61% ($P<0.001$), Dorsal White 55 % ($P<0.01$), Ventral Grey 37% ($P<0.001$) and Ventral White 43% ($P<0.001$) (Figure 18). The accompanying P values were generated from individual unpaired, two-tailed, t-tests of each region (Figure 18). On average this amounts to an overall reduction in spinal cord capillary density of approximately 49% (Figure 19). This confirmed the initial finding of a reduced spinal cord capillary density in late symptomatic SMA mice in a second mouse model of the disease.

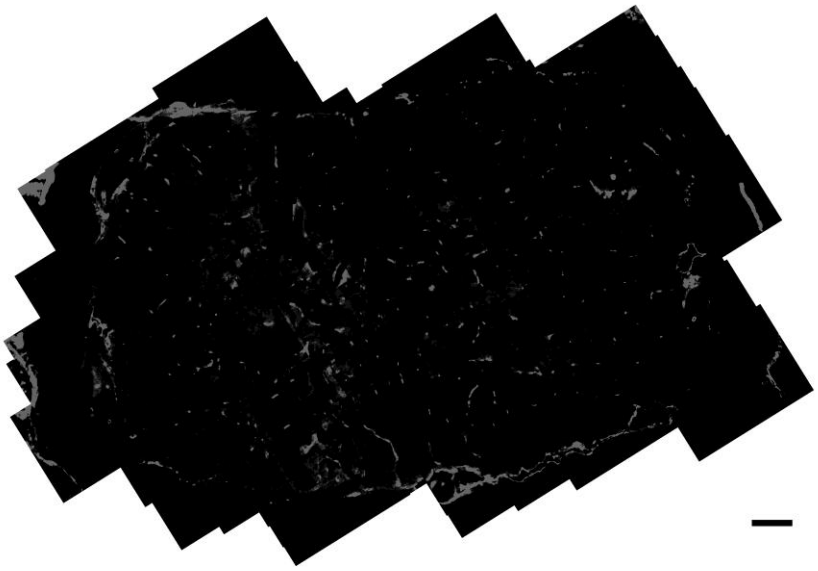

Figure 16 - P14 control SMNΔ7 spinal cord capillary bed. *Representative montage micrograph of P14 SMNΔ7 SMA control spinal cord visualised with PECAM 1. Individual images used to construct montage of entire section are 10 x magnification. Scale bar equals 200µm.*

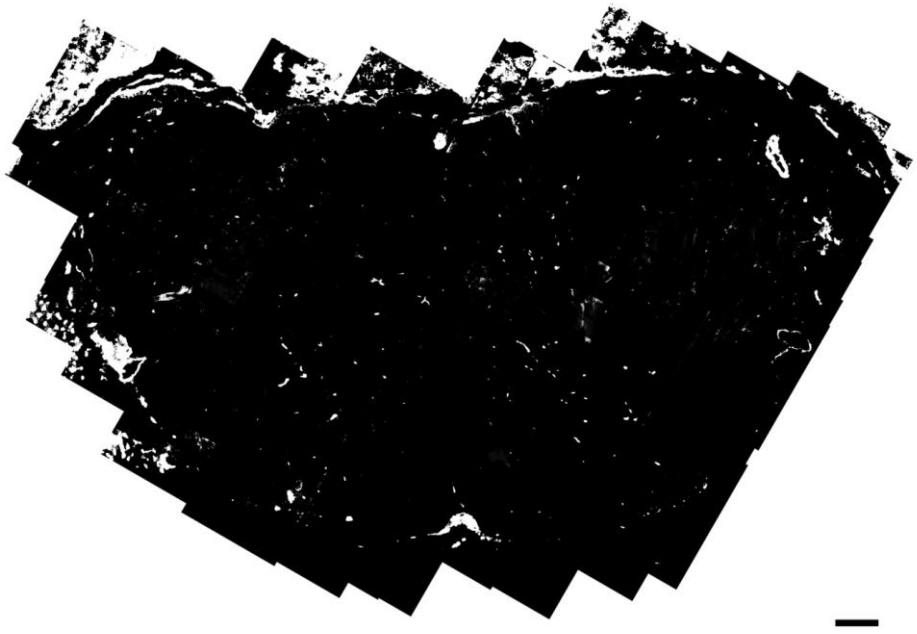

Figure 17 - P14 SMNΔ7 SMA spinal cord capillary bed *Representative montage micrograph of P14 late symptomatic SMNΔ7 SMA spinal cord visualised with PECAM 1. Individual images used to construct montage of entire section are 10 x magnification. Scale bar equals 200µm.*

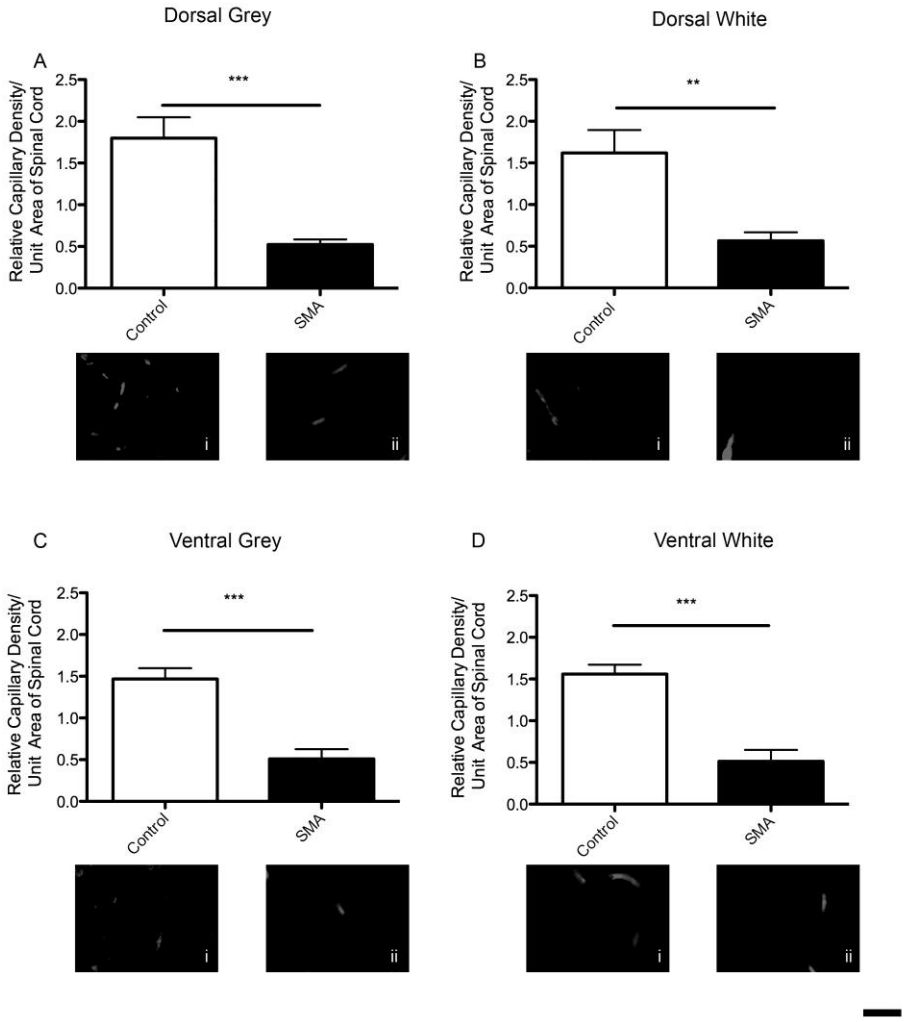

Figure 18 – Significant reductions in capillary density in all four spinal cord regions in P14 SMNΔ7 SMA mice. *Bar chart (mean ± s.e.m) quantification of capillary density in the four regions of the spinal cord of P14 SMNΔ7 SMA mice (black bars) and control littermates (white bars). Unpaired, two-tailed t-test,**=P<0.01, ***=P<0.001. N≥3 mice and n≥3 cords for each bar. Representative micrographs of PECAM 1 stained capillaries in each cord region in SMNΔ7 SMA and control littermates. 40 x magnification. Scale bar equals 50μm.*

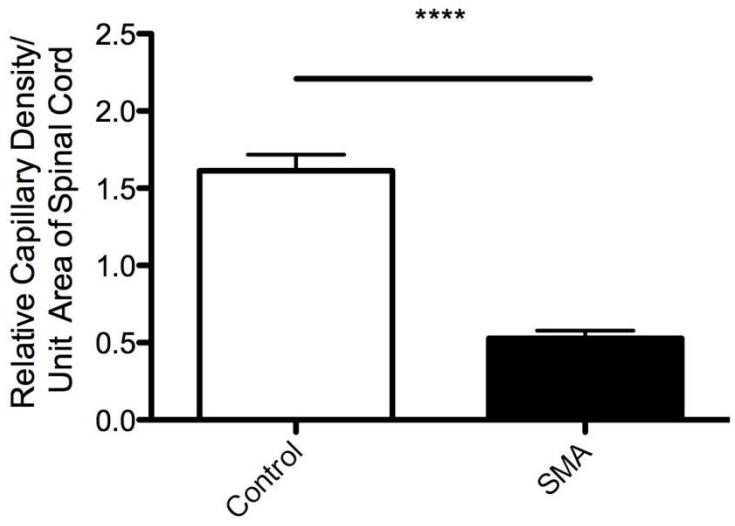

Figure 19 – Overall spinal cord capillary density in P14 SMNΔ7 mice. *Bar chart (mean ± s.e.m) quantification of overall spinal cord capillary density in 14 SMNΔ7 SMA mice (black bar) and control littermates (white bar). Unpaired, two tailed t-test, ***=P<0.001. N≥3 mice and n≥3 cords for each bar.*

3.3.5 Disrupted Claudin 5 expression in late symptomatic Taiwanese SMA mice

Capillaries in the spinal cord have a specialised barrier function and form the blood spinal cord barrier (BSCB). The BSCB is the term applied to the close association between neighbouring astrocytes and capillaries which controls the access of immune cells and plasma proteins to the spinal cord. The BSCB is composed of endothelial cells, their basement membranes, pericytes and the end feet processes of astrocytes (Bartanusz et al., 2011). In order to form this barrier properly, spinal cord capillaries must express key tight junction and adherens proteins. Tight junctional proteins such as Zona-Occludens 1 (ZO-1) and Claudin-5 (CL-5) found in capillary endothelial cells and are the key vascular components of the barrier while the water

transporter Aquaporin-4 (AQ-4) in astrocytes is essential for the maintenance of the physiological function of the BSCB. Any alterations to the normal expression and presence of these proteins can lead to disruption of the BSCB a defect commonly reported in ALS (Garbuzo-Daiz, 2007; Zhang et al., 2008; Nicaise et al., 2009; Zhang et al., 2009; Garbuzova-Davis et al., 2012 Miyazaki et al., 2011). Having identified a significant reduction in the capillary density of SMA spinal cords in two different mouse models of the disease we briefly examined the presence of three key BSCB proteins in late symptomatic P11 Taiwanese SMA mice.

Here, sections of P11 late symptomatic Taiwanese SMA and control littermate spinal cord have been double labelled with the isolectin GSL-1 staining the capillary bed and with each of the BSCB proteins of interest (Figure 20).

In control spinal cords complete co-localisation between capillaries and all three BSCB proteins is observed (Figure 20). In Taiwanese SMA cords GSL-1, AQ-4 and ZO-1 labelling co-localises (Figure 20) but not every GSL-1 labelled capillary is co-labelled with Cl-5 (Figure 20). GSL-1 and Cl-5 co-labelling is present in large but not in small capillaries in the sections (Figure 20). This suggests that while elements of the BSCB are present in late symptomatic P11 Taiwanese SMA mice, the barrier is not fully formed.

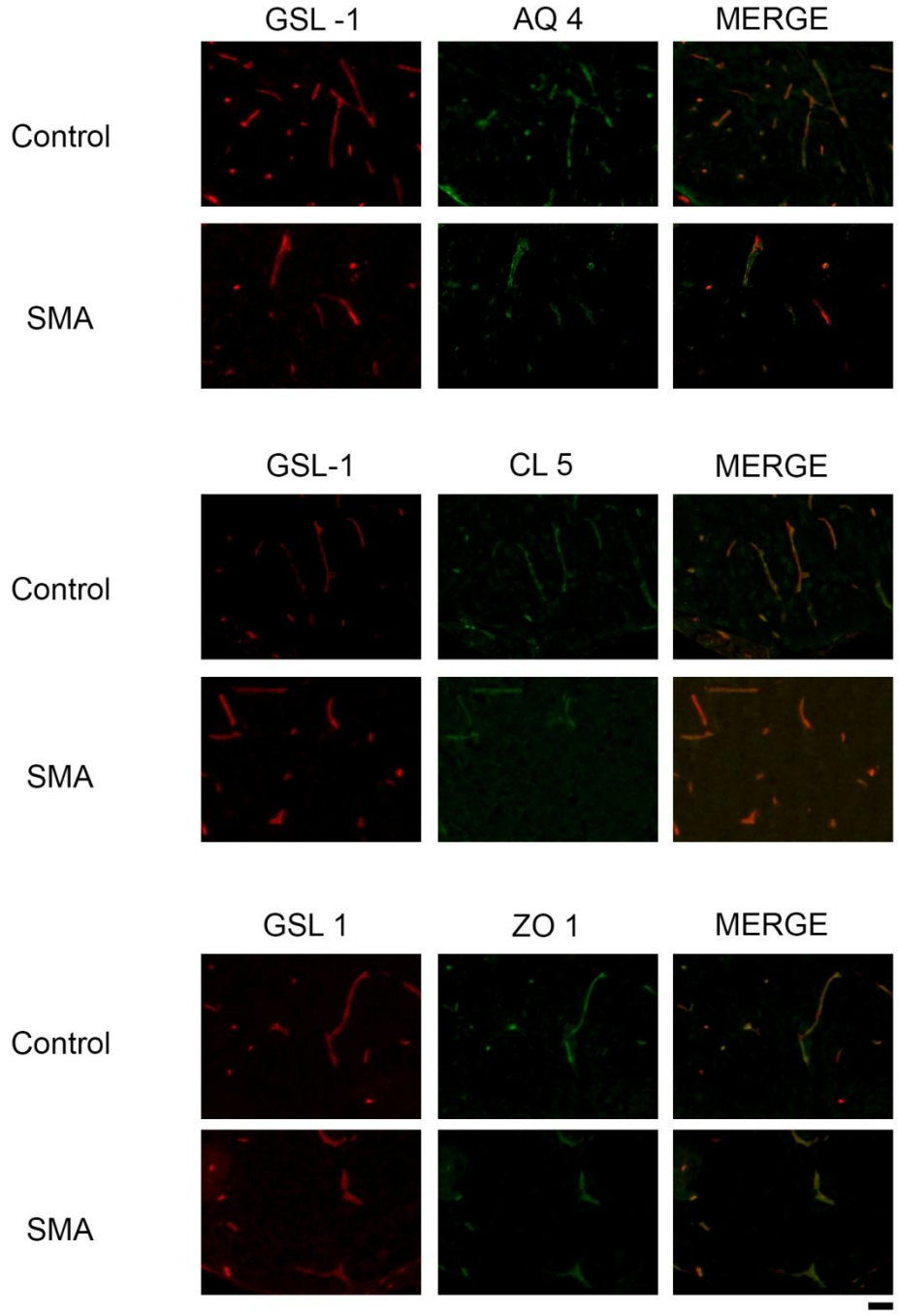

Figure 20 – Claudin 5 expression is disrupted in late symptomatic Taiwanese SMA mice while Aquaporin 4 and Zona Occludens 1 appear normal.
Representative micrographs of P11Taiwanese SMA and control spinal cord visualised in red with GSL-1 and in green with Aquaporin 4, Claudin 5 and Zona Occludens 1. 20 x magnification. Scale bar equals 50µm.

Having established a reduction in capillary density in both Taiwanese and SMN Δ7 SMA spinal cords, we next sought to investigate the effects of this capillary defect on the tissue of the spinal cord itself.

Along with nutrients and metabolites, blood vessels deliver oxygen to the body tissues. This oxygen reaches the cells of organs and tissues by diffusing through the thin walls of the capillary beds within the tissue. Oxygen diffuses from capillaries in such a way that cells nearer vessels are more oxygenated than those further away from vessels. Any alteration in the number of vessels supplying a tissue or the distance of a cell from supplying vessels will affect the level of oxygen which will reach that tissue or cell. The findings of this chapter show an overall reduction of 61% in spinal cord capillary density in P11 Taiwanese SMA mice when compared to control littermates (Figure 9). When examined regionally, a 62% reduction in capillary density was seen in the ventral grey region of P11 Taiwanese SMA mice when compared to the same region in control littermates (Figure 8). This reduction is particularly interesting, given that the ventral grey region houses the cell bodies of the lower motor neurons which degenerate and are eventually lost in SMA. To determine how the relationship between capillaries and motor neurons is affected by this reduction, sections of P11 Taiwanese SMA and control littermate spinal cords were double labelled with the capillary marker PCAM1 and the motor neuron marker SM1-32 (Figure 21). These double labelled sections were from adjacent slides to those used for the calculation of capillary density in P11 Taiwanese SMA and control littermate spinal cords.

3.3.6 Reduction in the number of capillaries surrounding motor neurons in late symptomatic P11 Taiwanese SMA mice

When control and Taiwanese SMA spinal cords were double stained with PECAM 1 and SM1-32, differences in the relationships between capillaries and motor neuron cell bodies were immediately apparent (Figure 21). In control spinal cords may capillary profiles were observed surrounding motor neuron cell bodies. In this representative image no fewer than 12 capillaries are seen in the field of view surrounding a cell body (Figure 21). In contrast, far fewer capillary profiles were observed in the field of view surrounding the remaining Taiwanese SMA motor neurons. In this representative image only 6 capillary profiles can be clearly identified (Figure 21). This reduction is in line with the 60% reduction in capillary density that has already been measured in this region of these P11 Taiwanese SMA spinal cords (Figure 21). In control spinal cords capillary profiles were observed in close proximity to cell bodies (Figure 21). However, in Taiwanese SMA spinal sections few, if any capillaries were seen in close relation to cell bodies (Figure 21). This is consistent with the pattern of vessels seen in the P11 Taiwanese SMA montage images where large sections of the cord appear devoid of capillaries (Figure 5). These example images are by no means conclusive, but serve illustrate the point that the association between capillaries and motor neurons is significantly altered in P11 Taiwanese SMA mice. To determine the physiological implications of such alterations on the motor neurons, the presence or absence of tissue hypoxia in the spinal cord (neurones and glia) was investigated using Pimonidazole Hydrochloride, an injectable marker of tissue hypoxia.

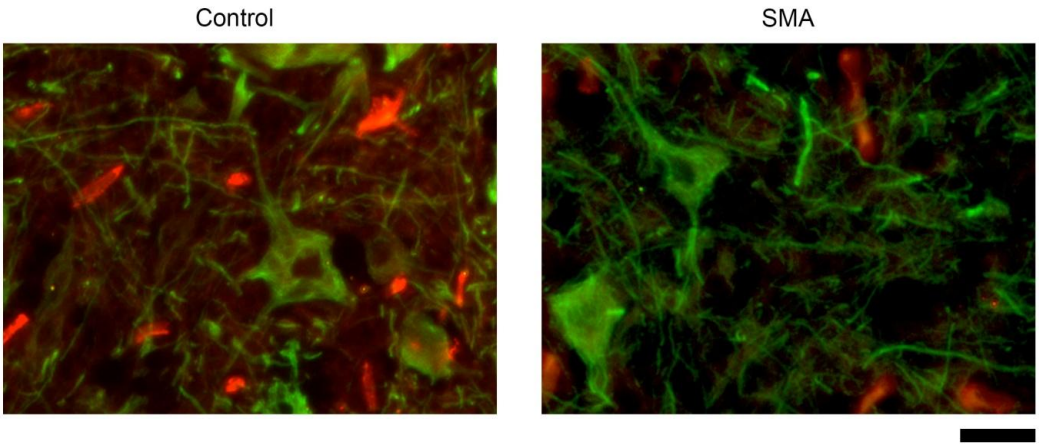

Figure 21 – The number of capillaries surrounding motor neurons is reduced in late symptomatic Taiwanese SMA mice. *Representative micrographs of motor neurons visualised with SM1-32 (green) and the capillary bed visualised with PECAM 1 (red) in late symptomatic P11 Taiwanese SMA and control spinal cords. Images are 20 x magnification. Scale bar equals 50µm.*

P11 late symptomatic Taiwanese SMA mice have a severe disease phenotype displaying drastic weight loss and muscle wasting along with pronounced motor deficits. At this state of disease progression, invasive procedures, such as the injection required to administer PIMO, are not ethically approved. To ensure minimal discomfort to the animals, a younger age and less severe disease status was required. The previous findings of this chapter have identified a significant reduction in capillary density in Taiwanese SMA spinal cords at P5 (Figure 14). This reduction is in line with that seen at the late symptomatic P11 timepoint (Figure 9). At P5 mice display a significant capillary defect in the spinal cord but their overall disease phenotype is mild enough to gain approval for injection experiments. P5 was therefore chosen as the optimal age for administration of PIMO to Taiwanese SMA and control littermates.

3.3.7 Increase in the number of hypoxic cell bodies in the ventral horn of SMA spinal cords

Pimonidazole Hydorchloride (PIMO) binds to the thiol groups of proteins in hypoxic cells. These hypoxic cells can then be identified by a primary antibody which targets the PIMO-thiol adducts and a peroxidise conjugated secondary antibody which visualises the hypoxic cells via the DAB reaction. To ensure the reliability of this procedure a series of controls were conducted alongside every staining experiment. Spinal cords sections, from Taiwanese SMA and control littermates that had been dosed with PIMO, were treated with secondary antibody and DAB but not primary antibody. A second set of sections, from the same mice, were treated with DAB only but not primary or secondary antibody. Both groups of sections were then counterstained with Cressyl Fast Violet (Figure 22). In both control groups no DAB staining was observed in any region of the spinal cord or surrounding vertebrae and muscle (Figure 22). This was still the case when the length of DAB incubation was tripled. These control experiments suggest that any DAB staining observed is a result of proper PIMO action and not as a result of inappropriate secondary binding or endogenous peroxidise activity in the cells.

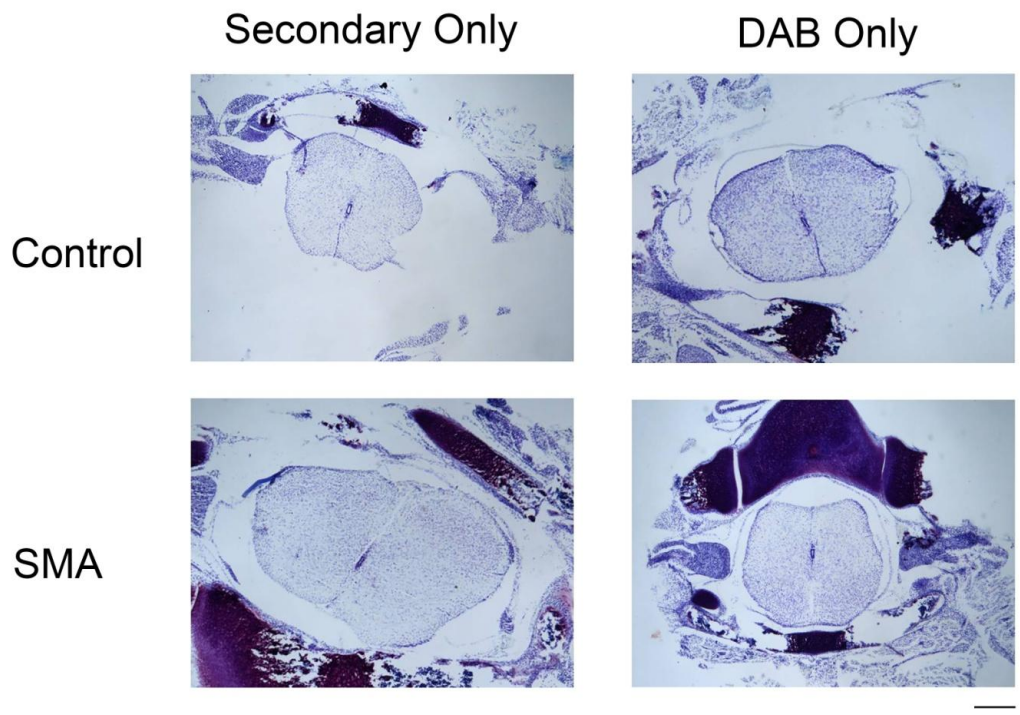

Figure 22 – No erroneous DAB staining in control staining procedure. *Representative micrographs of secondary antibody only and DAB only control sections from P5 symptomatic Taiwanese SMA mice and control litter mates injected with the hypoxia marker PIMO. Spinal cords are counterstained with Cressyl Fast Violet. Images are 10x magnification. Scale bar equals 200 µm.*

When examined by eye, very few DAB positive cells were observed in the spinal cord of control PIMO dosed mice. In contrast, numerous DAB positive cells were clearly seen in the spinal cord of Taiwanese SMA mice (Figure 23). Given that the ventral horn of the spinal cord houses motor neuron cell bodies and the importance of these cells in SMA, we focused on this region in particular (Figure 23). Here a clear difference in the number of DAB positive cells can be seen between the control and Taiwanese SMA sections (Figure 23). To quantify this observation, the number of DAB positive cells in the ventral horn of the spinal cord in both Taiwanese SMA and control littermates was counted using Image J (NIH) software.

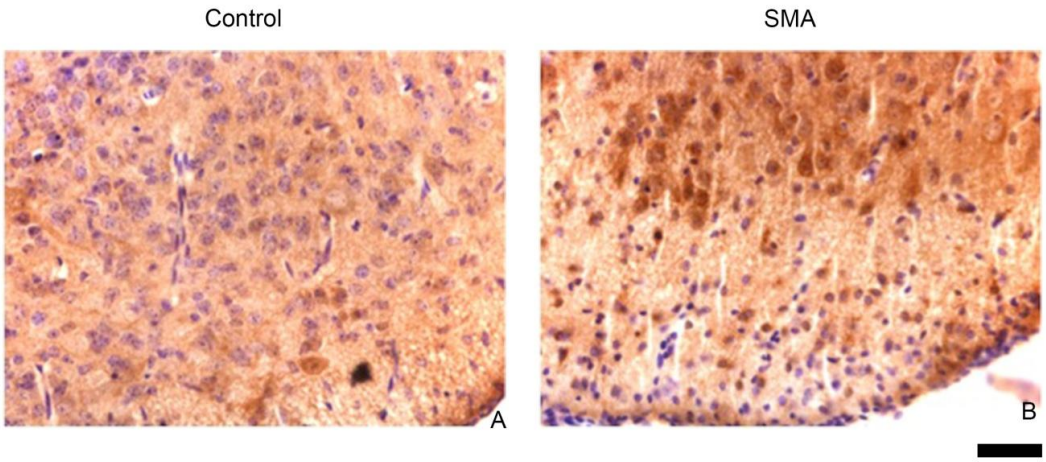

Figure 23 – Increase number of DAB positive cells in the ventral region of P5 Taiwanese spinal cord. *Representative micrographs of DAB visualisation of PIMO labelled hypoxic cells in ventral horn of P5 symptomatic Taiwanese SMA mice and control littermates. Spinal cords counterstained with Cressyl Fast Violet. Images are 40x magnification. Scale bar equals 50µ.*

The ventral horn of the spinal cord was identified by CFV Nissl staining. In this region the number of Nissl and DAB co-labelled cells were counted. In Taiwanese SMA mice the number of Nissl and DAB co-labelled cells was significantly increased in comparison to control spinal cords ($P<0.001$, unpaired, two-tailed, t test) (Figure 25). The average number of cells which were Nissl and DAB positive, in control spinal cords being 2.2 and 7.4 in Taiwanese SMA mice, amounting to a 3.3 fold increase in Nissl+DAB positive cells in Taiwanese SMA mice when compared to control littermates (Figure 25). This suggests that there is an increase in the number of hypoxic cells in the ventral horn of Taiwanese SMA spinal cords.

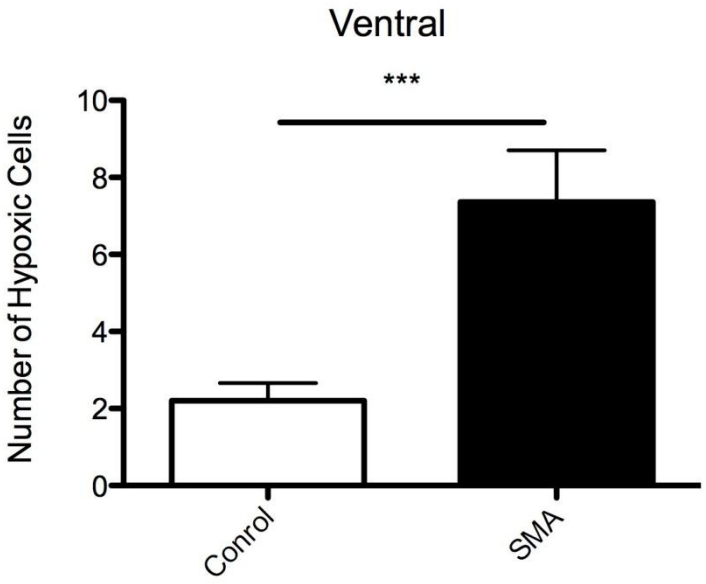

Figure 24 - Significantly increased number of hypoxic cells in the ventral region of P5 Taiwanese spinal cord. *Bar chart (mean ± s.e.m) quantification hypoxic cells in ventral horn of symptomatic P5 Taiwanese SMA mice (black bar) and control littermates (white bar). Unpaired, two-tailed, t-test. *** = P<0.001 N≥3 mice, n≥3 cords, n≥27 sections and n≥ 54 images for each bar.*

3.4 Discussion

In this chapter the capillary bed of the spinal cord in two mouse models of SMA was investigated. The findings of this chapter show that the capillary bed of the spinal cord is significantly altered in SMA mice.

The results of this chapter show first, that the vasculature of both Taiwanese SMA and control spinal cord mice conforms to the grey-white matter balance previously described in human and murine spinal cord vasculature (Sturrock, 1980; Brockstein, 1993).

Second, these findings show that the capillary density of the spinal cord is dramatically reduced by 61% in Taiwanese SMA mice when compared to control littermates at a late symptomatic time point (P11). This reduction in density was observed throughout the cord, in both the grey and white matter and in both the dorsal and ventral horns. The dorsal and ventral cord regions are supplied by anatomically and functionally discrete capillaries, which do not anastomose with one another (Sturrock, 1980; Brockstein, 1993). Observing a reduction in capillary density in each of these regions suggests a widespread defect in spinal cord vasculature in Taiwanese SMA mice.

Third, this work revealed that while dramatically reduced at a late symptomatic (P11) timepoint the capillary density of the Taiwanese SMA spinal cord was not significantly different from control littermates at birth ($P>0.5$, One way ANOVA, with post hoc Tukey). At birth, Taiwanese SMA mice are presymptomatic and show no neuromuscular pathology (Hseih-li et al., 2001; Reissland et al., 2010). By P6-7 Taiwanese SMA mice are regarded as symptomatic displaying a phenotype of

reduced body weight, organ pathology, diarrhoea, muscle wasting and motor neuron degeneration (Hseih-li et al., 2000; Reissland et al., 2010; Schreml et al., 2013). At P5 the capillary beds of control and SMA spinal cords were observed to be significantly different ($P<0.001$, One way ANOVA, with post hoc Tukey). These findings suggest that the capillary defect observed in SMA skeletal spinal cord is a postnatal phenomenon which occurs in line with the appearance of motor neuron pathology.

Fourth, this investigation confirmed the presence of the spinal cord capillary defect seen in a second mouse model of SMA at a late symptomatic timepoint. Capillary density in P11 Taiwanese SMA and P14 SMNΔ7 SMA mice is comparable. P11 Taiwanese SMA mice retain 47% of control littermate density and SMNΔ7 SMA mice retain 51% of control littermate density. This suggests that the spinal cord capillary defects observed are not an epiphenomenon of mouse genetics but a consistent SMA disease phenotype.

Fifth, preliminary investigations of the blood spinal cord barrier revealed defects in the expression of the key BSCB tight junction protein Claudin 5 in P11 late symptomatic Taiwanese SMA mice. While Claudin 5 was present in large capillaries, it was not detected in smaller capillaries in SMA mice. This may suggest a defect in the BSCB related to the expression and accumulation of Claudin 5 in Taiwanese SMA mice.

Finally, the findings of this chapter show an increase in the number of hypoxic cells in the ventral horn of Taiwanese SMA spinal cords when compared to control littermates. Given their location, it is likely that many of these hypoxic cells are

neurones and that many of these neurones are motor neurones. This increase in hypoxic cells is observed at an early stage in disease progression. Taiwanese SMA mice display reduced body weight, muscle wasting and motor neuron degeneration at P6-P7. An increase in hypoxia in the spinal cord could contribute to these pathological changes, in particular the degeneration of motor neurons, the defining pathology of SMA.

3.4.2 Vascular contribution to motor neuron degeneration

The findings of this chapter describe a reduced capillary density in the spinal cords of SMA mice. Importantly this reduced density is seen at an early timepoint in the progression of the disease. It is possible that this reduction in vessel number could contribute to the pathogenesis of SMA, particularly the degeneration of motor neurons. A 10-15% reduction in the total length and number of spinal cord capillaries results in a 30-45% reduction in spinal cord blood flow (Zhang et al., 2008). A similar decreased perfusion of the cord occurs in response to spinal cord injury. This is a rapid response with reduced perfusion seen with 30 minutes of injury (Means et al., 1978). Such reductions in spinal cord perfusion have been shown to lead to the degeneration of motor neurons (Oosthuyse et al., 2001).

Vascular Endothelial Growth Factor (VEGF) is essential for angiogenesis, the process by which new blood vessels are formed (Carmeliet, 2000). VEGF is particularly sensitive to oxygen levels in tissue and is upregulated by more than ten times by very slight decreases in tissue oxygen level (Dor & Kesket, 1997; Semenza 2000). This response is mediated by hypoxia inducible factors which bind to the hypoxia response element of the VEGF promoter (Semeza, 2000). When this

hypoxia response element was deleted in mice, the hypoxia induced expression of VEGF was blunted, particularly in neural tissue such as peripheral nerve and the spinal cord (Oosthuyse et al., 2001). While the density and structure of capillaries in the spinal cord of these mice appeared normal, vascular perfusion in the spinal cord was halved (Oosthuyse et al., 2001). As a result, motor neurons in the ventral horn of the spinal cord degenerated, with 30% of ventral horn motor neurons being lost entirely. This loss of motor neurons lead to severe muscle weakness in the mice which presented with a phenotype very similar to that of ALS with hindlimb clasping, muscle weakness and progressive immobility (Oosthuyse et al., 2001). This study suggests that motor neuron degeneration and subsequent motor neuron disease symptoms can be caused by inadequate blood supply to motor neurons. This presents a potential mechanism by which capillary defects in the spinal cord may contribute to motor neuron loss in SMA.

3.4.3 Effects of Hypoxia on blood barrier composition

In this chapter defects in the expression of the tight junctional protein Claudin -5 were observed. Although not entirely absent, the expression pattern of Claudin-5 was altered. A similar alteration of Claudin-5 expression is reported in the vasculature of mice exposed to hypoxic conditions (Koto et al., 2007).

Under normal conditions Claudin-5 is observed in the plasma membrane of retinal microvascular endothelial cells. To observe the effects of hypoxia on this expression, neonatal mice were housed in hypoxic chambers for the first 7 days of life and their retinas collected. Reduced Claudin-5 immunostaining was observed in the retinal vasculature. This reduction was further confirmed by a 41% decrease in Claudin-5

protein expression, as measured by western blotting, in the retinas from hypoxic conditions when compared to normoxic conditions (Koto et al., 2007). As the retina is part of the central nervous system, the retinal vasculature displays similar barrier qualities to that of the brain and spinal cord. To determine the effects of this reduction in a key tight junctional protein on the barrier functions of the retinal vasculature, tracer experiments were conducted. The small nuclear label Hoechst and the larger fluorescently conjugated lysine-flexible dextran were injected into the left ventricle of heavily anesthetised hypoxic and normal oxygen conditioned mice. The larger dextran was seen in the vascular lumen with little to no observable leakage into the surroundings in the vasculature of both the normal and hypoxia condition retinas. In contrast, enhanced extravasation of the Hoescht was seen in the hypoxic retinal vasculature, as identified by nuclear staining of retinal glial and neural cells by the Hoescht (Koto et al., 2007). These findings suggest that the expression of Claudin-5 is altered in response to hypoxia and that this affects the permeability of the retina vasculature to small molecules.

In this chapter an increase in the number of hypoxic cells was observed in the spinal cord of P5 Taiwanese SMA mice. When examined, the expression pattern of Claudin-5 in the spinal cord vasculature was also altered in Taiwanese SMA mice when compared to control littermates. These alterations were observed at the later P11 timepoint. It is possible that increased levels of hypoxia in the Taiwanese SMA spinal cord has contributed to these alterations in Claudin-5 expression. The particular sensitivity of Claudin-5 to hypoxia could explain why it appears to be the only blood spinal cord barrier component affected in the Taiwanese SMA mice. This could in turn be a factor in motor neuron damage resulting via a leaky BSCB.

3.4.4 Weaknesses of Study

Although every attempt was made to ensure that this study was as robust as possible, there are areas of weakness that should be noted: the delivery route of the hypoxia marker PIMO to the body tissues and a potential phenotype drift in the Taiwanese colony.

Once administered the hypoxia marker PIMO is distributed to the body tissues via the vasculature. Given that we observe defects in the vasculature of SMA mice it could be suggested that this may not be the ideal route to administer an investigative label. However, while we see a reduction in the number of blood vessels in SMA spinal cords, vessels are still present within the tissue in sufficient number for the animals to live. This suggests that while the vascular system may be deficient in SMA mice, it still functions well enough to be compatible with life. This combined with other benefits of the PIMO method identify it as an appropriate methodological approach to identify the presence of hypoxia in SMA tissues.

PIMO is a stable, safe and non-toxic marker of tissue hypoxia. Doses of 200mg/kg, over three times the dosage used in these experiments, have been safely delivered to P3 neonatal mice without any adverse side effects (Freeburg and Abraham 2004). Given the defects observed in multiple body systems the Taiwanese SMA mice, including the lungs and digestive tract (Schreml et al., 2013), PIMO is an ideal tool to administer without exacerbating the disease. Along with these animal health benefits, PIMO allows for the identification of hypoxia in identifiable cellular structures within a tissue.

Unlike measurements of hypoxia using probes, the imuunoperoxidase methodology of PIMO allows for the specific identification of hypoxic cells in a structure, not just an overall tissue reading of oxygen levels. By using Cressyl Fast Violet Nissl staining alongside the DAB PIMO labelling, the exact cellular location of hypoxia in the Taiwanese SMA spinal cords was identified.

Shortly after completion of this project it became apparent that Taiwanese SMA mice were not surviving to P11. When the colony was initially established Taiwanese SMA mice survived on average for 11 to 12 days. In the weeks following this investigation this average survival had decreased to 8 to 9 days. These shorter lived mice showed similar motor impairments, in particular a difficulty in righting ability, at P6-7 as the original, longer lived mice. However, these mice displayed more severe diarrhoea which was apparent earlier than that seen in the P11 surviving mice. This suggested an increase in the severity of systemic defects in the mice. Upon examination multiple abnormalities were seen in Taiwanese SMA organs including an accumulation of white fluid in the abdomen and discolouration of the liver and lungs. Many organs, including the heart, liver and spleen were also found to be disproportionately small in the Taiwanese SMA mice. While similar defects were observed in the longer surviving P11 mice, they were more pronounced in the reduced survival mice. This increase in systemic pathology could explain why Taiwanese SMA mice began to die earlier and could also be the underlying reason for the apparently more severe vascular defect observed at the P5 timepoint, which was the last timepoint to be collected in this study. This suggests that the severity of the capillary defect is linked to disease severity. This is a common pattern in many phenotypical and clinical aspects of SMA, with the severest Type I patients

displaying the most pronounced motor defects (Lung & Wang 2008) and abnormalities in multiple body systems including cardiovascular (Rudnik-Schoneborn, 2008) and metabolic systems (Bowerman et al., 2012). Milder forms of the disease show less motor impairment, with most Type III patients meeting all major motor milestones (Lung & Wang, 2008). Fewer systemic perturbations are reported in the less severe forms of the disease.

3.4.5 Conclusion

From these results we can conclude that the extent of capillary bed is altered in SMA mouse model spinal cord. The density of capillaries in SMA spinal cord is reduced in comparison to control cord. This reduction in capillary density was found to be post natal phenomenon which occurred throughout the cord, in both the grey and white matter as well as the dorsal and the ventral horns. A significant increase in the number of hypoxic cell bodies was also observed in the ventral horn of SMA mouse model spinal cord.

Chapter 4: Treatment with the HDAC inhibitor SAHA ameliorates skeletal muscle capillary defects in a mouse model of SMA

4.1 Introduction

At present there is not cure for Spinal Muscular Atrophy. After a diagnosis of the most severe Type I form of the disease, palliative care is currently the only clinical option. However, given its monogenetic basis (Lefebrve, 1995), SMA is a suitable target for genetic intervention. These interventions focus on replacing the lost SMN1 gene or enhancing the level of full length SMN protein produced by the SMN2 gene.

Viral gene therapy strategies aim to reintroduce the SMN1 gene into SMA cells and tissues, with the hope of restoring depleted SMN levels. Studies using viral SMN1 delivery have reported an increase in SMN levels in both isolated human cells (Azzouz *et al.,* 2004) and mouse model (Azzouz *et al.,* 2004) cells and tissues. Lentivector SMN1 delivery restored SMN levels in Type 1 patient fibroblasts (Azzouz *et al.,* 2004; Bevan et al., 2010; Foust et al., 2010; Valori et al., 2010; Dominguez et al., 2011). Intramuscular injections of the same vector in the SMNΔ7 mouse model of SMA resulted in restoration of SMN levels in motor neurons, reduction in motor neuron death and an increase in life expectancy (Azzouz *et al.,* 2004). Although effective in peripheral tissues, lentivector packaging prevents delivery of the SMN1 gene across the blood brain barrier to the central nervous system. In 2009 Foust *et al.,* reported the bypassing of the blood brain barrier by the self-complimentary adeno-associated virus serous number 9 (scAAV9). Delivery of the SMN1 gene by scAAV9 viral means has been used by multiple groups with reported rescue of motor neuron function, improved neuromuscular physiology and

increased life span (Foust et al., 2010; Valori et al., 2010; Dominguez et al., 2011). Importantly, improvement of non-neuromuscular tissues has been reported post scAAV9 SMN1 delivery. In 2010 Bevan et al., described improvements in ventricular remodelling and a resolution of cardiac arrhythmia in SMNΔ7 mice treated with scAAV9 SMN1.

While replacement of SMN1 shows promise as a treatment for SMA in animal models, effective gene therapy in patients has yet to be reported. However, another potential treatment approach, involving the amplification of full length Smn production by the remaining SMN2 gene, has been shown to improve the SMA phenotype in both SMA mouse models and patients.

In comparison to the SMN1 gene, SMN2 only produces 10% full length, fully functioning Smn protein (Burghes & Beattie 2009). When SMN1 is lost in SMA, the comparatively low levels of full length Smn produced by the remaining SMN2 gene cannot fully compensate for the loss of SMN1. It is this drastic reduction in Smn protein levels that results in the SMA phenotype. A significant correlation between the level of Smn and SMA disease severity has long been established. Early studies of the SMN genes reported a putative link between SMN protein levels and SMA disease severity, detailing a more marked reduction in SMN protein levels in the liver and spinal cord of more severe Type I patients, when compared to milder Type III patients (Lefebvre et al., 1997). More in depth studies involving patients of all SMA types have elucidated a significant correlation between SMN2 copy number and SMA severity (Feldkotter et al., 2002).

80% of Type I patients possessed one or more copies of SMN2, while 82% of Type II patients carried three SMN2 copies and 96% of Type III patients were found to possess three or four SMN2 genes (Feldkotter et al., 2002). Patients with even greater SMN2 copy numbers, up to five and six copies display even milder SMA phenotypes (Wirth el al., 2006). This correlation is also observed in animal models of the disease (Hsieh et al., 2000; Monani et al., 2000).

The severity of pathology evident in mice models correlates with the amount of full length Smn protein present (Hsieh et al., 2000), with higher levels of Smn resulting in milder SMA phenotypes. It has also been reported that mice lacking endogenous Smn but carrying eight human SMN2 copies show no SMA phenotype (Monani et al., 2000). Taken together this human and animal evidence highlights the importance of SMN2 as a modifier of the disease. The particular suggestion that the phenotypic severity of SMA can be modulated by the amount of Smn produced by SMN2 makes it an attractive target for SMA therapeutics. Levels of Smn can be amplified by genetically increasing SMN2 copy number (Monani et al., 2000) or by enhancing the transcription of the SMN2 gene present. One such transcription enhancement method is the use of Histone Deacetlyase (HDAC) inhibitors which act on the machinery responsible for condensing DNA.

Almost the entire genomic DNA is packaged into the nuclesome, the basic unit of chromatin, by histone proteins (Bradbury, 1992), highlighting the fundamental importance of histone proteins and their interactions in the regulation of gene expression. Nucleosomes are an octomeric structure which contain two molecules of each of the four histone proteins; H2A, H2B, H3 and H4 (Grunstein 1997). DNA is wound tightly around this histone core and this tight association prevents the DNA

from being freely available for transcription (Grunstein 1997). However, modification of the exposed terminal amino acids of the histone core loosens the association between it and the DNA permitting access to the DNA and initiating transcription (Grunstein, 1997). These terminal amino acids are freely available for modification by acetlylation, methylation and phosphorylation. Of these modifications, acetylation is most well understood.

Acetylation of histones occurs at the highly conserved lysine residues of the histone N-termini (de Ruijter, 2003). This acetylation is a dynamic process and is a key component of the regulation of gene expression. While acetylation of histones promotes DNA transcription (Alfrey et al., 1964, Hebbs et al., 1988, Lee et al., 1993), deacetylation has been shown to have repressive transcriptional activity. Efficient and effective transcription relies on the balance between acetylation and deacetylation of histones. Reduction in acetylation silences genes (Durrin et al., 1991), while hyperacetylation impairs the ability of histones to regulate nuclesome structure (Bauer etal., 1994, Garcia-Ramirez 1995) and also increases the access of transcription factors to DNA (Lee et al., 1993). The level of histone acetylation occurring in the nucleus is key to controlling transcription. This level of acetylation is determined by the balance of histone acetyltransferases and deacetlylases (Grunstein 19997). By altering the balance in favour of one or the other, chromatin structure and therefore transcription can be reversibly modulated. A key player in maintaining this balance is the Histone Deacetylase (HDAC) family.

HDACs are multi-subunit enzyme complexes within the nucleus that are responsible for the targeted deacetylation of histones (de Ruijter, 2003). The Classical HDAC family is composed of Class I and the Class II HDAC enzymes. While these enzymes

share approximately 82% sequence identity their expression profiles differ. Class I HDACs are expressed in the majority of tissues, while the expression of Class II HDACs is more restricted (de Ruijter 2003). Independent of class, the HDAC enzymes function in the same manner: by removing acetyl groups from the histones of the nucleosome. This tightens the association between the nucleosome and DNA, restricting transcription factor access to the DNA and so repressing transcription (Strahl & Allis, 2000; Wade, 2001; Yoshida et al., 2001). The action of HDAC enzymes can be inhibited by a class of compounds and molecules known as HDAC inhibitors, which act by blocking the enzyme's active site. These include, amongst others, short chain fatty acids such as butyrate, phenylbutyrate and valproic acid (de Ruijter, 2003). Given their ability to enhance transcription, HDAC inhibitors provide an attractive means by which the levels of full length Smn protein produced by the SMN2 gene could be increased. Multiple studies have taken advantage of HDAC inhibitor activity in an attempt to find possible SMA therapeutics.

Work involving HDAC inhibitor treatment in SMA has reported positive effects in mouse models and in patient cells. Application of sodium butyrate to isolated SMA lymphoid cells resulted in an increase in the level of full length Smn *in vitro.* While dosing of SMA mice increased Smn expression in spinal cord motor neurons *in vivo* and improved SMA symptoms (Chang et al., 2001). Application of the chemically similar Phenylbutyrate to patient fibroblasts also resulted in increased SMN expression in SMA cells (Andressai et al., 2004). Benzamide treatment of SMA patient fibroblasts resulted in a seven fold increase in SMN2 protein expression (Riessland et al., 2006). Other studies using SMA patient fibroblasts have shown a similar increase in SMN2 protein product when treated with Valproic acid (Sumner

et al., 2003, Brichta et al., 2004). Valproic acid has been the subject of many clinical trials, with varying degrees of success.

In 2006 Weihl et al., reported improved muscle strength in SMA adults who had been treated with Valproate for 8 months. However, another trial focusing on non-ambulatory children who were treated with L-Carnitine and Valproic acid showed no improvement in muscle strength or function (Kissel et al., 2011). It is worth noting that severity of SMA differed significantly between these two trial groups which could explain the marked difference in results between the trials. HDAC inhibitors other than Valproic acid have shown promise as possible SMA therapeutics, including Trichostatin A, which has been reported to have positive effects at both the protein and phenotype (Avila et al., 2007; Narver et al., 2007) level.

Daily dosing SMNΔ7 SMA mice with Trichostatin A increased SMN2 transcript and protein levels in neural and muscle tissue, while also improving survival duration, attenuating weight loss and improving motor function (Avila et al., 2007). When combined with nutritional support Trichostatin A improved survival of SMNΔ7 mice by 170% (Narver et al., 2007). More recent work has focused on the FDA approved HDAC inhibitor suberolynalidehydroxamic acid (SAHA).

In 2006 Hahnen et al., reported the ability of SAHA to increase SMN transcript levels at very low micromolar concentrations and emphasised its low toxicity when administered daily. Since then SAHA has been shown to improve the SMA phenotype in two mouse models of SMA (Riessland et al., 2010). Treatment of pregnant $Smn^{-/-}$:$SMN2^{tg/tg}$ mice with SAHA was able to rescue the embryonic lethality of SMN loss, producing SMA offspring. While 25mg/kg daily dosing of

Tawainese SMA mice increased Smn RNA and protein levels in multiple tissues, increased life span by 30% and improved motor ability as well as neuromuscular pathology (Riessland et al., 2010). SAHA treatment also ameriolates the muscular pathology observed in Taiwanese SMA mice (Mutsaers et al., 2011). These beneficial effects of SAHA treatment in SMA mice and tissues along with its FDA approved status make SAHA a very attractive possible therapeutic in SMA.

JNJ is a hydroxamic derivative which is chemically related to the potent HDAC inhibitor LBH589. LBH589 has previously been shown to increase SMN protein levels ten fold in SMA patient fibroblasts (Garbes et al., 2009), Importantly, LBH589 was able to promote SMN production in cells which were unresponsive to other HDAC treatment (Garbes et al., 2009). While JNJ retains a similar potency to LHB589 (Deleu et al., 2009; Schreml et al., 2013), it has an improved pharmacological profile and increased half life (Deleu et al., 2009). These improved pharmacological features make JNJ an appealing HDAC inhibitor to investigate as a potential therapeutic in SMA. In this chapter we investigate the effect of SAHA treatment on the capillary defect we observe in SMA skeletal muscle. Along with this well established HDAC, we also investigate the effects of the novel HDAC JNJ-2648158 (JNJ) on the capillary defect.

Based on the evidence that HDAC inhibitors can increase Smn protein levels and that the SMA phenotype in turn is improved by this increase, we hypothesised that ubiquitously increasing Smn levels via treatment with HDAC inhibitors would ameliorate the capillary defect we observe in SMA skeletal muscle.

Here a selection of hindlimb and body wall muscles from mice treated with the HDAC inhibitors SAHA and JNJ were analysed to assess the effect of postnatal increase of Smn levels on the skeletal muscle capillary defect. Capillary density in these muscles was quantified using immunohistochemical staining and fluorescent microscopy of the capillary bed along with quantitative fluorescent western blot measurements of a key endothelial marker. Morphological aspects of the skeletal muscle capillary bed, such as the alignment between capillaries and their underlying muscle fibres, as well as the calibre of capillaries were analysed using fluorescent microscopy. Treatment with the HDAC inhibitor SAHA was found to ameliorate the capillary defect observed in late symptomatic Taiwanese SMA mice. Capillary density, when measured via immunohistochemical staining of the capillary bed and via quantitative fluorescent western blotting of the endothelial marker PECAM 1, was significantly increased in SMA mice treated with SAHA when compared to untreated SMA mice. Capillary alignment and calibre was also improved in SAHA treated mice. Treatment with JNJ was found to produce a small but not significant increase in capillary density.

4.2 Methods

4.2.1 Ethics statement

All breeding and animal experiments were carried out in Cologne and approved by the local animal protection committee and conducted in accordance with guidelines established by the Landesamt fur Natur, Umwelt and Verbraucherschutz NRW in Germany. *In vivo* experiments involving JNJ-26481585 were performed under the reference number 9.93.2.10.31.07.292.

4.2.2 Animal husbandry

Taiwanese FVB.Cg-Tg(*SMN2*)2Hung *Smn1*^{tm1Hung}/J were bred and maintained in micro-isolation chambers in the mouse facility of the Institute of Genetics, Cologne according to guidelines established by the Landesamt fur Natur, Umwelt and Verbraucherschutz NRW in Germany.

4.2.3 Drug Administration

4.2.3.1 Suberoylanilidehydroxamic Acid (SAHA)

Litters of Taiwanese SMA mice, including both SMA mice and control littermates, were treated orally via a feeding needle with the HDAC inhibitor suberolynalidehydroxamic acid (SAHA). Mice were dosed twice daily from day of birth (P0) with 2.5mg/kg of SAHA dissolved in DMSO or the equivalent volume of DMSO alone as a control.

4.2.3.2 JNJ-26481585 (JNJ)

Litters of Taiwanese SMA mice, including both SMA affected and control littermates, were treated orally via a feeding needle with the HDAC inhibitor JNJ-2648158 (JNJ). Mice were dosed every other day from day of birth (P0) with 2.5µg of JNJ until P2 (P0 and P2 timepoints). At P4 the JNJ dose was increased to 5 µg.

4.2.4 Tissue Collection

All mice were humanely sacrificed via euthanasia in accordance with protocols established by the Landesamt fur Natur, Umwelt and Verbraucherschutz NRW in Germany. Initial tissue collection and dissection was performed in Germany by Julia Schreml.

4.2.4.1 SAHA treated mice

Mice treated with SAHA were sacrificed at P10. *Quadriceps* and *gastrocnemius* muscles from the hindlimb were dissected from the mice. The *quadriceps* muscles were immediately frozen on dry ice and stored individually at -80°C until shipment on dry ice to Edinburgh for analysis. The *gastrocnemius* muscles were removed intact and fixed in 4% paraformaldehyde, washed and embedded in paraffin wax for storage before shipment to Edinburgh.

4.2.4.2 JNJ treated mice

Mice treated with JNJ were sacrificed at P5. Initial pre-fix dissection of the *transverses abdominus* (TVA) muscle was conducted in Germany. In brief, the skin from the trunk of the mouse was carefully removed leaving the underlying abdominal wall intact. The rib cage and attached abdominal musculature was

dissected out and fixed in 4% paraformaldehyde for 20 minutes. The fixed preparations were stored in 1xPBS for shipment to Edinburgh.

4.2.5 Genotyping

Retrospective genotyping of the mice was performed in Germany by Julia Schreml as per the Taiwanese genotyping protocol described in detail in earlier chapters (Chapter 2).

4.2.6 Quantitative Fluorescent Western Blotting

Total protein was isolated from the *quadriceps* muscles by homogenisation in RIPA buffer (Pierce, 89900). Proteinase inhibitor cocktail (Thermoscientific, 1861278) was added to the RIPA buffer at a concentration of 5µg/ml. 30µl of RIPA buffer was added to each muscle sample. Following homogenisation the samples were centrifuged at 14,000rpm for 20 minutes. A BCA assay was then conducted to determine protein concentration in the samples, using a micro BCA Assay kit (Pierce, 23235). A master mix was made up using the following volumes per sample and standard; 500µl reagent A, 480µl reagent B and 20µl reagent C. Enough master mix was made to analyse each sample and standard in duplicate (1ml per sample). A protein standard curve was produced by adding increasing volumes of 2mg/ml of BSA albumin protein standard (Pierce, 23209) to the master mix. 1ml of mix was transferred to appropriately labelled 1.5ml Eppendorf tubes to which 1µl of corresponding sample was added. The samples were briefly vortexed and then incubated at 60°C for one hour. Following incubation, samples were transferred to cuvettes and their absorbance measured at 562nm on a Thermo Scientific spectrophotometer. The absorbance readings from the standard samples were used to

produce a standard curve. Using the equation of the line $y = mx + c$ the concentration of the experimental samples was calculated. After doing so, 15mg of protein per lane was chosen as the optimum loading concentration for western blotting. Samples were diluted with the appropriate volume of autoclaved, deionised water to prepare 10µl for loading. To aid loading 5µl of NuPAGE LDS Sample Buffer (Novex, NP0007) was added to each sample. The samples were then incubated at 98°C for 2 minutes before loading into 4-12% precast NuPageBisTris gradient gels (Novex, NP0323BOX) along with 5µl of Sharp Pre-stained protein standard (Novex, LC5800). Samples were run at 80V for 5 minutes, to ensure even entry of the samples into the gel, and then at 170V for 45 minutes. The gels were then removed from their precast casing and trimmed. The gels were then transferred to PVDF membranes (NuPAGE,) in transfer buffer (NuPAGE,) at 24Mv 16 hours. Following overnight transfer, the membranes were moved to 50ml falcon tubes and incubated with 5mls Odyssey blocking buffer (Licor, 402-467-0700) at room temperature, on a rolling platform for at 30 minutes. After this initial blocking, a fresh 5ml of blocking buffer was added to the membranes along with Tween-20 at a concentration of 1:1000. Primary antibodies were added to the blocking buffer and tween solution, platelet cell adhesion molecule 1 (PECAM 1: R&D Systems, AF3628, 130kDa) was added at a concentration of 1:1600. β Actin (Abcam, ab8226, 42 kDa) at a concentration of 1:1600 was added as a loading control. The membranes were then incubated overnight at 4°C on a rolling platform. Following incubation with the primary antibodies the membranes were washed for 6x5 minutes in 0.1M PBS. Corresponding Odyssey secondary antibodies were then applied to the membranes along with fresh blocking buffer and Tween-20 for an incubation period of 90

minutes, at room temperature, on a rolling platform. Both in Donkey antigoat IRDye 680 (Odyssey) and Rabbit antimouse IRDye 800 (Odyssey) were used at a concentration of 1:1600. The membranes were washed again for 6x5 minutes in 0.1M PBS before being dried and scanned at 600 and 800nm on a Licor Odyssey scanner. Quantification of the blots was performed on single channel scans. Bands were identified according to their molecular weight and their arbitrary fluorescence intensity calculated by odyssey software.

4.2.7. Sectioning of Gastrocnemius muscles

Gastrocnemius muscles were processed and embedded in paraffin wax in Germany prior to dispatch. The embedded muscles were section at 10µm on a Leica microtome. Adjacent sections from the beginning, middle and end of tissue ribbons were floated out in a water bath at 42°C and mounted on charged slides, creating a series of sections from throughout the whole muscle.

4.2.8 Dissection

Upon arrival the initial *transverses abdominus* (TVA) preparations were dissected and prepared for immunohistochemistry as described in detail in earlier chapters (Chapter 2).

4.2.9 Immunohistochemistry

4.2.9.1 Sectioned SAHA treated Gastrocnemius muscles

Slides of sectioned *gastrocnemius* muscle were deparaffinised in xylene for 20 minutes (two separate xylene solutions for 10 minutes each). After dewaxing the slides were rehydrated in a descending ethanol series (100% x2, 90%, 70% and 50%)

for 5 minutes in each ethanol percentage. Slides were then washed for 5 minutes in 0.1M PBS on a rocking platform before antigen retrieval was performed using sodium citrate buffer (pH6). Initially slides were washed in the buffer for 10 minutes at room temperature on a rocking platform. After this low temperature incubation the slides were boiled in citrate buffer for 20 minutes in a microwave. After this heat treatment the slides were left in the buffer for 20 minutes to cool to room temperature. Following cooling the slides were washed for 2x5 minutes in 0.1% Triton-PBS. Slides were blocked in immunoglobulin G protease-free standard blocking solution (0.2% BSA, 0.5% Triton-X 100 (TX100) in PBS) for 1 hour at 4° C before overnight incubation with goat anti mouse PECAM-1 primary antibody (R&D Systems Cat. No. AF3628) at a concentration of 1:750 in standard blocking solution at 4°C. The following day slides were washed for 6x5 minutes in 0.1M PBS at room temperature on a rocking platform. After washing slides were incubated with donkey anti goat Cy3 conjugated secondary antibody (Jackson ImmunoResearch Laboratores Inc) made up in standard block at a concentration of 1:250, for 1 hour at 4° C in the dark. Slides were washed for the final time for 6x5 minutes in 0.1M PBS, at room temperature on a rocking platform. At all times slides were protected from exposure to light. Following this final washing series slides were mounted with glass coverslips in Mowiol (10% Mowiol, Polyscience Inc, 20% glycerol, 50% 0.2M Tris buffer pH 8.5, 3% 1,4-diazobicyclooctane made up in distilled water). The 1,4-diazobicyclooctane acts as an anti-fade reagent. The mounted slides were left overnight in the dark, at room temperature to set before visualisation and imaging the following day.

4.2.9.2 Whole mount JNJ treated TVA muscles

To label the skeletal muscle capillary bed, intact TVA muscles were labelled with the rhodamine-conjugated lectin Griffoniasimplicifolia-1 (GSL-1). As described in earlier chapters, GSL-1 is not an antibody and does not require many of the staining procedures used in antibody based immunohistological protocols. Muscles were exposed to 5µg/ml αBTX conjugated to FITC (made up in 0.1M PBS) for 10 minutes to label post-synaptic acetylcholine receptors. Muscles were then washed 2x5 minutes in 0.1M PBS. To label the skeletal muscle capillary bed, muscles were incubated with Rhodamine conjugated Griffonia Simplicifolia Lectin 1 (GSL-1) at a concentration of 1:100, made up in 0.1M PBS, for one hour, at room temperature, on a rocking platform. Following this incubation muscles were washed for 6x5 minutes in 0.1M PBS before being mounted in Mowiol on glass slides, with glass coverslips. The resulting slides were left to set overnight in the dark at room temperature before visualisation and imaging the following day.

4.2.10 Imaging

Micrographs for the calculation of capillary density were captured using a standard inverted epifluorescence microscope (Olympus 1X71) combined with a chilled CCD camera (Hammamatsu C4742-95) and OpenLab (Improvision) image capture software. Cy3 and rhodamine labelled capillaries were imaged using 570 emission optics. FITC labelled capillaries and post-synaptic acetylcholine receptors were imaged using 520 emission optics.

4.2.11 Quantification and Analysis

4.2.11.1 Sectioned Gastrocnemius muscles

Any sections with poor staining or those that had been damaged during the sectioning or staining procedure were excluded from analysis. For capillary density calculations a minimum of 10 fields of view per muscle section were taken with a x20 objective, 0.4 NA. Care was taken to ensure that images were obtained from areas where the muscle was cut in the longitudinal plane by viewing muscle fibre orientation in phase contrast.

4.2.11.2 Whole mount TVAs

Any muscles with poor quality staining or those that had been damaged during dissection were excluded from analysis. For capillary density calculations a minimum of 40 fields of view per muscle were taken with a x40 objective, 0.8 NA. Any fields of view where excessive overlying connective tissue interfered with imaging were excluded from further analysis. If excluded fields of view amounted to five or more in an individual muscle the entire muscle in question was discarded from further analysis. Images were captured in every third field of view across the entirety of the muscle.

4.2.11.3 Quantifying capillary density

Images from both sectioned and whole mount muscles were first enhanced in Adobe Photoshop (CS4) for contrast and brightness. This ensured that definite vessel borders were visible and also prevented any fine capillary structures from being lost and discounted. Any out of focus images where capillaries appeared blurred or those

where background was too high to completely isolate capillary structures were excluded from further analysis. Using Image J (NIH) the enhanced images were converted to binary. In the resulting binary images capillaries were assigned black and muscle background white, allowing for the ratio of black to total white pixels to be calculated. This produced a value for capillary area per field of view. By calculating the area of a x40 field of view, it was then possible to calculate the area of capillaries in mm^2 per mm^2 of muscle.

4.2.11.4 Quantifying capillary calibre

Muscle capillary calibre (diameter) was measured in the PECAM 1 stained sections of the gastrocnemius muscle. Measurements were taken from the same images used to quantify capillary density. A measuring grid was overlain onto the images using Image J (NIH) and every capillary found at the intersection of gridlines was measured. The shortest distance across the capillary was measured. Measurements were not taken at capillary bifurcations. If the same capillary crossed multiple gridlines it was measured only once, at the first gridline encountered.

4.2.11.5 Analysis

All data were collected using Microsoft Excel software and were graphed and analysed using GraphPad Prism software. Charts shown are mean ± s.e.m. In all analyses statistical significance was considered to be $p < 0.05$. Tests used are detailed in figure legends.

4.3 Results

Having established the presence of a capillary defect in flat muscles of the body wall and described it in detail, we sought to investigate the capillary bed of another group of muscles. Limb muscles are known to be affected in SMA patients (Monani, 2005; Tsirikos and Baker, 2006; Wirth et al., 2006; Russman 2007; Farrar et al., 2009) and show motor defects in a variety of mouse models of the disease (Monani et al., 2000; Hsieh Li et al., 2000). Here we examine the vasculature of the hindlimb *gastrocnemius* muscle, which is known to display alterations in molecular mechanisms in Taiwanese SMA mice (Mutsaers et al., 2011). In comparison to the thin, flat, relatively two dimensional muscles of the body wall, the *gastrocnemius* muscle is much thicker, comprising multiple muscle fibres in a large muscle belly. In order to apply our novel method of capillary density quantification (Chapter 2) the *gastrocnemius* muscle was embedded in paraffin wax and sectioned on a Leica microtome. The capillary bed in the resulting sections of muscle was visualised using the endothelial marker PECAM 1.

4.3.1 Hindlimb muscles of late symptomatic Taiwanese SMA mice show similar capillary bed defects as flat muscles form the body wall

On initial inspection it was evident that the capillary bed of the Taiwanese SMA *gastrocnemius* muscle was altered in comparison to control littermates (Figure 1A,B). The number of capillaries present in sections from SMA muscle (Figure 1B) appeared to be less than that of control muscles (Figure 1A). Further, the arrangement of capillaries within the muscle appeared to differ. When compared to images from control and SMA P11 late symptomatic Taiwanese TVA muscles (Figure 1C,D), the alterations observed in the *gastrocnemius* muscle sections

appeared similar, with both displaying an obvious reduction in capillary density and more subtle impairments in capillary organisation and arrangement. As it is the most striking difference between the two conditions, the apparent reduction in capillary density seen in the SMA *gastrocnemius* muscle was chosen for initial analysis.

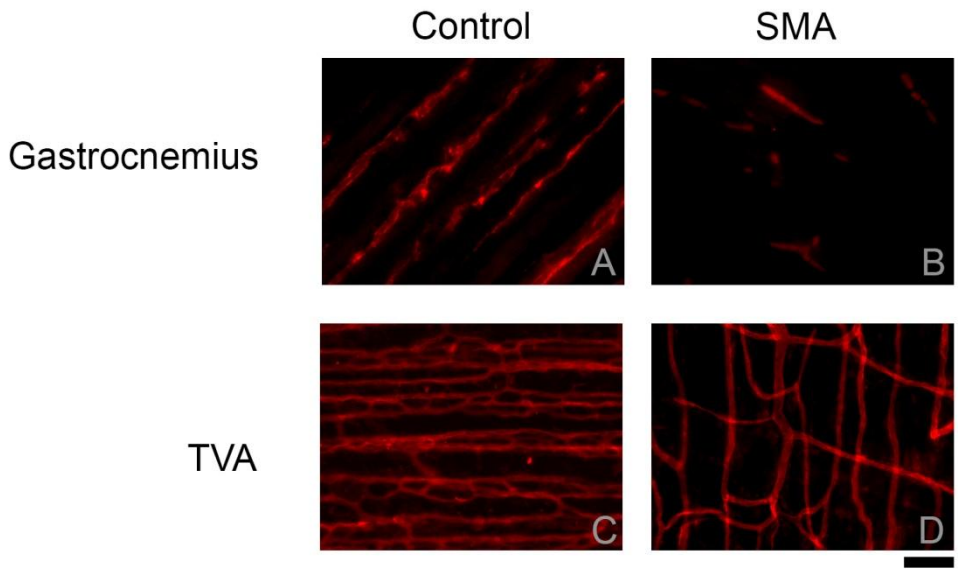

Figure 1-Alterations to gastonemius capillary bed are comparable to those seen in the TVA. *Representative micrographs of PECAM 1 labelled capillary bed in gastrocnemius (A,B) and TVA (C,D) muscles in control and SMA littermates. Images are 20x magnification. Scale bar equals 50µm.*

4.3.1.1Capillary density of gastrocnemius muscle is significantly reduced in late symptomatic Taiwanese SMA mice

Capillary density in the *gastrocnemius* muscle sections was measured using the novel method described in detail in Chapter 2. In brief, PECAM 1 labelled images of the capillary bed were captured at 20x magnification and their contrast enhanced in Adobe Photoshop to ensure no loss of fine capillary structure. The resulting images

were converted to binary using Image J software and the ratio of total black to white pixels calculated. This provided a value for total capillary area per field of view, which was then converted to capillary area per mm^2 of muscle. When the resulting values for control and Taiwanese SMA *gastrocnemius* muscle capillary density were compared a significant ($P<0.0001$, unpaired two-tailed students t-test) and dramatic difference between the two conditions was observed (Figure 2A). In comparison to control littermates, the capillary density of P11 late symptomatic *gastrocnemius* Taiwanese SMA muscle was reduced by 81% (Figure 2A). Having confirmed that the capillary density is drastically reduced in P11 Taiwanese SMA *gastrocnemius* muscle, the other notable defects in the capillary bed were then investigated and in particular, the arrangement of the capillaries within the muscle itself.

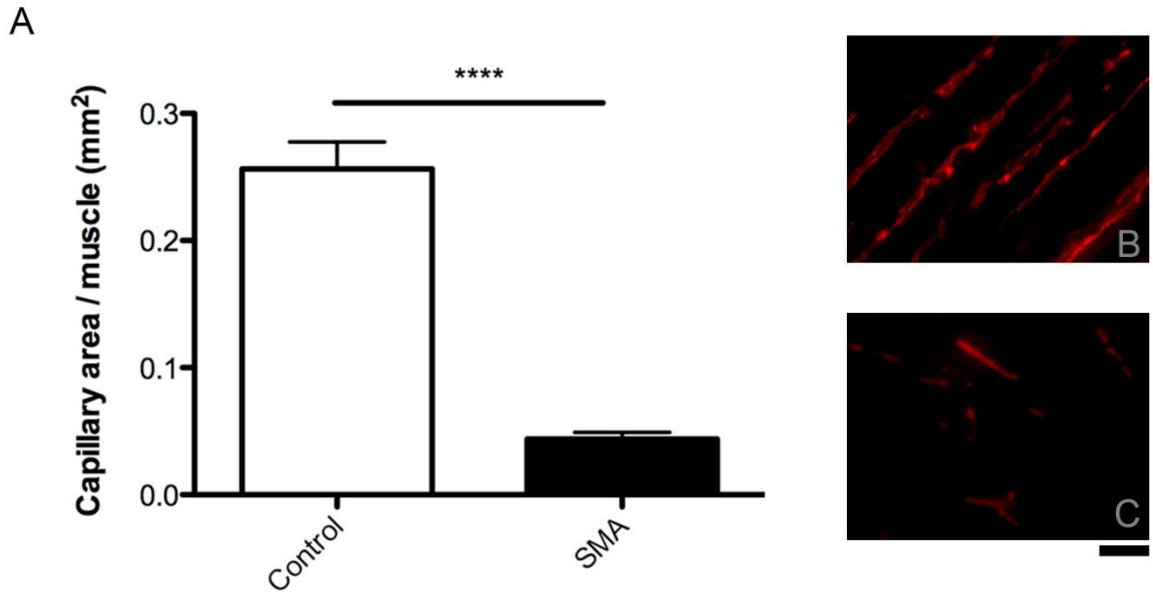

Figure 2 – Capillary density is significantly reduced in late symptomatic SMA gastrocnemius muscle*. (A) Bar char (mean±s.e.m) quantifying capillary density in gastrocnemius muscle of P11 control and SMA mice. Unpaired, two-tailed t-test, ****P<0.00001. N≥3 mice for each bar and n≥6 muscles for each group. Representative micrographs of PECAM 1 labelled capillary bed of P11 control (B) and SMA (C) gastrocnemius muscle. Images are 20x magnification. Scale bar equals 50µm.*

4.3.1.2 Impaired organisation of the skeletal muscle capillary bed

When initially examined the arrangement of capillaries within the *gastrocnemius* muscle sections appeared altered between control and Taiwanese SMA mice (Figure 1A,B). With control capillaries displaying a more linear, parallel arrangement (Figure 1A) than their SMA counterparts. To investigate the arrangement of the capillaries within the muscle further phase contrast images of the muscle fibres underlying capillaries were captured and compared (Figure 3A,3B). Here it can be seen that the overlying capillaries form a parallel arrangement with their underlying muscle fibres and can be seen to run the length of the muscles fibres (Figure 3A, 3C). In comparison, capillaries in the Taiwanese SMA *gastrocnemius* muscle only rarely display a close, parallel association with their underlying muscle fibres (Figure 3B,D) and instead appear as shortened, isolated vessels lacking the regular arrangement expected in the tissue (Figure 3D). The phase contrast images captured (Figure 3A,B) confirm that the capillaries compared from both the control and Taiwanese SMA mice are from regions of the muscle where fibres are sectioned in a longitudinal plane. This ensures that the differences observed between the control and Taiwanese SMA capillary beds are not due to comparison between muscle regions of different fibre orientation.

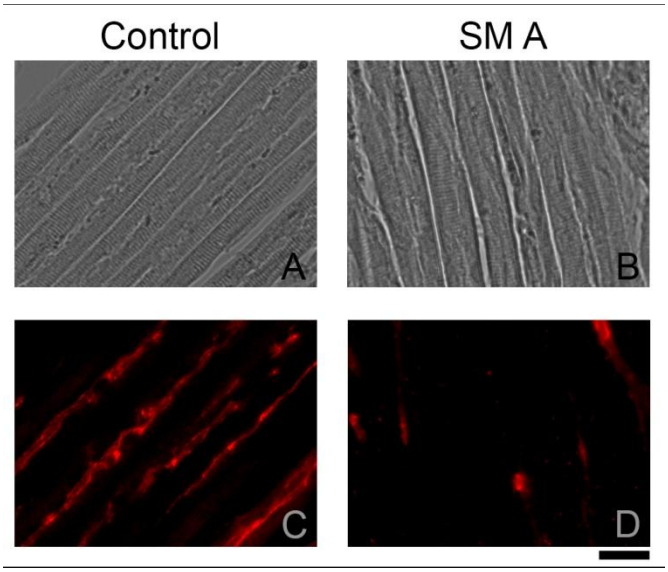

Figure 3 – Alignment of capillaries with underlying muscle fibres is altered in late symptomatic Taiwanese SMA mice*. Representative phase contrast images of muscle fibres from P11 control (A) and SMA (B) gastrocnemius muscles and PECAM 1 labelled capillaries directly overlying the corresponding phase captured muscle fibres (C, D). Images are 20x magnification. Scale bar equals 50µm.*

4.3.1.3 Increase in capillary calibre in late symptomatic Taiwanese SMA mice

When examining the structure of the capillary bed of TVA muscles in more detail the calibre of capillaries in SMA muscle was found to be increased in comparison to control littermates. As the capillary bed of the *gastrocnemius* muscle had been found to possess similar decreases in density and alterations in arrangement as the TVA muscle, capillary calibre in the sectioned *gastrocnemius* muscle was measured.

Capillary calibre was measured in longitudinal portions of the gastrocnemius muscle. The orientation of muscle fibres was confirmed by viewing the muscle under phase contrast before capturing the PECAM 1 labelled fluorescent images of the capillary bed. When quantified the calibre of capillaries in Taiwanese SMA gastrocnemius muscle was significantly greater in comparison to control littermates ($P<0.05$,

unpaired, two-tailed, students t-test). On average control capillaries were approximately 1.4µm in diameter, while Taiwanese SMA capillaries were approximately 1.6µm (Figure 4A), representing a significant average 14% increase in capillary calibre in Taiwanese SMA mice ($P<0.05$, unpaired, two-tailed, t test). When individual capillary calibres were presented in scatter plot format a slightly wider distribution of calibres was evident in the Taiwanese SMA muscle when compared to controls. This suggests a greater degree of variation in the diameter of SMA capillaries than control vessels. While this spread is not as great as was observed in the LALc muscle (Figure, Chapter 2), it shows a similar trend with Taiwanese SMA capillaries skewed towards larger diameters. In comparison to the large number of capillaries measured in the LALc muscle, 1650 profiles from ≥6 muscles, far fewer capillaries were available for measurement in the *gastrocnemius* muscle. This is due to the use of sectioned tissue rather than whole mount muscle.

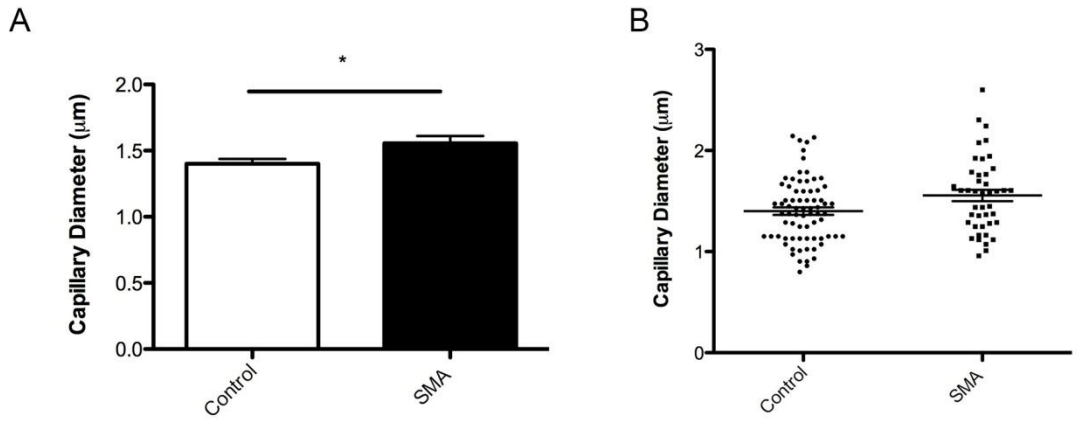

Figure 4 – Increased capillary calibre in P11 Taiwanese SMA gastrocnemius muscle. (*A) Bar chart (mean ±s.e.m) quantification of capillary calibre in the gastrocnemius muscle of P11 SMA Taiwanese mice (black bar) and control littermates (white bar). Unpaired, two-tailed t-test, * = P<0.05. N≥181 profiles from ≥6 muscles from ≥3 mice for each bar. (B) Scatter plot of capillary calibres showing distribution of calibres for each condition.*

4.3.2 Treatment with SAHA ameriolates the capillary bed defects observed in late symptomatic SMA mice

Identifying and characterising the same defects in the capillary bed of P11 late symptomatic Taiwanese SMA *gastrocnemius* muscle as we previously described in the cranial and TVA muscles, presented the opportunity to investigate the impact of SMA therapeutics on the capillary defect. In comparison to the cranial and TVA muscles, the muscles of the hindlimb are easy to identify and dissect intact. This allowed for the collection of skeletal muscle from mice undergoing drug trials in another lab. For this investigation the particular drug of choice was the histone deacetylase inhibitor (HDACi) suberolynalidehydroxamic acid (SAHA), which has been shown to increase Smn protein levels two-fold in P11 late symptomatic Taiwanese SMA gastrocnemius muscles (Mutsaers et al., 2011). Mice were treated twice daily from birth with a 2.5mg/kg dosing regimen. At P11 mice were sacrificed and skeletal muscles were collected for both morphological and molecular analysis. Having examined the morphological defects in the capillary bed in detail, the morphology of Taiwanese SMA skeletal muscle treated with SAHA was analysed first, starting with the most striking defect; the decrease in capillary density.

4.3.2.1 Increase in capillary density in SAHA treated Taiwanese SMA mice

When compared to control littermates, capillary density in P11 late symptomatic Taiwanese SMA *gastrocnemius* muscle was reduced by 81% ($P<0.0001$, unpaired, two-tailed, students t-test) (Figure 2). When Taiwanese SMA mice were treated twice daily with 2.5mg/kg SAHA the capillary density appeared, by eye, to be

improved in comparison to DMSO treated SMA mice (Figure 5B,C). When quantified the capillary density of SAHA treated Taiwanese SMA *gastrocnemius* muscle was 52% of the density measured in control littermates (Figure 5D). This represents a significant ($P<0.05$, One Way ANOVA with Tukey post hoc test) 2.6 fold increase in capillary density when compared to DMSO treated Taiwanese SMA *gastrocnemius* muscle (Figure 5D). This suggests that treatment with the HDAC inhibitor SAHA is capable of significantly ($P<0.05$, One Way ANOVA with Tueky post hoc test) improving capillary density in Taiwanese SMA skeletal muscle.

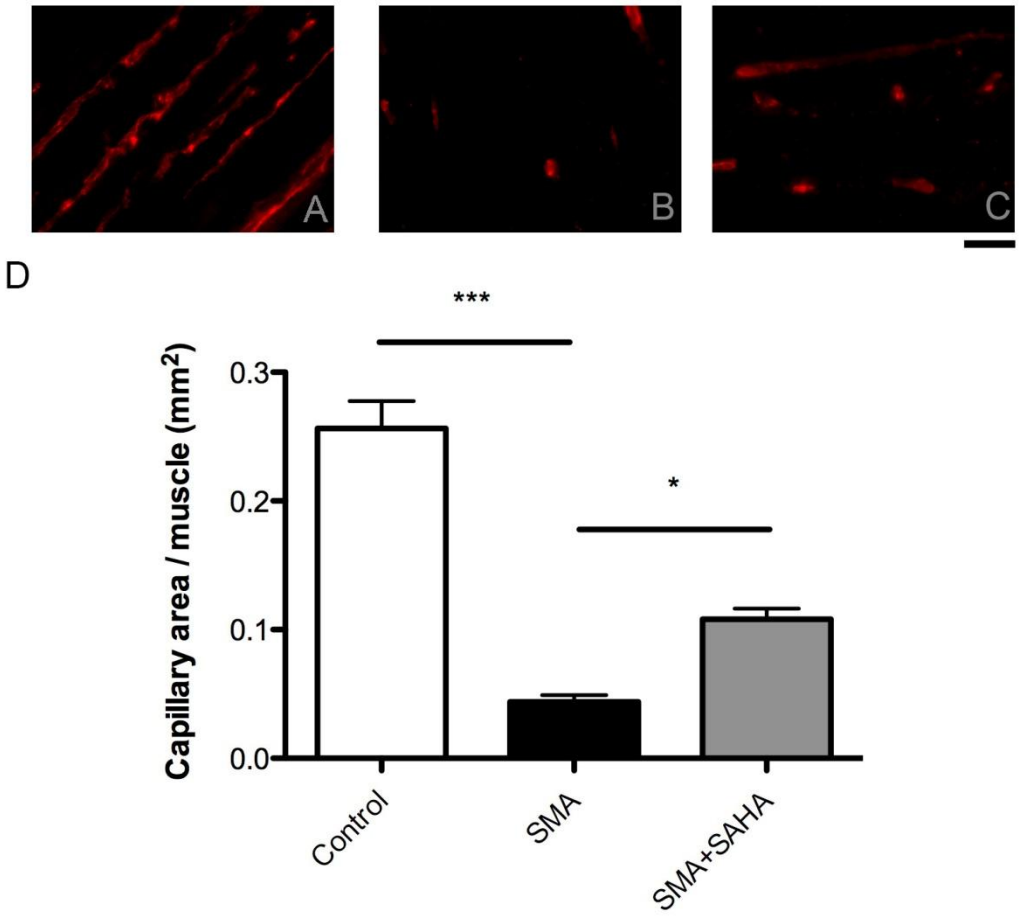

Figure 5 – Treatment with SAHA increases capillary density in late symptomatic Taiwanese SMA mice. *Representative micrographs of PECAM 1 labelled capillary bed in the gastrocnemius muscle of P11 control (A), SMA (B) and SAHA treated SMA (C)Taiwanese mice. Images are 20x magnification. Scale bar*

*equals 50µm. (D) Bar chart (mean±s.e.m) quantifying capillary density in P11 gastrocnemius muscle of control, SMA and SAHA treated SMA Taiwanese mice. Unpaired, two-tailed t-test, *** =P<0.0001, *=P<0.05. N≥3 mice and n≥6 muscles for each bar.*

4.3.2.2 Improvement in capillary and muscle fibre alignment in SAHA treated Taiwanese SMA mice

Having established that treatment with SAHA is capable of increasing capillary density in Taiwanese SMA skeletal muscle (Figure 5), the effect of SAHA treatment on other morphological defects in the capillary bed was then investigated.

The capillaries within P11 late symptomatic Taiwanese SMA *gastrocnemius* muscle displayed a more disorganised association with their underlying muscle fibres than their control counterparts (Figure 3). With capillaries in control muscle displaying a regular, parallel arrangement while capillaries in SMA muscle showed little association with muscle fibre orientation and a more dispersed vessel arrangement (Figure 3). A small improvement in the arrangement of capillaries could be seen by eye in Taiwanese SMA skeletal muscle treated with SAHA (Figure 6). In these muscles, a greater number of capillaries were observed running in parallel with their underlying muscle fibres (Figure 6C). This suggests that treatment with SAHA not only increases capillary density in skeletal muscle but also improves the overall architecture of the capillary bed. A key feature of capillary bed architecture is the structure of the vessels themselves, in particular capillary diameter, a feature we know to be affected in SMA skeletal muscle. Along with delivering nutrients,

capillaries are involved in gas exchange across their vessel walls. The surface area available to take part in this exchange is directly proportional to the diameter of the vessel. Large vessels will have a smaller surface area available for this exchange than several smaller vessels. Alterations to the diameter of capillaries will impact upon the area available for gaseous exchange in the tissue.

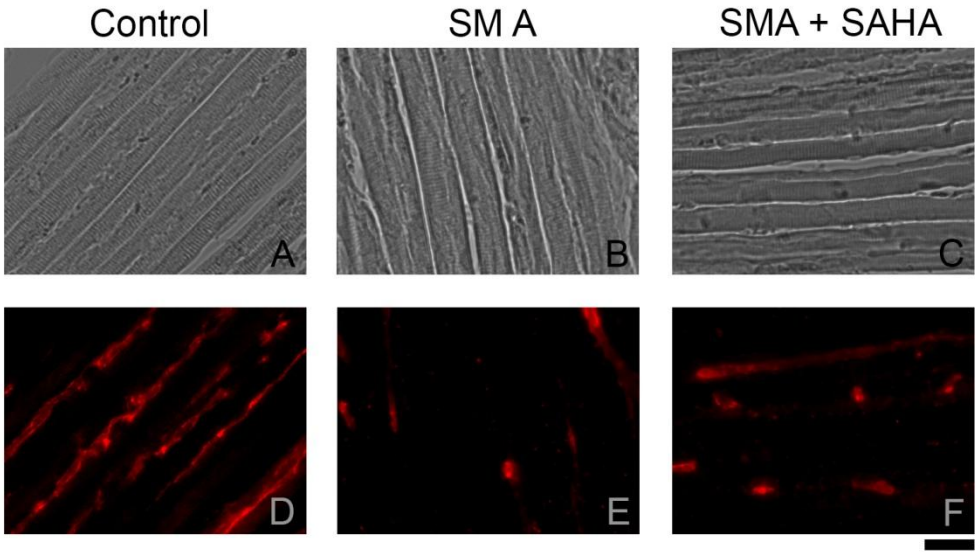

Figure 6 – Treatment with SAHA improves the relationship between capillaries and their underlying muscle fibres*. Representative phase contrast micrographs of control (A), SMA (B) and SMA mice treated with SAHA (C). Representative micrographs of the PECAM 1 labelled control (D), SMA (E) and SMA mice treated with SAHA (F) capillaries directly overlying the corresponding phase captured muscle fibres. Images are 20x magnification. Scale bar equals 50 µm.*

4.3.2.3 Restoration of capillary calibre in SAHA treated Taiwanese SMA mice

Capillary calibre was greater by 14% in P11 late symptomatic Taiwanese SMA gastrocnemius capillaries in comparison to control vessels (Figure 4). Capillary calibre in SAHA treated Taiwanese SMA gastrocnemius muscle was on average 1µm. This is a significant ($P<0.001$, One Way ANOVA with Tukey post hoc test)

40% reduction in comparison to the 1.6µm average calibre recorded in DMSO treated Taiwanese SMA *gastrocnemius* muscle. This suggests that along with the increase in capillary density and improvements in capillary bed architecture, treatment with SAHA restores capillary calibre in P11 late symptomatic Taiwanese SMA skeletal muscle.

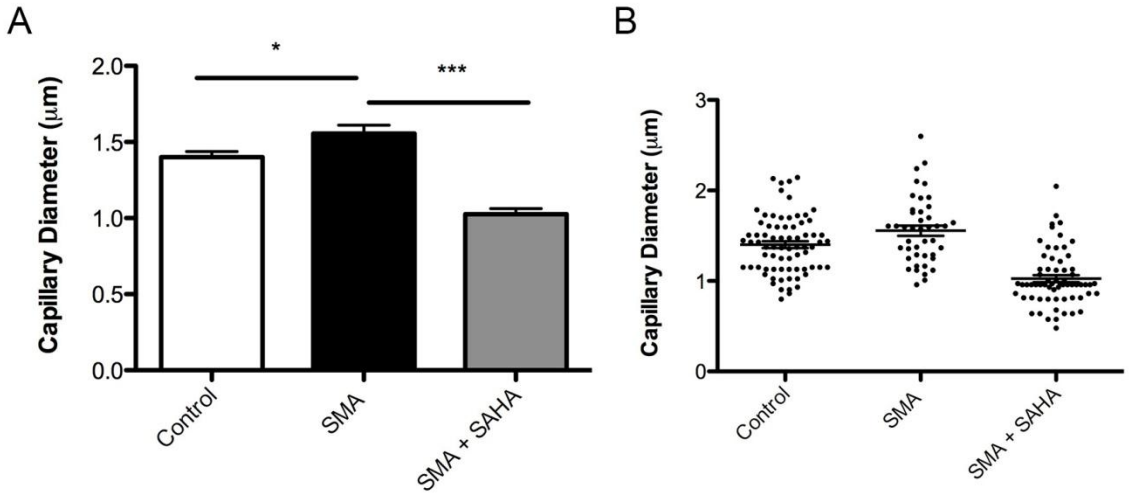

Figure 7 – Treatment with SAHA restores capillary calibre in P11 Taiwanese SMA mice. *Figure 4 - (A) Bar chart (mean ±s.e.m) quantification of capillary calibre in the gastrocnemius muscle of P11 SMA Taiwanese mice (black bar) control mice (white bar) and SMA Taiwanese mice treated with SAHA (grey bar).One Way ANOVA, with Tukey post hoc test, * = P<0.05, ***P<0.0001. N≥181 profiles from ≥6 muscles from ≥3 mice for each bar. (B) Scatter plot of capillary calibres showing distribution of calibres for each condition.*

4.3.3 Measuring protein levels of the key endothelial marker, PECAM 1, is a reliable means of assessing capillary density

Along with the fixed gastrocnemius muscle collected for morphological analysis of the capillary bed, fresh frozen *quadriceps* muscle were also collected and shipped to Edinburgh for analysis. This provided the opportunity to assess the capillary bed of skeletal muscle using molecular techniques, in particular quantitative fluorescent

western blotting. Initially, the accuracy and reliability of this method for assessing capillary density had to be determined.

4.3.4. Significant decrease in PECAM 1 protein levels in late symptomatic Taiwanese SMA mice

Throughout this work PECAM 1 has been successfully used to visualise the capillary bed of skeletal muscle, in both flat muscles of the body wall and the *gastrocnemius* muscle of the hindlimb. Given the reliability of the endothelial marker PECAM 1 (primary antibody R&D Systems Cat. No. AF3628) to label the capillary bed in a variety of skeletal muscles, it was chosen to conduct western blot analysis of the *quadriceps* muscles using this antibody.

Western blots for the PECAM 1 protein in *quadriceps* muscles of P11 late symptomatic Taiwanese SMA and control littermates showed abundant levels of the PECAM 1 protein in control *quadriceps* and reduced levels in SMA muscles (Figure 8). When quantified, in arbitrary fluorescence units, PECAM 1 protein expression in Taiwanese SMA *quadriceps* was found to be significantly ($P<0.001$, unpaired, two-tailed, students t-test) reduced by 82% in comparison to control littermates (Figure 8B). This reduction is almost identical to the 81% reduction in capillary density observed in the P11 late symptomatic Taiwanese SMA *gastrocnemius* muscles reported earlier in this chapter (Figure 2). This near identical measurement of capillary density by morphological means and molecular determination of PECAM 1 protein presence suggests that measuring PECAM 1 protein levels in tissue is an accurate and reliable means of assessing capillary density.

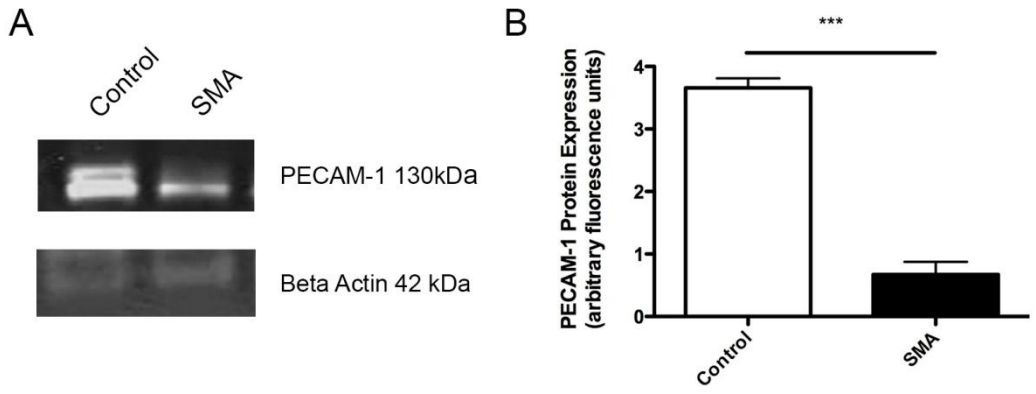

Figure 8- Western blotting of PECAM 1 reliably detects reductions in skeletal muscle capillary density. (*A) Western blot of PECAM 1 (~130kDa) and β Actin (~42kDa) of P11 Control and Taiwanese SMA quadriceps muscles. A western blot was carried out to measure the expression of the endothelial cell junctional protein PECAM 1. An antibody against PECAM 1 was used to probe protein samples extracted from P11 quadriceps muscles. In the control sample a strong band was detected at approximately 130kDa, the molecular weight of PECAM 1 protein. In the SMA sample a fainter band was present at 130kDa. β Actin was used as a loading control, with bands of similar intensity and weight present in both control and SMA samples.(B) Bar chart (mean±s.e.m) quantifying PECAM 1 expression in P11 control (white bar) and SMA (black bar) quadriceps muscles. Unpaired, two-tailed t-test, ***=P<0.0001. N≥3 mice and n≥6 muscles for each bar.*

4.3.5 Treatment with SAHA significantly increases capillary density in late symptomatic Taiwanese SMA mice

Initial western blots determined that measurement of PECAM 1 protein expression is a reliable means of assessing capillary density. Analysis of protein levels in SAHA treated *quadriceps* muscle revealed the sensitivity of the method in detecting changes in the capillary bed.

On first inspection, a band of intermediate intensity was observed in the blot of Taiwanese SMA *quadriceps* muscles treated with SAHA when compared to control and DMSO treated SMA mice (Figure 9A). While not as intense as the band

produced in the control protein sample, the 130kDa band observed in the SAHA treated Taiwanese SMA sample was larger and brighter than that observed in the DMSO treated Taiwanese SMA mice (Figure 9A). PECAM 1 protein expression measured in arbitrary fluorescence units was significantly greater in SAHA treated Taiwanese SMA mice than in DMSO treated Taiwanese SMA littermates ($P<0.05$, One Way ANOVA with Tukey post hoc test). In comparison to DMSO treated Taiwanese SMA mice, PECAM 1 protein expression was increased by 2.6 fold in SAHA treated Taiwanese SMA mice. This is almost identical to the 2.5 fold increase in capillary density measured by morphological methods in SAHA treated Taiwanese SMA *gastrocnemius* muscles. Taken together these findings suggest that treatment with the HDAC inhibitor SAHA significantly improves the capillary defect observed in P11 late symptomatic Taiwanese SMA skeletal muscle. And also, that capillary density can be reliably and accurately assessed by quantitative fluorescent western blot measurement of PECAM 1 protein expression.

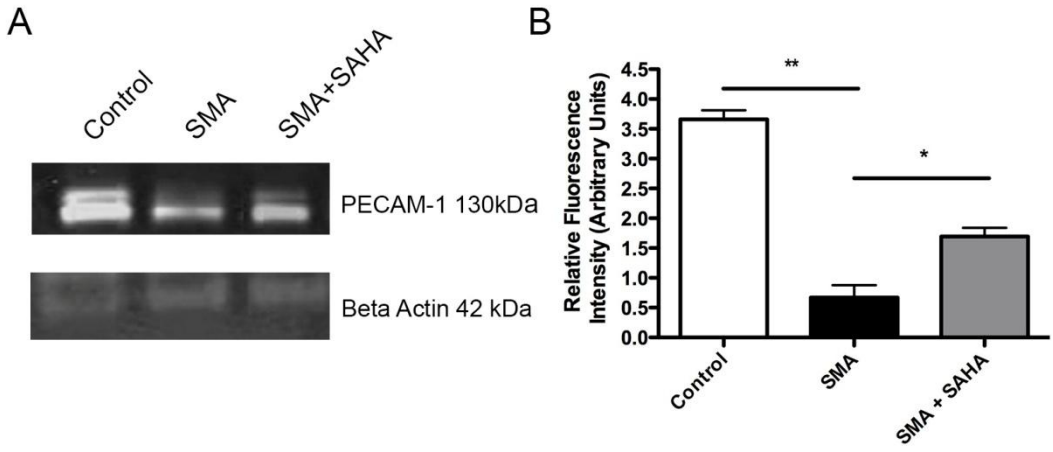

Figure 9 – Treatment with SAHA increases PECAM 1 protein expression in Taiwanese SMA skeletal muscle. *(A) Western blot of PECAM 1 (~130kDa) and β Actin (~42kDa) of the quadriceps muscles of P11 Control, SMA and SMA mice treated with SAHA. β Actin was used as a loading control, with bands of similar intensity and weight present in all three samples. Images for control and SMA*

*samples are reproduced from Figure 8. The band detected at approximate 130kDa in the SAHA treated SMA sample was of intermediate intensity, being brighter than the untreated SMA sample the band but not as intense as the band detected in the control sample.(B) Bar chart (mean±s.e.m) quantifying PECAM 1 expression in P11 quadriceps muscle of control (white bar), SMA (black bar) and SMA mice treated with SAHA (grey bar).One Way ANOVA, with Tukey post hoc test, **=P<0.001, *=P<0.05.N≥3 mice and n≥6 muscles for each bar.*

4.3.6 Treatment with the novel HDACi JNJ produces a small but not significant improvement in capillary density

These investigations highlighted the beneficial effects of HDAC inhibitor treatment on the capillary defect observed in SMA skeletal muscle. The HDAC inhibitor used, SAHA, is an FDA approved drug and is currently involved in phase two clinical trials (Riessland et al., 2010). These factors make it a highly attractive therapeutic to investigate. Another potential HDAC inhibitor of interest is the novel HDAC inhibitor JNJ, which is far more potent in action than SAHA. To investigate the effects of this novel HDAC inhibitor on the capillary defects in SMA skeletal muscle, the TVA muscle of JNJ treated mice were collected and analysed.

The TVA muscle from P5 early symptomatic JNJ treated Taiwanese SMA mice, DMSO treated Taiwanese SMA mice and their control littermates were dissected and the capillary bed labelled with the fluorescently labelled GSL -1 isolectin. Capillary density of the TVA muscle was then measured as previously described (Chapter 2). Initial observations of the stained capillary bed revealed a reduction in capillary density in Taiwanese SMA TVA muscle when compared to control littermates (Figure 10B,C). When quantified, capillary density in Taiwanese SMA mice was reduced by 30% in comparison to control littermates (Figure 10A). Inspection of the

JNJ treated Taiwanese SMA TVA muscle revealed no readily observable difference in the capillary bed when compared to DMSO treated Taiwanese SMA muscle, with JNJ treated muscle showing no real improvement in organisation or arrangement. Capillary density in the JNJ treated Taiwanese SMA TVA muscle also appeared to be unaffected. When analysed capillary density in JNJ treated Taiwanese SMA TVA muscle was found to be 6% greater than that recorded in DMSO treated SMA muscle, a small but not significant increase in capillary density (ns, One Way ANOVA with Tukey post hoc test).

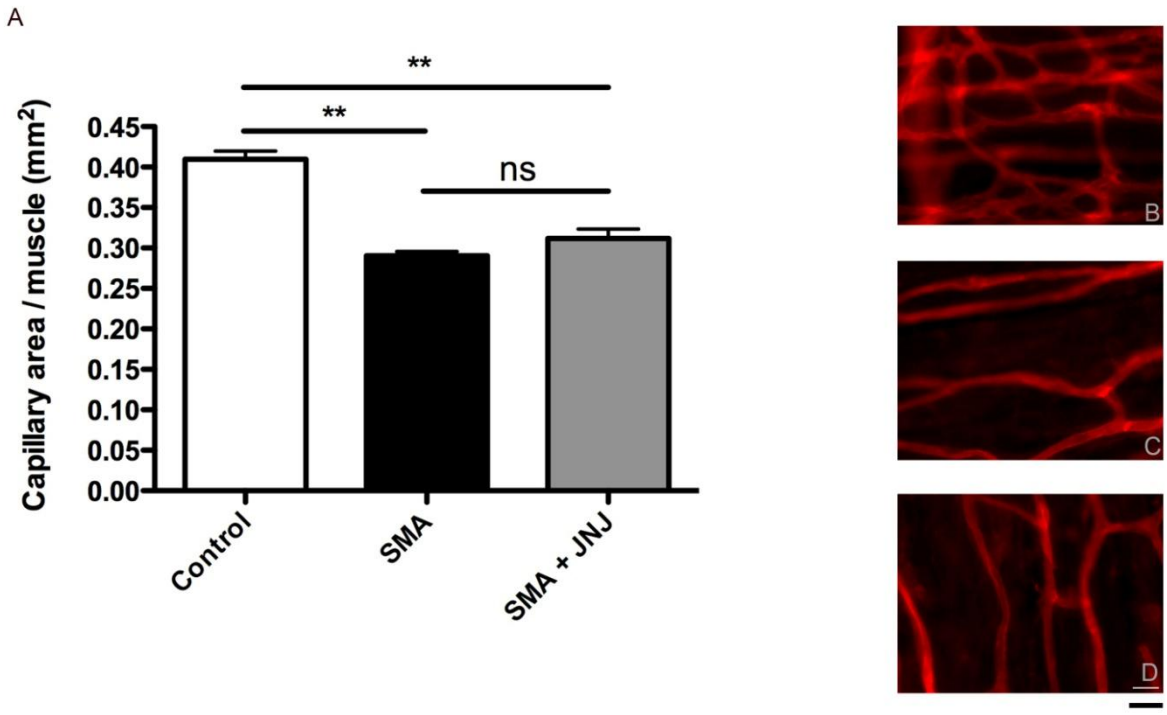

Figure 10 – Treatment with JNJ provides a small but not significant improvement in skeletal muscle capillary defects*. (A) Bar chart (mean±s.e.m) quantifying capillary density in P5 TVA muscle of control (white bar), SMA (black bar) and SMA Taiwanese mice treated with JNJ (grey bar). One Way ANOVA, with Tukey post hoc test, **=P<0.001, ns= no significant difference. Representative micrographs of PECAM 1 labelled capillary bed of the TVA muscle of P5 control (B), SMA (C) and SMA mice treated with JNJ (D). Images are 20x magnification. Scale bar equals 50µm.*

4.4 Discussion

The findings of this chapter show that ubiquitously increasing Smn protein levels via treatment with the HDAC inhibitor SAHA ameliorates the skeletal muscle capillary defect in SMA mice. Initially the results of this chapter show that the skeletal muscle capillary bed of SMA hindlimb muscles show a similar reduction in capillary density and display similar alterations to the architecture of the bed as flat muscles from the body wall. Taken together with the results of earlier chapters this work confirms that the capillary defect we observe in SMA mice is present in muscle tissue regardless of fibre type or body position.

Secondly these findings show that measuring tissue levels of the endothelial marker PECAM 1 is a sensitive and robust means of assessing capillary density. Quantitative fluorescent western blotting techniques detected an approximately 82% reduction in the levels of the endothelial marker PECAM 1 in SMA *quadriceps* muscles. This reduction in PECAM 1 protein is almost identical to the approximately 81% reduction in capillary density observed in SMA *gastrocnemius* muscles when capillary density was analysed morphologically by PECAM 1 immunostaining. When analysing SAHA treated tissue, blotting was able to detect a two fold increase in PECAM 1 levels. The same two fold increase in density that was determined by morphological analysis of the *gastrocnemius* muscle. These data suggest that quantitative fluorescent western blotting of PECAM 1 protein is a sensitive and reliable means by which to assess capillary density in tissue. Blotting for PECAM 1 can be used not only to confirm morphological assessments of capillary density but given the reliable and robust results it produces could also be used to assess tissue

capillary density independent of other assessment techniques. This may be of particular use to tissues which do not easily lend themselves to histological analysis.

Thirdly this work shows that daily dosing with the HDAC inhibitor SAHA, which is known to increase SMN levels two fold in muscle (Mutsaers et al., 2011), increased capillary density and improved the architecture of the skeletal muscle capillary bed. This increase in capillary density was observed when hindlimb muscles were assessed both morphologically and molecularly. A 2.6 fold increase in capillary density was observed in the sectioned *gastrocnemius* muscles of SAHA treated SMA mice when compared to DMSO dosed SMA mice. A similar 2.5 fold increase in the protein levels of the endothelial marker PECAM 1 in SAHA treated SMA *quadriceps* muscles when compared to DMSO dosed SMA quadriceps was also observed. This increase in capillary density is directly proportional to the increase in Smn levels previously reported by the same SAHA dosing regimen (Riessland et al., 2010, Mutsaers et al., 2011) and suggests that the severity of the capillary defect is directly linked to the level of Smn protein in muscle.

SAHA treatment was also shown to improve the architecture of the SMA skeletal muscle capillary bed. In SMA *gastrocnemius* muscle the arrangement of the capillary bed was found to be altered. SMA capillaries showed poor alignment with underlying muscle fibres and had larger calibre than control capillaries, both alterations that have been reported in previous chapters in the flat muscles of the body wall. Here it was seen that treatment with SAHA improved these alterations, in particular rescuing the enlarged calibre of SMA capillaries. The improvement of these alterations by SAHA treatment, which increases Smn protein levels, suggests

that active molecular signalling downstream of Smn regulates various aspects of capillary morphology.

Lastly it was observed that treatment with the novel HDAC inhibitor JNJ produced a small but not significant increased in capillary density in the *transverses abdominus* (TVA) muscle. Based on its potency (Delue et al., 2009) and ability to significantly increase the levels Smn protein *in vitro* and *in vivo* (Schreml et al., 2013) we hypothesised that JNJ treatment would improve the capillary defect in SMA mice. While JNJ treatment resulted in a 2 % increase in capillary density of *TVA* in Taiwanese SMA mice this was not significantly different from the 29% density seen in DMSO treated SMA mice. Failure of JNJ treatment to significantly improve the capillary defect may be due to the shorter JNJ treatment regimen determined by the earlier time point at which the animals were sacrificed in the JNJ study (P5) in comparison to the SAHA study (P10).

4.4.2 Linking Smn and the vasculature

The results of this chapter suggest that increasing Smn levels ameliorates the capillary bed defect observed in SMA skeletal muscle. This suggests a link between Smn and the signals which control the development and growth of capillaries. As previously described in earlier chapters (Discussion of Chapter 2), many of the signals which control vascular development are also used by the nervous system and vice versa. This cooperative use of patterning, outgrowth and developmental signals between the two systems is termed the neurovascular link. Given this evidence that neural and vascular systems share key signalling molecules and growth factors during development, it is reasonable to suggest that Smn, which has been shown to

play key roles in the development of skeletal muscle (Fidzianska and Wado 1990, Shafey et al., 2008, Rajeda et al., 2007, Stahas et al., 2008, Walker et al., 2008,Lee et al., 2011, Mutsaers et al., 2011) may also share molecular mechanisms with the vascular system. One potential candidate for such interaction is the Notch signalling pathway.

The Notch receptor and its ligands form a cell-cell communication pathway which plays vital roles in the development of the nervous system (Louvi and Artavanis-Tsakonas 2006, Cau et al., 2008, Pierfelice et al., 2011) and in the regulation of angiogenesis in the vascular system (Carmeliet 2005, Bray 2006, Roca and Adams 2007, Benedito et al., 2009, Ehling 2013). In both systems Notch signalling links the fate decision of one cell to those surrounding it. In the nervous system this is key in determining the neuronal or glial fate of progenitor cells during embryonic development (Louvi and Artavanis-Tsakonas 2006). In the vascular system Notch signalling determines the fate of endothelial cells at the leading edge of the growing vascular front (Ehling 2013), pushing cells to an actively sprouting "tip cell" nature or a quiescent "stalk cell" (Benedito et al., 2009), controlling where new vessels arise and so determining formation of the vascular network. Investigations have shown that disruption of notch signalling can drastically alter the formation of the developing vascular network (Benedito et al 2009).

Over-activation of the Notch signalling pathway has been shown to result in reduced branching of vessels, a delay in the extension of the growing vascular front to reach its target and an impairment in the structural organisation of vessels within networks (Benedito et al., 2009). Importantly, a similar over-activation of the Notch signalling pathway has recently been reported in SMA.

In astroglioma cells transduced with a lentiviral shSMN construct, used to deplete Smn protein levels, the expression of the Notch ligand and its receptors were found to be increased (Caraballo-Miralles et al., 2013). Significantly, in SMNΔ7 SMA mice increased Notch signalling was observed in the motor neurons of the spinal cord (Caraballo-Miralles et al., 2013). This study suggests that decreased levels of Smn can result in over expression of the constituents of the Notch signalling pathway and over activation of the pathway itself.

Taken together these studies suggest a possible link between Smn protein and the Notch signalling pathway, where decreased levels of Smn protein results in the over activation of the Notch signalling pathway (Caraballo-Miralles et al., 2013), which has been shown to cause drastic defects in angiogenesis (Benedito et al., 2009).

4.4.3 Weaknesses of Study

Although every attempt was made to ensure that this study was as robust as possible, there are areas of weakness that should be noted. Ideally, Smn protein levels in the quadriceps muscles should have been measured along with PECAM 1 levels. Given the young age of the mice (P10) the muscles collected were particularly small in size. This meant that a relatively small volume (30µl) of RIPA buffer was used to isolate total protein from homogenised muscle. Once centrifuged this resulted in a small volume of sample, which only permitted enough blots to measure PECAM 1 and loading control (β Actin) levels to be measured. As the tissue for this study was generously provided by a group out with our lab which no longer ran SAHA mice trials, collection of more tissue to perform this experiment was not possible. However, we can be confident that Smn protein levels were increased in the tissue

we examined as the muscles we analysed were taken from the exact same mice which were shown to have a twofold Smn increase in adjacent hindlimb skeletal muscles in the study by Mutsaers et al., in 2011.

Another point to note is the length of the JNJ trial. Ideally, to compare the effectiveness of SAHA and JNJ both HDAC inhibitor treatment regimens should be the same. Again the tissue for this study was generously provided by the same group as the SAHA tissue, out with our lab. While their study encompassed a longer treatment window, they required later time point muscle tissue for their own work and analyses. However, the small improvement that we see, even with the shortened treatment regimen, suggests that given a lengthier treatment timeline JNJ could well have a significant effect on capillary density in SMA skeletal muscle.

4.4.4 Conclusion

From these results we can conclude that ubiquitously increasing Smn levels using the HDAC inhibitor SAHA significantly increases capillary density and improves the capillary bed defects in Taiwanese SMA mice.

Chapter 5: Endothelial cell culture and retinal vasculogenesis in a mouse model of SMA

5.1 Introduction

In the previous chapters of this thesis we have identified and characterised a severe defect in the capillary bed of skeletal muscle and the spinal cord, in a variety of mouse models of SMA. While our studies involving HDAC inhibitor treatment of SMA mice have suggested a link between Smn protein levels and the severity of these defects, the underlying mechanism responsible for the capillary defects observed has not been established. In this chapter we present a selection of experimental paradigms which will help to determine the root cause of capillary defects in SMA.

Investigations of vascular development and control have been undertaken using a range of experimental approaches in a variety of animal models. Classical observations routinely utilise the transparent nature of chick embryos and xenopus larvae (Clark, 1918; Clark, 1939) to study the formation and growth of vessels in fine detail (Clark, 1919; Clark, 1939). Similar advantages are found in the transparent zebrafish embryo (Dodd et al., 2000) where organ and tissue development are well characterised and understood. This combined with the relative ease of genetic manipulation and protein knockdown, resulting in a large mutant zebrafish library, makes zebrafish a popular and advantageous model for the study of vascular development. While a zebrafish model of SMA is available (McWhorter et al., 2005), we have chosen to utilise experimental approaches which will allow us to investigate vascular development in our chosen model species, the mouse.

First, Taiwanese SMA and control endothelial cells will be examined in culture. This will establish if the defects in structure and number that we observe at the vessel level are a result of inherent defects in the growth and morphology of the constituent cells of capillaries themselves. Second, the capillary network of the retina in Taiwanese SMA and control littermate mice will be investigated. In mice the entire capillary network of the retina forms postnatally, making it a particularly useful preparation for investigating angiogenesis and the signalling pathways involved. Together these investigative tools should provide insight into the cause of capillary defects in SMA.

5.1.2 Endothelial Cells

All blood vessels are lined by a monolayer of endothelial cells. In the larger veins and arteries, blood vessel walls are composed of multiple layers of cellular and extracellular materials, while capillary walls are composed solely of endothelial cells covered by a loose scattering of pericytes (Figure 1).

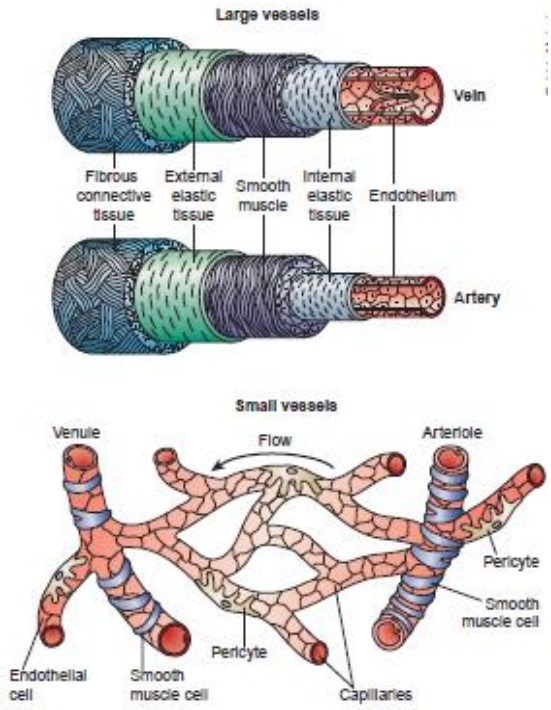

Figure 1 – Figure taken from Cleaver & Melton 2003 to show the difference in vessel wall composition between arteries, veins and capillaries.

This endothelial lining is important in all vessels, regulating vascular homeostasis via the release of vasodilating and vasoconstricting factors, with the balance of these factors ensuring appropriate organ perfusion. Alterations to normal endothelial function is critical in many pathological conditions and can lead to the development of atherosclerosis, thrombosis and vasospasm (Shimokawa, 1999). Any defects in the endothelium will be particularly pertinent in capillaries, which are comprised almost solely of endothelial cells.

Endothelial cells are highly diverse showing regional specifications depending on the size of the vessel and the organ their vessels are found in (Cleaver & Melton, 2003). The endothelial cells found in capillaries are flat and elongated while the endothelial

cells of large vessel endothelium are polygonal and much thicker (Thorin & Shreeve, 1998). In skeletal muscle, brain, spinal cord, heart and lungs endothelial cells form a continuous endothelium with no gaps between cells, forming continuous capillaries. In endocrine and exocrine glands and the small intestine 80-100nm gaps called fenestrations are present between endothelial cells resulting in fenestrated capillaries. Discontinuous capillaries, such as the sinusoids of the liver, have large lumens, numerous fenestrations and almost no basal lamina (Pasqualini et al., 2002). These differences in endothelial cell association reflect the different functions of the tissue the capillary bed resides in. Continuous capillaries are found in the nervous system where they contribute to the formation of the brain and spinal cord blood barriers to protect the nervous system from toxic substances. While the liver readily involved in filtering the blood, requires discontinuous, permeable sinusoids. These tissue specific differences in the capillary bed are a result of signals sent from the surrounding tissue to the endothelial cells.

Evidence of this tissue micro-environment signalling to endothelial cells comes from heterotopic transplantation experiments in quail embryos. Blood vessels taken from neural tissue of very young embryos, which had yet to be vascularised, was transplanted into host chick embryos and mesoderm which had yet to be vascularised was grafted into the brain of chick embryos. Peripheral vessels which grew into the grafted neural tissue developed the morphology and histology of the blood brain barrier, while neural vessels growing into a graft of mesodermal tissue lost their barrier characteristic (Stewart et al., 1981). This suggests that the structural characteristics of endothelial cells develop in response to factors in their local

environment. Similar findings were reported in a later study using heart tissue grafting in mice (Aird et al 1997).

Von Willebrand Factor (vWF), a binding protein important in platelet adhesion, is expressed solely by endothelial cells, although not by all endothelial cells. The differential expression of vWF by endothelial cells was revealed by transgenic mice in which the vWF gene was coupled to a LacZ reporter. vWF expression was observed in the brain, heart and skeletal muscle endothelial cells but not a variety of other tissues including in the liver, spleen, lung or kidney (Aird et al., 1997). These findings show endothelial cell specialisation at the gene expression level, alongside the structural specialisations described earlier in the introduction (Thorin & Shreeve, 1998; Pasqualini et al., 2002). In further experiments using this mouse line, the heart of a donor mouse was transplanted subdermally into the ear of a host mouse. The presence of the heart in the ear resulted in the LacZ expression of vWF in the auricular blood vessels of the host that was not observed prior to transplant. This suggests that not only are the structural characteristics of endothelial cells influenced by their surrounding environment but that gene expression in endothelial cells is determined by their surrounding environment. Not only can the surrounding tissue environment influence the nature of endothelial cells, it can also regulate vessel architecture and organisation. This is achieved by signalling through endothelial cells via local angiogenic agents, specifically the VEGF family (D'Amore & Ng, 2002).

Vascular Endothelial Growth Factor (VEGF) regulates multiple endothelial cell behaviours including the initial patterning of endothelial cells in the embryo, the recruitment of endothelial cells during wound healing and in tumour angiogenesis,

along with the maintenance of endothelial cells in normal tissue (Ferrara & Alitalo, 1990). Locally secreted VEGF signals have also been shown to drive endothelial cell development (Stone et al., 1995; Ng et al., 2001; Mukouyama et al., 2002).

VEGF from the alveoli of the lungs has been shown to pattern pulmonary vasculature formation (Ng et al., 2001). In situ hybridisation for the VEGF188 isoform in the lungs revealed high levels of expression in Type II alveolar epithelial cells. Targeted deletion of the VEGF188 isoform resulted in defects in the formation of the pulmonary vasculature, including a reduction in the number of capillaries in the lung and a miss-localisation of larger vessels which were found uncharacteristically close to the pleural surface (Ng et al., 2001). This reduced capillary number and disorganisation of the vascular network is reminiscent of the capillary defects we have previously described in the skeletal muscle (Chapter 2) and spinal cord (Chapter 3) of SMA mice. Similar patterning of blood vessels by local VEGF is observed in the skin (Mukouyama et al., 2002).

Mukouyama and co workers observed that arteries were aligned with peripheral nerves in embryonic mouse limb skin. To determine if this alignment was the result of coordinated nerve and vessel growth several mutant mouse lines were examined. Neurogenin1/Neurogenin2 null mice lacking peripheral sensory nerves showed improper arteriogenesis, with altered vessel morphology and a reduced expression of arterial markers. This suggests that peripheral arteries and nerves follow the same pattern of growth. To test this potentially linked system further, the pattern of limb arteries were studied in mice with mutations in the axon guidance gene Semaphorin 3A. These mice displayed disorganised peripheral nerve growth but despite this

disorganisation the blood vessels still aligned with the nerve (Mukouyama et al., 2002). This suggests that signals secreted from the nerves pattern blood vessel growth in skin. Similar to the lungs this signal was identified by immunological, RT-PCR and *in vitro* cell experiments, as VEGF (Mukuoyama et al., 2002).

Taken together these experiments show that the tissue surrounding endothelial cells is important in determining endothelial cell characteristics, gene expression and the structure of the vessels they form. Studies have revealed that endothelial cells are not passive recipients of external tissue signals but actively signal their local tissue environment. Endothelial cells produce multiple growth factors and cytokines and possess a variety of cell-surface molecules (Vapaatalo & Mervaala, 2001). All of which suggest that endothelial cells are readily capable of participating in communication with their surrounding tissues. In particular, disruption of endothelial derived VEGF results in defects in the surrounding organ (Kimato et al., 1997; Zeng et al., 1998).

Loss of VEGF signalling has been shown to cause defects in the structure and function of the kidney (Kitamoto et al., 1997; Gerber et al., 1998). Blocking endogenous VEGF signalling in the kidney epithelium causes a reduction in nephron number (Gerber et al., 1998) and abnormal glomerular structure which resulted in systemic oedema (Kitamoto et al., 1997). Overexpression of endothelial VEGF has been shown to be just as damaging to the organisation and structure of the lung (Zeng et al., 1998). Enhanced VEGF expression in the developing lung endothelium resulted in an increase in the size of the main pulmonary vessels, suggesting enhanced vasculogenesis. However, the branching morphology of the lung was

adversely affected, with a decrease in the number of terminal buds along with an inhibition of alveolar cell differentiation (Zeng et al., 1998). These studies suggest a role for endothelial cell signalling in the normal development of the kidney and lungs. The necessity of endothelial cells in the normal functioning of multiple organs including the heart (Rouleau et al., 1993; Brutsaert et al., 1998), pancreas (Lammert et al., 2001) and liver (Matsumoto et al., 200; LeCouter et al., 2003) has been reported in multiple studies. Importantly, defects in the structure and function of these organs have been reported in SMA patients (Rudnick-Schoneborn et al., 2008; Bowerman et al., 2012) and mouse models of the disease (Vilte et al., 2004; Bevan et al., 2010; Heier at al., 2010; Hau et al., 2011; Shababi et al., 2010, Bowerman et al., 2014).

Defects in both the structure (Rudnick-Schoneborn et al., 2008; Shababi et al., 2010) and coordinated beating (Heier et al., 2010; Bevan et al., 2010) of the heart are commonly reported in SMA patients and mice. 75% of Type I patients display atrial and septal defects and a high incidence of hypoplastic left heart syndrome (Rudnik-Schoneborn et al., 2008). Arrhythmia and bradycardia are also reported in mice models of the disease (Heier et al., 2010) with this impaired function leading to early heart failure (Bevan et al., 2010). Similar defects in structure and function are reported in zebrafish and mice where the endothelium of the heart, the endocardium, has been disrupted (Strainer et al., 1996).

Deletion of the endocardium in zebrafish embryos disrupts normal cardiac development and results in defects of the heart chambers, with smaller ventricles and dilated atria in the mutant fish. A reduced contractility of the heart is also noted in

these mutants (Stainer et al., 1996). This suggests that the endocardium is important for not only the proper development of cardiac structure but also cardiac function. This role of the endocardium in cardiac contractility is also suggested by studies involving physical disruption of the endocardium in mice (Roulea et al., 1993).

When the endocardium of mouse hearts was physically disrupted, by injection of Triton-X-100 into the coronary arteries of the heart, the contractile properties of the ventricular papillary muscles were affected (Roulea et al., 1993). Both the duration and strength of papillary muscle contraction was reduced, suggesting that the endocardium is capable of modulating the contractility of the myocardium.

Taken together these studies suggest that the endocardium is critical in ensuring the proper structural development and normal functioning of the heart. Any defects in the endothelial cells, which form the endocardium, could precipitate structural and functional defects in the heart. Given the defects we have observed in SMA capillaries it is possible to suggest that defects of their comprising endothelial cells could be a contributing factor to the structural and functional defects seen in SMA patients and mice models. Endothelial cells are also crucial in the development of the pancreas and liver, two other organs that display abnormalities in SMA (Vitte et al., 2004; Hau et al., 2011; Bowerman et al., 2012; Bowerman et al., 2014).

Severe impairment of liver development is seen in mice where the exon 7 element of murine Smn has been specifically deleted in the liver (Vitte et al., 2004). Atrophy of the liver was evident along with a failure of the tissue to regenerate which resulted in late embryonic death (Vitte et al., 2004). These findings suggest that Smn is essential for the normal development and growth of the liver. Similar defects regarding

development and growth of the liver are observed in mutant mice lacking endothelial cells in the liver (Matsumoto et al., 2001).

In mutant mice where endothelial cells were prevented from forming in the liver the overall growth of the organ was reduced. Defects were also observed at the cellular level when hepatocytes failed to differentiate (Matsumoto et al., 2001). Communication between endothelial cells and differentiated hepatocytes is essential for the release of growth and survival factors (LeCouter et al., 2003). Defects in the release of circulating factors could have potentially widespread systemic effects, such as those caused by the pancreatic defects observed in SMA (Bowerman et al., 2012).

In 2B model SMA mice, an imbalance in pancreatic cell type is observed, with a high number of glucagon releasing α cells resulting in a reduced number of insulin producing β cells (Bowerman et al., 2012). Along with this alteration in the cellular composition of the pancreas several defects in glucose homeostasis were also reported including hyperglycemia, hyperglucogonemia and glucose resistance (Bowerman et al., 2012). Importantly similar cellular and metabolic defects are also found in SMA patients (Bowerman et al., 2012). Endothelial cells have also been reported to be particularly important in the proper development of pancreatic cells (Lammert et al., 2003). Removal of abdominal aorta region endothelium in developing Xenopus embryos resulted in the absence of pancreatic gene expression in the mesoderm and a failure of pancreatic cells to differentiate (Lammert et al., 2003).

Taken together these studies imply that the endothelium is a source of developmental signals in organogenesis. This suggests that as well as ensuring appropriate nutrient delivery and waste removal, the endothelium, and its constituent endothelial cells, is a key modulator of organ formation and development. These studies suggest that systemic impairment in the functioning of the endothelium could cause widespread organ defects, a situation that is observed in multiple mouse models of SMA (Hamilton & Gillingwater 2013) and is increasingly apparent in SMA patients (Dahl et al., 1975; Musch et al., 1975; Crawford et al., 1998; Rudnick-Schonebon et al., 2008; Araujo et al., 2009; Bowerman et al., 2012).

Our previous findings have detailed a dramatic capillary defect in SMA mice in comparison to control littermates. Based on the knowledge that endothelial cells are the major cellular component of capillaries and on the evidence that perturbations in endothelial cells can cause organ abnormalities similar to those observed in SMA patients and animal models, we hypothesised that the form and function of endothelial cells could be altered in SMA. Therefore, endothelial cells were isolated from symptomatic Taiwanese SMA and control littermate mice and grown in culture. The morphology, growth and histological characteristics of the cells were analysed using immunohistochemical staining and fluorescent and light microscopy. SMA endothelial cells were found to express reduced levels of the Smn protein when compared to control endothelial cells. When compared to control endothelial cells, the morphology, growth rate and expression of the endothelial marker PECAM 1 in SMA endothelial cells was found to be no different.

5.1.3 The Retina

The murine retina has long been the preferential experimental preparation for studying vascular development. This is due to the fact that the entire retinal vasculature develops postnatally, with the majority of vessel development occurring with the first two weeks of postnatal life (Blanks & Johnson, 1986). This postnatal development allows for the observation of vascularisation from its initial stages until completion. In addition to this, murine retinas are small and very thin, allowing for the visualisation of their entire vascular system in flat, whole mount preparations without the need for sectioning. Multiple studies have capitalised on the advantages of the retina to study vasculogenesis and angiogenesis in detail.

The initial blood supply within the developing eye is a transient capillary network within the hyaloid. The hyaloids vascular network extends from the back of the eye, where the hyaloids artery emerges with the optic nerve, to the developing lens. This network of capillaries supplies the lens and the primary vitrous of the developing eye. In mice the hyaloid network forms at E10.5 and is completed by E13.5. By P16 the entire hyaloids vessel network is completely regressed (Albè, et al., 2009). During this period of postnatal regression the vessels of the retina form.

The blood vessels of the retina are arranged in two planar layers and formed by three stages of vascular differentiation (Connolly et al., 1988). In the initial phase the superficial layer of the retina is vascularised. This stage occurs between P0 and P10 where retinal vessels begin to extend radially from the optic disc to the peripheral edge of the retina. Between P2 and P8 the growth of the vessels lags behind the growth of the retina and so the peripheral edge of the retina remains temporarily

avascular. By P10 the retina has reached its mature dimensions and the vessels extend to the edge of the retina. By this stage the vessels also display the characteristic radial arrangement seen in the retina (Connolly et al., 1988).

In the second phase of development the vascularisation of the deeper retinal layers occurs. By P4 primordial vessels appear in the deeper layer of the retina. These primitive vessels are polygonal in appearance and so can be differentiated from the more mature superficial layer vessels which assumed a more radial appearance (Connolly et al., 1988).

In the third phase of vascularisation the capillary network in the retina beings to mature. By P7 a primitive capillary network is readily observable in the nerve fibre layer of the retina. This primitive network is made purely of capillaries. As the capillary plexus matures the vessels are remodelled, with some vessel walls thickening to form arteries, arterioles, veins and venules and some vessels regressing. This process of remodelling then moves to the deeper layers of the retina to form mature vascular networks throughout the layers of the retina (Connolly et al., 1988). By P14 this remodelling is complete and the vascular network in the retina has the appearance of an adult vascular pattern. In this pattern a variety of vessel diameters are seen with large vessels radiating from the optic disc to the ora serrata with smaller vessels branching between them to form a highly arborised pattern. Although the retina retains this appearance into adult life remodelling of the retina vasculature is observed as late as P45 (Connolly et al., 1988). This highlights the dynamic nature of the retinal vasculature which can also be seen in the response of the retinal vasculature to pathology and disease.

As the vasculature of the retina forms in response to hypoxia and hypoxic signalling, any disruption of the oxic conditions of the eye results in drastic alterations in the retinal vasculature and can result in Retinopathy of Prematurity (ROP), a common cause of blindness in premature infants (Dorrell & Friedlander, 2006). In humans, retinal vasculogenesis occurs during the second and third trimester and so can be incomplete in premature infants. Hyperoxia treatment is common in the care of premature infants, in an effort to ease respiratory distress. However, these high levels of oxygen can disturb normal retinal vascular development (Dorrell & Friedlander, 2006) Hyperoxia blunts vessels and causes pre-existing vessels to regress. When the infant is returned to normal oxygen conditions this underdeveloped vasculature results in retinal hypoxia, which induces pathological neovascularisation (Madan & Penn, 2003). Without normal developmental regulation, these new vessels are structurally and functionally compromised and these defects eventually lead to retinal detachment and significant visual impairment (Patz, 1986). As the developmental stage of the vasculature of the retina in newborn mice approximates that of premature human infants (Connolly et al., 1988), neonatal mice are an ideal system to model ROP.

In mice models of ROP, newborn pups are subjected to hyperoxic conditions for the first 5 days of postnatal life. In these hyperoxic conditions the hypoxia normally experienced by the retina following increased neural activity does not occur and so the hypoxia induced VEGF expression that drives retina vascularisation is downregulated. As a result no central retinal vessels are formed (Smith et al., 1994). Once the mice are returned to normoxic conditions the under-perfused retinal tissue becomes overtly hypoxic. This extreme hypoxia induces a strong and uncontrolled

secretion of VEGF. This excessive VEGF expression leads to pathological neovascularisation in the retina, including the formation of vascular buds in the avascular vitrous humor of the eye (Smith et al., 1994). Pathological vessel growth is also observed in forms of Age-Related Macular Degeneration (AMD: Saint-Geneiz & D'Amore, 2004).

Exudative AMD is characterised by the pathological growth of vessels into the sub-retinal space. These new vessels are particularly leaky in comparison to the retinal vasculature which possess a more barrier like nature given the position of the retina within the central nervous system (Connolly et al., 1988). The leaky nature of these invading vessels leads to the accumulation of blood and fluid in the posterior portion of the retina. This swelling eventually leads to detachment of the retina and the loss of vision (Saint-Geneiz &D'Amore, 2004). Alterations to the composition and structure of retinal vessels are also observed in Diabetic Retinopathy (Saint-Geneiz & D'Amore, 2004).

Of the variety of ocular complications that arise in diabetes, Diabetic Retinopathy is classed as the most severe (Frank, 2004). In its earliest forms the condition is present in almost all Type 1 and Type 2 patients who have lived with the disease for 20 years (Frank, 2004). In the condition the structure and organisation of retinal blood vessels is altered. Vessels appear torturous and irregular is diameter, with thickened basement membranes. Vessels also show a loss of pericytes and an increase in permeability which results in multiple microaneurysms and haemorrhages which cause visual loss (Frank, 2004).

The pathological growth of vessels observed in these conditions results from interference in the fine control of vessel growth and development. Angiogenesis, the growth of new vessels, is a complicated, multi stage process with each stage requiring the control and interaction of numerous signalling systems. In early angiogenesis, endothelial cells must respond to external proliferative growth factor and cytokine signals (Provis et al., 1997). These new endothelial cells must then organise themselves into a vessel like structure. This involves the finely controlled breakdown of the extracellular matrix (ECM: Stetler-Stevenson and Yu 2001) which the endothelial cells must then navigate through to reach their desired location. To do so the endothelial cells must communicate with ECM receptors and then utilise cell-cell adhesion molecules to form primitive vessels (Ingber, 2002). These primitive vessels must then be remodelled to form the mature vascular network. This involves pruning of excess vessels (Ishida et al., 2003) and structural alterations of the remaining vessels, including thickening of the basement membrane and acquisition of appropriate mural cells (Das & McGuire, 2003). This process requires the interaction of multiple cell types and signalling pathways. Due to its multiple advantages, the retina provides an ideal preparation for the study of this complex control of vascular development, which involves the action of growth factors, signalling pathways and the influence of non vascular cells (Dorrell & Friedlander, 2003).

In addition to the crucial role of VEGF in initiating vascular development, numerous studies utilising the retina have identified a variety of growth factors which are also involved in initiating vascular development. Placental growth factor (PGF) (Feeny et al., 2003), platelet derived growth factor (PDGF) (Fruttiger et al., 1996) and basic

fibroblast growth factor (bFGF: Friedlander et al., 1995) have all been identified as key initiators of vascularisation. Along with this initiating role, growth factors also play a regulatory role in angiogenesis, in particular, insulin-like growth factor (IGF) which regulates VEGF signalling (Smith et al., 1999). Interruption of IGF action, by antagonism of the IGF-1 receptor, prevents the proliferation and migration of endothelial cells delaying retinal vascularisation (Smith et al., 1999) and resulting in a retinal phenotype similar to that observed in ROP (Hellstrom et al., 2001). In addition to growth factor signalling, several other signalling pathways are crucial to the formation and development of the retinal vasculature, in particular the Notch signalling pathway which controls angiogenesis (Krebs et al., 2000; Carmeliet 2005; Bray 2006; Hoffman & Iruela –Arispe 2007; Roca and Adams 2007; Benedito et al., 2009; Ehling 2013;).

Initial studies involving Notch mutant mice revealed the importance of Notch signalling in angiogenesis, with mice lacking the Notch 1recpetor displaying severe defects in angiogenic vascular remodelling (Krebs et al., 2000). These defects began embryonically with mutant embryos being able to form primary vascular networks but failing to remodel these putative structures into mature vascular networks (Krebs et al., 2000). Further studies investigating the localisation and distribution of the Notch 1 receptor ligands hinted at the complexity of the Notch signalling pathway (Hofman & Iruela-Arispe, 2007). The Notch 1 receptor has multiple ligands including Jagged 1 (Jag1) and Delta-like 4 (Dll4). Immunological analysis of their distribution during the postnatal development of the retinal vasculature revealed a widespread expression of Dll4 in the vasculature but a more restricted pattern of Jag1 expression, (Hofman & Iruela-Arispe, 2007) suggesting distinct roles for the ligands

during angiogenesis. These ligands were later found to have opposing effects in angiogenesis. While Jag1 is highly pro-angiogenic, Dll4 inhibits endothelial tip cell sprouting (Benedito et al., 2009). Disruptions to the balance of these ligands results in drastic angiogenic defects (Benedito et al., 2009).

Specific loss of the Jag1 ligand in endothelial cells results in a reduced retinal vasculature. In mice lacking endothelial Jag1 the area of retina covered by vessels was reduced and the vessel present had fewer branch points and a decrease in tip cell number at the growing angiogenic front (Benedito et al., 2009). Overexpression of Jag1 in endothelial cells promoted endothelial cell sprouting and increased the number of tip cells (Benedito et al., 2009). Similar alterations to the retinal vasculature are observed when the normal astrocyte population of the retina is altered (Fruttiger et al., 1996; Dorrell et al., 2002).

In the embryonic retina, astrocytes emerge from the optic nerve and radiate to the peripheral edge of the retina forming a template which endothelial cells colocalise with and follow during their postnatal expansion across the retina (Dorrell et al., 2002). When this astrocyte network is prevented from forming, the vascular network also fails to develop (Fruttiger et al., 1996). Conversely, excessive astrocyte number results in an overly dense vascular pattern (Dorrell et al., 2002). These findings highlight the importance of cells beyond the vascular system in normal retinal vascular development.

Taken together these studies not only highlight the multitude of factors involved in initiating, controlling and regulating angiogensis in the retina, but they also emphasise how alterations in any single factor can result in drastic alterations to

normal vascular network formation and development. Interestingly many of the elements involved in retinal angiogenesis have been implicated in SMA (Caraballo-Miralles et al., 2013)

Alterations to the Notch signalling pathway have been reported in Smn deficient cells *in vitro* and *in vivo*. When Smn protein levels were reduced in astroglioma cells, using lentiviral shSMN, the expression of the Notch receptor and it's ligands in the cells were found to be increased (Caraballo-Miralles et al., 2013). Importantly, a similar pattern of increased Notch pathway expression was also reported *in vivo*. When analysed, the motor neurons of SMNΔ7 SMA mice displayed increased levels of Notch signalling (Caraballo-Miralles et al., 2013). This study suggests that decreased levels of Smn can result in over expression of the constituents of the Notch signalling pathway and over activation of the pathway itself, which has been shown to result in drastic angiogenic defects in the retina (Benedito et al., 2009). As well as this increase in signalling pathway activation, an increase in the number of glial cells is a commonly reported feature of SMA (Araki et al., 2003; Garcia-Cabezas et al., 2004; Kuru et al., 2009; Caraballo-Miralles et al., 2013).

Gliosis in the spinal cord has been reported in Type I and Type II SMA patients (Araki et al., 2003; Garcia-Cabezas et al., 2004; Kuru et al., 2009) and has also been reported in the SMNΔ7 mouse model of SMA (Caraballo-Miralles et al., 2013). If this increase in glial cell number is consistent throughout the nervous system, a significant impact on the retinal vasculature could be observed, given that both an increase and a decrease in astrocyte number can alter the formation and structure of the retinal vasculature (Fruttiger et al., 1996; Dorrell et al., 2002).

Our previous findings have shown a significant capillary defect in SMA skeletal muscle and spinal cord, in comparison to control littermate tissue. Based on the advantages of the retina as an experimental tool we chose to investigate vascular development in SMA mice using the retina. Based on our previous findings of capillary defects in multiple tissues and the evidence that signalling pathways which control retinal vascular development are altered in SMA, we hypothesised that the retinal vasculature could be altered in SMA. Therefore, retinas were collected from Taiwanese SMA mice and control littermates at varying stages of disease progression. The development of the retinal vasculature was analysed using immunohistochemical staining and fluorescent microscopy. Significant defects were observed in the form and extent of the vasculature of SMA mice in comparison to control retinas. These defects were observed at a presymptomatic disease timepoint and became increasingly worse as the disease progressed.

5.2 Methods

5.2.1 Ethics Statement

All animal experiments were approved by a University of Edinburgh internal ethics committee and were performed under license by the UK Home Office (Project License number 60/3891).

5.2.2 Animal Husbandry

(SMN2)2Hung Smn1^{tm1Hung}*/J* mice (originally received from Brunhilde Wirth in Koln) on a congenic FVB background were maintained as heterozygous breeding pairs under standard SPF conditions in animal care facilities in Edinburgh. All animal procedures and breeding were performed in accordance with Home Office and institutional guidelines. Retrospective genotyping was carried out using standard PCR protocols detailed in previous chapters (Chapter 2).

5.2.3 Genotyping of Taiwanese SMA mice

Retrospective genotyping of Taiwanese SMA and control littermates was performed as previously described in earlier chapters (Chapter 2).

5.2.4 Isolation and Culture of Mouse Endothelial Cells

Isolation and culture of mouse lung endothelial cells was performed by modifying protocols described by Lim & Luscinskas (2006).

5.2.4.1 Preparation of Plates

Collagen Type I (BD Biosciences) was diluted in acetic acid at a concentration of 50µg/ml. This solution was deposited onto 13mm glass coverslips in individual wells of sterile 24 well plates at a concentration of 5µg/cm^2. The coverslips were left under

sterile conditions for 2 hours before being washed twice with sterile PBS (Invitrogen) and left under sterile conditions to air dry before use. Coverslips were coated fresh on the day of tissue collection.

5.2.4.2 Tissue Collection

P7 Taiwanese SMA mice and control littermates were sacrificed by an overdose of anaesthetic administered via intraperitoneal (IP) injection of sodium pentabarbitol (Euthenal). Lungs were removed from the mice under sterile conditions and immersed in sterile PBS. Taiwanese SMA and control lungs were separated into two groups. Once in sterile PBS,the lungs were gently minced using fine scissors before being lysed Collagenase A (Roche). The minced lung was added to 5 mls of 0.1% Collagenase A (Roche) and heated in a water bath at 37°C for one hour. Tubes were periodically agitated by hand during incubation.

5.2.4.3 Culture System

Following incubation with Collagenase A (Roche) the resulting lung cell suspension was passed through a round end glass cannula 12 times before being filtered through a 100µm cell sieve (BD Falcon SLS 352360) which was then washed with 5mls of EGM2 media (Lonza CC-3162). The sieved suspension was then centrifuged at 400G for 15 minutes with the resulting pellet re-suspended in fresh EGM2 media. 120µl of the cell suspension was added to each coverslip which were then incubated at 37°C with 5% CO_2 for at least 4 hours before an additional 250µl of EGM2 media was added to each well. Cells were incubated for 24 hours at 37°C with 5% CO_2 before the media was removed and replaced with 350µl of fresh media. Cells were

incubated at 37°C with 5% CO_2 until cells reached 90% confluence, normally achieved by 10 days. During this period media was changed every two days.

5.2.4.4.Immunohistochemistry

When cells had reached the desired confluence, coverslips were rinsed 3 times with 0.1M PBS and fixed with 4% PFA for 10 minutes at room temperature. Cells were then permeabilised by incubating coverslips with ice-cold methanol for 15 minutes at -20°C. Coverslips were then rinsed 3 times with 0.1M PBS to remove any remaining methanol. The cells were then incubated with modified blocking buffer (1% BSA in 0.1M PBS) for an hour at room temperature. Following blocking, cells were incubated with primary antibodies against PECAM 1, Vessel Endothelial Cadherin (VE-cadherin) and SMN for one hour at room temperature: PECAM 1 (R&D Systems, AF3628) at a concentration of 1:500, VE-Cadherin (Abcam ab7047) at a concentration of 1:50 and SMN (BD Biosciences) at a concentration of 1:100 made up in blocking buffer. Following this incubation cells were rinsed 6 times with blocking buffer before being incubated with secondary antibodies for one hour at room temperature: donkey anti-goat Cy 3 conjugated secondary antibody (Jackson ImmunoResearch Laboratories Inc) at a concentration of 1:250 and anti-mouse dylite 488 conjugated secondary antibody (Dako) at a concentration of 1:100 made up in blocking buffer. The cells were then rinsed 6 times with blocking buffer. For nuclear staining DAPI was applied to the cells for 3 minutes before being washed rinsed 6 times with 0.1M PBS. Coverslips were then mounted on glass slides with mowiol (Calbiochem) and left overnight at room temperature, in the dark to set before imaging the following day.

5.2.4.5 Imaging

Phase contrast images of growing cells were captured using a standard inverted epifluorescence microscope (Olympus 1X71) combined with a chilled CCD camera (Hammamatsu C4742-95) and OpenLab (Improvision) image capture software. Micrographs for cell purity and protein expression were captured using a Zeiss LSM 710 laser scanning confocal microscope (20 x objective/ 0.4 NA; 40 x objective/ 1.3 NA oil objective). 488nm,543nm and 633nm laser lines were used for excitation. All images were captured using identical confocal settingsto allow for the comparison of expression levels between Taiwanese SMA and control cultures. Resulting images were prepared using Adobe Photoshop CS 6.

5.2.4.6 Quantification and Analysis

A minimum of two confocal images were captured per slide. Cell number was counted using the Cell Counter plugin for Image J (NIH). Endothelial cell culture purity was calculated as the percentage of cells in representative micrographs that were immunostained by all three markers (PECAM 1, VE-Cadherin and DAPI). SMN and PECAM 1 expression levels in Taiwanese SMA and control cells were measured using Image J (NIH). Using Image J (NIH) the area, integrated density and mean grey value of individual cells in a 20 x magnification image were measured. To obtain a measurement of background, area, integrated density and mean grey value were measured in multiple regions lacking fluorescence. To calculate Corrected Total Cell Fluorescence (CTCF) the following formula was used:

CTCF = Integrated Density – (Area of selected cell x Mean fluorescence of background readings

All data were collected using Microsoft Excel software and were graphed and analysed using GraphPad Prism software. Charts shown are mean ± s.e.m. In all analyses statistical significance was considered to be $p < 0.05$. Tests used are detailed in figure legends.

5.2.5 Investigating Retinal Vasculature

5.2.5.1 Tissue Collection

Neonatal SMA mice and control littermates up to the age of P5 were sacrificed by immersion in ice followed by decapitation. Pups above the age of P5 were sacrificed by an overdose of anaesthetic administered via intraperitoneal (IP) injection of sodium pentabarbitol (Euthenal). The mice were monitored closely following injection until no breath was observed and no footpad or tail responses were evoked.

5.2.5.2 Dissection

To expose the eye, a small incision was made in the skin adjacent to the eyelid. The skin was then reflected to reveal the eyeball. The eyeball was then removed by inserting forceps into the socket and gently pulling. The eyeball was then fixed in 4% paraformaldehyde (PFA) for two hours, at room temperature, on a rocking platform. Following fixation the preparation was repeatedly rinsed in 0.1M PBS to remove excess fixative. All post-fix dissection was performed in 0.1M PBS.

The eyeball was pierced with a syringe needle at the edge of the lens. Small scissors were inserted into this hole and the initial incision was continued around the circumference of the lens allowing it to be freed from the eyeball. The aqueous humour, which had solidified as a result of fixation, was removed and any fibrous

hyaloid vessels were gently cleaned away. At this point the eyeball was fixed for a further two hours in 4% PFA, at room temperature, on a rocking platform. Following this second period of fixation the outer pigment layer of the eyeball was gently removed from the inner retinal layer, leaving the retina free for staining.

5.2.5.3.Immunohistochemistry

Retinas were permeabilised overnight in 1% BSA 0.5% PBS at 4° on a rocking platform. The following day retinas were rinsed twice in 0.1M PBS and were washed for 2x5 mins in PBlec (1% triton PBS containing 0.1Mm $CaCl_2$, 0.1Mm $MgCl_2$ and 0.1Mm $mNCl_2$). Retinas were then incubated in rhodamine conjugated GSL-1 at a concentration of 1:25 made up in PBlec for 4 hours at room temperature on a rocking platform. The retinas were then washed for 5x5 minutes in 0.1M PBS before being left overnight in fresh 0.1M PBS at 4° on a rocking platform to additionally wash the samples. Following overnight washing the retinas were inspected under a microscope and any remaining hyaloids vessels were removed. Four cuts were made into the retinas which were then flat mounted in PBS on glass slides with glass coverslips ready for imaging.

5.2.5.4 Imaging

Micrographs were captured using a standard inverted epifluorescence microscope (Olympus 1X71) combined with a chilled CCD camera (Hammamatsu C4742-95) and OpenLab (Improvision) image capture software. Rhodamine labelled capillaries were imaged using 550nm excitation and 570nm emission optics.

5.2.5.5 Quantification and Analysis

Any retinas with poor quality staining or those that had been damaged during dissection were excluded from analysis. 10 x magnification images of whole retinas were captured and were enhanced for contrast and brightness in Photoshop CS 6. This ensured that definite vessel borders were visible and also prevented any fine capillary structures from being lost and discounted. Any out of focus images where capillaries appeared blurred or those where background was too high to completely isolate capillary structures were excluded from further analysis. The resulting images were analysed using AngioTool software (National Cancer Institute) which was used to semi-automatically calculate: the area of retina covered by capillaries, the total number of branch points in the capillary network and the total number of capillary end points to provide quantitative values with which to compare retinal vascular development. All images were analysed blind.

All data were collected using Microsoft Excel software and were graphed and analysed using GraphPad Prism software. Charts shown are mean ± s.e.m. In all analyses statistical significance was considered to be $p < 0.05$. Tests used are detailed in figure legends.

5.3 Results

Having identified and characterised defects in the development and morphology of capillaries in SMA mice, we sought to investigate the underlying cause of such alterations to vessel number and structure. Here we examine the growth and morphology of the major cellular constituent of capillaries, the endothelial cell, which were isolated from the lungs of P7 symptomatic Taiwanese SMA mice and control littermates. Observing any differences in growth rates or morphology between control and Taiwanese SMA endothelial cells in vitro could provide insight into the differences between control and SMA capillaries in vivo.

5.3.1 Comparable growth rate and morphology of Taiwanese SMA and control endothelial cells

In the first 5-6 days following isolation the cells in both the control and Taiwanese SMA cultures displayed elongated and irregular cytoplasm with a large single nucleus (Figure 2) This is consistent with previous reports of endothelial cell morphology early in culture (Pomerate & Slick, 1963). The P1 post isolation these cells were spread widely over the surface of the coverslip, with few neighbouring cells in contact (Figure 2 A,D). By 5 days post isolation small islands of more closely associated cells were apparent in groups across the surface of the coverslip (Figure 2 B,E).

Between P5 to P10 post isolation these islands of cells became more densely packed and the morphology of the cells altered. Cells still contained a single nucleus, but which now appeared more oval in shape. The cytoplasm became broader with less distinct borders than was seen in the younger cells. These changes are consistent with

previous reports of endothelial cell morphology as the culture period progresses (Gimbrone et al., 1973). As the cells reached confluency, both the Taiwanese SMA and control cultures displayed the classical, characteristic cobblestone morphology of endothelial cells in culture (Figure 2 C, F). Here cells formed single layer mats with densely packed cells at the centre, radiating out to more loose association at the edge of cell islands. These islands of cobblestone cells covered the majority of the cover slip surface with only a few regions of more irregular shaped cells separating the islands. The cobblestone morphology observed in these cultures is consistent with the morphology described in cultured endothelial cells obtained from both human (Gimbrone et al., 1973) and murine (Lim & Luscinskas, 2006) tissues and isolated by both magnetic bead (Marelli-Berg et al., 2000) and FACs sorting (Fehrenbach et al., 2009) techniques.

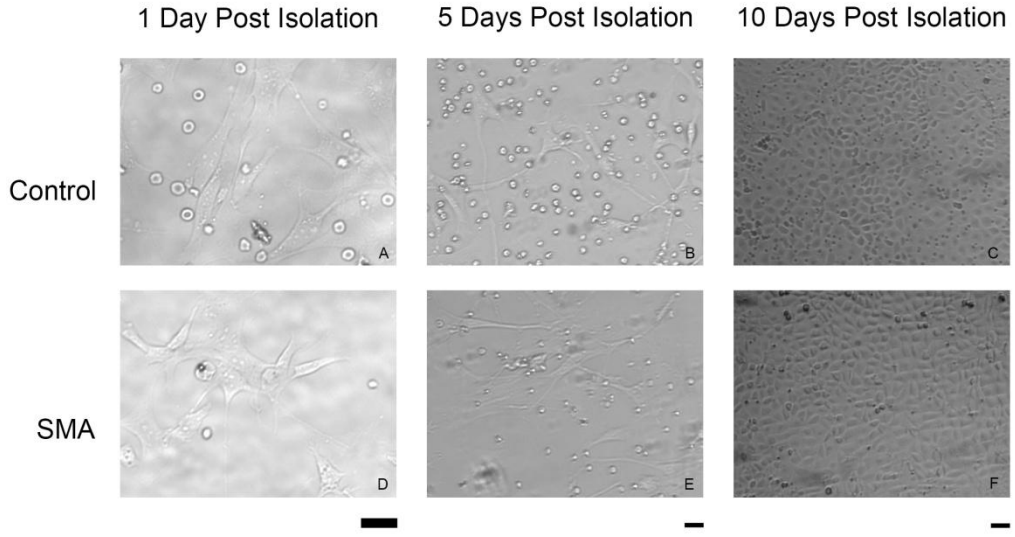

Figure 2- Comparable growth and morphology of control and Taiwanese SMA endothelial cells. *Representative phase contrast micrographs of control (littermate) and Taiwanese SMA cultures at 1 (A, D), 5 (B, E) and 10 (C, F) days post isolation. By 10 days post isolation the characteristic cobblestone morphology of Endothelial Cell mats is apparent in both control (C) and Taiwanese SMA (F) cultures. Images A and D are 20 x magnification. Images B,C,E and F are 10 x magnification. Scale bars for all images equal 50µm.*

5.3.2 Purity of Endothelial Cells

Having established that the isolated cells from both Taiwanese SMA mice and control littermates displayed the morphological characteristics of endothelial cells in culture we next examined the histological characteristics of the cells. To determine the purity of the cultures, Taiwanese SMA and control endothelial cells were double labelled the endothelial cell markers PECAM 1 and VE-Cadherin (Lim and Luscinskas, 2006) (Figure 3). PECAM 1, the endothelial tight junctional protein used in previous investigations to label skeletal muscle and spinal cord capillaries, and VE-cadherin another junctional protein specific to endothelial cells. Cells were also labelled with the nuclear marker DAPI (Figure 3). Endothelial cell purity was calculated as a percentage of cells that were immunostained for all three markers, with DAPI labelled cells counted as the total number of cells present. Taiwanese SMA and control endothelial cell purities were 91.73% and 92.45% respectively (Figure 4). These results represent a relatively high level of purity in each culture and also show no significant difference in purity levels between Taiwanese SMA and control endothelial cell cultures ($P>0.05$, unpaired, two-tailed t –test) (Figure 4). Importantly these results showed no obvious differences in the staining pattern of the endothelial markers PECAM 1 and VE-Cadherin between Taiwanese SMA and control endothelial cells (Figure 3).

PECAM 1 and VE-Cadherin expression appeared identical in both control and Taiwanese SMA endothelial cells. Both markers can be seen throughout the cytoplasm but are absent from the nuclei, which is consistent with previous reports of these markers in isolated endothelial cells (Fehrenbach et al., 2009). In addition to similar distribution and localisation, the intensity of expression is also comparable

between control and Taiwanese SMA endothelial cells. All images of the endothelial cells were taken using identical confocal settings. These results suggest that the presence of these two endothelial cell markers is not altered in SMA. This is consistent with our previous work where we were able to identify the SMA capillary bed both immunohistochemically and via quantitative fluorescent western blotting using PECAM 1. Absence or dysfunction of PECAM 1 in SMA mice would have prevented these investigations.

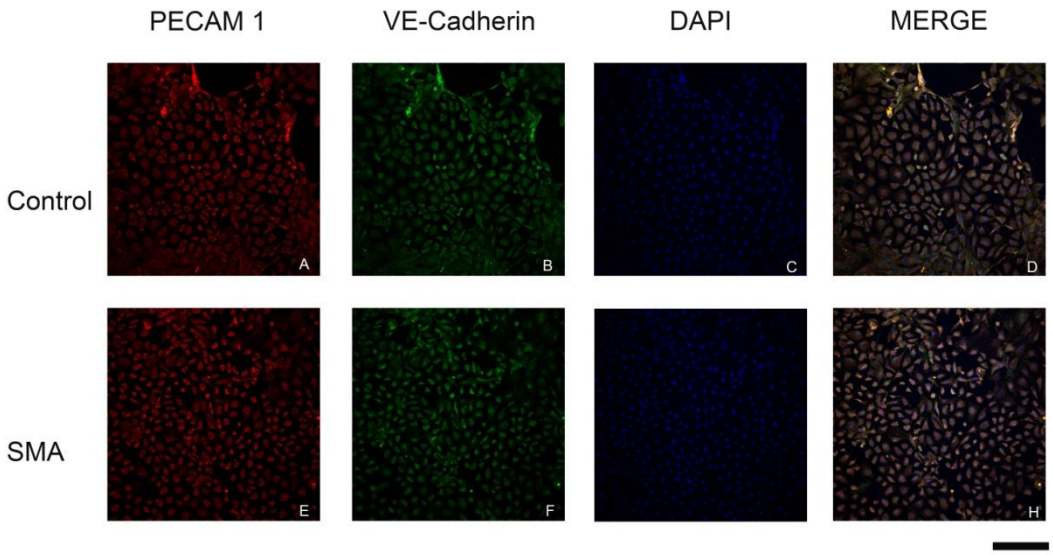

Figure 3 – Taiwanese SMA and control littermate endotheial cells express key endothelial markers. *Representative confocal micrographs of Endothelial Cells immunostained with PECAM 1 (red), VE-Cadherin (green) and DAPI (blue). Images are 20 x magnification. Scale bar equals 50µm.*

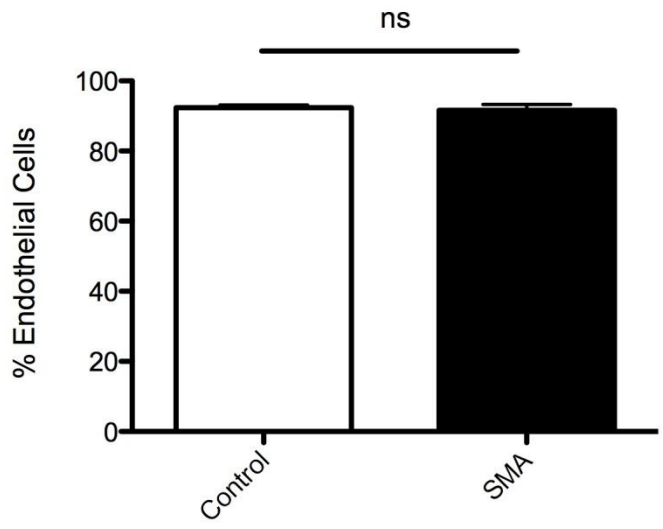

Figure 4 –Endothelial cell purity. *Bar chart (mean ± s.e.m) quantification of triple labelled cells in control (white bar) and Taiwanese SMA (black bar) cultures. Unpaired, two-tailed t-test, ns = no significance P>0.05. N≥9 mice, n≥36 coverslips and n≥72 images per bar.*

5.3.3 Decreased Smn expression in Taiwanese SMA Endothelial Cells

Having identified a high level of purity in and consistency between Taiwanese SMA and control endothelial cell cultures, we next sought to investigate the expression of Smn in the isolated endothelial cells. Cells were labelled for Smn protein along with PECAM 1 and DAPI as in previous studies (Figure 5). When imaged, using identical confocal settings, a clear difference could be seen between the level of Smn expression in Taiwanese SMA and control endothelial cells, with control endothelial cells appearing far brighter than their Taiwanese SMA counterparts (Figure 5 B, F). When quantified, Smn expression was significantly greater in control than Taiwanese SMA endothelial cells ($P<0.05$, unpaired, two-tailed, t test) (Figure 6). Smn expression in Taiwanese SMA endothelial cells was reduced by 67% in comparison to control endothelial cells (Figure 6). This is consistent with the approximately 60%

reduction in Smn expression reported in isolated Taiwanese SMA Schwann cells (Hunter et al., 2014). This suggests that the reduction in Smn levels observed in the endothelial cells is in line with the reduction of Smn protein observed in other SMA body tissues and regions.

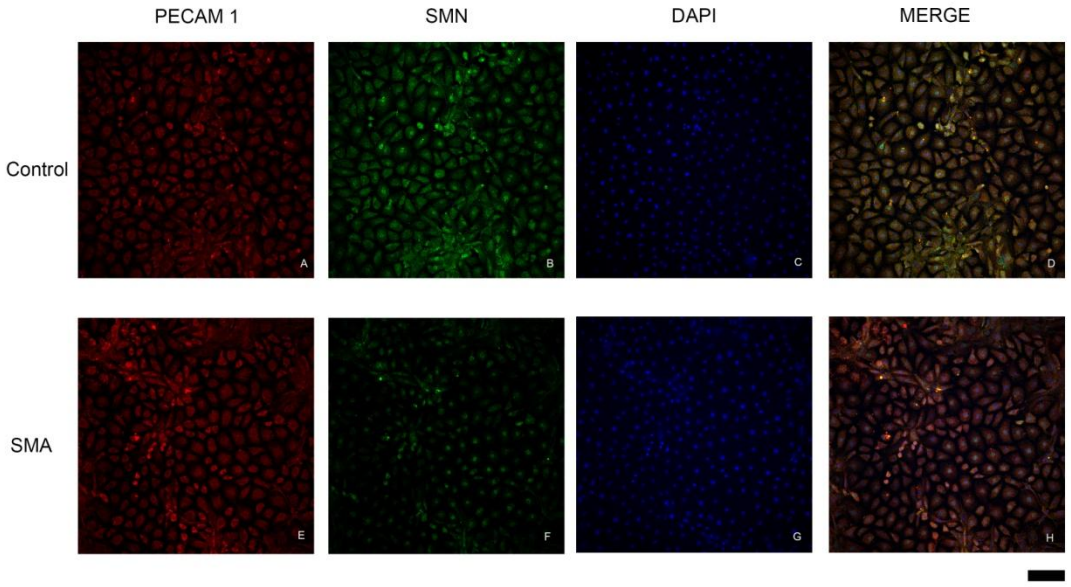

Figure 5 – Smn expression in Taiwanese SMA and control littermate endothelial cell cultures. *Representative confocal micrographs of Endothelial Cells immunostained with PECAM 1 (red), SMN (green) and DAPI (blue). Images are 20 x magnification. Scale bar equals 50µm.*

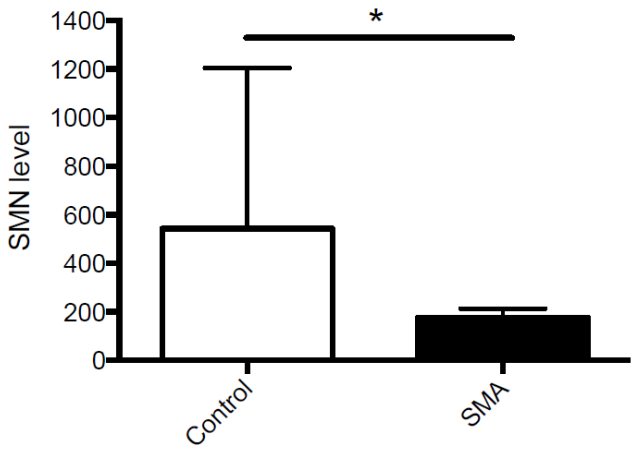

Figure 6 – Reduced Smn expression in Taiwanese SMA endothelial cells in culture. *Bar chart (mean ± s.e.m) quantification of Smn expression in cells in control (white bar) and Taiwanese SMA (black bar) cultures. Unpaired, two-tailed t-test, . N≥9 mice, n≥36 coverslips and n≥72 images per bar.*

5.3.4 Severe defects in capillary network of Taiwanese SMA retinas

Having identified no obvious defects in the growth, morphology and immunohistochemical profile of Taiwanese SMA endothelial cells, other than SMA levels, we sought to further investigate the development of capillary networks in SMA mice. Here we examine the growth of the retinal vasculature of Taiwanese SMA and control littermate mice from a variety of disease stages. Observing any differences in the morphology and growth of the capillary network between Taiwanese SMA and control retinas could provide insight into how the capillary defects we have observed in other tissue have arisen.

Upon initial inspection of P11 retinas, dramatic differences between the vasculature of control and Taiwanese SMA mice were readily observable (Figure 7). In control retinas the vascular network could been seen extending all the way to the peripheral

edge of the retina while in Taiwanese SMA mice a large portion of the retina remained avascular (Figure 7). Along with this reduction in vessel coverage, striking alterations to the morphology of the vascular network were also apparent. In control retinas large, almost straight vessels could be seen radiating from the centre of the retina to the periphery. From these large radiating vessels, numerous branching vessels arise forming the densely packed, tight looped capillary network similar to that observed in control skeletal muscle. No such similar organisation was observed in the Taiwanese SMA littermate retinal vasculature. Here, instead, a much more loose and open vascular network was apparent. Unlike their control counterparts no large radiating vessels were observed, instead a collection of poorly organised vessels were seen. These vessels had few branches, which were separated by large open spaces, resulting in a sparse network appearance. To analyse these morphological differences in more detail, the images from both control and Taiwanese SMA retinas were analysed using AngioTool software.

AngioTool is free software, developed by the National Cancer Institute, specifically to analyse the morphology of vascular networks and key elements of their structure and development. Given the particular differences in the vascular that we observed by eye, and our knowledge of capillary defects in SMA from our previous findings, we chose four particular important elements of retinal vasculature to measure; the area of the retina covered by vessels, the number of vessel branch points, the number of endpoint vessels at the vascular front and finally lacunarity. Lacunarity is a measure of how patterns fill gaps, where patterns with high numerical value for lacunarity, have large gaps between their constituent elements.

When measured, the area of retina covered by vessels was significantly reduced in P11 Taiwanese SMA mice when compared to control littermates ($P<0.0001$ unpaired, two-tailed t test) (Figure 8A). In control mice 39.4% of the retina was covered by vessels, this was reduced to only 17% in Taiwanese SMA littermates, amounting to a 57% reduction in the total vessel area in P11 Taiwanese SMA retinas. This reduction is in line with the 45% and 61% reduction in vessel density recorded in P11 SMA skeletal muscle and spinal cord respectively. This suggests that the reduction in vessel number is consistent across tissues and importantly, given that SMA is classed as a motor neuron disease, at a consistent level in a tissue which lacks skeletal muscle or motor neurons. Along with this overall reduction in area, other important structural components of the retinal vascular network were also reduced in P11 Taiwanese SMA mice (Figure 8A).

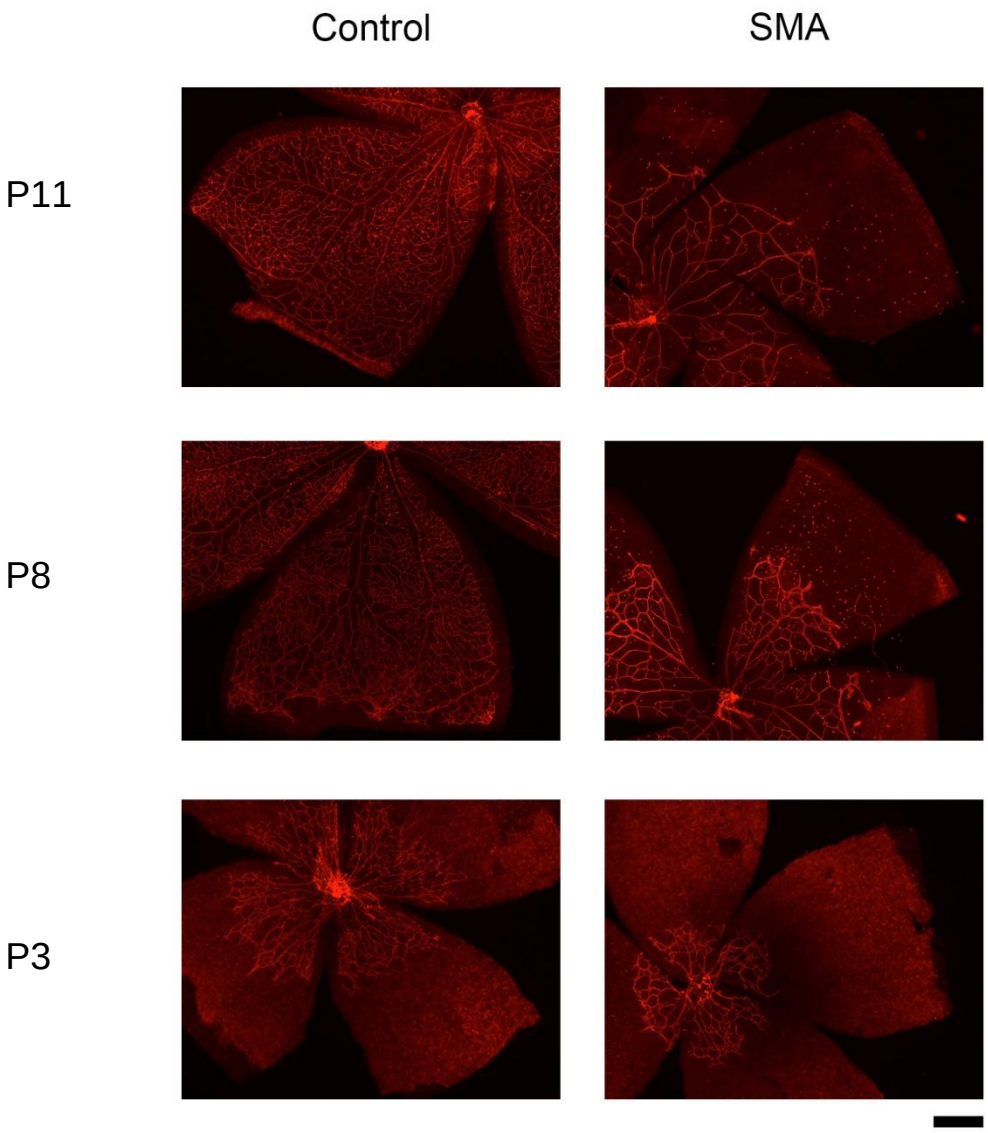

Figure 7 – Severe capillary defects are present at presymptomatic and late disease stages in Taiwanese SMA retinas. *Representative micrographs of GSL-1 labelled capillary bed of the retina in presymptomatic P3, symptomatic P8 and late symptomatic P11 Taiwanese SMA mice and control littermates.*

The number of vessel branch points was significantly reduced in P11 Taiwanese SMA mice when compared to control littermates ($P<0.0001$, unpaired, two-tailed t test) (Figure 8B). In P11 control retinas the average number of vessel branch points was 506, in P11 Taiwanese SMA mice this was reduced to 94.5, representing a

dramatic 81% reduction (Figure 8B). Along with this reduction in vessel branch number, the number of terminal vessels at the vascular front was also significantly reduced in P11 Taiwanese SMA mice in comparison to control littermates ($P<0.0001$, unpaired, two-tailed t test) (Figure 8C).

The average number of terminal vessels in P11 control retinas was 301.3 compared to an average of 85 in Taiwanese SMA retinas, calculated as a large, 72% reduction in endpoint vessels between control and Taiwanese SMA retinas (Figure 8C).

Taken together these findings detail a reduction in the number of vessels in the retina and a decrease in the branching of vessels. This results in a more open, loose arrangement of vessels seen in the P11 Taiwanese SMA retina in comparison to the dense, tightly packed capillary loops seen in their control littermate retinas (Figure 7). This is reflected in a 450% increase in average lacunarity in P11 Taiwanese SMA mice (0.9) in comparison to control littermates (0.2) (Figure 8D).

These alterations to the vascular network of P11 Taiwanese SMA mice are dramatic. P11 is a late symptomatic timepoint in the Taiwanese mouse model of SMA. To identify is such drastic alterations are present at earlier timepoints in disease progression two further timepoints were analysed; the symptomatic P8 and presymptomatic P3 timepoints.

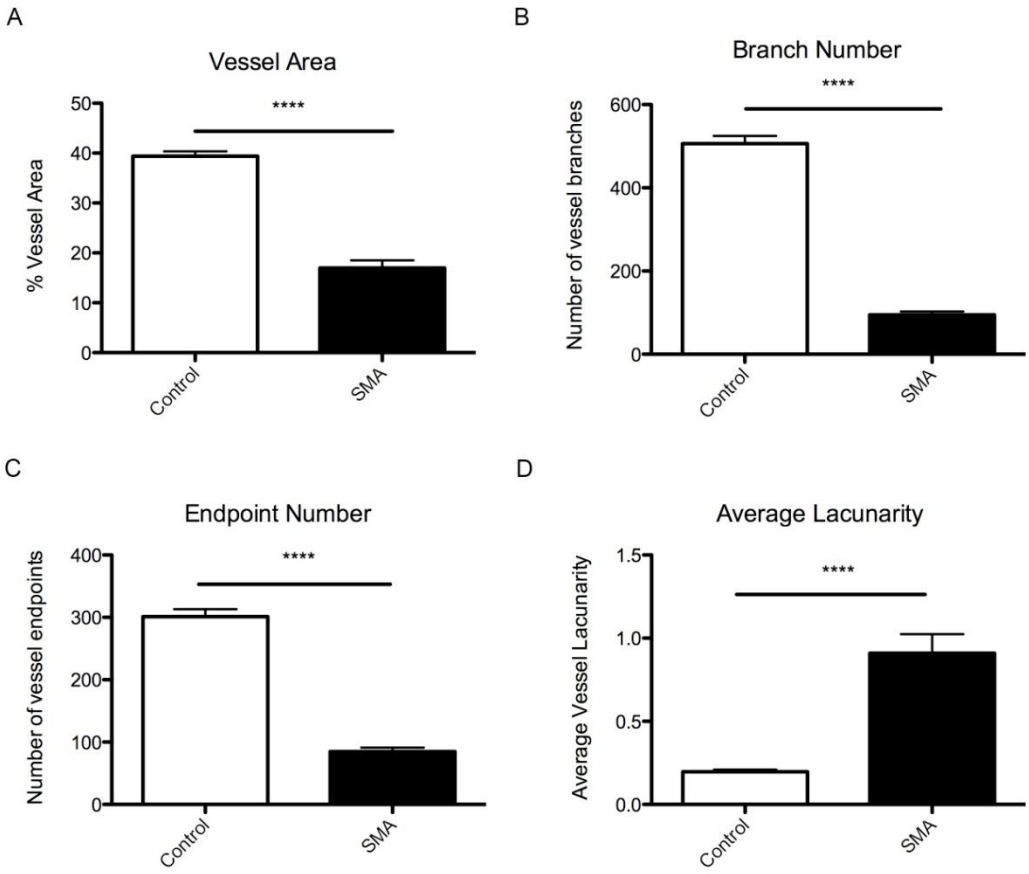

Figure 8 – Significant alterations to key vascular network features in P11 Taiwanese SMA mice. *Bar chart (mean ± s.e.m) quantification of the vessel area (A), branch number (B), endpoint number (C) and average lacunarity (D) of late symptomatic P11 Taiwanese SMA and control littermate retinas. Unpaired, two-tailed, t-test. **** = P<0.0001 N≥3 mice and n≥3 retinas for each bar.*

Initial observations of P8 Taiwanese SMA and control littermate retinas revealed a similar pattern of alterations to the retina vasculature in Taiwanese SMA mice as that seen at P11 (Figure 7). In P8 control retinas, almost all of the vessels have reached the periphery of the retina, with only small isolated pockets of the periphery not possessing a vessel covering. Again in the P8 Taiwanese SMA retinas, as was observed at P11, the vessels have failed to reach the periphery of the retina, with a large peripheral section of the retina remaining avascular, suggesting a reduction in overall vessel area similar to that observed at P11. In fact, a 56% reduction in vessel

area between P8 control and Taiwanese SMA retinas was recorded (Figure 9A), almost identical to the 57% reduction seen at P11 (Figure 8A). To add to this, further analysis of the structure of the vascular network revealed comparable defects in the P8 Taiwanese SMA mice as those found in P11 Taiwanese SMA mice.

Average vessel branch number in P8 control mice was 550.8 while P8 Taiwanese SMA retinas had an average of 142.3 vessel branch points (Figure 9B). This is equivalent to a 75% reduction in vessel branch number, on a smaller but similar scale to the 81% reduction in branching recorded at P11 (Figure 8B). Analysis of the number of endpoint vessels followed a similar trend (Figure 9C).

The average number of end vessels in P8 control retinas was 233.4, while this number was reduced to 93.5 in P8 Taiwanese SMA mice, a reduction of 60% (Figure 9C). Again, such dramatic alterations to these factors will impact upon the lacunarity of the P8 Taiwanese SMA retinal vasculature. Here, as was seen at P11, a large increase in lacunarity was observed, with lacunarity in P8 Taiwanese SMA mice being 318% greater than that of control littermates (Figure 9D). These findings at P8, although not as severe as those measured at P11, still reflect dramatic alterations to the retinal vasculature. This suggests that these defects are not merely a disease end stage symptom but that they are present at earlier timepoints in the disease progression. To assess if vascular defects in the retina are present prior to the onset of disease symptoms, the retinas of presymtpomatic P3 Taiwanese SMA and control littermate mice were examined.

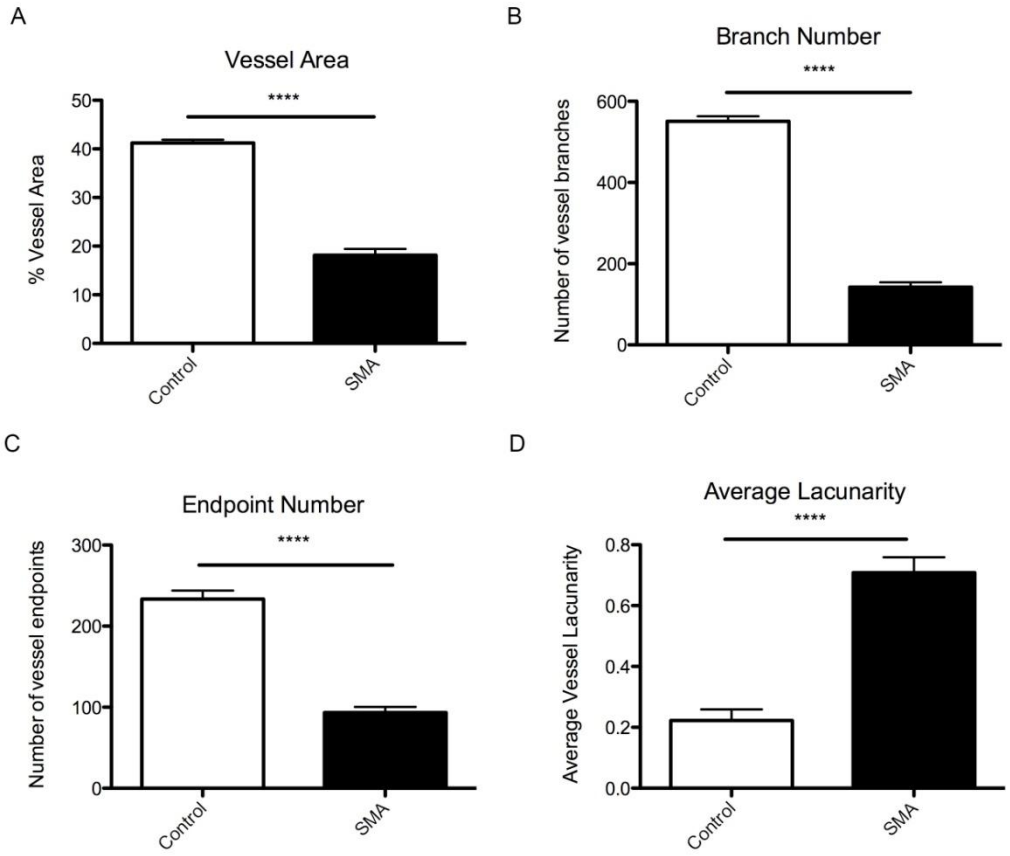

Figure 9 - Significant alterations to key vascular network features in P8 Taiwanese SMA mice. *Bar chart (mean ± s.e.m) quantification of the vessel area (A), branch number (B), endpoint number (C) and average lacunarity (D) of symptomatic P8 Taiwanese SMA and control littermate retinas. Unpaired, two-tailed, t-test. **** = P<0.0001 N≥3 mice and n≥3 retinas for each bar.*

In control P3 retinas the vascular network appeared less well developed than the control P8 and P11 retinas (Figure 7). This would be expected given the postnatal developmental time course of the retinal vasculature (explained in detail in the introduction of this chapter). Vessels can be seen emerging from the optic disc and extending across the more central regions of the retina (Figure 7). Unlike the P8 and P11 control retinas, no large radiating vessels are observed, with the majority of vessels retaining an immature, polygonal plexus appearance. This, again, is consistent with the normal time course development of the retina vasculature. At first glance the P3 Taiwanese SMA retinas appear more similar to the control vascular

network that at any other timepoint investigated (Figure 7). However, closer inspection reveals that the P3 Taiwanese SMA vasculature is markedly different from that of their control littermates.

P3 control vessels may still possess more loosely packed vessels at the growing vascular front than the P8 and P11 control networks but they do display the beginnings of the mature, densely packed vascular network in their more central regions (Figure 7). The P3 Taiwanese SMA mice however display the open looped, loose structure throughout their networks (Figure 7). Large gaps between adjacent vessels are evident, even at this early stage, in the P3 Taiwanese SMA retinas, which are not present in the more developed regions of the control retina networks (Figure 7). The smaller vascular network in the P3 control mice is reflected in the smaller vessel area value of 16.8% (Figure 10A). This however is still 45% greater than the 9.4% the P3 Taiwanese SMA retina covered by vessels (Figure 10A). Here we see that even at this early, presymptomatic timepoint a significant 55% reduction in vessel area is observed in Taiwanese SMA mice when compared to control littermates ($P<0.0001$, unpaired, two-tailed, t test) (Figure 10A). Significant reductions were also observed in vessel branch number ($P<0.0001$, unpaired, two-tailed, t test) (Figure 10B) and the number of endpoint vessels ($P<0.0001$, unpaired, two-tailed, t test) (Figure 10C) in P3 Taiwanese mice when compared to control littermates.

Average vessel branch number in P3 control retinas was 135.6 (Figure 10B). This was reduced by 50% to 68.8 in Taiwanese SMA littermates (Figure 10B) and a 40%reduction in the total number of endpoint vessels was also seen in Taiwanese SMA mice when compared to control littermates (Figure 10C). Along with these

alterations, lacunarity was also significantly different between control and Taiwanese SMA mice (P<0.0001, unpaired, two-tailed, t test) (Figure 10D). The lacunarity of P3 control retinas, 0.9, was much greater than that recorded at the older P8 and P11 timepoints, 0.22 and 0.2 respectively. This is due to the much less densely packed, immature vascular network present in the P3 control retinas. However, the lacunarity of P3 Taiwanese SMA retinas was still almost double that measured in control retinas, totalling 1.7. Even at the early developmental stage of P3 the retinal vasculature of the Taiwanese SMA mice is drastically altered from that of control mice. This suggests that defects in the SMA retinal vasculature occur early in its development.

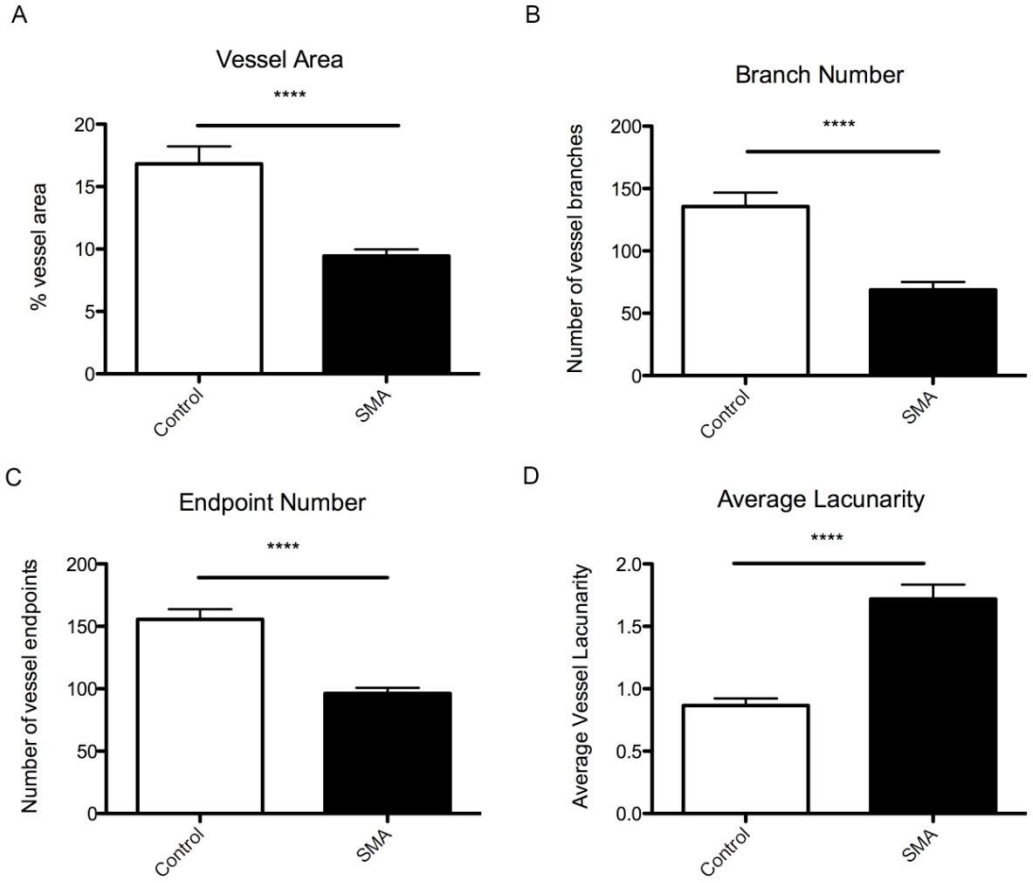

Figure 10 - Significant alterations to key vascular network features in P3 Taiwanese SMA mice. *Bar chart (mean ± s.e.m) quantification of the vessel area (A), branch number (B), endpoint number (C) and average lacunarity (D) of presymtpomatic P3 Taiwanese SMA and control littermate retinas. Unpaired, two-tailed, t-test. **** = P<0.0001 N≥3 mice and n≥3 retinas for each bar.*

When data from these three timepoints is presented together (Figure 11) it can clearly be seen that the vascular defects in SMA retinas are established early in the disease and that they become progressively worse as the disease progresses (Figure 11). Drastic alterations in all of the key points measured are already evident at the presymptomatic P3 timepoint (Figure 10. Figure 11) and these differences increase in magnitude as the disease progresses (Figure 11). At each timepoint examined a significant difference is observed between control and Taiwanese SMA mice for each point of interest measured ($P<0.0001$, One Way ANOVA with post hoc Tukey) (Figure 11). While the reduction in total vessel area remains relatively constant (50% at P3, 56% at P8 and 57% at P11) (Figure 11A), the values for branch number (Figure 11B), end vessel number (Figure 11C) and lacunarity (Figure 11D) all increase in magnitude as the disease progresses.

The percentage reduction in branch number increases from 50% at P3, to 75% at P8, to 81% at P11 (Figure 11B). Similarly, the reduction in end vessel number increases from 40% at P3, to 60% at P8, to 72% at P11 (Figure 11C). Finally, the increase in lacunarity increases from 188% at P3, to 318% at P8, to 450% at P11. This pattern could provide insight into how the vascular defects in the retina arise and progress, particularly with regard to the decrease in vessel branching and the reduction in the number of vessels at the growing vascular front of the developing vasculature. This

suggests that the mechanisms responsible for controlling these two processes would be particularly interesting to investigate in Taiwanese SMA retinas.

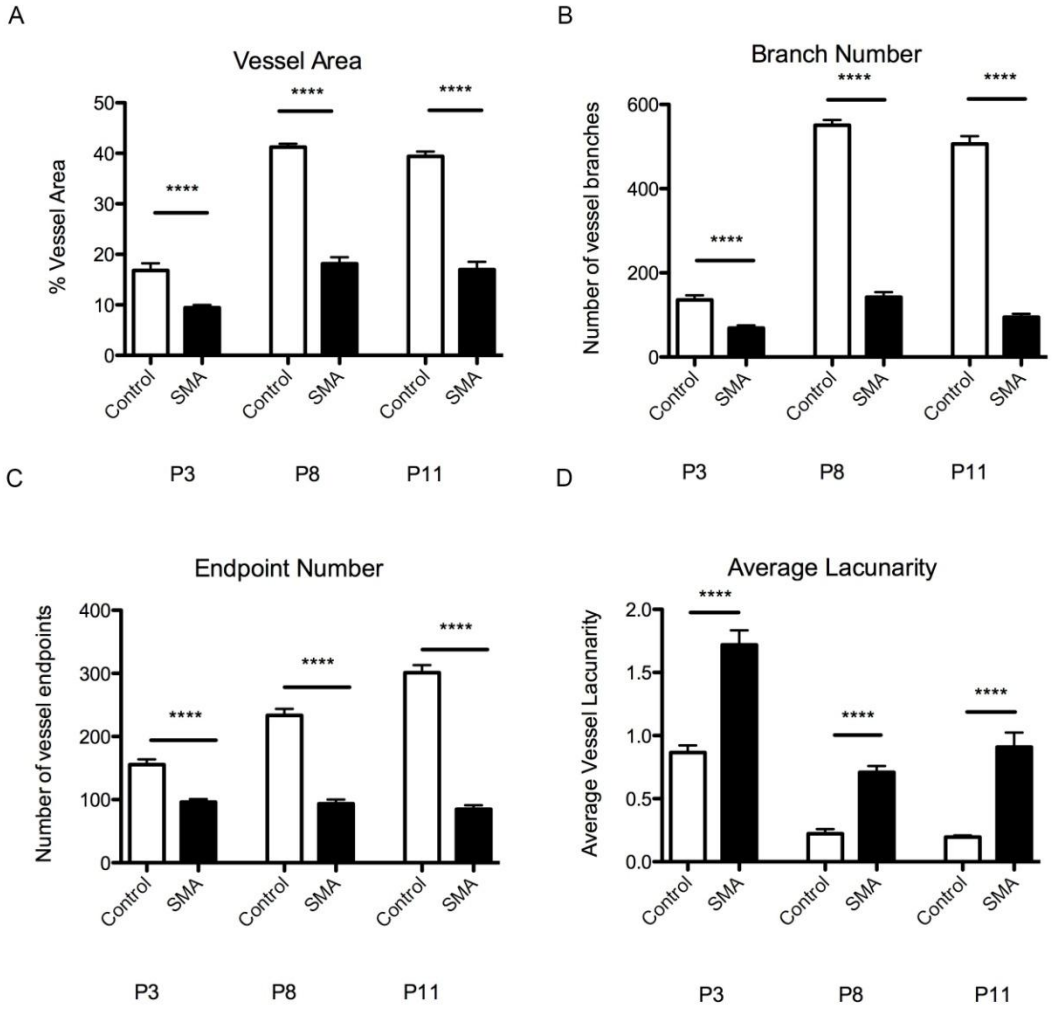

Figure 11 – Retinal capillary defects are established presymptomatically in Taiwanese SMA mice and persist as the disease progresses. *(A) Bar chart (mean ± s.e.m) quantification of the vessel area in presymptomatic P3, early symptomatic P8 and late symptomatic P11 Taiwanese SMA retinas (black bars) and control littermates (white bars). (B) Bar chart (mean ± s.e.m) quantification of vessel branch number in presymptomatic P3, symptomatic P8 and late symptomatic P8 Taiwanese SMA retinas (black bars) and control littermates (white bars). (C) Bar chart (mean ± s.e.m) quantification of vessel endpoint number in presymptomatic P3, symptomatic P8 and late symptomatic P11 Taiwanese SMA retinas (black bars) and control littermates (white bars). (D) Bar chart (mean ± s.e.m) quantification of average lucanarity in presymptomatic P3, early symptomatic P8 and symptomatic*

*P11 Taiwanese SMA retinas (black bars) and control littermates (white bars). One Way ANOVA with Post hoc test Tukey. ****=P<0.0001. N≥3 mice and n≥3 retinas per bar.*

5.4 Discussion

5.4.1 Isolation and culture of SMA endothelial cells

In this first part of the chapter endothelial cells were, for the first time, isolated from SMA mice and cultured. The findings of this chapter show that the morphology, growth and complement of endothelial cell markers of SMA endothelial cells is comparable to that of control endothelial cells.

Initially the results of this chapter show that endothelial cells isolated from P7 symptomatic SMA lungs are viable and can be successfully cultured in a sufficient density and at a high percentage purity for in excess of 10 days. This suggests that primary cultures of murine SMA lung endothelial cells are a reliable investigative tool for future study in SMA.

Second, these findings show that Smn expression is reduced in SMA endothelial cells in comparison to control endothelial cells. This is consistent with the ubiquitous nature of the Smn protein and further confirms the systemic reduction of Smn in SMA and the utility of this culture system for studying a relatively homogeneous, primary cell culture system in SMA research.

Third, this work has shown that SMA endothelial cells in culture express the endothelial cell marker PECAM 1 in a comparable fashion to control endothelial cells. This is consistent with our previous findings where we were able to label capillaries in SMA skeletal muscle and spinal cord using PECAM 1 and along with our use of GSL-1 labelling of the capillary beds, suggests that the reduction in capillary density we observe in these tissues is not an artefact of staining.

Forth, it was observed that SMA endothelial cells grow at the same rate as control endothelial cells in culture. Endothelial cells isolated from SMA lungs reached the desired confluency after the same number of days post-isolation as those isolated from control lungs.

Finally, this investigation revealed that SMA endothelial cell morphology does not differ from control endothelial cells, with both groups displaying the characteristic cobblestone morphology of endothelial cells in culture. These findings suggest that the growth and form of endothelial cells is not altered in SMA. Given that SMA endothelial cells display the classical endothelial cell morphology and grow at the same rate as control endothelial cells it is possible to suggest that defects in the growth and structure of endothelial cells are not responsible for the defects we observe in SMA capillaries. Rather, it is possible that either the response of the endothelial cells to exogenous factors is different or perhaps their ability to branch in response to such factors is compromised. However, studies to investigate these possibilities were beyond the limits of the current study.

5.4.1.2 Weaknesses of Study

Although every attempt was made to ensure that this study was as robust as possible, there is an area of weakness that should be noted: the crude isolation of endothelial cells.

In an initial study magnetic dynabead isolation protocols were used to isolate endothelial cells. In brief, sheep anti-rat IgG Magnetic dynabeads (Invitrogen Life Technologies 11035) were coated overnight with anti-rat PECAM 1 primary antibody (BD Pharmigen 558736) and incubated with the lung suspension for affinity

binding of the beads to endothelial cells. The endothelial cells were then separated from the suspension using a DynnaMag^{TM}-15 magnet (Invitrogen Life Technologies 12301D). After several magnetic isolation and washing steps the resulting bead and cell pellet was resuspended in EGM2 media and cultured in the same manner as described earlier in the methods section of this chapter.

On the first attempt this protocol produced endothelial cells from P7 control mice but no cells in the Taiwanese SMA suspension were found to bind to the beads. This was attributed to faults in the preparation of the Taiwanese SMA lung tissue, particularly over-mincing. To optimise tissue preparation and handling techniques the experiment was repeated multiple times in P7 CD1 litters. CD1 mice were chosen as they produce large litters of mice, all of which are the same genotype. During these trial experiments the number of cells in the suspension was counted using Trypan Blue dye (Sigma T6146) and a Haemocytometer (Sigma Z359629-1EA). Cell number was counted after incubation with collagenase, following centrifugation and resuspension, after incubation with the beads and after magnetic separation and resuspension. Cell number was found to be consistent, on average 42,050 cells per µl, at every stage up until magnetic separation. Following separation of the beads from the suspension, no cells were observed in the suspension. This suggested that endothelial cells were not binding to the beads. To ensure proper coating of the beads with the PECAM 1 antibody, trial experiments were run increasing the length of incubation time of beads and antibody and separate experiments where the method of incubation was altered from rocking to rolling and end-over-end incubation. In each trial a failure of cell and bead binding was observed. This suggested that the antibody was no longer binding to the beads. At this time a fresh batch of PECAM 1

antibody was purchased and trial experiments using CD1 litters were repeated. Again high numbers of cells were recorded at every stage of the protocol up until magnetic separation. Following magnetic separation no cells were observed in the suspension. At this point, due to time constraints, it was decided to abandon the use of the magnetic isolation protocol and to culture the cells obtained directly from the centrifuged lung suspension. The data presented in the results section of this chapter is from these experiments.

Direct culturing of the lung suspension produced cultures of a high density and purity, with 92% of cells in culture being identified as endothelial cells. Using this method we were able to analyse the growth and morphology of SMA endothelial cells in culture, obtaining consistent data across multiple cultures. While this method was appropriate for these preliminary investigations into the basic nature of SMA endothelial cells, more in depth future experiments may require a more stringent isolation technique.

5.4.1.3 Future Work

The results of this chapter show that endothelial cells isolated from symptomatic Taiwanese SMA mouse lungs not only survive in culture but that they are comparable in appearance and basic characteristics to endothelial cells isolated from control littermate pups. Taiwanese SMA endothelial cells grow at a similar rate to control endothelial cells, achieve the characteristic morphology of endothelial cells in culture and express the endothelial markers PECAM 1 and VE-Cadherin despite a 60% reduction in Smn expression. These results are not entirely unexpected, given the findings of the previous chapters of this thesis.

Despite the defects in vessel density, organisation and calibre observed in SMA skeletal muscle and spinal cord, the capillaries present in SMA tissue appear intact and robust (Chapter 2, Chapter 3). The capillaries present were can be labelled with both PECAM 1 and GSL-1, with consistent staining patterns in control and SMA tissue (Chapter 2). This suggests that the endothelium of SMA capillaries itself is similar to that of control capillaries. This is consistent with the findings of this chapter which show no difference between the nature of Taiwanese SMA and control endothelial cells in culture.

The preliminary investigations undertaken in this chapter have established that it is possible to isolate and culture murine SMA endothelial cells. Here we have begun to characterise SMA endothelial cells, observing their initial growth, morphology and the expression of key markers and proteins. Any further studies should seek to characterise SMA endothelial cells in more detail, particularly their expression of important angiogenic factors and their ability to form endothelial tubes.

In this chapter we have analysed the expression of two endothelial markers and the Smn protein in Taiwanese SMA endothelial cells. Observing expression of both PECAM 1 and VE-Cadherin in our cultured cells, along with their characteristic morphology, allowed for the confident identification of the cells as endothelial in nature. Measuring the intensity of Smn staining showed that endothelial cells isolated from Taiwanese SMA mice express reduced level of Smn in comparison to control cells, confirming the ubiquitous loss of Smn in SMA. Future studies should expand this profile to include critical components of the signalling pathways which initiate and regulate vascular development, in particular the Notch signalling pathway warrants future investigation.

Endothelial cell targeted alterations in the expression level of the Notch 1 receptor and its ligands cause dramatic alterations in vascular development, with overexpression being as detrimental as loss of function (Benedito et al., 2009). The loss of the Jagged 1 Notch 1 receptor in endothelial cells resulted in a decrease in vascular density and a reduction in vessel branching (Benedito et al., 2009). This phenotype is very similar to that observed in SMA capillary beds, making the Jagged 1 ligand an attractive target for future investigation.

Initially, the expression of Jagged 1 could be investigated morphologically in SMA endothelial cells using immunohistochemical staining. This would allow for the localisation of Jagged 1 in endothelial cells to be examined and the measurement of Jagged 1 staining intensity. To further validate these morphological measurements, quantitative fluorescent western blot techniques could be used to determine the expression of Jagged 1 at the protein level. These experiments would provide insight into a key regulator of angiogenesis in SMA. Importantly, the culture of isolated endothelial cells also allows for the process of angiogenesis itself to be examined.

Maintained under the correct conditions, endothelial cells will form networks of endothelial tubes, which appear almost identical to *in vivo* capillary beds (Folkman and Haudenschild, 1980). These tubes first appear approximately 20 days after initial plating of endothelial cells. The tubes form from the alignment of as few as 5-10 endothelial cells (Folkman and Haudenschild, 1980). Vacuoles appear in these cells which extend from one cell to the next, joining together to form a single, continuous, longitudinal lumen (Kamei et al., 2006). These tubes then undergo remodelling, similar to that observed in *in vivo* angiogenesis, with the appearance of new and the retraction of unwanted branches (Folkman and Haudenschild, 1980). Future

investigations should aim to extend the culture period described in this chapter to examine the formation of endothelial tubes by SMA endothelial cells. Our preliminary findings suggest that the growth and morphology of SMA endothelial cells in culture appears normal. This proposed experiment would determine if cultured SMA endothelial cells are also capable of forming endothelial tubes. Previous studies have shown that endothelial cells require no other cell type to form endothelial tubes in culture (Folkman and Haudenschild, 1980). Examining the ability of SMA endothelial cells form endothelial tubes would be a relatively simple further investigation, requiring little alteration to the current culturing methodology.

5.4.1.4 Conclusion

From these results we can conclude that the growth and morphology of isolated Taiwanese SMA endothelial cells in culture is comparable to that of control endothelial cells. Isolated SMA endothelial cells express lower levels of Smn protein than control endothelial cells, but show no apparent differences in endothelial marker presence.

5.4.2 The Retina as an investigative tool

In the second part of this chapter the developing vascular network of the retina was examined in Taiwanese SMA mice. The findings of this chapter show significant and dramatic defects in the form and extent of the retinal vascular network in Taiwanese SMA mice.

Initially the results of this chapter show drastic defects in the vascular network of late symptomatic P11 Taiwanese SMA retinas. These alterations include a reduction in total vessel area, a decrease in the number of vessel branching points, a decrease in

the number of terminal endpoint vessels and an increase in the lacunarity of Taiwanese SMA retinas when compared to control littermates. Observing such dramatic alterations in the vasculature of a tissue devoid of skeletal muscle and motor neurons suggests that the vascular defects observed in SMA mice are not a consequence of the neuromuscular pathology present in the disease. This implies the presence of an independent systemic defect in the vascular system of Taiwanese SMA mice.

Second, analysis of younger mice revealed that these defects are present in SMA retinas at earlier disease timepoints. Symptomatic P8 Taiwanese SMA retinas appeared very similar to late symptomatic P11 Taiwanese SMA retinas, displaying an almost identical reduction in vessel area and comparable alterations in branching, end vessel number and lacunarity. Importantly these defects were also observed at a presymptomatic timepoint. Presymptomatic P3 Taiwanese SMA retinas showed significant alterations in vessel area, branching, end vessel number and lacunarity when compared to control littermates. These alterations, while on a smaller scale than those observed at a later timepoint, were dramatic. This suggests that the defects observed in Taiwanese SMA retinal vasculature begin early in the development of the retinal vascular network and worsen as the disease progresses.

5.4.2.1 Disruption of Retinal Angiogenesis

The results of this chapter suggest that the development of the retinal vasculature is disturbed in SMA mice. Similar defects to those that we observe in SMA retinas have been reported in the retinas of mice where the key cell-fate determining Notch signalling pathway has been disrupted (Benedito et al., 2009). Loss of the Notch 1

ligand Jagged 1 from endothelial cells results in a phenotype very similar to that seen in Taiwanese SMA retinas, with a reduction in the area of the retina covered by vessels, a reduction in the number of vessel branch points and a decrease in the number of endothelial tip cells at the growing angiogenic front of the developing vascular network (Benedito et al., 2009). Immunohistochemical studies of the Notch ligands have revealed specific expression patterns of the Jagged 1 and the Dll4 Notch ligands in the developing retina (Hoffman and Iruela-Arispe, 2006).

The expression of the Jagged 1 is restricted to stalk cells of the growing vasculature and arterial branch points (Hoffman and Iruela-Arispe, 2006). The Dll4 ligand however is found throughout the retinal vascular network in stalk cells, capillaries and arterial endothelial cells. Crucially Dll4 is the only Notch ligand found in the endothelial tip cells leading vessel sprouts at the growing vascular front ((Hoffman and Iruela-Arispe, 2006). This suggests a key role for Dll4 in sprouting angiogenesis.

D114 is responsible for determining the fate of sprouting endothelial tip cells (Hellstrom et al 2007; Suchting et al., 2007). High expression of Dll4 in tip cells activates the Notch signalling pathway and suppresses tip cell phenotype in adjacent stalk cells preventing them from forming capillary sprouts. The ratio of tip to stalk cells in the developing vascular network is crucial for its proper formation. The correct balance of quiescent stalk cells and sprouting tip cells ensures the formation of proper capillary loops allowing for proper tissue perfusion (Hellstrom et al., 2007). This balance is achieved through the negative regulation of tip cell formation by Dll4-Notch signalling (Hellstrom et al., 2007; Suchting et al, 2007).

Over-activation of the Dll4-Notch signalling pathway in the retina results in a phenotype very similar to that observed in Taiwanese SMA retinas, with a 35% decrease in the number of sprouts at the growing vascular front and an overall reduction in vessel density of 45% (Hellstrom et al., 2007). In contrast, the reduced Dll4-Notch signalling found in $Dll4^{+/-}$ mice results in a 75% increase in sprouting tip cells at the vascular front, a 125% increase in vessel branching and an 80% increase in the area of retina covered by vessels (Suchting et al., 2007). These studies emphasise the importance the fine control of Notch signalling in angiogenesis. These studies describe how an alteration to Notch signalling level, be that enhanced or suppressed activation, can lead to aberrant vessel network formation. In particular, how enhanced Notch signalling, via the Dll4 ligand, results in a vascular phenotype very similar to that observed in SMA mice. Importantly, increased activation of the Notch signalling pathway has recently been reported in Smn depleted cells and SMA mice (Caraballo- Miralles et al., 2013).

When Smn protein level was depleted in astroglioma cells using lentiviral shSMN, the expression of the Notch ligands Jagged1 and Delta 1 was increased by 5 to 6 fold and the expression of the Notch receptor itself was increased 4 fold (Caraballo-Miralles et al., 2013). Similar increases in ligand and receptor expression were found in the spinal motor neurons of SMNΔ7 SMA mice. Expression of Jagged 1, Delta 1 and Notch were increased by 281%, 249% and 215% respectively, in comparison to control motor neurons (Caraballo- Miralles et al., 2013). To determine if the increased expression of these components of Notch signalling pathway resulted in activation of the Notch pathway the expression of Ngn3 was measured as activation of the Notch signalling pathway inhibits Ngn3 expression. In SMA motor neurons

Ngn3 expression was reduced by 54% in comparison to control motor neurons (Caraballo- Miralles et al., 2013), suggesting an activation of the Notch signalling pathway in SMA motor neurons.

In combination with the findings of this chapter, these studies provide an interesting avenue for future investigation: Notch signalling in vascular development in SMA.

5.4.2.2 Future Work

In this chapter severe defects were found in the development of the retinal vasculature in Taiwanese SMA mice. These defects are consistent with those observed in a variety of studies where the signals controlling of angiogenesis have been disturbed (Hellstrom et al., 2007, Suchting et al., 2007, Benedito et al., 2009). One of these master control pathways, the Notch signalling pathway, shows aberrant activation in SMA motor neurons and cultured cells where Smn levels have been depleted (Caraballo-Miralles et al., 2013). Inappropriate activation of this same Notch signalling pathway has been shown to result in a vascular phenotype which closely resembles the vascular defects we observe in SMA tissues (Hellstrom et al., 2007, Benedito et al., 2009). Based on this evidence, the Notch signalling pathway is a prime candidate for further investigation in SMA. Given the many advantages of the retina as an investigative tool, it would be the most suitable experimental approach to utilise for these future studies.

Given that previous studies have identified a highly specific expression pattern of the Notch 1 receptor and its ligands (Jagged 1, Dll4 and Delta 1), any future investigations should initially examine the distribution and location of the Notch 1 receptor and its ligands in the developing Taiwanese SMA retina. Due to the

postnatal development of the retinal vasculature these expression profiles can be examined immunohistochemically at every stage of angiogenesis. This would determine if any miss-localisation of the key elements of the signalling pathway were present in Taiwanese SMA retinas. The intensity of receptor and ligand expression could also be analysed from these stained preparations. Previous studies have shown an increase of Notch ligand immunoreactivity in SMA tissue in excess of 200% in comparison to control tissue (Caraballo- Miralles et al., 2013). Similar measurements could be made in Taiwanese SMA and control littermate retinas. To further validate these morphological measurements quantitative fluorescent western blot techniques could be used to determine the expression of Notch signalling elements at the protein level in the retina.

These investigations would identify any miss-localisation or altered protein expression levels of the Notch signalling pathway elements. To identify functional alterations of the Notch signalling pathway itself, the expression of the Ngn 3 protein could be examined. The expression of Neurogenin 3, a key protein in differentiation, is controlled by Notch signalling. Activation of the Notch signalling pathway results in the suppression of Ngn 3 expression (Caraballo- Miralles et al., 2013). A 54% reduction in Ngn 3 expression has previously been reported in SMA tissue where the Notch signalling pathway was aberrantly activated (Caraballo- Miralles et al., 2013). Ngn 3 expression could be analysed both morphologically and molecularly in the retina using western blotting, giving insight into the activation status of the Notch signalling pathway in Taiwanese SMA mice. Results from this study could then form the basis of investigations into if and at what stage the Notch signalling pathway is actively disrupted.

In several studies, enhanced activation of the Notch signalling pathway has resulted in a vascular phenotype that mirrors the phenotype we observe in SMA tissue (Hellstrom et al., 2007, Suchting et al., 2007, Benedito et al., 2009). Based on this, investigating the effects of Notch inhibitor administration on SMA vasculature would be an interesting future experiment to conduct in Taiwanese SMA mice.

These particular potential future studies are attractive routes of investigation as they could all be conducted in the Taiwanese SMA mouse line and would require no additional mouse lines. Much of our understanding of vascular defects in SMA comes from our work in the Taiwanese mouse line and in the wider SMA field the Taiwanese SMA line is well characterised and appreciated. These proposed experiments would take advantage of the previous knowledge we have gained working with the Taiwanese SMA mice and combine it with well established experimental approaches used in angiogenic research.

5.4.2.3 Conclusion

From these results we can conclude that the form and extent of capillary bed is altered in SMA mouse model retinas, a tissue which lacks muscle and motor neurons. The percentage area of retina covered by capillaries in SMA mice is reduced in comparison to control retinas and the organisation of the capillary network within the SMA retina is impaired. These alterations were observed at a presymptomatic disease timepoint and increased in magnitude as the disease progressed.

5.4.3 Overall Conclusion

Further work is required to identify the underlying mechanisms responsible for the capillary defects observed in SMA model mice. The experimental approaches outlined in this chapter provide ideal tools to conduct these future investigations.

General Discussion

6.1 Overview of Results

The work presented in this study has described novel, significant and robust defects in widespread capillary beds in SMA. Specifically, the form and extent of skeletal muscle, spinal cord and retinal capillary beds are significantly reduced in both extent and complexity in SMA mice. Analysis of postnatal development in these tissues revealed that capillary beds appear normal at birth with defects developing after birth and either slightly prior to or in parallel with the signature neuromuscular pathology seen in SMA mouse models. Similar capillary defects were also described in the retina, a tissue devoid of skeletal muscle and motor neurons, and also in skeletal muscles resistant to denervation and which show no neuromuscular pathology. These findings imply that the defects observed in the vascular system of SMA mice are not a secondary consequence of neuromuscular pathology, but rather are the result of defects intrinsic to the vascular system. Further investigation of the growth and morphology of endothelial cells, the major cell component of capillaries, suggested that these defects are not in the basic properties of endothelial cells. This suggests a more complex interaction between endothelial cells and surrounding or supporting cells. One important question is whether these dramatic defects in the capillary bed of tissues, where reductions in vessel density are close to 50%, result in compromised blood supply. Investigations of tissue hypoxia in vivo in SMA mice, revealed that these reduction in vessel density do in fact result in a significantly increased number of hypoxic cell bodies in the spinal cord of SMA mice. This increase in tissue hypoxia was seen at an early symptomatic timepoint and suggests a novel and exciting, possible sequence of events leading up to motor neuron damage.

Here tissue hypoxia could contribute to damage in the neuromuscular and other systems. Experiments in which levels of Smn protein were artificially increased using HDAC inhibitors, resulted in an amelioration of vascular defects suggesting that the severity of these vascular defects is linked to the level of tissue Smn, and therefore likely amenable to therapies which increase Smn levels.

6.2 Investigating mechanisms underlying the SMA capillary phenotype

In this thesis, the capillary phenotype in SMA mice models has been identified and characterised. Future work should look to elucidating the molecular and cellular mechanisms underlying the aberrant vascularisation observed. To examine such mechanisms microarray and proteomic techniques could be employed.

In previous chapters a method for isolating and culturing endothelial cells from SMA mice and control littermates was described (Chapter 5). This technique presents an opportunity to determine the molecular consequences of Smn depletion in endothelial cells at both the genetic and proteomic level. Previous microarray analysis of Severe SMA mouse model tissue has been performed on neurological tissue, notably the spinal cord (Murray et al., 2010). Analysis of SMA spinal cord revealed significant changes in gene expression when compared to control littermates. At presymptomatic timepoints only three genes were significantly altered by more than 1.5 fold but by the P5 late symptoamtic timepoint the expression of 160 genes was significantly changed by 1.5 fold or more (Murray et al., 2010). A similar high degree of change in expression is also observed in Severe SMA mice at the protein level.

In a recent study iTRAQ comparative proteomics was used to analyse hippocampal synaptosomes form pre and late symptomatic Severe SMA model mice (Wishart et al., 2014). In comparison to controls, the expression of 52 of the 150 unique proteins identified in the synaptosome were altered by more than 20% in SMA synaptosomes (Wishart et al., 2014). Critically, analysis of raw proteomics data using software such as Ingenuity Pathway Analysis (IPA) software allows for the grouping of related proteins into functional clusters. This means that changes in individual proteins can be linked to modifications in functional pathways. Applying this protocol to SMA and control endothelial cells would highlight not only the presence of any altered proteins in SMA endothelial cells in comparison to controls but also how these changes might impact on critical molecular pathways. A similar approach has recently been applied cells isolated from the nervous system of SMA model mice.

In their 2014 work Hunter et al., performed iTRAQ comparative proteomics and IPA software analysis on Schwann cells isolated and cultured from Taiwanese SMA mice and control littermates. This work showed similar robust results as those obtained from SMA tissue samples (Mutsaers et al., 2011), suggesting that proteomics is an appropriate and potentially illuminating procedure to investigate SMA endothelial cells.

Future experiments should refine the endothelial cell primary culture methodology to produce consistent purity and yield of endothelial cells. These cells should then be subjected to both microarray and proteomic analysis. These experiments would allow for the quantification and comparison of the genome and proteome of SMA and control endothelial cells, potentially highlighting genes and proteins for further examination. Here the pathway analysis software would be particularly useful in

identifying any changes in functional pathways that could underpin the capillary defect. Any differences seen in gene or protein expression could be validated in a variety of ways.

To confirm any differences in gene expression quantitative real time PCR could be used. This technique could be applied first to the isolated endothelial cells and then to a variety of other tissues in SMA model mice. These may include the larger vessels of the vascular system, the tissues known to display capillary defects (skeletal muscle, spinal cord and retina) and other organs which are known to display defects in SMA (see Hamilton and Gillingwater, 2014 for review). After evaluating the expression of the selected genes the effects of over- or under-expressing the same genes on the vascular system could be screened in zebrafish.

Any genes found to be upregulated in SMA endothelial cells, in comparison to control cells, could be over-expressed in zebrafish using over-expression constructs introduced into developing zebrafish embryos. Genes found to be down-regulated in SMA endothelial cells, in comparison to control cells, could be knocked down by injecting zebrafish embryos with oligonucleotide morpholinos which would reduce the expression of that gene by blocking transcription or modification of the target mRNA. In both cases the effects of the over-expression or knock down of the genes on the development of the zebrafish vasculature could be assessed using confocal microscopy techniques such as live imaging. This would help to determine if the identified genes were involved in the development of the aberrant vasculature seen in the SMA mouse models. Any such interesting results from the zebrafish studies could then be carried forward into murine models.

Mouse models could be generated which lack or over-express genes seen to cause effects in the vascular system in the zebrafish. These models would determine if such genetic alterations could result in a similar capillary phenotype as that observed in SMA model mice. Investigations could also be conducted involving targeted replacement or removal of genes in existing SMA model mice. These studies would determine the effect of restoring or blocking such genes on the capillary defect in SMA. Tissue specific approaches could also be employed to tease apart the involvement of the capillary defect in the neuromuscular pathologies seen in SMA.

At the protein level, any differences highlighted between the proteome of SMA and control endothelial cells could be validated using western blotting. Again this confirmatory technique could be applied first to the isolated endothelial cells and then to a variety of other tissues in SMA model mice. These could include the vessels, heart, liver, lung, small intestine and spleen which are known to have altered proteomes (Wishart et al., 2014) along with alterations in their structure and function (see Hamilton and Gillingwater, 2014 for review). Having analysed molecular expression, it would be prudent to examine the morphological expression of any indentified proteins of importance using immunohisto- and immunocytochemistry. This could be performed on the isolated endothelial cells and then expanded to the other tissues of interest. In this incidence the retinal preparation described in previous chapters (Chapter 5) would be particularly useful. Using this preparation the expression of any indentified protein of interest could be followed throughout the entire process of vascularisation. Such experiments would provide information about the presence, absence or mislocalisation of highlighted proteins during the process of vasculogenesis. This could provide insight into the involvement of these proteins in

the development and progression of the capillary defect. Importantly, examination of the retina in human SMA patients would be a non-invasive and relatively simple procedure to conduct. This would require capturing images of the retina which is performed as part of routine eye examinations. This would provide a rapid means of assessing the morphology of the capillary bed in SMA patients. This could help determine if the capillary phenotype observed in multiple mouse models translates to the human disease. This study should be combined with molecular analysis of any key genes and proteins identified by mouse microarray and proteomics data. This would determine if the same pathways and mechanisms which underpin the murine capillary defect are translated into the human disease.

6.3 Importance of Systemic Defects in SMA

While numerous studies, using a variety of therapeutic approaches, report improvements in motor phenotypes and pathologies in mouse models of SMA, in many of these the survival of these animals is only minimally extended.

Studies using Antisense Oligonucleotides targeting the erroneous splicing of the SMN2 gene have been reported to increase the expression levels of full length Smn protein and improve the SMA phenotype (Osman et al., 2012; Passini et al., 2012). ASO treated mice show improved weight gain, reduced loss of motor neuron cell bodies and an improved motor function as a result of improved muscle physiology and function (Osman et al., 2012; Passini et al., 2012). However, ASO treated SMNΔ7 SMA mice only survive for an additional 2 (Osman et al., 2012) to 5 (Passini et al., 2012) days in comparison to untreated SMNΔ7 SMA mice. A

comparable 4 day extension of survival is seen in SMNΔ7 SMA mice treated with aminoglycosides used to enhance translation of full length Smn from the SMN2 gene (Mattis et al., 2009). Viral delivery of the SMN1 gene has dramatically different effects on survival, depending on the route of administration (Azzouz et al., 2010; Foust et al., 2010,Valori et al., 2010; Dominguez et al., 2011).

The survival of SMNΔ7 SMA mice was extended by 3 to 5 days when the scAAV9 viral vector was used to deliver the SMN1 gene to the central nervous system (Azzouz et al., 2010; Foust et al., 2010). When the SMN1 gene, within the scAAV9 viral vector, was delivered systemically via the vasculature, SMNΔ7 SMA mouse survival was increased by between 60 (Valori et al., 2010) and 200 days (Dominguez et al., 2011). These studies suggest that SMA therapeutics must be delivered systemically to have a major impact on survival. However, therapeutics with a systemic activation, such as histone deacetylase inhibitors, show a varying degree of success in extending lifespan (Chang et al., 2001; Avila et al., 2007; Narver et al., 2008; Riessland et al., 2010; Schreml et al., 2013).

Early HDAC inhibitor trials using Sodium Butyrate improved SMA mouse survival by an average of 7 days (Chang et al., 2001). Investigations combining another HDAC inhibitor, Trichostatin A, and nutritional support showed an increase in lifespan of over 3 weeks (Narver et al., 2008). However, other studies using HDAC inhibitor treatment show only a mild 3 day increase in lifespan (Avila et al., 2007; Riessland et al., 2010) or no improvement at all (Schreml et al., 2013). While these studies demonstrate the variability in the outcome of HDAC inhibitor treatment, they also began to identify the presence of non neuromuscular pathologies in treated SMA mice (Chang et al., 2001; Avila et al., 2007; Schreml et al., 2013).

Treatment with Sodium Butyrate was seen to increase full length Smn protein and improve SMA symptoms but the longer surviving, treated mice developed necrosis of the tail (Chang et al., 2001) and SMA mice, whose survival was extended using Trichostatin A, developed diarrhoea (Avila et al., 2007). This extension of survival, although brief, revealed the presence of defects beyond the neuromuscular system in SMA mice. Since these studies, exploratory autopsies and histological investigations of SMA mice have revealed widespread organ defects (Vitte et al., 2004; Bevan et al., 2010; Heier et al., 2010; Shababi et al., 2010; Wishart et al, 2010; Hua et al., 2011; Bowerman et al., 2012; Gogliotti et al., 2012 Schreml et al., 2013).

Development of the brain is compromised in SMA mice (Wishart et al, 2010), along with the development and function of the heart (Shababi et al., 2010; Heier et al., 2010; Bevan et al., 2010; Gogliotti et al., 2012), the formation and growth of the liver (Vitte et al., 2004, Hua et al., 2011) and the cell fate and function of the pancreas (Bowerman et al., 2012). In depth histological analysis has also revealed compromising structural defects in the lungs and intestine of SMA mice (Schreml et al., 2013). Importantly, while potent HDAC inhibitor treatment was able to improve motor function in SMA mice, no improvement in any of these significant organ defects was observed and the survival of SMA mice was not increased (Schreml et al., 2013). A recent study has suggested that differences in the molecular basis of organ and neuromuscular pathologies could explain why neuromuscular phenotypes are improved in certain treatments and organ pathologies are not (Wishart et al., 2014).

A recent study has revealed widespread disruption of ubiquitin homeostasis in SMA mice, which in turn results in disturbances of β-catenin signalling in the

neuromuscular system (Wishart et al., 2014). Inhibition of β-catenin signalling was seen to alleviate neuromuscular pathology including improved motor function, reduced motor neuron loss, restored muscle fibre size and reduced NMJ pathology. However, weight gain was not improved and survival was not increased. Post-mortem examination revealed widespread gross organ defects. When β-catenin signalling was investigated, the perturbations found in the neuromuscular system were not seen in the organs. This suggests that pathology in the neuromuscular system and the organs are driven by distinct mechanisms (Wishart et al., 2014).

These studies emphasise the need for the systemic treatment of SMA. Therapeutic approaches which target only the neuromuscular system will not fully treat SMA. These studies suggest that systemic pathologies are life limiting factors in the course of SMA. Therefore a better understanding of the involvement of organ and systemic pathologies in SMA is required. This would not only improve current standards of patient care but would also lead to a re-evaluation of the therapeutic approaches used in SMA treatment.

6.4 Conclusion

The work described in this study characterises vascular defects in SMA and has taken the first steps to address the mechanisms underlying them. In summary, it has shown that;

1) The form and extent of capillary beds in skeletal muscle, spinal cord and retina are dramatically altered in mouse models of SMA.

2) These vascular defects are postnatal phenomena which occur independently of neuromuscular pathology.
3) The capillary defects seen do not appear to be a consequence of defects in endothelial cell morphology or growth.
4) The reduction in vessel density in tissue has physiological consequences.
5) The severity of these vascular defects is linked to the level of Smn in tissues and these defects are amenable to therapies which increase Smn levels.

This study will hopefully aid future work aimed at defining the underlying cause of vascular defects in SMA, and be of benefit for the development of clinically relevant therapeutic strategies for SMA.

References

Aird, W.C. et al., 1997. Vascular bed-specific expression of an endothelial cell gene is programmed by the tissue microenvironment. *J. Cell Biol.,* 138(5), pp.1117-24.

Albè, E. et al., 2009. Proteomic Analysis of the Hyaloid Vascular System Regression during Ocular Development. *J. Proteome Res.*, 7(11), pp.4904-13.

Allfrey,V.G. 1977. Chromatin and Chromosome Structure. Academic, New York, pp.167–91.

Andreassi, C. et al., 2004. Phenylbutyrate increases SMN expression in vitro: relevance for treatment of spinal muscular atrophy. *Eur. J. Hum.Gen.,* 12 (1), pp.59-65.

Araujo, A.P., Araujo, M. & Swoboda, K.J., 2009. Vascular perfusion abnormalities in infants with spinal muscular atrophy. *J Pediatr.,* 155(2), pp.292-4.

Araki, S. et al., 2003. Neuropathological analysis in spinal muscular atrophy type II. *Acta Neuropathol.,* 106, pp.441-48.

Arnold, A.S. et al., 2004. Reduced expression of nicotinic AChRs in myotubes from spinal muscular atrophy I patients. *Lab Invest.*, 84(10), pp.1271-8.

Authier, F.J. et al., 1996. Necrotizing myopathy with pipestem capillaries and minimal cellular infiltration: A case associated with cutaneous signs of dermatomyositis. Neurology., 46(5), pp.1448-51.

Avila, A.M. et al., 2007. Trichostatin A increases SMN expression and survival in a mouse model of spinal muscular atrophy. *J Clin Invest.*, 117(3), pp.659-71.

Azzouz, M. et al., 2004. Lentivector-mediated SMN replacement in a mouse model of spinal muscular atrophy. *J Clin Invest.*, 114(12), pp.1726-31.

Bartholdi, D. et al., 1997. VEGF mRNA induction correlates with changes in the vascular architecture upon spinal cord damage in the rat. *Eur. J. Neurosci.,* 9(12), pp.2549-60.

Bauer, W.R. et al., 1994. Nucleosome Strucutral Changes Due To Acetylation. *J. Mol. Bio.,* 236(3), pp.685-90.

Benedito, R. et al., 2009. The Notch Ligands Dll4 and Jagged1 Have Opposing Effects on Angiogenesis. *Cell.,* 137, pp.1124-35.

Bevan, A.K. et al., 2010. Early heart failure in the SMNDelta7 model of spinal muscular atrophy and correction by postnatal scAAV9-SMN delivery. *Hum Mol Genet.*, 19(20), pp.3895-905.

Blank, J.C. & Johnson, L.V. 1986. Vascular atrophy in the retinal degenerative RD mouse. J. *Comparative Neurology.,* 254(4), pp. 543-53.

Boillee, S. et al., 2006. ALS: A disease of motor neurons and their nonneuronal neighbors. *Neuron.,* 52(1), pp. 39-59.

Borisov, A.B. et al., 2000. Remodeling of the vascular bed and progressive loss of capillaries in denervated skeletal muscle. *Anatomical Record.*, 258(3), pp. 292-304.

Bowerman, M. et al., 2012. Glucose metabolism and pancreatic defects in spinal muscular atrophy. *Ann Neurol.*, 72(2), pp.256-68.

Bowerman, M. et al., 2012. Glucose metabolism and pancreatic defects in spinal muscular atrophy. *Ann Neurol.*, 72(2), pp.256-68.

Bray, S.J. 2006. Notch signalling: a simple pathway becomes complex. *Nat. Rev. Mol.Cell. Bio.*, 7(9), pp.678-89.

Brichta, L. et al., 2003. Valproic acid increases the SMN2 protein level: a well-known drug as a potential therapy for spinal muscular atrophy. *Hum. Mol. Gen.*, 12(19), pp.2481-9.

Briese, M. et al., 2009. Deletion of smn-1, the Caenorhabditis elegans ortholog of the spinal muscular atrophy gene, results in locomotor dysfunction and reduced lifespan. *Hum Mol Genet.*, 18(1), pp.97-104.

Brockstein, B. et al., 1994. Blood supply to the spinal cord: anatomic and physiologic correlations. *Annals of Vascular Surgery.*, 8(4), pp.394-9.

Bruijn, L.I. et al., 1997. ALS-linked SOD1 mutant G85R mediates damage to astrocytes and promotes rapidly progressive disease with SOD1-containing inclusions. *Neuron.*, 18(2), pp. 327-38.

Brutsaert, D.L. et al., 1998. Cardiac endothelium and myocardial function. *Cardiovascular Research.*, 38(2), pp.281-90.

Brzustowicz, L.M. et al., 1995. Linkage disequilibrium and haplotype analysis among Polish families with spinal muscular atrophy. *Am J Hum Genet.*, 56(1), pp.210-15.

Burghes, A.H. & Beattie, C.E., 2009. Spinal muscular atrophy: why do low levels of survival motor neuron protein make motor neurons sick? *Nat Rev Neurosci.*, 10(8), pp.597-609.

Caraballo-Miralles, V. et al., 2013. Notch Signaling Pathway Is Activated in Motoneurons of Spinal Muscular Atrophy. *Int. J. Mol. Sci.*, 14, pp.11424-37.

Carmeliet, P. & Tassier-Lavigne, M., 2005 Common mechanisms of nerve and blood vessel wiring. *Nature Review.*, 436, pp. 193-200.

Carreau, A. et al., 2011. Why is the partial oxygen pressure of human tissues a crucial parameter? Small molecules and hypoxia. *J. Cell & Molecular Biology.*, 15(6), p. 1239-53.

Cau, E. et al., 2008. Notch resolves mixed neural identities in the zebrafish epiphysis. *Dev.*, 135(14), pp. 2391-401.

Cebasek, V. et al., 2009. 3D Visualization and Measurement of Capillaries Supplying Metabolically Different Fiber Types in the Rat Extensor Digitorum Longus Muscle During Denervation and Reinnervation. Journal of Histochemistry & Cytochemistry., 57(5), pp. 437-47.

Cebasek, V. et al., 2010. The estimation error of muscle capillary supply is significantly reduced by 3D method. *Microvascular Research.,* 79, pp. 40-46.

Chernukh, A.A.M & Alekseeva, N.N. 1975. Changes in capillary bed of skeletal muscle at various times after nerve section. *Bulletin of Experimental Biology and Medicine*., 80(9), pp. 1009-12.

Clark, E.R., 1918. Studies on the growth of blood vessels in the tail of the frog. *American Journal of Anatomy*., 23, pp. 37-88.

Clark, E.R., 1939. Microscopic observations on the growth of blood capillaries in the living mammal. *Amerian Journal of Anatomy*., 66, pp. 1-49.

Chang, J.G., (2001) Treatment of spinal muscular atrophy by sodium butyrate. Proc Natl Acad Sci USA 98:9808–13.

Chang, H.C. et al., 2008. Modeling spinal muscular atrophy in Drosophila. *PLoS One.*, 3(9), p.e3209.

Chan, Y.B. et al., 2003. Neuromuscular defects in a Drosophila survival motor neuron gene mutant. *Hum Mol Genet.,* 12(12), pp.1367-76.

Chou, S.M. & Fahadey, A.V. 1971. Ultrastructure of chromatolytic motorneurons and anterior spinal roots in a cause of Werdnig-Hoffman disease. *Journal of Neuropathology and experimental neurology.,* 30(3), pp. 368.

Cifuentes-Diaz, C. et al., 2002. Neurofilament accumulation at the motor endplate and lack of axonal sprouting in a spinal muscular atrophy mouse model. *Hum Mol Genet.,* 11(12), pp.1439-47.

Cleaver, O. & Melton, D.A. Endothelial signaling during development. *Nat. Med.,* 9(6), pp.661-8.

Cleveland, D.W. & Rothstein, J.D. From Charcot to Lou Gehrig: Deciphering selective motor neuron death in ALS. *Nat. Rev. Neurosci.,* 2(11), pp.806-19.

Conolly, S.E. et al., 1988. Characterisation of vascular development in the mouse retina. *Microvascular Research.,* 36(3), pp. 275-90.

Crawford, T.O. et al., 1999. Abnormal fatty acid metabolism in childhood spinal muscular atrophy. *Ann Neurol.,* 45(3), pp.337-43.

D'Amore, P.A. & Ng, Y.S. 2002. Won't you be my neighbor? Local induction of arteriogenesis. *Cell.,* 110(3), pp.289-92.

Dachs, E. et al., 2011. Defective neuromuscular junction organization and postnatal myogenesis in mice with severe spinal muscular atrophy. *J Neuropathol Exp Neurol.*, 70(6), pp.444-61.

D'Amico, A., Mercuri, E., Tiziano, F.D. & Bertini, E., 2011. Spinal muscular atrophy. *Orphanet J Rare Dis.*, 6(71).

Dalcanto, M.C. & Gurney, M.E. 1994. Development of central nervous system pathology in a murine transgenic model of human amyotrophic lateral sclerosis. Am. J. Path., 145(6), pp. 1271-9.

Das, A. & McGuire, P.G. 2003. Retinal and choroidal angiogenesis: pathophysiology and strategies for inhibition. *Progress in Retinal and Eye Research.,* 22(6), pp. 721-48.

Dedkov, E.I. et al., 2002. Resistance vessel remodeling and reparative angiogenesis in the microcirculatory bed of long-term denervated skeletal muscles. *Microvascular Research.,* 63(1), pp.96-114.

Deleu, S. et al., 2009. The effects of JNJ-26481585, a novel hydroxamate-based histone deacetylase inhibitor, on the development of multiple myeloma in the 5T2MM and 5T33MM murine models. *Leukemia.*, 23(10), pp.1894-903.

De Ruijter, A.J. et al., 2003. Histone deacetylases (HDACs): characterization of the classical HDAC family. *Biochem. J.*, 370, pp. 737-49.

Devisser, M. et al., 1989. Early ultrastructural alterations in adult dermatomyositis - capillary abnormalities precede other structural changes in muscle. *Journal of the Neurological Sciences.*, 94(1-3), pp.181-92.

Dickson, B.J. 2002. Molecular mechanisms of axon guidance. *Science.,* 298 (5600), pp. 1959-64.

Dodd, A. et al., 2000. Zebrafish: bridging the gap between development and disease. *Hum. Mol. Gen.,* 9(16), pp. 2443-49.

Dominguez, E. et al., 2011. Intravenous scAAV9 delivery of a codon-optimized SMN1 sequence rescues SMA mice. *Hum Mol Genet.*, 20(4), pp.681-93.

Dommisse, G.F. 1974. Blood supply of spinal cord- critical vascular zone in spinal surgery. *Journal of Bone & Joint Surgery, British Volume.* B56(2), pp.225-35.

Donnenfeld, H. et al., 1984. Deposits of IGG and C-3 in the spinal cord and motor cortex of ALS patients. *J. Neuroimmunology.,* 6(1), pp.51-7.

Dorrell, I.M & Friedlander, M. 2006. Mechanisms of endothelial cell guidance and vascular patterning in the developing mouse retina. *Progression in Retinal and Eye Research.,* 25(3), pp.277-95.

Dubowitz, V., 1999. Very severe spinal muscular atrophy (SMA type 0): an expanding clinical phenotype. *Eur J Paediatr Neurol.*, 3(2), pp.49-51.

Durrin, L. K. et al., 1991. Yeast histone H4 N terminal sequence is required for promoter activation in vivo. *Cell*., 65, pp. 1023–31.

Ehling, M. et al., 2013. Notch controls retinal blood vessel maturation and quiescence. *Development.,* 140, pp.3051-61.

Eichmann, A. et al., 2005. Neural guidance molecules regulate vascular remodeling and vessel navigation. *Genes & Development.,* 19(9), pp. 1013-21.

Engelhardt, J.I. et al., 1993. Lymphocytic infiltrates in the spinal cord in amyotrophic lateral sclerosis. *Archives of Neurology.,* 50(1), pp.30-6.

Erzen, I. et al., 2000. Fiber types in the mouse levator auris longus muscle: A convenient preparation to study muscle and nerve plasticity. *Neurosci. Res.,* 59(5), pp. 692-97.

Estruch, R. et al., 1992. Microvascular changes in skeletal muscle in idiopathic inflammatory myopathy. Human Pathology., 23(8), pp. 888-85.

Fan, L. & Simard, L.R., 2002. Survival motor neuron (SMN) protein: role in neurite outgrowth and neuromuscular maturation during neuronal differentiation and development. *Hum Mol Genet.*, 11(14), pp.1605-14.

Fehrenbach, M.L. et al., 2009. Isolation of murine lung endothelial cells. *American Journal of Physiology - Lung Cellular and Molecular Physiology.,* 296(6), pp. L1096-103.

Felderhoff-Mueser, U. et al., 2002. Severe spinal muscular atrophy variant associated with congenital bone fractures. *J. Child Neurol.,* 17(9), pp. 718-21.

Feldkötter, M. et al., 2002. Quantitative analyses of SMN1 and SMN2 based on real-time lightCycler PCR: fast and highly reliable carrier testing and prediction of severity of spinal muscular atrophy. *Am J Hum Genet.,* 70(2), pp.358-68.

Feeny, J.F. & Watterson, R.L. 1946. The development of the vascular pattern within the walls of the central nervous system of the chick embryo. *Journal of Morphology.,* 78, pp. 231.

Ferrara, N. & Alitalo, K. 1999. Clinical applications of angiogenic growth factors and their inhibitors. *Nat. Med.,* 5(12), pp.1359-64.

Fidzianska, A. et al., 1990. Acute Infantile Spinal Muscular-Atrophy - Muscle Apoptosis As A Proposed Pathogenetic Mechanism. *Brain.,* 113, pp.433-45.

Folkman, J. & Haudenschild, C. 1980. Angiogenesis Invitro. *Nat.,* 288(5791), pp. 551-6.

Foust, K.D. et al., 2009. Intravascular AAV9 preferentially targets neonatal neurons and adult astrocytes. *Nat Biotechnol.,* 27(1), pp.59-65.

Foust, K.D. et al., 2010. Rescue of the spinal muscular atrophy phenotype in a mouse model by early postnatal delivery of SMN. *Nat Biotechnol.*, 28(3), pp.271-4.

Frank, R.N. 2002. Diabetic Retinopathy. *New England J. Medicine.* 350(1), pp.48-58.

Fruttiger, M. et al., 1996. PDGF mediates a neuron-astrocyte interaction in the developing retina. *Neuron.,* 17(6), pp. 1117-31.

Garbes, L. et al., 2009. LBH589 induces up to 10-fold SMN protein levels by several independent mechanisms and is effective even in cells from SMA patients non-responsive to valproate. *Hum. Mol. Gen.,* 18(19), pp. 3645-58.

Garbuzova-Davis, S. et al., 2007. Evidence of Compromised Blood-Spinal Cord Barrier in Early and Late Symptomatic SOD1 Mice Modeling ALS. *PL0S ONE*., 2(11), DOI: 10.1371/journal.pone.0001205

Garbuzova-Davis, S. et al., 2007. Ultrastructure of blood-brain barrier and blood-spinal cord barrier in SOD1 mice modeling ALS. *Brain Research.,* 1157, pp. 126-37.

Garbuzova-Davis, S. et al., 2010. Reduction of Circulating Endothelial Cells in Peripheral Blood of ALS Patients. *PL0S ONE.,* 5(5), DOI: 10.1371/journal.pone.0010614

Garbuzova-Davis, S. et al., 2012. Impaired blood-brain/spinal cord barrier in ALS patients. *Brain. Res.,* 1469, pp.114-28.

Garcia-Cabezas, M.A. et al., 2004. Neonatal spinal muscular atrophy with multiple contractures, bone fractures, respiratory insufficiency and 5q13 deletion. *Acta Neuropathalogica.,* 107(5), pp. 475-8.

Gerhardt, H. et al., 2002. VEGF guides angiogenic sprouting utilizing endothelial tip cell filopodia. J. *Cell. Bio.,* 161(6), pp.1163-77.

Gerhardt, H. et al., 2004. Neuropilin-1 is required for endothelial tip cell guidance in the developing central nervous system. *Developmental Dynamics.,* 231(3), pp.503-09.

Gimbrone, M. et al., 1973. Growth and ultrastructure of human vascular endothelial and smooth muscle cells in culture. *J. Cell Biology.*, 59(2), pp. A109.

Gitler, A.D. et al., 2004. PlexinD1 and semaphorin signaling are required in endothelial cells for cadiovascular development. *Dev. Cell.,* 7(1), pp.107-16.

Glascock, J.J. et al., 2012. Decreasing disease severity in symptomatic, Smn(-/-);SMN2(+/+), spinal muscular atrophy mice following scAAV9-SMN delivery. *Hum Gene Ther.*, 23(3), pp.330-5.

Gogliotti, R.G. et al., 2012. Motor neuron rescue in spinal muscular atrophy mice demonstrates that sensory-motor defects are a consequence, not a cause, of motor neuron dysfunction. *J Neurosci.*, 32(11), pp.3818-29.

Grunstein, M. 1997. Histone acetylation in chromatin structure and transcription. *Nature*. 389, pp.349-352.

Gubitz, A.K., Feng, W. & Dreyfuss, G., 2004. The SMN complex. *Exp Cell Res.*, 296(1), pp.51-6.

Gurney, M.E. et al., 1994. Motor-neuron degeneration in mice that express a human Cu-Zn superoxide dismustase mutation. *Science.,* 264(5166), p. 1772-75.

Haaker, G. & Fujak, A., 2013. Proximal spinal muscular atrophy: current orthopedic perspective. *Appl Clin Genet.,* 6(11), pp.113-20.

Haddad, H. et al., 2003. Riluzole attenuates spinal muscular atrophy disease progression in a mouse model. *Muscle Nerve.*, 28(4), pp.432-7.

Hamilton, G. & Gillingwater, T.H., 2013. Spinal muscular atrophy: going beyond the motor neuron. *Trends in Molecular Medicine*, 19(1), pp.40-50.

Hahnen, E. et al., 2006. In vitro and ex vivo evaluation of second-generation histone deacetylase inhibitors for the treatment of spinal muscular atrophy. *J Neurochem* DOI:10.1111/j.1471–4159.2006.03868.x.

Haverkamp, L.J. et al., 1995. Natural-History of Amyotrophic-Lateral-Sclerosis in a Database Population - Validation of a Scoring System and a Model for Survival Prediction. *Brain.,* 118, pp.707-19.

He, Z.E & Tessier-Lavigne, M. 1997. Neuropilin is a receptor for the axonal chemorepellent Semaphorin III. *Cell,*. 90(4), pp.739-51.

Hebbes,T.R. et al., 1988. A direct link between core histone acetylation and transcriptionally active chromatin. *EMBO J.* 7, pp.1395–402.

Heier, C.R., Satta, R., Lutz, C. & DiDonato, C.J., 2010. Arrhythmia and cardiac defects are a feature of spinal muscular atrophy model mice. *Hum Mol Genet.*, 19(20), pp.3906-18.

Henderson, C.E. et al., 1987. Extracts of muscle biopsies from patients with spinal muscular atrophies inhibit neurite outgrowth from spinal neurons. *Neurology.*, 37(8), pp.1361-4.

Henkel, J.S. et al., 2004. Presence of dendritic cells, MCP-1, and activated microglia/macrophages in amyotrophic lateral sclerosis spinal cord tissue. *Annals. Neurol.,* 55(2), pp.221-35.

Hellstrom, A. et al., 2001. Low IGF-I suppresses VEGF-survival signaling in retinal endothelial cells: Direct correlation with clinical retinopathy of prematurity. *Proceedings of the National Academy of Science of The United States.,* 98(10)., pp. 5804-8.

Herzog, Y. et al., 2001 Differential expression of neuropilin-1 and neuropilin-2 in arteries and veins. *Mechanisms of Development.,* 109(1), pp. 115-9.

Hirano, A. et al., 1984(a). Neurofibrillary changes in a family with Amyotrophic Lateral Sclerosis (ALS). J. Neuropathy & Exp. Neurology., 43(3), pp. 310.

Hirano, A. et al., 1984(b). Fine structural study of neurofibrillary changes in a family with Amyotrophic Lateral Sclerosis. J. Neuropathy & Exp. Neurology., 43(5), pp. 471-80.

Hsieh-Li, H. et al., 2000. A mouse model for spinal muscular atrophy. *Nature genetics*, 24(1), pp.66-70.

Hoffman, J.J. & Iruela-Aripse, M.L. 2007. Notch signaling in blood vessels - Who is talking to whom about what? *Circulation Research.,* 100(11), pp. 1556-68.

Hua, Y. et al., 2010. Antisense correction of SMN2 splicing in the CNS rescues necrosis in a type III SMA mouse model. *Genes Dev.*, 24(15), pp.1634-44.

Hua, Y. et al., 2011. Peripheral SMN restoration is essential for long-term rescue of a severe spinal muscular atrophy mouse model. *Nature.*, 478(7367), pp.123-6.

Hunter, G. et al., 2014. SMN-dependent intrinsic defects in Schwann cells in mouse models of spinal muscular atrophy. *Hum Mol Genet.*.

Imperato, E.L. et al., 1997. Local changes in vascular architecture following partial spinal cord lesion in the rat. Exp. *Neurol.,* 145(2), pp.322-8.

Ingber, D.E. 2002. Mechanical signalling and the cellular response to extracellular matrix in angiogenesis and cardiovascular physiology. *Circulation Research.,* 91(10), pp. 877-87.

Ishida, S. et al., 2003. Leukocytes mediate retinal vascular remodeling during development and vaso-obliteration in disease. *Nat. Med.,* 9(6), pp. 281-8.

Ito, Y. et al., 2011. New insights into the pathogenesis of spinal muscular atrophy. *Brain Dev.*, 33(4), pp.321-31.

Johnson, D.G. & Dent, S.Y., 2013. Chromatin: receiver and quarterback for cellular signals. *Cell.*, 152(4), pp.685-9.

Jonsson, P.A. et al., 2004. Minute quantities of misfolded mutant superoxide dismutase-1 cause amyotrophic lateral sclerosis. *Brain.,* 127, pp. 73-88.

Kamei, M. et al., 2006. Endothelial tubes assemble from intracellular vacuoles in vivo. *Nat.,* 442(7101), pp. 453-6.

Kariya, S. et al., 2008. Reduced SMN protein impairs maturation of the neuromuscular junctions in mouse models of spinal muscular atrophy. *Hum Mol Genet.*, 17(16), pp.2552-69.

Kawasaki, T. et al., 1999. A requirement for neuropilin-1 in embryonic vessel formation. *Dev.,* 126 (21), 4895-902.

Kerr, D.A. et al., 2000. Survival motor neuron protein modulates neuron-specific apoptosis. *Proc Natl Acad Sci U S A.*, 97(24), pp.13312-7.

Kissel, J.T. et al., 2011. SMA CARNI-VAL TRIAL PART II: A Prospective, Single-Armed Trial of L-Carnitine and Valproic Acid in Ambulatory Children with Spinal Muscular Atrophy. *PLoS ONE.*, 6 (7), PP.1-11.

Kitamoto, Y. et al., 1997. A glomerulus is developed through angiogenesis mediated by vascular endothelial growth factor (VEGF). *Journal of the American Society of Nephrology.*, 9, pp. 361(A).

Kobayashi, Y. et al., 1983. Endothelial alterations of skeletal-muscle capillaries in childhood myopathies. Tohoku J. Exp. Med., 140(40), pp. 381-89.

Kolodkin, A.L. 1997. Semaphorin function in neuronal growth cone guidance. *J. Neurochem.*, 69, pp. S162-S162.

Kong, L. et al., 2009. Impaired synaptic vesicle release and immaturity of neuromuscular junctions in spinal muscular atrophy mice. *J Neurosci.*, 29(3), pp.842-51.

Koto, T. et al., 2007. Hypoxia disrupts the barrier function of neural blood vessels through changes in the expression of claudin-5 in endothelial cells. Am. J. Pathol., 170(4), pp.1389-87.

Krebs, L.T. et al., 2000. Notch signaling is essential for vascular morphogenesis in mice. *Genes & Dev.*, 14(11), pp. 1343-52.

Kuru, S. et al., 2009. An autopsy case of spinal muscular atrophy type III (Kugelberg-Welander disease). *Neuropathology.*, 29(1), pp. 63-7.

Lammert, E. et al., 2001. Induction of pancreatic differentiation by signals from blood vessels. *Science.*, 294(5542), pp.564-7.

LeCouter, J. et al., 2003. Angiogenesis-independent endothelial protection of liver: Role of VEGFR-1. *Science.*, 299(5608), pp.890-3.

Lee, D.Y. et al., 1993. Hayes, J. J., Pruss, D. & Wolffe, A. P. A positive role for histone acetylation in transcription factor access to DNA. *Cell*., 72, pp. 73–84 .

Lefebvre, S. et al., 1995. Identification and characterization of a spinal muscular atrophy-determining gene. *Cell.*, 80(1), pp.155-65.

Leonardi, A. et al., 1984. Cerebrospinal fluid (CSF) findings in amyotrophic lateral sclerosis. *J. Neurol.*, 213(2), pp.75-8.

Lim, Y.C. & Luscinskas, F.W. 2006. Isolation and culture of murine heart and lung endothelial cells for in vitro model systems. *Cell-cell interactions: methods and protocols.*, 341, pp. 141-154.

Ling, K.K., Gibbs, R.M., Feng, Z. & Ko, C.P., 2012. Severe neuromuscular denervation of clinically relevant muscles in a mouse model of spinal muscular atrophy. *Hum Mol Genet.*, 21(1), pp.185-95.

Lippa, C.F. & Smith, T.W. 1988. Chromatolytic neurons in Werdnig-Hoffmann disease contain phosphorylated neurofilamets. *Acta Neuropathologica.,* 77(1), pp. 91-4

Liu, Q. & Dreyfuss, G., 1996. A novel nuclear structure containing the survival of motor neurons protein. *EMBO J.*, 15(14), pp.3555-65.

Lorson, C.L. & Androphy, E.J., 2000. An exonic enhancer is required for inclusion of an essential exon in the SMA-determining gene SMN. *Hum Mol Genet.*, 9(2), pp.259-65.

Lorson, C.L., Hahnen, E., Androphy, E.J. & Wirth, B., 1999. A single nucleotide in the SMN gene regulates splicing and is responsible for spinal muscular atrophy. *Proc Natl Acad Sci U S A.*, 96(11), pp.6307-11.

Louvi, A. & Artavania-Tsakonas, S. 2006. Notch signalling in vertebrate neural development. Nat. Rev. *Neurosci.,* 7(2), pp.93-102.

Lu, X.W. et al., 2004. The netrin receptor UNC5B mediates guidance events controlling morphogenesis of the vascular system. *Nature.,* 432(7014), pp. 179-86.

Madan, A. & Penn, J.S. 2003. Animal models of oxygen-induced retinopathy. *Frontiers in Bioscience.* 8, pp. D1030-43.

Marelli-Berg, F.M. et al., 2000. Isolation of endothelial cells from murine tissue. *J. Immunological Methods.*, 244(1-2), pp. 205-15.

Martinez, T.L. et al., 2012. Survival motor neuron protein in motor neurons determines synaptic integrity in spinal muscular atrophy. *J Neurosci.*, 32(25), pp.8703-15.

Martínez-Hernández, R. et al., 2013. Synaptic defects in type I spinal muscular atrophy in human development. *J Pathol.*, 229(1), pp.49-61.

Martínez-Hernández, R. et al., 2009. The developmental pattern of myotubes in spinal muscular atrophy indicates prenatal delay of muscle maturation. *J Neuropathol Exp Neurol.*, 68(5), pp.474-81.

Matsumoto, K. et al., 2001. Liver organogenesis promoted by endothelial cells prior to vascular function. *Science.*, 294(5542), pp. 564-67.

McWhorter, M.L., 2003. Knockdown of the survival motor neuron (Smn) protein in zebrafish causes defects in motor axon outgrowth and pathfinding. *J Cell Biol.*, 162(5), pp.919-31.

Melki, J. et al., 1994. De novo and inherited deletions of the 5q13 region in spinal muscular atrophies. *Science.*, 264(5164), pp.1474-7.

Miyazaki, K. et al., 2011. Disruption of Neurovascular Unit Prior to Motor Neuron Degeneration in Amyotrophic Lateral Sclerosis. J. *Neurosci. Research.,* 89(5),pp. 712-28.

Miyazaki, K. et al., 2012. Early and progressive impairment of spinal blood flow-glucose metabolism coupling in motor neuron degeneration of ALS model mice. Journal of Cerebral Blood Flow and Metabolism., 32(3), pp.456-67.

Monani, U.R., 2005. Spinal muscular atrophy: a deficiency in a ubiquitous protein; a motor neuron-specific disease. *Neuron.,* 48(6), pp.885-96.

Monani, U.R. et al., 1999. A single nucleotide difference that alters splicing patterns distinguishes the SMA gene SMN1 from the copy gene SMN2. *Hum Mol Genet.,* 8(7), pp.1177-83.

Monani, U.R. et al., 2000. The human centromeric survival motor neuron gene (SMN2) rescues embryonic lethality in Smn(-/-) mice and results in a mouse with spinal muscular atrophy. *Hum Mol Genet.,* 9(3), pp.333-9.

Moyon, D. et al., 2001. Plasticity of endothelial cells during arterial-venous differentiation in the avian embryo. *Development.,* 128 (17), 3359-70.

Mukouyama, Y. et al., 2002. Sensory nerves determine the pattern of arterial differentiation and blood vessel branching in the skin. *Cell.,* 6, pp.693-705.

Musch, B.C. et al., 1975. A comparison of the structure of small blood vessels in normal, denervated and dystrophic human muscle. *Journal of Neuroscience*., 26 (2), pp.:211-34.

Murray, L.M. et al., 2008. Selective vulnerability of motor neurons and dissociation of pre- and post-synaptic pathology at the neuromuscular junction in mouse models of spinal muscular atrophy. *Human Molecular Genetics,* 17(7), pp.949-62.

Murray, L.M. et al., 2008. Selective vulnerability of motor neurons and dissociation of pre- and post-synaptic pathology at the neuromuscular junction in mouse models of spinal muscular atrophy. *Hum Mol Genet.,* 17(7), pp.949-62.

Murray, L.M. et al., 2010. Pre-symptomatic development of lower motor neuron connectivity in a mouse model of severe spinal muscular atrophy. *Hum Mol Genet.,* 19(3), pp.420-33.

Murray, L.M., Talbot, K. & Gillingwater, T.H., 2010. Review: neuromuscular synaptic vulnerability in motor neurone disease: amyotrophic lateral sclerosis and spinal muscular atrophy. *Neuropathol Appl Neurobiol.,* 36(2), pp.133-56.

Musch, B.C. et al., 1975. Comparison of Structure of Small Blood-Vessels in Normal, Denervated and Dystrophic Human Muscle. *J. Neurol. Sci.,* 26(2), pp.221-34.

Mutsaers, C.A. et al., 2011. Reversible molecular pathology of skeletal muscle in spinal muscular atrophy. *Hum Mol Genet.,* 20(22), pp.4334-44.

Narver, H.L. 2008. Sustained improvement of Spinal Muscular Atrophy Mice Treated with Trichostatin A Plus Nutrition. *Ann. Neurol.,* 64, pp. 465-70.

Newman, P.J. 1997. The Biology of PCAM. *Journal of Clinical Investigation*., 100(11), pp.3-8.

Nicaise, C. et al., 2009. Impaired blood-brain and blood-spinal cord barriers in mutant SOM-linked ALS rat. *Brain Research.*, 1301, pp.152-62.

Ng, Y.S. et al., 2001. Differential expression of VEGF isoforms in mouse during development and in the adult. *Developmental Dynamics.,* 220(2), pp.112-21.

Norton, W.L. et al., 1968. Evidence of microvascular injury in sclerodema and systemic lupus erythematosus- quantitative study of microvascular bed. *J. Lab. Clin. Med.,* 71(6), pp. 919.

Oosthuyse, B. et al., 2001. Deletion of the hypoxia-reponse element in the vascular endothelial growth factor promoter causes motor neuron degeneration. *Nature Genetics* 28(2), pp. 272-84.

Oprea, G.E. et al., 2008. Plastin 3 is a protective modifier of autosomal recessive spinal muscular atrophy. *Science.*, 320(5875), pp.524-7.

Osman, E.Y., Yen, P.F. & Lorson, C.L., 2012. Bifunctional RNAs targeting the intronic splicing silencer N1 increase SMN levels and reduce disease severity in an animal model of spinal muscular atrophy. *Mol Ther.*, 20(1), pp.119-26.

Palenia, P. et al., 2005. New insights into skeletal muscle phenotype of equine motor neuron disease a quantitative approach. *Acta Neuropathol.,* 109, pp. 272-84.

Parker, G.C. et al., 2008. Survival motor neuron protein regulates apoptosis in an in vitro model of spinal muscular atrophy. *Neurotox Res.*, 13(1), pp.39-48.

Passini, M.A. et al., 2011. Antisense oligonucleotides delivered to the mouse CNS ameliorate symptoms of severe spinal muscular atrophy. *Sci Transl Med.*, 3(72), p.72ra18.

Pasqualini, R. et al., 2002. Probing the structural and molecular diversity of tumor vasculature. *Trends in Molecular Medince.,* 8(12), pp. 563-71.

Patz, A. 1986. Observations on the retinopathy of prematurity. *Am. J. Opthalmology.* 101(3), pp. 390-90.

Pellizzoni, L., Yong, J. & Dreyfuss, G., 2002. Essential role for the SMN complex in the specificity of snRNP assembly. *Science.*, 298(5599), pp.1775-9.

Pierfelice, T. et al., 2011. Notch in the Vertebrate Nervous System: An Old dog with New Tricks. *Neuron.,* 69, pp. 840-55.

Pomerat, C.M. & Slick, W.C. 1963. Isolation and growth of endothelial cells in tissue culture. *Nat., 198*(488), pp. 859.

Poole, T.J & Coffin, J.D., 1989: Vasculogenesis and angiogenesis: Two distinct morphogenetic mechanisms establish embryonic vascular pattern. J Exp Zool., 251, pp. 224–31.

Provis, J.M et al., 1997. Development of the human retinal vasculature: Cellular relations and VEGF expression. *Exp. Eye. Res.,* 65(4), pp. 555-68.

Rajendra, T.K., et al (2007). A Drosophila melanogaster model of spinal muscular atrophy reveals a function for SMN in striated muscle. J. Cell Biol., 176, 831–841.

Ravits, J. et al., 2006. Focality of ALS: II. 3-D topography of motor neurons in post mortem spinal cords and the neuropathological gradient of degeneration. *Neurology.,* 66(5), pp.A244-5.

Rezania, K. & Roos, R.P., 2013. Spinal cord: motor neuron diseases. *Neurol Clin.,* 31(1), pp.219-39.

Risau, W. & Flamme, I., 1995. Vasculogenesis. *Annual Review Cell Developmental Biology*., 11, pp. 73-91.

Risau W (1997) Mechanisms of angiogenesis. Nature 386: 671-674.

Riessland, M. et al., 2010. SAHA ameliorates the SMA phenotype in two mouse models for spinal muscular atrophy. *Hum Mol Genet.,* 19(8), pp.1492-506.

Robertson, W.C. et al., 1978. Morphometric study of motorneurons in congenital nemaline myopathy and Werdnig-Hoffmann disease. *Neurology.,* 28(10), pp. 1057-60.

Roca, C. & Adams, R.H. 2007. Regulation of vascular morphogenesis by Notch signaling. *Genes & Dev.,* 21(20), pp.2511-24.

Rosen, D.R. et al., 1993. Mutations in Cu/Zn Superoxide-Dismutase gene are associated with familial amyotrophic lateral sclerosis. Nat., 362 (6415), pp.59-62.

Rossoll, W. et al., 2003. Smn, the spinal muscular atrophy-determining gene product, modulates axon growth and localization of beta-actin mRNA in growth cones of motoneurons. *J Cell Biol.,* 163(4), pp.801-12.

Roth, D.W. & Zonenshayn, M. 2003. Vascular anatomy of the spine. *Operative Techniques in Neurosurgery.,* 6(3), pp.116-21.

Rouleau, J.L. et al., 1993. Effect of dysfunctional vascular endothelium on myocardial performance in isolated papillary muslces. *Circulation Research.,* 72(4), pp. 768-77.

Rowland, L.P & Schneider, N.A. 2001. Medical progress: Amyotrophic lateral sclerosis. *New. Eng. J. Med.,* 344(22), pp.1688-700.

Rudnik-Schöneborn, S. et al., 2003. Classical infantile spinal muscular atrophy with SMN deficiency causes sensory neuronopathy. *Neurology.,* 60(6), pp.983-7.

Rudnik-Schöneborn, S. et al., 2008. Congenital heart disease is a feature of severe infantile spinal muscular atrophy. *J Med Genet.,* 45(10), pp.635-8.

Rudnik-Schoneborn, S. et al. (2010). Digital necroses and vascular thrombosis in severe spinal muscular atrophy. *Muscle & Nerve*., 42(1), pp.144-14

Ruiz de Almodovar, C. et al., 2009. Role and therapeutic potential of VEGF in the nervous system. *Physiological Reviews.* 89(2), pp. 607-48.

Schnorrer, F. & Dickson, B.J. 2004. Axon guidance: Morphogens show the way. *Current Biology.,* 149(1), pp. R19-21.

Schrank, B. et al., 1997. Inactivation of the survival motor neuron gene, a candidate gene for human spinal muscular atrophy, leads to massive cell death in early mouse embryos. *Proc Natl Acad Sci U S A.*, 94(18), pp.9920-5.

Schreml, J. et al., 2012. Severe SMA mice show organ impairment that cannot be rescued by therapy with the HDACi JNJ-26481585. *European Journal of Human Genetics.* 21, pp. 643–5.2

Shimokawa, H. 1999. Primary endothelial dysfunction: Atherosclerosis. *J. Molecular and Cellular Cardiology.*, 31(1), pp. 23-37.

Shwarz, Q. et al., 2004. Vascular endothelial growth factor controls neuronal migration and cooperates with Sema3A to pattern distinct compartments of the facial nerve. *Genes & Development.,* 18(22), pp.2822-34.

Shababi, M. et al., 2010. Cardiac defects contribute to the pathology of spinal muscular atrophy models. *Hum Mol Genet.*, 19(20), pp.4059-71.

Shafey, D., Côté, P.D. & Kothary, R., 2005. Hypomorphic Smn knockdown C2C12 myoblasts reveal intrinsic defects in myoblast fusion and myotube morphology. *Exp Cell Res.*, 311(1), pp.49-61.

Shafey, D. et al., 2008. Neurodevelopmental abnormalities in neurosphere-derived neural stem cells from SMN-depleted mice. *J. Neurosci. Res.,* 86(13), pp.2839-47.

Shanmugarajan, S. et al., 2009. Bone loss in survival motor neuron (Smn(-/-) SMN2) genetic mouse model of spinal muscular atrophy. *J. Pathol.,* 219(1), pp.52-60.

Shaw, P.J., 2005. Molecular and cellular pathways of neurodegeneration in motor neurone disease. *J Neurol Neurosurg Psychiatry.*, 76(8), pp.1046-57.

Singer, M.A. et al., 2006. Primary lateral sclerosis. Muscle & Nerve., 35(3), p.291-302.

Sleigh, N.J., Gillingwater, T.H. & Talbot, K., 2011. The contribution of mouse models to understanding the pathogenesis of spinal muscular atrophy. *Dis Model Mech.*, 4(4), pp.457-67.

Smith, L.E.H. et al., 1994. Oxygen-induced retinopathy in the mouse. Investigative *Opthalmology & Visual Science.* 35(1), pp. 101-11.

Smith, L.E.H. et al., 1999. Regulation of vascular endothelial growth factor-dependent retinal neovascularization by insulin-like growth factor-1 receptor. *Nat. Med.,* 5(12), pp.1390-5.

Soler-Botija, C. et al., 2002. Neuronal death is enhanced and begins during foetal development in type I spinal muscular atrophy spinal cord. Brain., 125(7), pp. 1624-34.

Steiman, G.S. et al., 1980. Infantile neuronal degeneration masquerading as Werdnig-Hoffmann disease. *Annals of Neurology.,* 8(3), pp. 317-24.

Stewart, P.A. et al., 1981. Developing nervous tissue induces formation of blood brain barrier characteristics in invading endothelial cells - a study using quail-chick transplantation chimeras. *Developmental Biology.,* 84(1), p.183-92.

Stalmans , I. et al., 2002. Arteriolar and venular patterning in retinas of mice selectively expressing VEGF isoforms. *J. Clin. Inves.,* 109(3), pp. 327-36.

Stathas, D., 2008. Spinal muscular atrophy: DNA fragmentation and immaturity of muscle fibers. *Acta Histochem.,* 110,pp. 53–58.

Stone, J. et al., 1995. Development of retinal vasculature is mediated by hypoxia induced vascular endothelial growth factor (VEGF) expression by neuroglia. *J. Neurosci.,* 15(7), pp. 4738-47.

Storkebaum, E. et al., 2005. Treatment of motoneuron degeneration by intracerebroventricular delivery of VEGF in a rat model of ALS. Nat. Neurosci. 8(1), pp. 85-92.

Strahl, B.D & Allis, C.D., 2000. The language of covalent histone modifications. *Nature.,* 403 (6765), pp.41-5.

Sturrock, B.B. 1990. An ultrastructural study of development of the leptomenix of the rabbit spinal cord. *Anatomischer Anzeiger.,* 170(1), pp. 73-7.

Suchting, et al., 2007. The Notch ligand Delta-like 4 (Dll4) negatively regulates endothelial tip cell formation and vessel branching. *Faseb. J.,* 21(5), pp. A15.

Sumner , C.J., 2003. Valproic acid increases SMN levels in spinal muscular atrophy patient cells. *Ann Neurol* 54:647–654.

Tessier-Lavigne, M. & Goodman, C.S. 1996. The molecular biology of axon guidance. *Science.,* 274 (5290), pp. 1123-33.

Thorin, E. & Shreeve, S.M. 1998. Heterogeneity of Vascular Endothelial Cells in Normal and Disease States. *Pharmacology & Therapeutics.,* 78(3), pp. 155-66.

Valori, C.F. et al., 2010. Systemic delivery of scAAV9 expressing SMN prolongs survival in a model of spinal muscular atrophy. *Sci Transl Med.,* 2(35), p.35ra42.

Vapaatal, H. & Mervaala, E. 2001. Clinically important factors influencing endothelial function. *Medical science monitor : international medical journal of experimental and clinical research.,*7(5), pp.1075-85.

Vitte, J.M. et al., 2004. Deletion of murine Smn exon 7 directed to liver leads to severe defect of liver development associated with iron overload. *Am J Pathol.,* 165(5), pp.1731-41.

Wade, P.A, 2001. Transcriptional control at regulatory checkpoints by histone deacetylases: molecular connections between cancer and chromatin. *Hum. Mol. Gen.,* 10(7), pp.693-8.

Wang, J. & Dreyfuss, G., 2001. Characterization of functional domains of the SMN protein in vivo. *J Biol Chem.,* 276(48), pp.45387-93.

Wang, J. et al., 2003. Copper-binding-site-null SOD1 causes ALS in transgenic mice: aggregates of non-native SOD1 delineate a common feature. *Hum. Mol. Gen.,* 12(21), pp. 2753-64.

Walker, M.P. et al., 2008. SMN complex localizes to the sarcomeric Z-disc and is a proteolytic target of calpain. *Hum. Mol. Gen.,* 17(21), pp.3399-410.

Will, C.L. & Lührmann, R., 2001. Spliceosomal UsnRNP biogenesis, structure and function. *Curr Opin Cell Biol.,* 13(3), pp.290-301.

Winkler, E.A. et al., 2013. Blood-spinal cord barrier breakdown and pericyte reductions in amyotrophic lateral sclerosis. *Acta Neuropathologica.,* 125(1), pp. 111-20.

Wirth, B. et al., 2006. Mildly affected patients with spinal muscular atrophy are partially protected by an increased SMN2 copy number. *Hum. Genet.,* 119, pp. 422–28.

Wishart, T.M. et al., 2010. SMN deficiency disrupts brain development in a mouse model of severe spinal muscular atrophy. 19(21), pp.4216-28.

Wishart, T.M. et al., 2014. Dysregulation of ubiquitin homeostasis and β-catenin signalling promote spinal muscular atrophy. *J. Clin. Inves.,* 124(4), pp. 1821-34.

Wolff, J.R. et al., 1975 Common morphogenetic aspects of various organotropic microvascular patterns. *Microvascular Research.*, 10, pp. 373-95.

Wong, P.C. et al., 1995. An adverse property of a familial ALS-linked SOD1 mutation causes motor-neuron disease characterised by vacuolar degeneration of mitochondria. *Neuron.,* 14(6), pp. 1105-16.

Woollam, D.H. & Millen, J.W. 1958. In discussion on vascular disease of the spinal cord. *Proceedings of the Royal Society of Medicine.,* 51, pp.540.

Workman, E., Kolb, S.J. & Battle, D.J., 2012. Spliceosomal small nuclear ribonucleoprotein biogenesis defects and motor neuron selectivity in spinal muscular atrophy. *Brain Res.,* 1462, pp.93-9.

Yoshida, M. eat al., 2001. Histone deacetylase as a new target for cancer chemotherapy. *Cancer Chemotherapy and Pharmacology.*, 48, pp.20-6.

Yuan, L. et al., 2004. Abnormal lymphatic vessel development in neuropilin 2 mutant mice. *Development.*, 129(20), pp.4797-06.

Zanetta, C. et al., 2014. Molecular, genetic and stem cell-mediated therapeutic strategies for spinal muscular atrophy (SMA). *J Cell Mol Med.*, 18(2), pp.187-96.

Zeng, X. et al., 1998. VEGF enhances pulmonary vasculogenesis and disrupts lung morphogenesis in vivo. *Developmental Dynamics.*, 211(3), pp.215-27.

Zhong, Z. et al., 2008. ALS-causing SOD1 mutants generate vascular changes prior to motor neuron degeneration. *Nature Neuroscience*., 11 (4), pp. 420-22.

Zhong, Z. et al., 2009. Activated protein C therapy slows ALS-like disease in mice by transcriptionally inhibiting SOD1 in motor neurons and microglia. *J. Clin. Inves.*, 119(11), pp. 3437-49.

Zlokovic, B.V. et al., 2005. Neurovascular mechanisms of Alzheimer's neurodegeneration. Trends in Neurosciences. 28(4), pp. 202-08.

Zlokovic, B.V et al., 2008. The blood-brain barrier in health and chronic neurodegenerative disorders. Neuron., 57(2),pp. 178-01.

Appendices

Appendix 1: List of Pulications

Somers E, Stencel Z, Wishart TM, Gillingwater TH, Parson SH. Density, calibre and ramification of muscle capillaries are altered in a mouse model of severe spinal muscular atrophy. Neuromuscular Disorders. 2012; 22(5): 435-442.

Somers E, Riessland M, Schreml J, Wirth B, Gillingwater TH, Parson, SH. 2013. Increasing SMN levels using the histone deacetylase inhibitor SAHA ameliorates defects in skeletal muscle microvasculature in a mouse model of severe spinal muscular atrophy. Neuroscience Letters. 2013; 544:100-104.

Schreml J, Riessland M, Paterno M, Garbes L, Rossbach K, Ackerman B, Kramer J, **Somers E**, Parson SH, Heller R, Berkessel A, Sterner-Kock, Wirth B. 2013. Severe SMA mice show organ impairment that cannot be rescued by therapy with the HDACi JNJ-26481585. European Journal of Human Genetics. 2013; 21(6); 643-652.

Wishart TM, Mutsaers CA, Riessland M, Reimer MM, Hunter G, Hannam ML, Eaton SL, Fuller HR, Roche SL, **Somers E**, Morse R, Young PJ, Lamont DJ, Hammerschmidt M, Joshi A, Hohenstein P, Morris GE, Parson SH, Skehel PA, Becker T, Robinson IM, Becker CG, Wirth B, Gillingwater TH. Dysregulation of ubiquitin homeostasis and beta-catenin signaling promote spinal muscular atrophy. Journal of Clinical Investigation. 2014; 124(4): 1821-1834.

Hunter G, Roche SL, **Somers E**, Fuller H, Gillingwater T. The influence of storage parameters on measurement of survival motor neuron (SMN) protein levels: Implications for pre-clinical studies and clinical trials for spinal muscular atrophy. Neuromuscular Disorders. *In press.*

Appendix 2: Conference Abstracts

The Joint Meeting of the Anatomical Society & Sociedad Anatómica Española Edinburgh 2012:

Increasing SMN levels using histone deacetylase inhibitors ameliorates the skeletal muscle capillary bed defect in a mouse model of severe Spinal Muscular Atrophy.

E Somers, J Schreml, M Riessland, B Wirth, S.H Parson.

Development of the capillary bed in spinal cord and peripheral nerve: Implications for the study of Motor Neuron Diseases.

K Hoban, **E Somers**, S.H Parson.

The Scottish Neuroscience Group Meeting Edinburgh 2013:

Significant reductions in spinal cord vascularity, including the ventral horn, in a mouse model of severe Spinal Muscular Atrophy

E Somers, K Hoban, S.H Parson.